"Functional insights into a *Plasmodium* sporozoite membrane protein (SIMP) and a Cysteine protease (SERA-3) reveals a role in maintaining pre-erythrocytic infectivity"

Thesis submitted to University of Hyderabad for the award of

Doctor of Philosophy

In Department of Animal Biology

By

Dipti Singh

14LAPH07

Department of Animal Biology

School of Life Sciences

University of Hyderabad

Hyderabad - 500 046

India

June 2022

UNIVERSITY OF HYDERABAD

Central University (P.O.), Hyderabad-500046, INDIA

DECLARATION

I, Dipti Singh hereby declare that the results of the study incorporated in the thesis entitled **"Functional insights into a *Plasmodium* sporozoite membrane protein (SIMP) and a Cysteine protease (SERA-3) reveals a role in maintaining pre-erythrocytic infectivity"** has been carried out by me under the supervision of **Prof. Kota Arun Kumar** and this work has not been submitted previously in part or full to this University or any other University for award of any degree or diploma.

Dated: 28-06-2022

Dipti Singh

University of Hyderabad
(A Central University by an act of Parliament)
Department of Animal Biology
School of Life Sciences
P.O. Central University, Gachibowli, Hyderabad-500046

CERTIFICATE

This is to certify that the thesis entitled "**Functional insights into a *Plasmodium* sporozoite membrane protein (SIMP) and a Cysteine protease (SERA-3) reveals a role in maintaining pre-erythrocytic infectivity**" submitted by **Dipti Singh** bearing registration number **14LAPH07** in partial fulfilment of the requirements for award of Doctor of Philosophy in the **School of Life Sciences** is a bona fide work carried out by her under my supervision and guidance.

This thesis is free of plagiarism and has not been submitted previously in part or in full to this or any other University or Institution for award of any degree or diploma.

Parts of the thesis had been published in following publications:

1. **Singh D**, Patri S, Narahari V, Segireddy RR, Dey S, Saurabh A, Macha V, Prabhu NP, Srivastava A, Kolli SK, Kumar KA. A Conserved *Plasmodium* Structural Integrity Maintenance Protein (SIMP) is associated with sporozoite membrane and is essential for maintaining shape and infectivity. **Mol Microbiol**. 2022 Mar 17. doi: 10.1111/mmi.14894) PMID: 35301756. Chaptor 2

Presented in the following conferences

1. **EMBL Conference: BioMalPar XVI: Biology and Pathology of the Malaria Parasite.** "A *Plasmodium berghei* conserved gene- *PBANKA_1422900* regulates salivary gland sporozoite infectivity". **Poster Presentation,** 18-19 May 2020, Virtual conference (International).
2. **International Symposium on Malaria Biology & 29th National Congress of Parasitology on Basic and Applied Aspects (ISMBNCP-2018).** A *Plasmodium berghei* conserved gene- *PBANKA_1422900* regulates salivary gland sporozoite infectivity". **Poster Presentation,** 1-3 November 2018, University of Hyderabad, India (International).

Further, the student has passed the following courses towards the fulfilment of course work required for the award of Ph.D.

S. No	Course Code	Name of Course	Credits	Pass/fail
1	AS 801	Analytical Techniques	4	PASS
2	AS 802	Research Ethics, Data Analysis and Biostatics	3	PASS
3	AS 803	Lab Work and Seminar	5	PASS

Supervisor

Dr. KOTA ARUN KUMAR
Professor
Department of Animal Biology
School of Life Sciences
University of Hyderabad
P.O. Central University, Gachibowli,
Hyderabad-500 046. Telangana. INDIA

Head of the Department

अध्यक्ष / HEAD I/C
जंतु जैविकी विभाग
Department of Animal Biology

Dean of the School

School of Life Sciences
University of Hyderabad
Hyderabad-500 046.

This thesis is dedicated to my parents

For their endless love, support and encouragement

Table of Contents

Acknowledgement ..... **i**
Abbreviations ..... **iii**

Chapter 1: Review of Literature **1**

1.1 History of Malaria 2
1.2 Epidemiology of Malaria 2
1.3 Cause of Malaria 3
1.4 Overview of *Plasmodium* Life cycle 4
1.4.1 Asexual development of parasite in the mammalian host 6
1.4.2 Erythrocyte stage 14
1.4.3 Gametocytogenesis 18
1.4.4 Sexual development in the mosquito vector 20
1.5 Clinical Manifestation of Malaria 27
1.6 Diagnosis and treatment 28
1.7 Malaria control measures and prophylaxis 29
1.8 Current challenges to achieve malaria elimination 32
1.9 *Plasmodium berghei* as model 33

Chapter 2. Functional investigation of a conserved *Plasmodium berghei* hypothetical gene *PBANKA_1422900* by reverse genetics **35**

2.1 Introduction 36
2.2 Materials and methods 39
2.3 Results 65
2.4 Discussion 87
2.5 Conclusion 89

Chapter 3. Functional investigation of *Plasmodium berghei* Serine Repeat Antigen 3 (PbSERA 3) **90**

3.1 Introduction 91
3.2 Materials and methods 98
3.3 Results 106
3.4 Discussion 116

Summary **119**

Refrences..... **121**

Publications

Anti-Plagiarism report



Acknowledgements



This Report would not have been conceivable without the fundamental and thoughtful help of numerous individuals.

I would like to express my deepest sense of gratitude to my supervisor ***Dr. Kota Arun Kumar***, for giving me an opportunity to work under his guidance, constant cooperation, and encouragement throughout my work. I am highly grateful to him for all the efforts he has put in for the successful completion of this thesis.

Besides my supervisor, I would like to thank my doctoral committee members: Prof. Manjula Sritharan and Dr. Bindu Madhava Reddy for constructive criticism and guidance.

I am thankful to present Head, Dept of Animal Biology, Prof Srinivasulu Kurukuti, and previous HOD's: Prof. Anita Jagota, Prof. Jagan Pongubala, Prof. B. Senthilkumaran, Prof. Manjula Sritharan and Prof. S Dayananda for providing the departmental facilities.

I am thankful to the present the Dean, School of Life Sciences, Prof. Dayananda Siddavattam, and former Deans Prof. Ramaiah, Prof M.N.V Prasad, Prof. Pallu Reddanna, and Prof. A.S. Raghavendra for providing the central facilities at the School of Life Sciences.

I am thankful to all the Departments of School of Life Sciences and faculty for providing the research facilities either in common facility or in their labs.

The support from Dr. Kota Arun Kumar's collaborators: Dr. N Prakash Prabhu for in silico analysis, Dr. Satish Mishra (CDRI) for providing MTIP antibody, Dr. Anand Srivastava (NIAB) for TEM studies and Dr. Anil Pasupulati (Dept of Biochem, UoH) for Phalloidin reagent is highly acknowledged.

The financial support from DBT, DST, CSIR, ICMR, UGC, PURSE and DBT-CREBB is highly acknowledged, I genuinely recognize the financial support through BBL non-net

fellowship and CSIR Direct SRF research fellowship.

I am thankful all my former lab mates - Dr. Jyothi, Dr. Maruthi, Dr. Surendra, Dr. Rameshwar, Dr. Mastan, Dr. Faizal, and Dr. Ravi, and present lab mates - Dr. Pallabi, Sandeep, Narhari, Smita, Sneha, Anusha and Chandan for their constant support and encouragement during my stay in lab. I am also thankful to Narasimha and Yadagiri for their assistance in the laboratory and Insectary.

I am thankful to all my friends in the HCU campus and SLS research scholar group.

I am extremely grateful to my **parents** and my **husband** for their unwavering love, support and patience throughout my life.

Above all, I owe my thanks to **Almighty,** for everything.

Thank you

Dipti…..

Abbreviations

ACT	Artemisinin combination therapy
AMA	Apical membrane antigen
Bp	Base pairs
BSA	Bovine serum albumin
CDK	Cyclin dependent kinase
cDNA	Complementary DNA
CDPK	Calcium dependent protein kinase
CELTOS	Cell traversal protein for ookinetes and sporozoites
CS	Circumsporozoite
DAPI	4', 6' diamidino-2 phenyl indole
DIC	Differential interference contrast
DMEM	Dulbecco's modified Eagle's medium
DNA	Deoxy ribonucleic acid
DOZI	Development of zygote inhibited
EBL	Erythrocyte binding like
EDTA	Ethylene diamine tetra acetic acid
EEF	Exo erythrocytic form
EMP	Erythrocyte Membrane Protein
FBS	Fetal bovine serum
FP	Forward primer
FLP	Flippase
FRT	Flippase recognition target site
GAP	Genetically attenuated parasite
GAPDH	Glyceraldehyde 3-phosphate dehydrogenase
GFP	Green fluorescent protein
HBV	Hepatitis B virus
hDHFR	Human Dihydrofolate reductase
HEPES	4-(2-hydroxyethyl)-1-piperazineethanesulfonic acid

HSPG	Heparin sulfate proteoglycan
IFN	Interferon
iRBC	Infected red blood cell
ITN	Insecticide treated net
Kb	Kilobase pairs
KO	Knockout
LB broth	Luria-Bertani broth
LISP	Liver specific protein
MAP/MAPK	Mitogen activated protein kinase
mRNA	Messenger RNA
MSP	Merozoite surface protein
MTIP	Myosin tail interacting protein
NEK	NIMA related kinase
Ng	nanogram
NIMA	Never in mitosis Aspergillus
OD	Optical density
P. falciparum	*Plasmodium falciparum*
P. malariae	*Plasmodium malariae*
P. knowlesii	*Plasmodium knowlesii*
P. ovale	*Plasmodium ovale*
P. vivax	*Plasmodium vivax*
PBS	Phosphate buffer saline
PEXEL	*Plasmodium* export element
PKG	cGMP dependent protein kinase/ protein kinase G
PL	Phospholipase
PUF	Pumilio and fem3 transcription binding factor
PV	Parasitophorous vacuole
PVM	Parasitophorous vacuolar membrane
RBC	Red blood cell
RH	Relative humidity

RNA	Ribonucleic acid
RP	Reverse primer
RPM	Revolutions per minute
RPMI	Roswel Park Memorial Institute medium
SAP	Sporozoite asparagine rich protein
SERA	Serine repeat antigen
SIAP	Sporozoite invasion associated protein
SIMP	Structural Integrity Maintenance Protein
SPECT	Sporozoite protein essential for cell traversal
SSH	Suppression subtractive hybridization
SUB1	Subtilisin like protease 1
TAE	Tris acetate EDTA
TBS	Tris buffer saline
TE	Tris EDTA
TRAP	Thrombospondin related anonymous protein
TSR	Thrombospondin related
UIS	Up regulated in infected salivary glands
UTR	Untranslated region
UV	Ultraviolet
WHO	World health organization
WT	Wild type
XA	Xanthurinic acid
^{o}C	Degrees Celsius
µg	Microgram
µL	Microliter
µM	Micrometer

Chapter 1: Review of Literature

1.1 History of Malaria

Malaria is a fatal disease caused by *Plasmodium* parasites that are transmitted through female Anopheles mosquito. Across the globe, nearly 350-500 million people get infected annually and approximately 1 million (mostly children) die of malaria each year in the African continent alone.

Its first references to its symptoms can be established in Hindu writings and early Chaldean, Chinese traditional mythology. In the 5th century B.C., Hippocrates had described the various aspects of malarial infection. In the 17th century, the Italians have devised the term *mal' aria* meaning "bad air" with reference to some foul-smelling vapors emanating from swamps situated in nearby Rome province. At around the same time, it was noted that the outer covering or bark of cinchona tree had a potential for the treatment of intermittent fevers. In the following years, a crucial breakthrough invention was made by Charles Louise Alphonse Laveran in the year 1880 that led to the discovery of transmissible stages of *Plasmodium* to mosquitoes- the gametocytes in the fresh blood samples, albeit at that time the complete life cycle of malaria was obscure. Approximately after 5 years, an Italian histologist named Camillo Golgi observed multiplicative asexual forms of parasites in the blood. In 1890, Patrick Manson proposed mosquitoes as probable vectors for transmission of malaria infection. Sir Ronald Ross, an army surgeon in the British military observed that the developing *Plasmodia* stages reside in the gut of mosquitoes, providing compelling evidence to Manson's theory. Using a bird model of experimental malaria, he made elegant observations and established the mosquito stages *Plasmodium* life cycle and was awarded Noble Prize in 1902 for this seminal contribution.

1.2 Epidemiology of Malaria

Human malaria is one of the deadliest diseases which is prevalent in tropical, subtropical, and temperate regions and remains a major health complication in terms of mortality and morbidity. Malaria transmission is affected by various factors like temperature and humidity, the genetic makeup of host, variation in virulence gene [1] etc. According to the WHO malaria report 2021, 241 million cases and 6,27, 000 deaths were reported in 2020 compared with 238 million cases and 7,36,000 deaths in the year

2000. African region was accounted for about 96% of cases, with an estimation of 228 million cases in 2020. India accounted for 2% of total cases in 2019 and contributed to the largest absolute decrease in malaria cases from about 23 million cases in 2000 to 6.3 million cases in 2020. In India, Odisha, Jharkhand, Chhattisgarh, Madhya Pradesh states contributed to approximately 74.1% of the total malaria burden in 2018 (http://www.nvbdcp.gov.in).

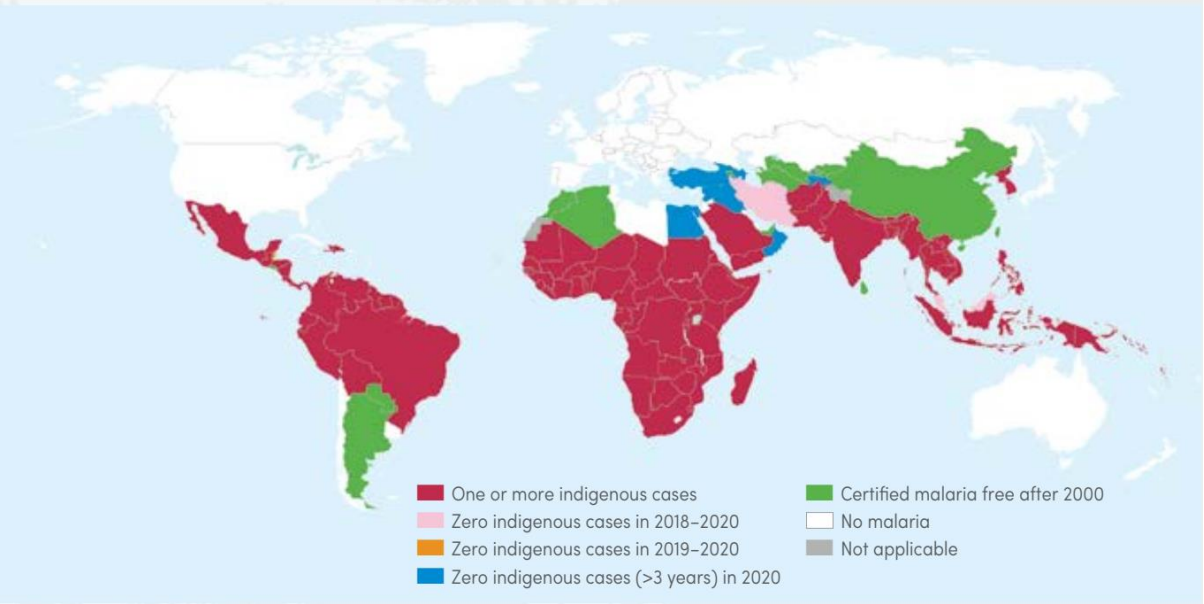


Figure-1. Countries with indigenous cases in 2000 and, their status by 2020. Image Source: WHO malaria report 2021).

1.3 **Cause of Malaria**

Malaria is caused by a unicellular protozoan parasite *Plasmodium* that belongs to phylum *Apicomplexa. Plasmodium* name was given because of its resemblance to multi-nucleated slime moulds with the same name [2]. The *Plasmodium* infection begins from asymptomatic phase that eventually leads to symptomatic infection, characterised by high fever, headache, chills, vomiting, nausea, and anaemia. The genus *Plasmodium* consists nearly 200 species and shows distinct morphology in blood stages in infected host. These *Plasmodium* species have been categorized into 14 sub genera based on their

appearance and distributed globally [3]. Five distinct *Plasmodium* species reported to infect human are *Plasmodium malariae* (*P. malariae*), *Plasmodium ovale* (*P. ovale*), *Plasmodium vivax* (*P. vivax*), *Plasmodium knowlesi* (*P. knowlesi*) and *Plasmodium falciparum* (*P. falciparum*). Among them, *P. vivax* and *P. falciparum* pose the biggest threat to humankind. *Plasmodium falciparum* is the most deadly species of malaria responsible for most deaths in the world, especially in Sub Saharan Africa region. In this region the incidences of malaria caused by *P. vivax* are less common due to the absence of Duffy antigen, however, in America, *P. vivax* cases are two times higher than *P. falciparum* [4].

1.4 **Overview of *Plasmodium* Life cycle**

Plasmodium has a very complex life cycle that shuttles around sexual and asexual developments and requires two physiologically different habitats i.e., vertebrate host and mosquito vector (Fig2). Female Anopheline mosquitos are the definitive host where parasites undergo sexual reproduction as well as forms sporozoites. Once these sporozoites enter the mammalian host via mosquito bite, they infect the liver cells to undergo a silent phase of hepatic schizogony. Upon release of hepatic merozoites into sinusoidal lumen initiates multiple iterative cycles of asexual multiplication within erythrocytes.

The life cycle of *Plasmodium* in mammalian host starts with the bite of a female *Anopheles* mosquito that delivers sporozoites in the skin of the vertebrate host [5]. These sporozoites migrate rapidly through the dermis, penetrate nearby capillaries, and enter into the circulatory system and reach the liver where they are selectively arrested. In liver, sporozoites infect hepatocytes by a productive invasion process involving parasitophorous vacuole (PV) formation. The PV is a unique organelle, in which the spindle-shaped sporozoites transform into a round exo-exoerythrocytic form or EEF. After multiple rounds of asexual replication, the mature EEFs release merozoites into liver sinusoidal spaces packaged in merosomes. These hepatic merozoites are liberated into bloodstream upon rupture of merosomes, that initiate erythrocytic cycle. The merozoites infect RBCs and develop into different stages like rings, trophozoites and multinucleated schizonts forming 16-32 merozoites by erythrocytic schizogony [6]. These merozoites will be released into bloodstream upon rupture of erythrocyte and

invade new RBC to continue the erythrocytic cycle. In this process, some of the rings are differentiated into sexual stages like male and female gametocytes that are terminal stages of the *Plasmodium* in the mammalian host and are transmissible to the mosquito vector [7].

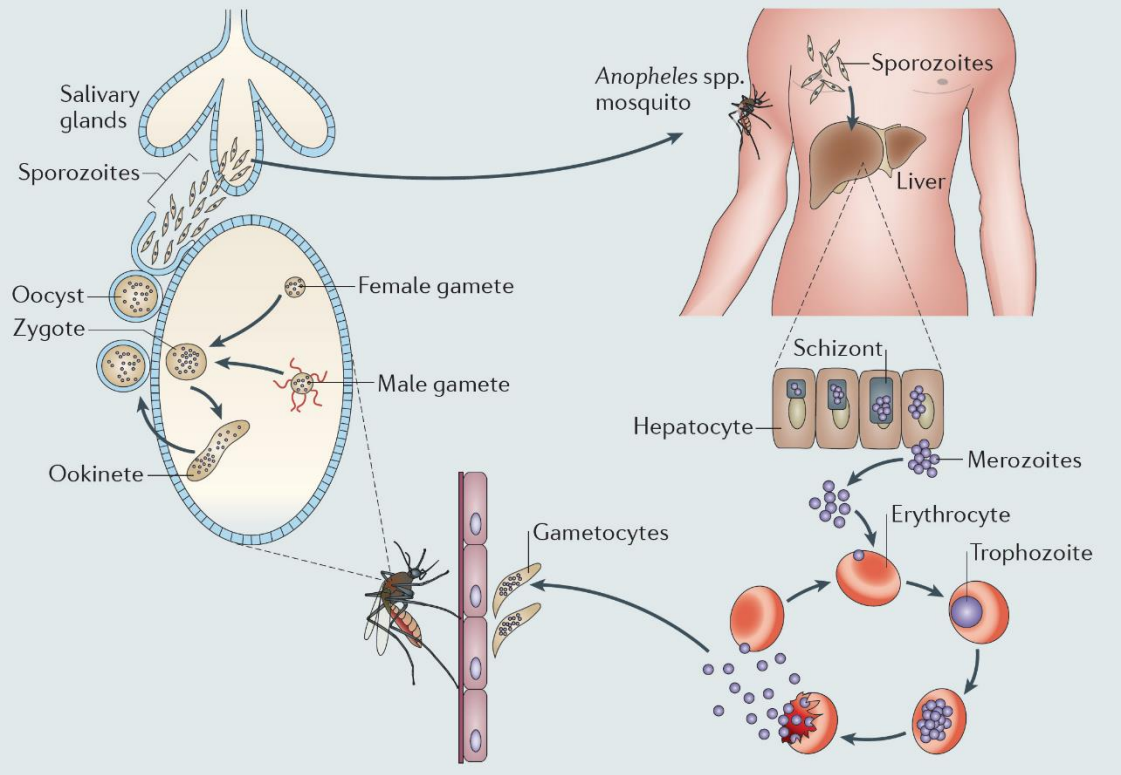


Figure 2. The life cycle of *Plasmodium.* *Plasmodium* life cycle in the vertebrates starts with the bite of a female *Anopheles* mosquito that delivers sporozoites in the skin of the vertebrate host, from where they glide through the dermis and reach the blood vessels. Through blood circulation, they reach to the liver, develop into exo-erythrocytic forms (EEFs) inside the hepatocytes. Following one round of asexual reproduction, the first generation hepatic merozoites are liberated into liver sinusoids packed in merosomes. Rupture of merosomes releases hepatic merozoites into the bloodstream to initiate an erythrocytic infection. In RBC, they go through a series of transformations resulting in ring, trophozoites, schizonts and gametocytes. Gametocytes are the sexual forms and the terminal stages of the life cycle in the vertebrate host. If a female *Anopheles* mosquito obtains a blood meal, at this point of time, they enter the lumen of the mosquito gut where sexual reproduction occur which results in zygote formation. The zygote transforms into a motile ookinete and by breaching the midgut epithelium, settles on the haemocoel side of the gut and develops into an oocyst. Sporulation occurs within the oocyst and upon completion of this process, the sporozoites are released into the haemocoel that make their way to the salivary glands.

Infection to a new mammalian host is initiated when sporozoites are inoculated in the skin when the mosquitoes happen to take a blood meal [8].

While obtaining the blood meal, mosquitoes take up gametocytes, the sexual forms of *Plasmodium* that enter the gut lumen. The male and female gametogenesis is triggered by the factors like change in pH, xanthurenic acid (mosquito-derived factor) and reduced temperature. The sexual gametes that emerged from their respective gametocytes, fuse and results into zygote formation that later transforms into a motile ookinete. These ookinete breaches the midgut epithelium and at the hemocoel side of the gut further develops into an oocyst. Sporozoites develop within the oocyst and upon maturation are released into the hemocoel. The sporozoites make their way to the salivary glands and are ready to infect a new host when mosquitoes take a blood meal.

Plasmodium parasite exhibits a tightly regulated stage-specific expression of proteins that have distinct functions central to each life cycle stage. The life cycle has three distinct phases- the pre-erythrocytic stage (asymptomatic stage), erythrocytic stage (symptomatic stage) and mosquito stage. The biology of these life cycle stages is described below.

1.4.1 Asexual development of parasite in the mammalian host

Infection in the mammalian host starts with a bite of female *Anopheles* mosquito. The bite inoculates 50 to 100 sporozoites into the skin [9-11]. It has been found that sporozoites which are inoculated by mosquito bite are more infectious compare to the sporozoites isolated from salivary glands and then injected intravenously [12]. While probing for a blood meal, the female *Anopheles* mosquito injects a few nanolitres of saliva into the dermis of the vertebrate host, which contains soluble components such as anticoagulants (thrombin), antihistamines, immunomodulators, vasodilators (tachykinin), and platelet aggregation inhibitors to enable blood intake, hence increasing sporozoite survival and enabling inoculation. [12-14].

1.4.1.1 Skin stage and hepatocyte invasion

Plasmodium sporozoites deposited in the vertebrate host skin are highly motile and reside in the skin for less than 4-5 mins. The change in environmental conditions may serve as a cue to activate sporozoite to begin the asexual cycle in mammalian host. From the injection site, the route of sporozoite journey to the bloodstream is poorly understood. It is speculated that sporozoites enter through capillaries that have been damaged by mosquito proboscis, or that sporozoites themselves have the ability to cross through capillary linings [15]. Most of sporozoites traverse through multiple cells using a substrate-dependent motility called gliding motility. [16-18]. Once the sporozoites enters the bloodstream, they are delivered through hepatic artery to the hepatic sinusoids, lined by specialised macrophages known as Kupffer cells and highly apertured endothelial cells. The sporozoites breach both these cell barriers and finally invade hepatocytes [19-21]. The molecular mechanism of cell traversal is well studied and several conserved sporozoite proteins are involved in the process. These proteins include SPECT 1 and 2 (sporozoite micronemel protein that are essential for cell traversal) [22, 23], phospholipase (PL) and Perforin like protein 1(PLP1) [24], [25]. Parasites lacking SPECT-1 or SPECT-2 proteins fail to traverse the host cells, though they were able to invade the cells under *in vitro* conditions, yielding fully mature exoerythrocytic forms (EEFs) or liver stages. However, parasites lacking both the genes resulted in impaired development and showed one day delay in prepatent period in mice [22, 23]. Disruption of *Pb* phospholipase impaired the sporozoite ability to migrate across the epithelial layers, resulting in a 90% reduction in sporozoite infectivity in the liver and one day delay in prepatent period [24].

After sporozoite reaches the liver by breaching different cell types, they get selectively arrested in the liver. Sporozoite retention in hepatic sinusoid is mediated by Circumsporozoite protein (CSP) and Thrombospondin-related adhesive protein (TRAP), that are major secretory antigens of sporozoite [26, 27]. It has been shown that recombinant CSP binds to highly sulphated heparan proteoglycans (HSPGs) present on hepatocytes in the Disse space- a region between hepatocyte and sinusoids. The fact that CSP of sporozoites can bind to the hepatocytes in this region is a highly remarkable and intelligent strategy adopted by sporozoites. The domains within CSP that interact with

hepatocytes are well characterised and include the N and C-terminal GAG binding regions and conserved regions I and II of CSP [28-30]. It has been reported that CSP is cleaved by cysteine protease and their proteolytic processing is required for interaction of CSP with hepatocytes [31]. The N-terminal cleavage of CSP is a function of a cysteine protease, as E-64 a cysteine protease inhibitor prevents the processing of CSP cleavage and hence host cell invasion [31]. The cleavage or processing of N-terminus exposes the C-terminus of CSP having adhesive thromospondin type1 repeat (TSR) domain that interacts with host HSPGs [32]. Later, TRAP is released by micronemes secretory organelles called onto the surface of sporozoite. TRAP protein has two adhesive domains: TSR domain and A domain that binds to host cell receptors (like HSPGs) [33]. In addition to this , another interaction between the C-terminal domain of intracellular TRAP and the sporozoite actin-myosin motor system [34] power a moving junction that enables parasite invasion of hepatocytes. The sporozoite invasion of hepatocytes is completely abolished when both the TSR domain and A domain domains are mutated [35]. Recently, it has been reported that *Plasmodium* TRAP protein binds with host integrin αvβ3 [36]. During the invasion process, host receptors also play important role. The mouse CD81 receptor, which belongs to the tetraspanin receptor family, is required for productive hepatocyte invasion but not for RBC invasion. The *Plasmodium yoelii* sporozoites failed to establish infection in CD81 KO mice [37]. It has been also reported that CD81 is essential for rhoptry discharge in the sporozoite [38, 39]. The scavenger receptor BI(SR-BI) affects sporozoite invasion in *Plasmodium berghei* and parasite development in hepatocytes in *P. falciparum* [40, 41]. In sporozoite invasion, role of Ephrin receptor A2 (EPHA2) has been also implicated [42]. Although higher expression of EPHA2 was corelated with increased invasion by *P. yoelii* sporozoites, It was later found that *Plasmodium* sporozoites can invade hepatocytes unassisted by EPHA2 [43].

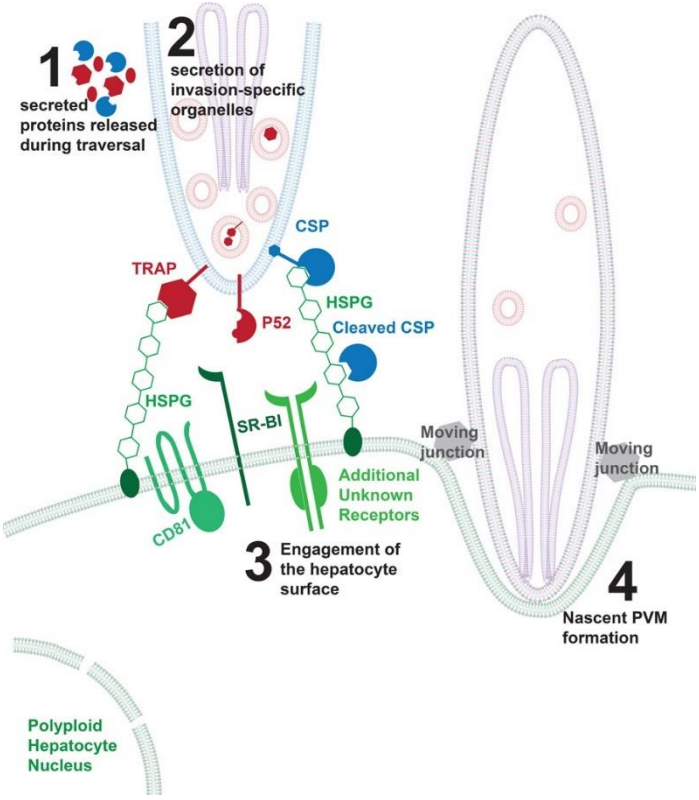


Figure 3. *Plasmodium* sporozoite invasion and early attachment to hepatocyte. 1&2) Sporozoite glides and traverse through skin and bloodstream that involves the secretion of several micronemal proteins. 3) After reaching liver sinusoids, for invasion, sporozoites proactively interact a hepatocyte. The interaction between CSP and host HSPGs is likely one of the factors involved in this binding. Host cell receptor like CD81 and SR-BI are also involved in hepatocyte invasion by interacting with parasite proteins. 4) Upon attachment, sporozoite initiate forming moving junction and nascent PVM [44].

Rhoptry and micronemal proteins are found in all parasite invasive stages, indicating that their secretion is crucial for the invasion process [45, 46]. The secretion of proteins from these secretory organelles coincide with actin-myosin motor system facilitates the invasion process, though the exact mechanism is poorly understood. The secreted proteins are thought to bind to ligands on the hepatocyte surface after secretory organelles discharge, resulting in a tight ring formation around the parasite [47, 48]. This complex is taken away from the apical end using same the actin-myosin motor complex which is used in gliding motility of sporozoite [48] in the formation of a moving junction which keep out host surface proteins, and finally resulting in the formation of PVM [47].

The host F-actin protein localizes to this moving junction [49], aids to stabilize this complex. The host actin-related protein (ARP) 2/3 appear to be employed to the moving junction, albeit it is unknown what signals drive this recruitment [49]. Two secretory proteins named as rhoptry neck protein 2 (RON2) and micronemal apical membrane antigen 1 (AMA1) form the moving junction to invade the red blood cell [50]. AMA1, RON2, RON4 and RON5 proteins are involved in tight junction formation between sporozoites and hepatocyte. RON4 was found to be essential for all invasive stages of *Plasmodium.* AMA1 is not required for sporozoite invasion in *P. berghei* [51]. Though, antibodies against AMA1 inhibit sporozoite invasion both in *vitro* and *in vivo* in *P. falciparum* [52] and *P. yoelii* [53] respectively. Moving junction formation during RBC invasion appears to be unaided of host proteins whereas membrane proteins of hepatocyte are required for sporozoite invasion. Elucidating the details of molecular mechanism of interactions could help with vaccine development to curb malaria at the liver stage.

1.4.1.2 Parasitophorous vacuolar membrane formation in hepatocyte

After migration through several cells, the sporozoites establish infection by subsuming themselves into a vacuolar structure, the parasitophorous vacuole membrane (PVM) that is partly made from host cell membrane. Within the PVM compartment, the spindle shaped sporozoites transform into a round exo-exoerythrocytic form (EEFs). The mechanism of PVM formation is obscure till date, but some reports suggest that it is formed by remodelling of host membrane components and by incorporation of parasite derived proteins [44]. As PVM separates parasites from host cell environment, it helps parasites to escape from immune responses of host. PVM is closely associated to host endoplasmic reticulum [47] and this interaction provides access to lipids and nutrients to parasites from host cell [54]. Two parasite micronemal proteins P36 and P52 are required for PVM formation. Depletion of these proteins resulted in early liver stage arrest with defect in PVM formation [55-57]. The PVM resident proteins like Up-regulated in Infective Sporozoites (UIS) 3 and UIS4, early transcribed membrane proteins (ETRAMPs) and Exported protein (EXP1) are all important for liver stage development. EXP1 interacts with the host apolipoprotein and required for the pre-erythrocytic development [58]. UIS3 is expressed in both sporozoite stage and liver stage. It interacts with the host cell derived autophagy protein LC3 affecting its inactivation and inhibition

of parasite autophagy process [59]. UIS3 also interacts L-FABP1(with liver fatty acid binding protein) that is likely to provide nutrition to parasite as L-FABP downregulation in hepatocytes impaired the parasite development while upregulation of L-FABP promoted the growth [60]. UIS4 is highly expressed in sporozoite and localized to parasitophorous membrane. In the absence of UIS4, *P. berghei* liver stage development was severely impaired [61]. UIS3/UIS4 knockouts showed defect in the EEF development within the hepatocytes and were unable to initiate blood stage infection that conferred sterile long-lasting immunity [61, 62]. Liver Specific Protein 1 (LISP1) is a PVM resident protein and essential for merozoite release [63]. Thus, PVM specific proteins play important role in host parasite interactions such as nutrition uptake, host cell remodelling etc. Exploring of PVM composition may aid in understanding the survival mechanism of parasite inside the hepatocyte, and its immune evasion techniques.

Through a specialized machinery, the parasite exports a repertoire of proteins into the cytoplasm of host cell, which are essential for host cell takeover. These proteins have a specific canonical motif called as *Plasmodium* export element/ host targeting sequence (PEXEL/HTS) with a conserved sequence RxLxE (x-any amino acid). This motif is present at the N terminus of a protein and found approximately 35 amino acids after the signal peptide [64, 65]. Although, the PEXEL/HT motif is not found in all proteins exported to the host cytosol. In fact, several PEXEL negative exported proteins-(PNEPs) also translocate to host compartment. CSP, the major surface protein of sporozoites have two typical PEXEL motifs that are required for export of the protein into the hepatocyte cytoplasm [66]. CSP inhibits the protein synthesis process by binding to the host ribosomes [67] and displace NFκB nuclear translocation therefore downregulating the expression of several genes regulated by NFκB, including genes that are involved in inflammation [68], Apart from CSP, only few liver exported protein has been studied so far: IBIS1, a transmembrane protein which is exported into the host cell at both the liver and blood stages [69]. SLTRiP is a tryptophan-rich protein is exported inside the host cell during early hours of liver stage infection [70]. Another protein named as LISP2 (liver specific protein 2) is exported into the host cytosol and nucleus during liver stage development. Gene targeting experiments revealed the role of LISP2 mutants in the liver stage, during formation of merozoites. Thus, the exported LISP2 affects host-parasite interactions required for intrahepatic development of *Plasmodium* [71].

1.4.1.3 Exoerythrocytic Forms (EEFs) development in hepatocytes

After successful productive invasion and formation of PVM inside the host cell, sporozoites rapidly dedifferentiate into EEFs. The IMC and the subpellicular network disassemble during dedifferentiation, resulting in a round parasite [72]. However, the sporozoites can develop into early EEFs *in vitro* in absence of host cells, suggesting that early EEF transformation does not require host factors [72, 73]. Intracellular liver stage parasites undergo schizogony, that involves rapid nuclear division without cytokinesis [74]. Cytokinesis takes place at very late liver stage development and finally forms thousands of exo erythrocytic merozoites from a single infected hepatocyte [75]. This scenario imposes a very high demand for fatty acids and other metabolites for development. Initially, it was thought that the parasite takes up lipids from the host [76]. However, the discovery of apicoplasts role in de novo fatty acid synthesis–through the fatty acid pathway II(FAS II) accounted for the lipid requirement of the parasite [77]. FabB/F, FabG, FabI and FabZ are the enzymes involved in FAS II pathway and needed during late liver stage development [78]. Liver stage schizogony is amongst the most dramatic cellular processes of *Plasmodium* that involves formation of several thousand merozoites and varies in different *Plasmodium* species. Rodent *Plasmodium* sporozoites (*P. berghei* and *P. yoelli)* take 2-3 days to transform into a fully mature liver stage having upto 29000 exo-erythrocytic merozoites [79, 80]. Liver stage development takes around 6-6.5 days in *P.falciparum*, with estimated 90,000 exo-erythrocytic merozoites wrapped in the fully mature liver stage parasite [81].

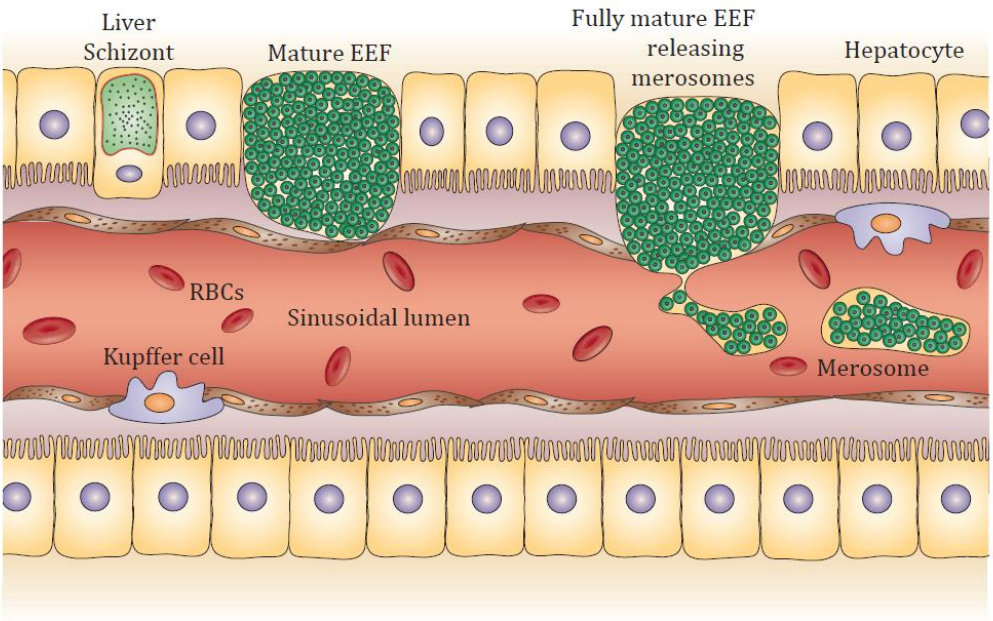


Figure 4. Hepatic merozoite exit from liver. The EEFs undergo schizogony to form thousands of hepatic merozoites. Following one round of asexual replication, the first generation merozoites are released into the liver sinusoids packed in sacs called merozomes, that are derived from both host and parasite plasma membrane to evade immune clearance by liver resident macrophages. The release of merosomes from fully mature EEFs into the bloodstream precludes them from being encountered by kupffer cells in the liver sinusoids. Rupture of merozomes release hepatic merozoites into the blood to initiate erythrocyte cycle. Image adapted from Surendra Kolli's thesis.

Once liver stage development completes in hepatocytes, these hepatic merozoites are released, packaged in membrane bound vesicles called merosomes. Merosomes are 12-18 microns in size and contain 100-200 merozoites. They facilitate host immune evasion from surveillance by Kupffer cells, which are highly phagocytic and are located in the liver lining of sinusoids. The merosomes are formed after parasite mediated degradation of PVM and host cell death [82, 83].

The process of PVM degradation is facilitated by parasite-derived cysteine protease and is blocked completely using a cysteine protease inhibitor, E64 [84]. Various proteins has been identified that play key roles in PVM rupture and egress of hepatic merozoites. Subtilisin like protease (SUB1) mutant parasites failed to rupture the PVM [85]. Similarly, Liver specific protein 1(LISP1) in *P.berghei* is involved in PVM degradation. LISP1 depleted parasites developed into fully mature merozoites but failed to degrade the PVM and egress from hepatocyte [63]. cGMP dependent protein kinase

(PKG) also has been reported to be involved in merozoite egress from hepatocytes [86]. Finally, merozoites are liberated from merosomes into the hepatic bloodstream by membrane breakdown, allowing them to infect RBCs and start the erythrocytic cycle [81, 86].

1.4.2 Erythrocyte stage

Exo-erythrocytic stages though are metabolically active yet are asymptomatic and clinically silent that liberate thousands of hepatic merozoites into the bloodstream. These free hepatic merozoites recognize and invade erythrocyte in a fast, three step process that includes pre-invasion, active invasion and echinocytosis [87, 88] which occurs within 2 min [89, 90]. The initial interaction of hepatic merozoites with erythrocytes is known as pre-invasion, however the molecular characteristics of this stage are not well understood. During the pre-invasion step, a hepatic merozoite establishes initial contact with erythrocytes, causing facile deformation the host cell membrane. Merozoite surface protein 1 (MSP1) present on the merozoite surface and mediates initial attachment of merozoite to RBC [91]. The merozoite then reorients itself in a manner that its apically localized organelles abut the cell surface. The specialised secretory organelles like Rhoptries, micronemes, and dense granules are found at the apical side of parasites that secrete surface proteins such as adhesins and invasins that aid the parasite's adhesion, invasion, and development in the host cell [92].

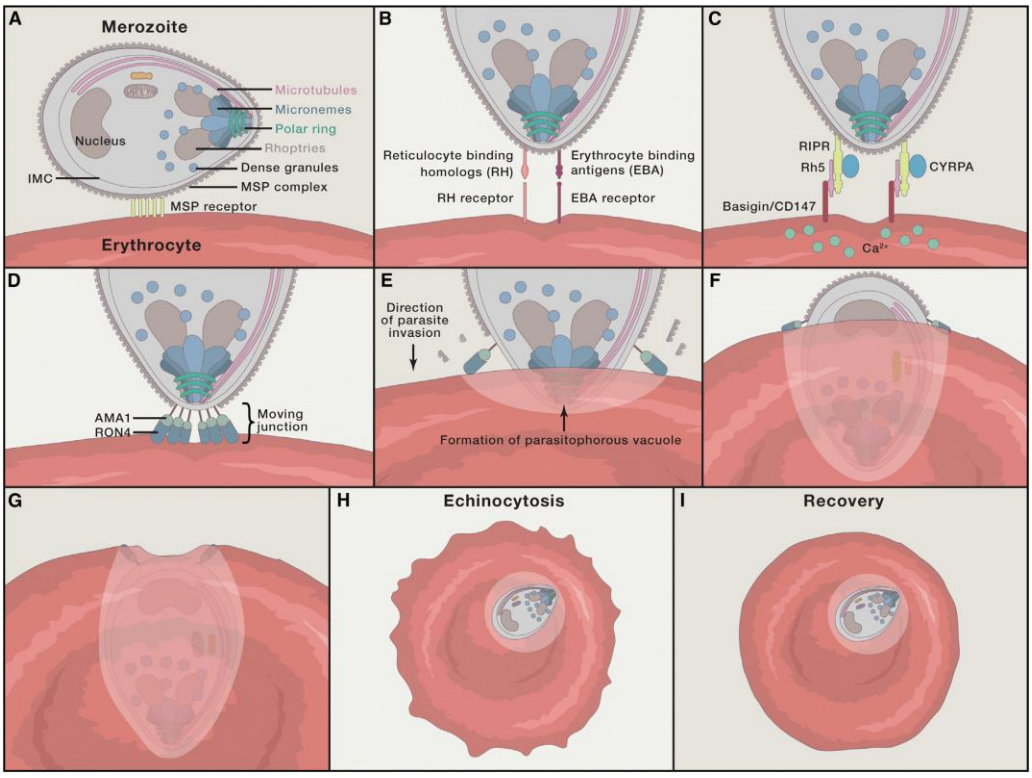


Figure 5. Erythrocyte invasion by merozoite. A) Merozoite-erythrocyte contact is mediated by weak interactions between erythrocyte receptor and merozoite surface proteins. B) Reorientation of merozoite occurs by wrapping the erythrocyte membrane around it and placing the apical end of parasite in interface with the erythrocyte membrane. C) The ligand-receptor interaction is mediated by the EBA protein and PfRh protein family members. The process is initiated with the binding of parasite PfRh5 complex to the host cell basigin receptor. D) This process is linked with a calcium flux inside erythrocyte and microneme secretion, which allows the RON complex to be deposited into the erythrocyte membrane and subsequently binding to AMA-1 directly for moving junction formation. E-G) The merozoite pushes into the erythrocyte membrane through reverse mobilisation of a merozoite actomyosin complex. This usually coincides with the release of rhoptry contents, which aid in the formation of PV membrane, which would enclose the parasite. H) Upon the sealing of the PV membrane and the erythrocyte plasma membrane, echinocytosis develop as a consequence of water loss from the erythrocyte cytoplasm. I) Following that, erythrocyte homeostasis gets rcovered. Image adapted from [93].

Merozoite reorientation is linked to membrane deformation and involves parasite ligand interactions such as the reticulocyte binding-like homologues (Rh) family proteins and the erythrocyte binding antigen (EBA) and receptors present on erythrocyte cell surface [88, 89, 93-95]. It has been shown that these parasite protein ligands bind specifically host cell receptors that includes glycophorin A, B, C and CR1 (complement

receptor 1) in a strain specific manner[95]. The *Pf*Rh and EBA proteins are also involved in the signalling activation that initiates the invasion process. *P. falciparum* merozoites are exposed to low K+ ion concentrations in plasma after being released from the host cell, which causes a jump in cytosolic calcium levels via a phospholipase C-mediated pathway, resulting in the release of EBA-175. Binding of EBA-175 binds glycophorin A receptor leads to rhoptries discharge. This study shows how important these protein families were, not only in binding to host erythrocytes, but also for downstream signalling events that are required for successful parasite invasion [96, 97]. Similarly, PfRh1 is also associated with Ca^{2+} signalling in the merozoites [98], and phosphorylation of the cytoplasmic tail of PfRh4 mediated by PfCK2 (*P. falciparum* casein kinase 2), is needed for parasite invasion via the PfRh4-CR1 mediated parasite-host interactions [99]. Calcineurin is also implicated in merozoite attachment, possibly by stabilising EBL and PfRh dimerization[100].

The merozoite seems to reorient after the erythrocyte is deformed, with the apical end aligning closely to the erythrocyte membrane. This interaction involves PfRh5, forming a complex with cysteine-rich protective antigen (CyRPA) and Rh5-interacting protein (PfRipr) [101, 102]. PfRh5 binds to the basigin receptor [103], which is required for merozoite invasion. PfRH5-basigin receptor interaction is required for the rhoptry discharge into the invaded erythrocyte, which is linked with a calcium spike, possibly owing to a pore formation on the erythrocyte surface [88, 104]. It was reported that invasion can be blocked by using specific antibodies that can prevent interaction between PfRH5 and basigin [103, 105].

The release from rhoptry organelles signals the start of the active invasion. RON complex (RON2,4 & 5) proteins are among the proteins released from the rhoptries, which all together forms a receptor for AMA1 protein binding localized on the merozoite surface [106-108]. The interaction between AMA1 protein and RON complex establish a moving junction between parasite and host cell that is considered to be completely parasite derived, results in the parasite attachment to erythrocytes in irreversibly manner [109-112]. The moving junction serves as an attachment site for the parasite to actively invade the host cell by using its actin-myosin motor machinary. Inhibiting the AMA1 and RON interaction prevents the invasion process [50, 108, 113].

As invasion proceeds, PV membrane is derived from host cell membrane components and parasite lipid rich rhoptries contents. Soon the merozoite produces a protective niche, within which the new daughter parasites are formed[94]. At the beginning of PVM formation, the interface between host and parasites appears like a ring, hence name as ring stage. Next, merozoite membranes at the posterior end, they fuse to enclose the parasite inside the PV and erythrocyte. Echinocytosis follows- the third invasion phase, a short period of host cell dehydration, shrinking and formation of spiky protrusions. It is possibly due to Ca^{2+} influx inside the erythrocyte during PfRh5 complex-basigin interaction. Echinocytosis was inhibited by reagents that block discharge of rhoptries, such as antibodies targeting PfRH5 or basigin [88]. After successful invasion, merozoite undergoes into a trophic phase followed by a replicative phase. Inside the erythrocyte, the parasite transforms into a trophozoite. The trophozoite develops by ingesting the cytoplasm of the host cell. Intracellular parasites breakdown haemoglobin and use it as a source of amino acids. The non-protein heme is toxic to parasite and therefore is converted to hemozoin, a malaria pigment [114]. Many anti-malarial drugs, such as mefloquine and chloroquine, prevent the formation and crystallisation of hemozoin, thus aiding parasite clearance [115]. Approximately after 18 h post invasion of RBC, the trophozoites develop into schizonts. The rapid intra-erythrocytic proliferation depends on the ability of the parasites to evade host defences which is possible due to antigenic variation. Antigenic variation refers to a phenomenon of differential expression in erythrocyte membrane protein 1 (PfEMP1) via a family of var genes (*Plasmodium* has 60 var genes). Every parasite expresses one var gene at a time in a mutually exclusive way while the other members of family remain transcriptionally silent [116]. Antigenic variation is attained by epigenetic regulation, the expression of monoallelic var transcripts, and the telomeric heterochromatin-mediated silencing of other var alleles [117]. At around 48hr post invasion, asexual schizogony is initiated that produces nearly 16-32 daughter merozoites. These merozoites egress RBC and invade new ones. This process continues in an iterative manner thus destroying the erythrocytes. The merozoite egress process is tightly regulated involving several protein kinases, such as the calcium-dependent protein kinase PfCDPK5 [118] and cGMP-dependent protein kinase (PfPKG) [119]. Merozoite egress from infected cells in *P. falciparum* is facilitated by MSP1 through subtilisin 1 (SUB1) mediated proteolytic processing on the surface of merozoite that activates it and helps to bind spectrin, a

cytoskeleton component of the erythrocyte. Parasite lacking surface bound MSP1 show severe egress defect, whereas mutant parasites expressing an improperly processed MSP1 display delayed egress [120]. Following one round of asexual blood stage replication, the released daughter merozoites infect new RBC and start another round of asexual replication. At the same time, a small population from freshly invaded merozoites transforms into male and female gametocytes, that are terminally differentiated sexual stages of parasite, that do not undergo further development, but can serves as stages that are transmissible to the female Anopheles mosquito [121].

1.4.3 Gametocytogenesis

The rate of sexual commitment differs between *Plasmodium* species and is influenced by a variety of environmental, genetic, and epigenetic factors. During preliminary research, it was discovered that chromosomal deletions result in the loss of gametocytogenesis while doing in vitro culture in *P. falciparum* and in mice in *P. berghei* [122, 123]. Genetic studies in *P. berghei and P. falciparum* established AP2-G as an important transcriptional activator of sexual commitment [124, 125]. In asexual parasites, the ap2-g locus is epigenetically repressed by heterochromatin protein 1 (HP1) [126] and histone deacetylase2 (HDAC2) [127]. In a recent study, it was shown that the GDV1 (gametocyte development 1) protein interacts directly with HP1 and activates the AP2-Gp2 locus, resulting in transcription of AP2-G and sexual commitment in a small group of schizonts [128]. Concomitant with such observations, PfGDV1 gene mutant parasites failed to produce gametocytes [129].

The development of gametocytes differs depending on the *Plasmodium* species and takes nearly 1–12 days and produce infectious sexually dimorphic male and female forms. *P. falciparum* shows the longest gametocyte development (9-12 days) with five morphologically distinct phases (stages I–V) [130]. In other species of *Plasmodium* that infect the aves, primates and rodent lineages, only slight morphological changes are noted during development of gametocyte with a cycle varying between 24h and 60 h [131]. A continuous layer of microtubules forms during gametocyte formation in *P. falciparum*. The microtubules are connected to inner membrane complex (IMC) present beneath the plasma membrane of the parasite. The formation of the IMC in *P. falciparum*

gametocytes correlates with cytoskeleton changes in infected RBCs (iRBCs), that includes integration of exported parasite antigens and finally results in reversible stiffening of the iRBC. [132, 133].

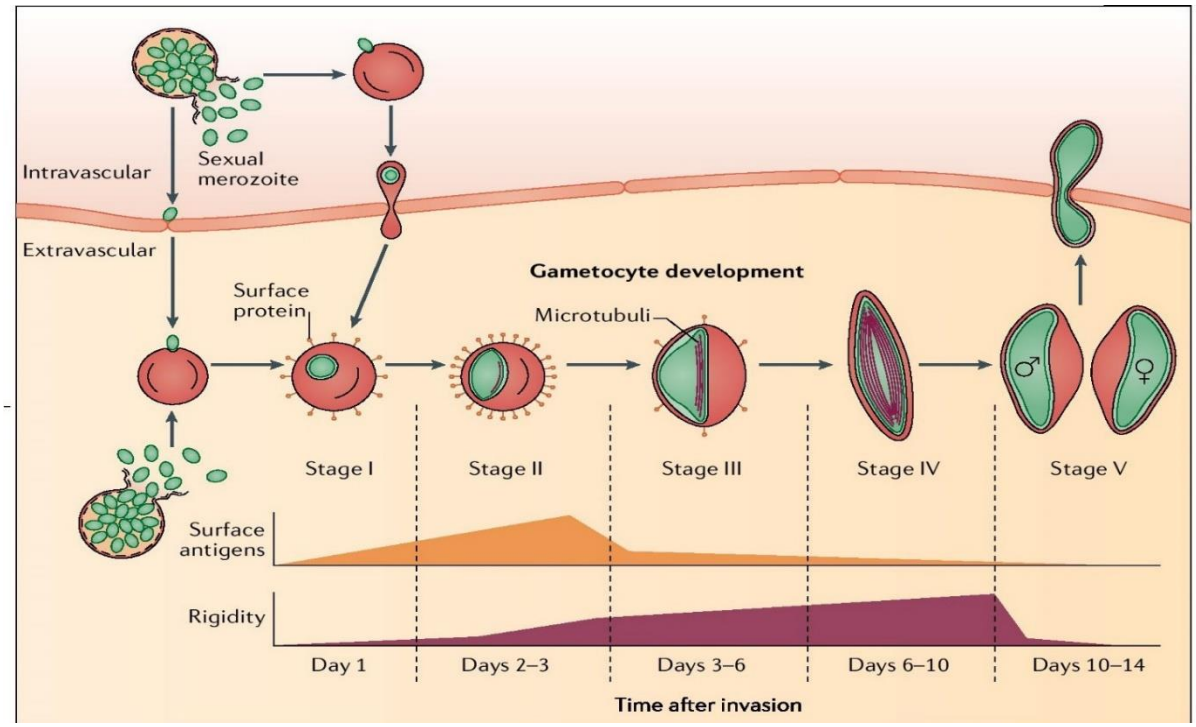


Figure 6. Gametocyte formation in *P. falciparum.* A subgroup of schizonts enter into the sexual cycle and produces sexual merozoites. These Merozoites and young gametocytes (in green) leave the sinusoids and enter the parenchyma to go to the bone marrow. On other hand, committed schizonts produce gametocytes in the parenchyma. Gametocytes develop from stage-I-IV in the bone marrow parenchyma. Remodelling of the erythrocyte membrane (red) results in transitory deposition of surface antigens (orange) and, a reversible increase in cellular stiffness (purple). When the deformability of stage V gametocytes is restored during maturation, they are released back into the blood, where they might be taken up by mosquito bite. Image adapted from [135]

As a result, gametocytes in stages II to stage IV are more rigid than gametocytes in stage V. Stage I gametocyte resembles the trophozoite stage and most of the gametocytes are sequestered in the bone-marrow to avoid splenic clearance. Only I and V stage gametocytes circulate in the peripheral blood [134]. The stage V gametocyte is only mature stage of the parasite that can survive in the mosquito vector. When mature gametocytes are taken up by a mosquito while taking a blood meal, they are activated by

a change in pH, a reduced temperature, a mosquito -derived factors such as xanthurenic acid (XA).

1.4.4 Sexual development in the mosquito vector

1.4.4.1 Gametogenesis

Sexual development begins with the bite of a female *Anopheles* mosquito on infected vertebrate host during a blood meal and during this process gametocytes are taken up by mosquito . In the mosquito midgut, gametes emerge from gametocytes by a process of gametogenesis, a process that is triggered by change in pH, presence of xanthurenic acid and reduced temperature [135]. Eight flagellated motile microgametes can be produced from a single male gametocyte. Gametogenesis is associated with intracellular Ca^{2+} mobilisation, that activates 3 rounds of DNA replication in male gametocytes, followed by endomitosis [136]. Parasites egress from the erythrocyte during this process and begin axoneme biosynthesis. Axoneme mobility is initiated in the penultimate step of male gametogenesis, and male gametes escape in the environment via the exflagellation process. [137]. Several kinases have been discovered as crucial components in process of male gametogenesis in *P. berghei*. cGMP-dependent protein kinase G (PKG) is critical for Ca^{2+} mobilisation on gametocyte activation by xantherunic acid [138]. Calcium-dependent protein kinase 4 (CDPK4) is required in the microgamete formation [136]. CDPK1 and CDPK2 also play key roles at different phases of male gametogenesis [139, 140]. A mitogen activated protein kinase (MAP-2) is essential for cellular differentiation in the process of male gametogenesis in both *P. falciparum* and *P. berghei* [141-143].

The activation and translation of numerous transcripts held under translational repression by the DDX6-class RNA helicase DOZI during in the female gametocyte is required for gamete formation. [144]. One female gametocyte produces a single macrogamete and exits the erythrocyte.

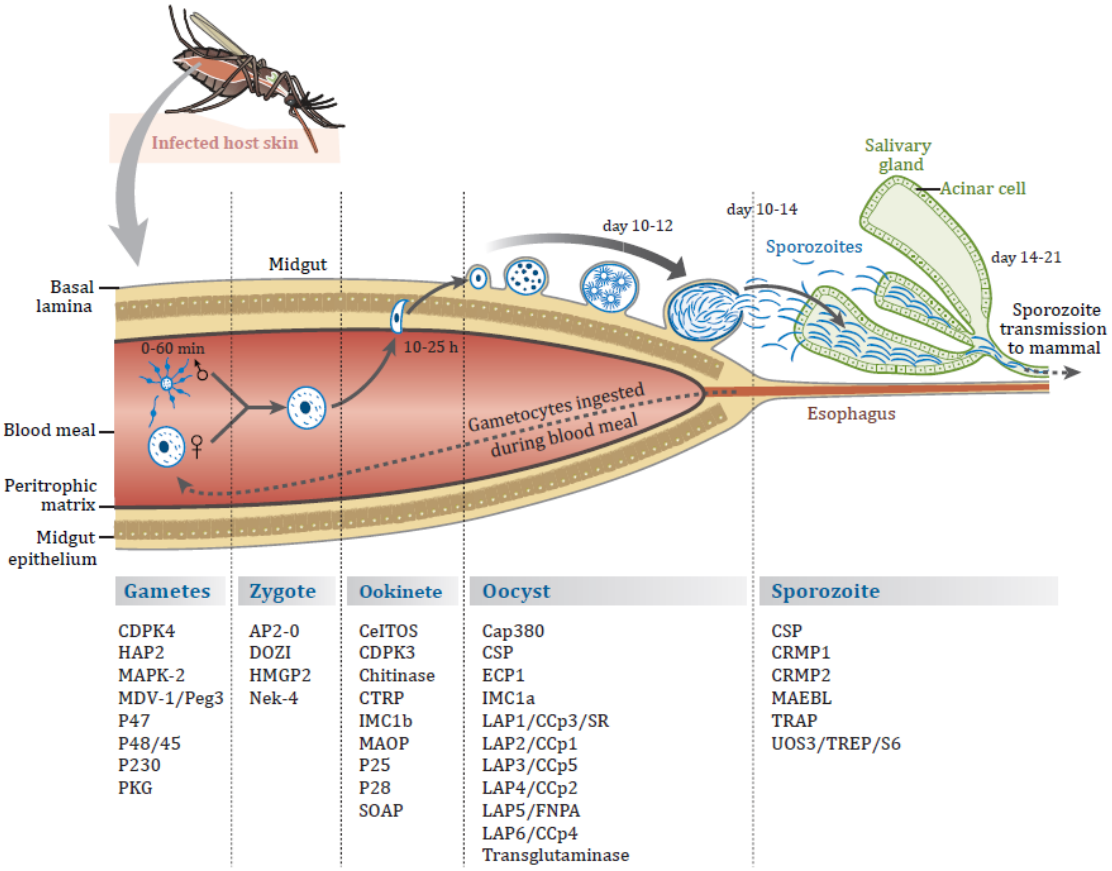


Figure 7. Plasmodium proteins required during mosquito stage development.

1.4.4.2 Fertilisation, ookinete formation and ookinete to oocyst transformation

Soon after gametogenesis (10min-1hr), fertilisation takes place in the lumen of mosquito midgut by fusion of haploid male and female gametes, resulting in the formation of a non-motile diploid zygote [145]. A number of proteins expressed by male and female gametes have been implicated to play essential roles in gamete fertilization and zygote formation [146, 147]. In the *Plasmodium* gamete stages, the conserved 6-cysteine family proteins have been shown to be essential. These proteins are surface localized and are important in cell-cell adhesions. P230, P230p, P48/45 and P47 are the conserved 6-cysteine family member proteins which are expressed in the gamete stage and critical role in gamete formation. P230 and P48/45 are male gamete specific proteins

and essential for male gamete fertility. P47, a paralog of P48/45, is expressed solely in female gametocytes, and its targeted disruption resulted in defective female gametes [147]. The male gametes contact female gamete through gamete adhesion that is mediated by Pfs48/45-P230 [148]. Targeted deletion of P230 revealed its role in the gamete formation and fertilisation [149]. *P. berghei* HAP2 was essential for fusion of male and female gamete membranes. Evidence from revere genetics have shown that P48/45, P47, P230, P25, and P28 are essential for gametogenesis and fertilization and thus considered as potential transmission blocking vaccine candidates [150, 151].

Within 3 hours of fertilization, the diploid zygote undergoes meiosis to become tetraploid [145, 152]. The spherical zygote transforms into an elongated motile structure-ookinete. It has been shown that NIMA1 (never in mitosis Aspergillus 1) related kinase NEK-2 and NEK-4 are required for zygote development and ookinete development form zygote [153, 154]. The motile ookinetes that are still in lumen of mosquito midgut, invade midgut epithelium and reach the basal side before transforming into oocyst. The first barrier which ookinetes pass is a chitin rich peritrophic matrix that is present on the apical side of midgut. The chitinase secreted by parasite degrades peritrophic matrix of midgut [155]. Ookinete adheres to epithelial apical cells by disrupting cell membrane with the help of members that belong to the PPLP family (perforin like protein (PPLP) family) [156]. The ookinetes traverse through the peritrophic matrix before migrating to the epithelial layer of the midgut of the mosquito [157]. Ookinete surface localised proteins - P25 and P28, having GPI anchor and EGF domain protect the ookinete from the proteolytic activity in the midgut. Parasites lacking either P25 or P28 fail to traverse midgut epithelium and do not form oocyst [158]. Ookinetes, like other *Plasmodium* motile stages, have actin-myosin-based gliding motility. The components and machinery that facilitates gliding motility is conserved among all the apicomplexan members [159]. The components of gliding machinery include an actin-myosin motor, an inner membrane complex (IMC), and accessory proteins such as gliding associated proteins (GAP45), (GAP50) and MyoA tail interacting protein (MTIP) [160-163]. The circumsporozoite and TRAP related protein (CTRAP), and calcium dependent protein kinase (CDPK3) have been shown to be essential for ookinete motility and infectivity. Deletion of CDPK3 and CTRAP resulted in non-motile ookinete that were unable to invade midgut [164, 165]. Ookinetes bind to the midgut basal lamina after migrating through the epithelium of the midgut and become sessile. It further transforms into oocysts beneath the basal lamina,

that is thought to be beneficial for the parasite as the developing oocyst is hidden from the mosquito immune system. A small number of ookinetes that traverse through the midgut epithelium and mature into oocysts are crucial to the malaria parasite's survival in the mosquito vector and its transmission to the vertebrate host. This transition ~~a~~ccounts for a considerable fraction of parasite loss. Ookinetes must overcome several obstacles to successfully develop into oocysts.

1.4.4.3 Development of oocyst and sporulation

Oocyst is extracellular and longest developmental stage of the *Plasmodium* life cycle that lasts for nearly 10-14 days for maturation [166]. The oocysts grow from 2-3 μm in diameter to 50-60 μm in diameter throughout development, extending the surrounding of basal lamina [167, 168]. During the development, the parasite secretes an amorphous capsule that completely encases the oocyst's surface. The capsule remains as a bi-layered structure, where the outer membrane is made of mosquito derived laminins and inner layer (oocyst plasma membrane) is surrounded by a dense coat of cirumsporozoite protein (CSP) [169, 170]. This oocyst capsule protects the parasite from mosquito immune system. The oocyst undergoes numerous mitotic divisions, resulting in a multinuclear syncytium [171]. The cytoplasm of the oocyst eventually segregates and subdivides into sporoblasts, which serve as budding centres for hundreds of sporozoites [172]. The sporoblasts are formed by the invagination of oocyst plasma membrane which leads to the retraction of cytoplasm into lobular structures.

CSP play a key part in sporozoite development in the oocyst. CSP expression starts few days after oocyst develpment and gradually accumulates on plasma membrane of oocyst [173]. In sporoblasts, CSP is present on the plasma membrane, endoplasmic reticulum and in the cytoplasm [174-176]. It has been reported that CSP is required for sporoblast formation and then sporozoites. Parasite lacking CSP, failed to form oocyst sporozoites [177]. Another study found that the GPI-anchor domain of CSP is required for the sporoblasts formation and cytokinesis, and that interfering with the position of this causes developmental defects [178]. Oocyst development ends with the formation of thousands of sporozoites, which finally bud out from the sporoblasts [179]. The budding process begins midway thorough oocyst development with the help of microtubule organizing centres (MTOCs). MTOC facilitate the apical complex and nuclei formation that

are integrated into daughter cells following cytokinesis [173]. Female gametocytes and ookinetes specific LAPs (lectin adhesive-like proteins) have demonstrated a key role in sporozoite formation [180-184].The sporozoite budding from sporoblasts appears to be asynchronous and occurs in successive waves. After budding from sporoblasts, the mature sporozoites take on a crescent form. The crescent shape is thought to be caused by an uneven distribution of microtubules connected to IMC of sporozoites [185, 186]. Membrane complex 1 (IMC1) is a key protein of the IMC, and its targeted disruption revealed that it has critical function in sporozoite motility and maintaining the crescent form [185]. Thousands of sporozoites are released from oocyst into mosquito heamolymph following the completion of sporulation. Several parasite proteases play important role in egress process. A egress cysteine protease 1 (ECP-1 or PbSERA5) is essential for sporozoite egress from oocysts. Targeted gene disruption of ECP-1 resulted in normal oocyst containing viable sporozoites that fail to egress from oocyst [187]. Disruption of the Sporozoite invasion-associated protein (SIAP-1) eliminated the ability of parasites to undertake gliding motility. These mutant parasites did not egress from the oocyst efficiently [188]. An aspartic protease Plasmepsin-VIII (PM-VIII) deletion showed defect in sporozoite egress from oocysts with impaired gliding motility [189]. Lastly, TRP1, a member of the TRAP family, has also been implicated in sporozoite egress from the oocyst. The TRP depleted parasites were not able to egress from oocysts [190]. Thousands of sporozoites which are liberated into the hemolymph migrate to the salivary gland by gliding motility, where they remain lodged in salivary gland lobes until inoculated into the vertebrate host through mosquito bite [166, 191, 192].

1.4.4.4 Salivary gland recognition and invasion by sporozoites

The salivary glands of mosquitos are a paired organ, with one medial and two lateral lobes in each half. When sporozoites are liberated from the oocyst, they travel through the haemocoel by hemolymph flow [166]. Despite the fact that sporozoites can infect any mosquito organ, they prefer to adhere to the distal parts of the salivary gland lobes [191, 193, 194]. *In vitro* studies using low-light video microscopy revealed that a chemotactic attraction may have a role in recognition of salivary glands. Since sporozoites selectively glide towards unheated salivary gland extracts, but randomly to other mosquito organs or towards extracts of salivary gland that is heat inactivated at 56°C for

30 minutes. Other independent studies also provide evidence that antibodies against salivary gland proteins inhibit parasites from invading the salivary glands [195, 196] supporting the idea of receptor mediated recognition. Touray et al. [197] revealed that following residence of sporozoites in salivary glands, they lose their capacity to reinvade the glands, implying a temporal expression of specific ligand on the surface of hemolymph sporozoites, committing its attachment to the basal lamina of the salivary glands.

The attached sporozoites travel through the secretory acinar cells to reach the salivary gland duct. Invasion and transmigration via acinar cells are thought to take place in transient vacuoles formed by invagination of acinar cell membrane [191]. However, the nature and molecular make up of such transitory vacuoles are unknown. Several proteins have been identified that aid sporozoite attachment to salivary glands. CSP is a most abundantly expressed sporozoite protein that has been extensively studied and spans its membrane uniformly [170, 173, 193, 198]. Peptides corresponding to CSP N-terminus (Region I) have been demonstrated to bind preferentially to the distal medial and lateral lobes of salivary glands [199]. Furthermore, *P. berghei* mutant parasites that that carry copy of *P. gallinaceum* CSP showed a defect in penetration of salivary glands [200]. Additionally, it has been also demonstrated that antibodies against CSP reduce sporozoite invasion of salivary glands [201, 202]. The TRAP is another parasite protein required for attachment and salivary glands invasion. TRAP is also required for gliding motility of sporozoite. TRAP null mutant parasites could not invade the salivary glands [27]. Mutations on the extracellular region of TRAP revealed that these regions are important for attachment and invasion of salivary glands [35, 203]. These domains, which serve as a connection between the transmembrane protein and the actin-myosin motor, are also involved in hepatocyte invasion [35, 203, 204]. TRAP is expressed in the secretory organelle of parasites called micronemes. The expression starts in the oocyst and becomes more prominent sporozoite stages. TRAP is also expressesd during the asexual stage of the life cycle [203, 205, 206].

Several reverse genetics studies have identified several proteins that are involved in gliding motility and salivary gland invasion. The rhoptry neck protein 2 (RON2) is RON2 has a n important role in salivary gland invasion as RON2-deficient parasites did not efficiently invade the salivary glands [207]. MAEBL proteins are expressed in all sporozoite forms and required for salivary gland invasion. MAEBL-deficient *P. berghei* sporozoites could not attach to basal lamina of salivary glands [208]. Deletion of PCRMP

(Cysteine Repeat Modular Proteins) 1 and 2 revealed that these proteins are required for salivary gland invasion. PCRMP1$^-$ or 2$^-$ parasites produced the same number of sporozoites as the wild type however, none of these spozozoites were detected inside or attached to the salivary gland showing an inability to recognise and invade the salivary glands [209]. Another protein UOS3, also known as TRAP-related protein (TREP), and S6 have TRAP-like domains. Disruption studies of UOS3 in *P. berghei* or *P. yoelii* revealed reduction in sporozoite numbers found in salivary glands, indicating that these parasites were unable to invade salivary glands [210-212]. Deletion of LIMP protein in *P. berghei* resulted in severely impaired gliding motility of sporozoites as well as showed significant reduction in their salivary gland invasion [213].

1.4.4.5 Sporozoite maturation

Plasmodium parasite development in the mosquito vector completes when sporozoites reach the salivary gland ducts. While waiting to be transmitted to a vertebrate host, sporozoites go through maturation process that allows them to migrate and infect a wide range of cells in the mammalian host. Generation of transgenic fluorescent sporozoites aided the analysis of early events during mammalian host infection using live cell imaging approaches [5, 214-217]. Initial studies showed that the salivary gland sporozoites are programmed in irreversibly manner to infect the vertebrate host [197]. Salivary gland sporozoites exhibit gliding motility and are highly infectious *in vivo* and *in vitro*, whereas oocyst sporozoites are not [18]. These preliminary data show that sporozoites in the salivary glands differ from oocyst sporozoites [218]. During their salivary gland invasion, sporozoites are thought to develop competence for natural transmission. Two translational repression processes have recently been discovered to be functional in maturation of sporozoites [219]. This study showed that different transcriptional repertoires are linked with various distinct sporozoite phenotypes. Functional characterization of UIS genes revealed that they encode proteins that serve key functions at different phases of the pre-erythrocytic stage of *Plasmodium* life cycle. UIS3 and UIS4 encode two transmembrane proteins that have been reported to be required for successful completion of liver stage development [62]. In rodent malaria model, the UIS3(-) and UIS4(-) mutant sporozoites have been found to induce complete, sterile protection against natural transmission, comparable to the radiation

attenuated sporozoites [61]. The major surface protein CSP present on the sporozoite surface serves many biological functions during pre-erythrocytic stage development. CSP processing is necessary for sporozoite gliding motility, which is essential for host cell invasion and traversal [31].

The proteolytic cleavage of CSP commences the signalling events that lead to host cell invasion [220]. CSP is also involved in the liver stage development [68]. These findings imply that transcriptional regulation is crucial for parasite development. Another study showed that after transmission of sporozoite to the mammalian host, the temperature shift causes an increase in the transcript abundance of a set of genes implicated in hepatocyte infection [221]. These functional investigations show that mature sporozoites are well-prepared to adapt to a new host environment after transmission.

.

1.5 **Clinical Manifestation of Malaria**

Malaria is a febrile disease with a 7-days or longer incubation period (The median time between sporozoite inoculation and the manifestation of the first clinical symptom). Malaria symptoms are caused by *Plasmodium* parasites development in the human RBCs. The duration of the incubation period is determined by both parasite and host factors. The parasite factors are species and strain of infecting parasite, epidemiology (parasite transmission intensity, prevalence rates, disease incidence) and the host factors are the immune status, age, genetic constitution, health, and nutritional status [222]. Incubation period with *P. falciparum* infection last for 9-14 days which is shortest while incubation period with non-*P. falciparum* infection takes longer time due to presence of hypnozoites form in liver: 12-17 days in *P. vivax*, 16-18 days in *P. ovale* and 8-40 days (longest) in *P. malariae* [223].

The clinical symptom of malaria appears similar to flu-syndrome during the erythrocytic stages of the malaria parasite and common in all *Plasmodium spp.* In the erythrocytic stage cycle, disease symptoms appear when RBCs lyse and release daughter merozoites and toxins (hemozoin) into the blood, initiating host defensive responses. The host immune response further triggers cytokine release and stimulates the production of reactive nitrogen species to clear asexual and sexual parasite forms except for rings as they are heat resistant [224, 225]. Each asexual erythrocytic cycle lasts around 48 hours

for *P. falciparum*, *P. ovale*, and *P. vivax* whereas it takes 72 hours in *P. malariae*. After each cycle, the host has symptoms such as fever (hallmark of malaria), chills, dizziness, headache, body aches, and perspiration. Infection with *P. falciparum* can result in severe or complicated malaria if left untreated resulting in conditions like severe anaemia, cerebral malaria, jaundice, renal failure, and hypoglycemia [226, 227].

1.6 **Diagnosis and treatment**

For nearly a century, the gold standard for malaria diagnosis has been analysing Giemsa-stained blood smears under the light microscope to identify the malaria parasite. However, accurate diagnosis needs the necessary expertise, or else it can lead to misdiagnosis. Microscopy identification is time-consuming and inappropriate for high throughput applications and determining species at low parasitemia and detection of mixed infections. Several other methods of malaria diagnosis have been developed recently which include Rapid Diagnostic Tests (RDTs), Serological tests [228, 229]. RDTs are easy to use, provide fast results, and are more affordable. All RDTs work by detecting malaria antigen in human blood such as histidine rich protein II (HRP-II) and lactate dehydrogenase (pLDH) or aldolase through immune-chromatographic detection [230]. RDT kits are suitable for diagnosis of both *P. vivax* and *P. falciparum* malaria effectively and rapidly. Serological tests are also based on principle antigen antibody interaction. This test detects antibodies against parasites by using enzyme-linked immunosorbent assay (ELISA) [231, 232]. These tests measure prior exposure rather than detecting current infection. Traditional laboratory diagnostic procedures are effective, but they have significant disadvantages. It is necessary to develop novel procedures with high sensitivity and specificity while avoiding subjective variation. Recent advances in molecular biological technologies, such as polymerase chain reaction (PCR), microarray, flow cytometric (FCM) assay techniques, mass spectrometry (MS), and loop-mediated isothermal amplification (LAMP), have contributed to effective malaria diagnostic strategies.

The major goal to treat malaria is to control transmission to other healthy individuals, minimise infection reservoirs and stop emergence and spread of antimalarial resistance. Antimalarial treatment is only given to patients who have had a

parasitological diagnosis confirmed by microscopy or RDT. There are number of antimalarial therapeutic alternatives available today. The therapeutic and treatment choice are determined by a several parameters including *Plasmodium* strain, drug efficacy, availability, low cost, and geographical region, which may contain drug resistant species [233]. The majority of drugs used in treatment of malaria are active against the blood stages of parasite, and these include chloroquine, mefloquine, sulfadoxine, pyrimethamine, artemisinin, etc. Drugs like chloroquine, mefloquine inhibit the crystallization of hemozoin (insoluble crystalline form heme) within the food vacuole of blood stage parasite, thus killing parasite by accumulating toxic free heme produced by haemoglobin degradation [115]. Primaquine is efficient against hypnozoites and a small number of gametocytes. Primaquine metabolites interferes with gametocyte electron transport system by causing severe oxidative damage in parasites [234]. Artemisinin and its derivatives seem to be activated by cleavage of endoperoxide bridge after interacting with heme and ferrous oxide, resulting in the formation of free radicles that kills the parasite [235]. The emergence of drug resistance is a major issue fight against malaria. Artemisinin-based combination therapies (ACT) are routinely employed in this scenario. ACTs slows the parasite multiplication rate and clear the parasites as combination drugs have various mode of action against development of parasite. Artesunate–amodiaquine, artesunate–mefloquine, artemether–lumefantrine, dihydroartemisinin–piperaquine and artesunate–sulfadoxine–pyrimethamine are currently available ACTs. Although majority of drugs are effective during asexual stage, only a few drugs target the sexual stage or gametocytes, owing to which malaria transmission is not effectively controlled.

1.7 **Malaria control measures and prophylaxis**

Control measures include vector control and inhibition of sexual stages of parasites in humans, as well as the use of mosquito repellent liquids and coils to prevent mosquito bites. Other malaria-control strategies include the use of window screens and insecticide-treated nets (ITNs). Paris green pesticide has been effective in killing both larvae and pupae that inhabit the stagnant waters- where mosquitoes prefer to lay eggs. Gambusia is a larvivorous fish that is cultivated to kill mosquito larvae. Adult mosquitoes can be

killed by indoor residual spraying (IRS) with dichlorodiphenyltrichloroethane (DDT), which opens sodium ion channels in neurons [236]. However, with the emergence of insecticide resistance in the major malaria vector species against the common insecticides, regular mosquito population monitoring and use of alternative or new insecticides has become necessary. The environmental conditions have a significant impact on malaria transmission. In endemic settings, awareness of environmental management practises, vector control, and parasite understanding aid in the fight against malaria transmission.

Even though several drugs to cure malaria are available, prophylactic vaccines are more effective due to the emergence of drug-resistant parasites. Despite decades of research, there is no commercially available and successful malaria vaccine that gives sterile and long-lasting immunity [237]. Immunisation with radiation-attenuated sporozoite elicits immunity that is protective against challenge with live infections sporozoites [238]. Over or under irradiation of sporozoites, on the other hand, results in inadequate immunity and sometimes leads to break through infection. These limitations pose logistics that are impractical to consider irradiated sporozoites as vaccines for large endemic populations. To overcome these constraints, developing effective subunit vaccines is another practically feasible approach, provided immunologically relevant epitopes are identified and their correlates of protection established. In line with this approach, the recently, RTS,S/AS01 subunit vaccines (Mosquirix) targeting the circumsporozite protein (CSP) of malaria parasite has showed promising result with ~30% reduced risk of severe malaria in newborns and young children [239]. RTS,S is a combination of hybrid protein particle and ASO1 (a multi component adjuvant). The RTS,S vaccine construct comprise central repeat (hence 'R') and C-terminal regions containing T cell epitopes (hence 'T') of circumsprozoite protein, that is fused to hepatitis B surface antigen ('S) and together called as RTS [239, 240]. The RTS is expressed in yeast with hepatitis B "S" expression cassettes, resulting in the production of S and RTS polypeptides that spontaneously co-assemble into mixed lipoprotein particles (or "RTS,S") with the CSP segment on their surface [240]. RTS,S is a first malaria vaccine which obtained regulatory approval by WHO for its widespread use among children in sub-Saharan Africa regions where *Plasmodium falciparum* transmission is moderate to high.

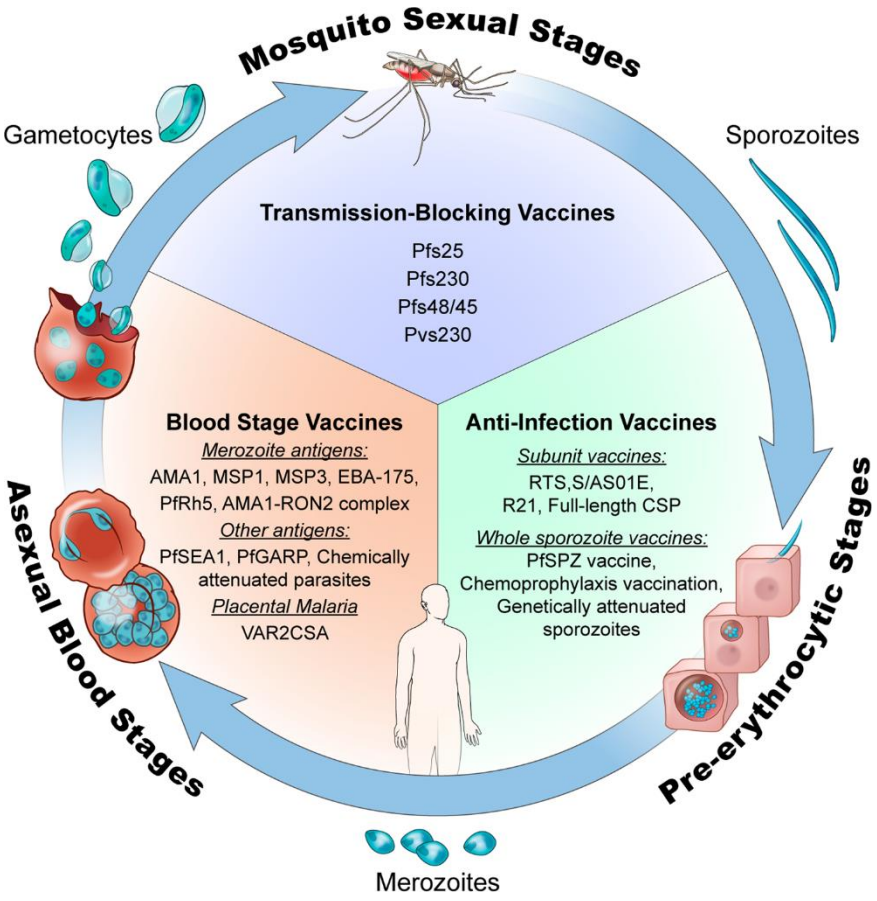


Figure 8. life cycle stages of *Plasmodium* and vaccine candidates that target respective stage. Image Source[241].

A second malaria vaccine R21 has shown 77% efficacy in phase IIb trials. R21 is a novel pre-erythrocytic vaccine candidate for malaria. R21 vaccine also encompasses the C-terminus and central repeats of circumsporozoite protein co-assembled into virus like particles in yeast. However, it lacks the excess hepatitis B surface antigen which is found in RTS,S. In clinical trials, R21 vaccine was given with two different doses of adjuvant Matrix-M (MM) to children aged 5-17 months in three dose manner in Nanoro, Burkina Faso and showed 77% efficacy. R21 is the first malaria vaccine to achieve that will be beyond the World Health Organization's (WHO) aim of 75% efficacy against the deadly disease. A larger Phase III trial including 4,800 infants aged 5 to 36 months in four countries is now ongoing [242]. Owing to their lower efficacy there is pressing need to develop effective vaccines to combat malaria. Current malaria vaccine development efforts include a variety of strategies aimed at targeting different stages of parasite

development: pre-erythrocytic vaccines- prevention of disease, blood-stage vaccines- elimination of disease, and sexual stage vaccines- transmission-blocking.

1.8 **Current challenges to achieve malaria elimination**

Malaria has been a major worldwide health problem for many years to the mankind and multi-stage life cycle of parasite poses a significant obstacle in the fight against disease. Malaria has been successfully managed in several endemic countries, such as Sao Tome and Principe, Zambia, Gambia, Zanzibar, Rwanda, and Kenya, leading to a reduction in malaria-related mortality. The remarkable elimination of malaria in several parts of the world was mostly achieved through vector control, showing that rehabilitated efforts are needed in this field, other than existing insecticide-based strategies. However, mosquitoes are developing resistance to insecticides as a result of extensive usage across many endemic countries. Emergence of resistance against artemisinin drug have been reported in five countries like Thailand, Vietnam, Cambodia, Laos and Myanmar [243]. Despite the availability of combination therapy, the emergence of resistance against anti-malarial drug remains a constant threat. Malaria is also being transmitted by travellers who move from drug-resistant areas to other places where the disease has been eradicated. For transmission blocking strategies, development of therapeutics that kills mature gametocytes is required as these stages are resilient to anti-malarial treatments due to their lower metabolic activity. Only Pfs25 and Pfs28, which are surface antigens expressed on zygote and ookinete stage of parasite, are employed in transmission blocking vaccines [244, 245]. Recombinant Pfs25 was highly immunogenic after being conjugated with EPA (Pseudomonas aeruginosa exoprotein A) adjuvant, resulting in transmission blocking immunity [246]. Many of the parasite proteins that have yet to be characterized may play a major role in disease dissemination and parasite development, making them potential novel therapeutic targets for effective vaccine development. More research into the parasite biology is required for the development of new drugs and vaccines required to prevent and cure malaria.

1.9 *Plasmodium berghei* as model

The study of malaria parasite and its complex interactions with both human and mosquito host has been extremely challenging. In malaria research, development of a continuous *in-vitro* culture for *P. falciparum* has been a pivotal event (Jensen & Trager, 1978). It has enabled research into several aspects of parasite biology, leading to key breakthroughs that have unveiled the details of cellular and molecular biology of the parasite. However, these laboratory culture conditions have its own limitation to study malaria parasite such as limited access to human tissue samples, inability to explore all life cycle stages of parasite or study host pathogen interactions and slow accumulation of adaptations within laboratory stains of parasite [247]. Model malaria parasites have been used to overcome these challenges, providing unique insights into development of parasite and its interactions with mosquito vector and mammalian hosts. They have improved our the understanding of mosquito and liver-stage biology particularly by making it more tractable. Model malaria parasites developed in controlled laboratory conditions allow for extensive *in vitro* and *in vivo* studies at various life cycle stages of parasite. The rodent malaria system has been a useful model also for its ease of handling and breeding. There are several naturally occurring rodent malaria species like *Plasmodium berghei*, *Plasmodium yoelii*, *Plasmodium vinckei* and *Plasmodium chabaudi* well adapted for laboratory use [248].

Plasmodium berghei is employed as a model organism in our laboratory. *Plasmodium berghei*, which was first identified from African thicket rats, is one of the most widely used rodent malaria parasite model. It allows study of synchronized asexual blood stage development, gametocyte formation, subsequent mosquito stages and *in vivo* development in mammalian host [249], an advantage that can overcome ethical considerations inherent to *P. falciparum* line. Comparative genomic analyses have showed that *P. falciparum* and *P. berghei* have a high degree of conservation (almost 80%) [250-252]. *P. berghei* parasites are more suitable for vaccine and drug development since they can be genetically modified using standard genetic engineering tools such as single crossover or double crossover homologous recombination, promoter swap approach, and conditional silencing at sporozoite stages. These tools can be used to investigate the gene function at a particular stage of the life cycle. This organism is more tractable due to

the availability of reporter parasite lines such as GFP, mCherry, luciferase, and gametocyte defective lines.

Chapter 2. Functional investigation of a conserved *Plasmodium berghei* hypothetical gene *PBANKA_1422900* by reverse genetics

2.1 Introduction

The life cycle of *Plasmodium* in mammalian host starts with the bite of a female *Anopheles* mosquito that delivers sporozoites in the skin of the vertebrate host [253]. The sporozoites make their way to the liver, where they transform into exo-erythrocytic forms. Following exo-erythrocytic schizogony, the first generation merozoites are packaged in a membrane bound structure called merosomes [82] that are extruded into sinusoids. Rupture of merosome releases parasites into the blood stream, that initiates an erythrocytic cycle. In RBC, the parasites replicate asexually and go through a series of transformations resulting in rings, trophozoites, schizonts and gametocytes.

Gametocytes are the sexual forms and the terminal stages of parasite in the mammalian host. These forms enter the gut of a female *Anopheles* mosquito during a blood meal. Sexual reproduction occurs in the lumen of gut, resulting in a zygote that transforms into a motile ookinete. The ookinete breaches the midgut epithelium and settles on the haemocoel side of the gut and further develops into oocyst. Sporozoites developing within the oocyst, upon maturation are released into the hemocoel that make their way to the salivary glands and infect a new host when these mosquitoes take a blood meal [254].

Sporozoites are eukaryotic cells that are delimited by a trilamellar pellicle consisting of plasma membrane and two closely opposed inner membranes called inner membrane complex (IMC) [163]. The sporozoites move using a substrate dependent motility called gliding motility [34], - a cell movement that is dependent on coordinated and well-orchestrated interaction between a macromolecular complex,-the glideosome, actin, a glideosome associated protein and transmembrane proteins [255]. Glideosome is a molecular complex whose core consists of Myosin A (MyoA), that belongs to class XIV and mainly functions in regulating gliding motility and host cell invasion [160, 256, 257]. Structurally, the MyoA lacks a tail domain, but its neck region binds two light chains- a myosin tail domain interacting protein (MTIP) and an essential light chain [258, 259]. MTIP links MyoA to the glideosome and the inner membrane complex. Post translational modifications leads to assembly of molecular complex following Ca^{2+} signaling and the energy required for sporozoite movement is likely produced by the relocation of glycolytic enzymes in close proximity of the glideosome [255]. Below the IMC are the

microtubules, that provide mechanical support to the sporozoites [260]. The invasins bind to substratum or host cell receptors on extracellular side and to the components of actomyosin motor towards the cytoplasmic side of sporozoite using adaptors proteins, for example- glycolytic enzymes like aldolase [261]. This linkage transduces the force through the cell membrane allows continuous forward movement of sporozoites concomitant with rearward traction of parasite-substrate interactions [159].

The ability of sporozoites to move from their site of deposition, breach multiple biological barriers, attach or commit to a suitable host cell, and infect by forming a replication-competent organelle, the parasitophorous vacuole (PV) is a function of a highly organized apical complex consisting of a set of cytoskeletal structures—apical rings, microtubules and specialized secretory organelles— micronemes, rhoptries, and dense granules [260]. An arsenal of proteins, that also serve as bonafide markers, sort to these compartments and assist in mediating all the aforementioned sporozoite specific functions and is arguably the most elaborate invasion machinery in any class of pathogens. As sporozoite surface proteins interacts with hepatocytes that has immense potential for therapeutic intervention, the past decade has seen a surge in defining its complement using high through put mass spectrometry approaches [262-264]. Most noteworthy, these investigations reiterated that invasion and signalling related proteins are membrane resident [262-264], IMC components can access the extracellular side of PM and the major surface proteins of sporozoite- the CSP and TRAP bear potential glycosylation sites in their TSR (thrombospondin type 1 repeat) motif [263]. Additionally, several proteins that constitute the glideosome and others that regulate transcription and translation are phosphorylated [264]. More recently, it has been documented that during maturation in salivary glands, the sporozoites temporally regulate protein expression by two overlapping, and independent programs of translational repression [265]. This allows precise expression of genes that mediate one or more functions highly specific for oocyst egress or invasion of salivary glands and hepatocytes.

While most sporozoite membrane proteins achieve one or more functions specific to hepatocyte commitment [266, 267], motility [27, 210] and invasion [27, 268], not much is known about proteins that maintain the sporozoite shape and structure. Herein, we have selected this *PBANKA_1422900* for functional characterisation based on two important criteria: 1: *PBANKA_1422900* was one of the highly upregulated transcripts in

gametocytes, midgut sporozoites[269], and 2: protein was detected majorly in salivary gland sporozoites [219]. Alignment of amino acids sequence of *PBANKA_1422900* with rodent and human *Plasmodium* species revealed that *PBANKA_1422900* is a highly conserved protein across all the *Plasmodium* species, however, it has no orthologs or conserved functional domains in other species.

In this current study, we deleted *PBANKA_1422900* by double homologous recombination and did phenotypic characterization of *PBANKA_1422900* KO parasites across all the *Plasmodium* life cycle stages. While *PBANKA_1422900* KO parasite did not manifest any defect in asexual blood stages, sexual stages, oocyst development, and salivary gland colonization. However, *PBANKA_1422900* depletion had a dramatic effect on sporozoite morphology, suggesting that it may function to maintain sporozoite structural integrity. Owing to this function of *PBANKA_1422900,* we referred to its product as SIMP- Structural Integrity Maintenance Protein. HA tagging at the C-terminus of SIMP revealed that it is localised to the plasma membrane and the non-permeabilization assay revealed PbSIMP HA tag to be extracellular. Since C-terminus of SIMP is highly conserved amongst *Plasmodium* species, these findings have important implications for utilising SIMP as a novel sporozoite specific vaccine candidate.

2.2 Materials and methods

2.2.1 Experimental animals and parasite lines

Six to eight weeks old female BALB/c, Swiss albino, or C57BL/6 mice were purchased from National Institute of Nutrition (NIN), Hyderabad, India and used for all animal experiments. All animal experiments were approved by Institutional Animal Ethical Committee and were in accordance with the CPCSEA guidelines. *Plasmodium* cycles were initiated by asexual propagation of WT GFP, *PbSIMP* KO line, *PbSIMP* complemented line and *Pb*SIMP 3XHA tagged line in Swiss Albino mice or BALB/c mice. To obtain the mosquito stages of *Plasmodium*, female *Anopheles* mosquitoes were allowed to obtain a blood meal from gametocyte positive mice carrying respective parasite lines. For analysis of pre-patency, C57BL/6 mice were infected with WT GFP and *PbSIMP* KO sporozoites by intravenous route.

2.2.2 Cell lines

HepG2 cell lines were procured from National Centre for Cell Science (NCCS), Pune, India. Cells were maintained in complete Dulbecco's modified Eagle's medium (DMEM)(Gibco) containing 25mM HEPES, 2mM L-glutamine and 4.5g/L glucose supplemented with 10% fetal bovine serum (FBS) (Gibco), 1X antibiotic antimycotic (Gibco).

2.2.3 Bacteria

Cloning and propagation of gene targeting constructs used for *Plasmodium* transfection, were done by using *E. coli* XL-1 Blue MRF cells (Δ(mcrA)183 Δ(mcrCB-hsdSMR-mrr)173 endA1 supE44 thi-1 recA1 gyrA96 relA1 lac [F′ proAB lacIqZΔM15 Tn10 (Tetr)]).

2.2.4 Plasmids

Following plasmids were used for molecular cloning, expression, and genetic manipulation of parasites:

1.pBC-GFP-hDHFR

2. pBC-3XHA-Hdhfr

3. pTZ57R/T

2.2.5 Bioinformatics Analysis

2.2.5.1 Retrieval of PBANKA_1422900 gene and protein sequences, sequence alignment analysis, sequence similarity localization probability of PbSIMP.

DNA and protein sequences of *P. berghei* SIMP and its orthologues were retrieved from PlasmoDB (www.plasmodb.org). Primers were designed based on the sequence information provided on these databases. MULTALIN (http://multalin.toulouse.inra.fr/multalin/) tool was used to check SIMP protein homology among *P. berghei*, *P. yoelii* and *P. chabaudi* which are rodent *Plasmodium* strains, and *P. falciparum* (human strain). Primers were designed based on the sequence information provided on these databases.

2.2.5.2 Phylogenetic analysis

The nucleotide sequence of *PbSIMP* was used as query for searching homologs in NCBI. The sequences were subjected to multiple sequence alignment using MUSCLE method, and the aligned sequences were used to generate the phylogenetic trees. Care was taken to consider only those sequences that were translating in frame with reference to the standard genetic code. The phylogenetic tree was generated using the Maximum Likelihood method and General Time Reversible model. The rates of substitution were analysed using the gamma distribution model.

2.2.5.3 Prediction for *Pb*SIMP localization probability and membrane binding.

The cellular localization probability PbSIMP was estimated using Phobius 1.01 server [270]. Phobius uses a hidden Markov model (HMM) approach to calculate the localization probabilities. Protscale [271] was used to calculate the Kyte-Doolittle hydropathy plot. For Kyte-Doolittle prediction, window size 19 was used. Expasy-TMpred and DTU-TMHM 2.0 were used to predict the transmembrane nature of the protein. Expasy-TMpred is based on TMbase [272], a database for naturally occurring transmembrane proteins, while DTU-TMHM 2.0 utilizes a hidden Markov model [273] to predict the transmembrane topology. For an unbiased prediction, multiple tools were selected.

2.2.5.4 Interaction network predictions for PbSIMP

STRING (Search Tool for the Retrieval of Interacting Genes/Proteins) interactions database was used to identify possible interaction networks for *PbSIMP* [274]. Although the network does not necessarily demonstrate direct protein-protein interactions, it does show a protein relationship to others by co-evolution, co-expression, and direct interaction evidence, and other methods. This network aids in understanding the function of the protein in a larger genomic context.

2.2.6 Primers

Primers were ordered and purchased from GCC biotech oligo support. Primers used in this study for amplification of *PbSIMP* sequences for quantitative real-time PCR, generation of knock out and transgenic plasmids, and for integration and clone confirmation PCRs are described below in table (1).

S. No	Primer designation	Primer used for	Primer sequence (5' to 3' direction)	Expected product size
1.	FP1	Generation *PbSIMP* KO construct	ATACTCGAGAGCATATATGTAATAAACCCC	615bp
2	RP1		ATAATCGATGTCGACTTATCTGGAGCCTTT GCTGTC	
3	FP2		ATAGCGGCCGCGCTGTCTTATCCAGTAGA	613bp

4	RP2		ATAGGCGCGCCTCATACATACACGAGAGC	
5	FP3	Confirmation of *PbSIMP* KO by integration PCR	TTTGTTTATGACAGGTTGATTCT	892bp
6	RP3		TTCCGCAATTTGTTGTACATA	
7	FP4		GTTGTCTCTTCAATGATTCATAAATAG	1050bp
8	RP4		TTATGTATTAACACGCTTTAGA	
9	FP5	Confirmation of *PbSIMP* KO clonal lines	TCAAATTTAGCTATTACATATG	357bp
10	RP5		TTGTCCATCGAAAAGCACATAT	
11	FP6	Confirmation of *Pb*SIMP GIMO line	GACAGGTTGATTCTCACAACA	1500bp
12	RP6		AAGAAAATGAGCTCCTTGTGG	
13	FP7		TGGTTGGTTCGCTAAACTGC	3000bp
14	RP7		TTTTATGTATTAACACGCTTTAGA	
15	FP8	Confirmation of *PbSIMP* GIMO complementation	GACAGGTTGATTCTCACAACA	1000bp
16	RP8		AGGTTCTCATTTAACAAACTTAC	
17	FP9		CATGCAAAACTAAAGTGTACA	890bp
18	RP9		TTTTATGTATTAACACGCTTTAGA	
19	FP10	Generation of *PbSIMP* HA localization construct	ATAGGGCCCTCAAATTTAGCTATTACATATG	662bp
20	RP10		ATACTCGAGAGCATTTTCTACTGGATAAGA	
21	FP11		ATAGCGGCCGCAACAAACAAATCTTCATGTTTG	585bp
22	RP11		ATAGGCGCGCCTCATACATACACGAGAGC	
23	FP12	Confirmation of *PbSIMP* HA integration	TTTTGCATGCGTCAATCCTTAT	751bp
24	RP12		GATCCTTAAGCGTAATCTGGAACATCG	
25	FP13		GTTGTCTCTTCAATGATTCATAAATAG	832bp
26	RP13		TTATGTATTAACACGCTTTAGA	
27	FP14	*PbSIMP* expression analysis by real time PCR	TCAAATTTAGCTATTACATATG	148bp
28	RP14		CTAGATCCTTTGGTATGACAA	
29	FP15	*Pb18SrRNA* expression analysis by real time PCR	AGCATTAAATAAAGCGAATACATCCTTAC	134bp
30	RP15		GGAGATTGGTTTTGACGTTTATGT	
31	FP16	*Pf*SIMP C-terminus recombinant protein expression	CGCGGATCCGGAGGGAAATGGGGATTCTT	597bp
32	RP16		CCGCTCGAGTTCCTTGTCCAATGGATATGAC	
33	SM-F	Amplification of positive-negative selectable marker cassette (hDHFR:yFCU)	GTCGACGGTATCGATAAGCTTGATATCGAATTCCTGCAGCCCAGCTTAATTCTTTTC	2831bp
34	SM-R		GCGGCCGCTCTAGGTACCCGAAATTGAAGGAAAAAAC	
35	3XHA-F	Annealing of 3XHA oligos to generate double stranded DNA with overhangs compatible to ligate with DNA digested using XhoI/BglII restriction sites	TCGAGGCTAGCAGATCTTACCCATACGATGTTCCAGATTACGCTTACCCATACGATGTTCCAGATTACGCTTACCCATACGATGTTCCAGATTACGCTTAAG	
36	3XHA-R		GATCCTTAAGCGTAATCTGGAACATCGTATGGGTAAGCGTAATCTGGAACATCGTATGGGTAAGCGTAATCTGGAACATCGTATGGGTAAGATCTGCTAGCC	

2.2.7 Total RNA isolation and cDNA synthesis

To study the gene expression of *PbSIMP*, total RNA was isolated from different life cycle stages of *P. berghei*. To isolate RNA from erythrocyte stages, Swiss albino mice were infected with asexual blood stages of *P. berghei* parasites, and once parasitemia reached to 10-12%, the blood was collected in a tube from mice by cardiac puncture in heparinized DMEM complete medium. The blood cells were lysed in 0.5% saponin solution and pelleted at 10,000 rpm for 5min at 4 °C. The Saponin lysis was done 2 times to ensure all infected erythrocytes were disrupted. Following 2 washes with 1x PBS, the sample was centrifugated at 10,000 rpm for 5 min. RNA was isolated from the parasite pellet. For RNA isolation from mosquito stages of parasite, 100 *P. berghei ANKA* infected *Anopheles* mosquitos were dissected to obtain the midguts and salivary glands on day 14 and day 18 respectively. Midguts and salivary glands were collected separately in a microcentrifuge tube maintained on ice and both the tissues were then mechanically disrupted using a plastic pestle. The disrupted tissue samples were centrifuged at 800 rpm at 4 °C for 3 min. The supernatant was collected containing partially purified sporozoites and taken for RNA isolation. For RNA isolation from liver stages, HepG2 cell cultures were infected with sporozoites, and cells were pelleted by centrifugation at different time points (17h, 25h, 38h, 48h, 65h, and merosomes). RNA was extracted from all these samples by using Ambion PureLink RNA mini kit (Cat No#12183020). RNA concentration was estimated using Nanodrop 2000 (Eppendorf) using nuclease-free water as blank. To remove DNA contamination, 2µg of purified RNA was added to reaction mixture containing 1X DNase I reaction buffer, 1U of DNase in a final volume of 10µl made up with DEPC treated water in a tube. Next, The reaction mixture was incubated at RT (room temperature) for 15 min. following this treatment, DNase I was neutralized by adding 1 µl of 25nm EDTA to the mixture and heat-inactivated at 65 °C for 10 min. Afterward, the remaining RNA was either stored at -80 °C for further use or subsequently processed to cDNA. cDNA was synthesized using MuLV reverse transcriptase (Applied Biosystems). The reaction mixture consisted of the following - 1X PCR buffer, 1µl of dNTPs (2.5mM each, Invitrogen, cat # R72501), 1µl of RNase inhibitor (Applied Biosystems, cat # N8080119), 1µl of random hexamers (for short length cDNA fragments) (Applied Biosystems, cat # N8080127) or Oligo (dT) primers (for full-length cDNA), 1µl of MuLV reverse transcriptase (Applied Biosystems, cat # AM2682) and 2µg of RNA used as a template. cDNA was generated using the Eppendorf master cycler PCR machine with the following thermal cycling conditions: 25

°C for 10 min, 42 °C for 20 min, 98 °C for 5 min. finally, the cDNA was synthesized and stored in aliquots at -20 °C

2.2.8 Quantitative real-time PCR analysis of *PbSIMP* expression in all the life cycle stages of *P. berghei*

The stage-specific expression *of PbSIMP* was analysed by the absolute quantification method. cDNA from rings, mixed-blood stages, Day 14 midgut sporozoites, Day 18-20 salivary gland sporozoites, and liver stages at 17h, 25h, 38h, 48h, 65h, and mersosomes were used. Gene-specific standards were generated for *PbSIMP* and *Pb18rRNA* (used as internal control) *by* amplifying 148bp and 180bp products respectively using *P. berghei* genomic DNA and ligated into PTZ57R/T vector followed by log dilution in a range from 10^2 to 10^7 copies per µl. The cDNA samples were run alongside gene-specific standards. The target gene was expressed as gene-specific standards' equivalents. For real-time analysis, the reaction was set up in a 96 well format plate consisting of 2X SYBR green mix (Biorad, Cat No#1708882), 0.25µM gene-specific primers, cDNA samples from different stages. qRTPCR run and detection was done using Eppendorf Real-Plex 2 qPCR machine. Normalized gene expression was obtained by taking the ratio of copy number of *PbSIMP /Pb 18S rRNA* for each sample.

2.2.9 Polymerase chain reaction

Genomic DNA from *P. berghei* wild-type parasites and additional sources with template DNA were used to perform PCR to generate DNA sequences for gene expression analysis, parasite genotyping, molecular cloning, and sequencing. The basic principle of this method is based on the ability of thermostable DNA polymerase to synthesize short fragments of single-stranded DNA complementary to target sequences using specific primers and deoxynucleotide triphosphates (dNTPs). Sequence specific primers were designed with 5'extensions including restriction sites to do molecular cloning. Taq DNA polymerase was used for analytical PCRs and iProof high fidelity DNA polymerase (Cat #1725301) was used for preparative PCRs.

Standard PCR reaction

1. 1x reaction buffer
2. 1.5 mM of Mgcl2
3. 200 µM of dNTPs
4. 0.2 µM of each primer
5. 10-50 ng of template DNA
6. 1 unit of DNA polymerase
7. Nuclease-free water

Standard PCR program

1. Initial denaturation	94 °C, 5 min
2. Denaturation	94 °C, 30 sec
3. Primer annealing	54 to 60 °C, 30 sec
4. Extension	72 °C, 30 sec to 3 min
5. Repetition of steps 2-4	30-35 cycles
6. Final extension	72 °C, 10 min
7. Hold	4 °C

2.2.10 Agarose gel electrophoresis

The agarose gel electrophoresis was employed to resolve, separate, and purify the DNA based on its size, charge, and conformation. DNA molecule is negatively charged owing to the presence of phosphate backbone, hence when DNA fragments are exposed to an electric field, they migrate towards positively charged anode. The migration rate depends on the size and conformation of DNA fragments. For standard analysis, 0.8-1% agarose gel was prepared by adding agarose (Lonza, Cat No# 50004) in 1X TAE buffer (Tris base, Acetic acid, and EDTA). The mixture was boiled in the microwave until the agarose was melted and allowed to cool down around 50-60 °C before adding ethidium bromide (EtBr) (0.5 µg/ml). This solution was loaded into a tray and immediately a comb was placed in the tray to make wells in the gel and was allowed to solidify. The DNA samples were mixed with 6XDNA loading dye along with 1kb DNA ladder (Thermo Scientific, Cat No# SM0333) and separated by 100-150 V for 1hr in 1XTAE running buffer. Later, the separated DNA fragments in agarose gel were visualized using a gel documentation system with Ultraviolet light (UV) illuminator.

2.2.11 Preparation of *Escherichia coli (E. coli) XL1 Blue MRF* competent cells by calcium chloride treatment and Transformation.

The ability of bacterial cells to transform or take up exogenous DNA is called competence. In some bacterial species, natural competence exists but most of the

laboratory bacterial strains do not possess natural competence. The bacterial cells must be made competent to take up the exogenous DNA. This competence can be artificially induced by chemical treatment. Competent cells with chemical induction are regularly used in cloning processes to produce recombinant DNA or proteins. Briefly, a frozen glycerol stock of XL-1 Blue MRF was inoculated in 10ml LB broth containing tetracycline antibiotic (Sigma, Cat no #87128) and incubated overnight at 37 °C in a incubator with 200 rpm. The following day, 20 ml of fresh LB broth having tetracycline was inoculated with 200µl of overnight bacterial culture and incubated for 2-3 hr till the optical density (OD_{650}) reached 0.4-0.5. After this, the bacterial culture was kept on ice for 30 min, which was followed by centrifugation at 6000 RPM for 10 min and supernatant was discarded. The pellet was resuspended in 10 ml of ice cold 0.1 M $CaCl_2$ and placed on ice for 1hr. Following incubation, the bacterial cells were centrifuged and pelleted at 6000rpm for 10 min. Finally, the pellet was resuspended in 3-4 ml of ice cold 13% glycerol in 0.1mM $CaCl_2$ and approximately 50 µl was aliquoted into 1.5 ml microcentrifuge tubes and stored in -80 °C (pre-treated with liquid nitrogen) for long term usage. These competent cells were further used for the transformation of ligation products or plasmids to produce large DNA quantities.

For transformation, a frozen vial of competent XL-1 blue cells was taken out and thawed on ice. Approximately 5-10 µl of ligation mixture or 50-100ng of plasmid was added to competent cells and stirred gently by a pipette tip. The mixture was immediately kept on ice for 20 min incubation and given heat shock at 42°C for 90 seconds for DNA uptake, followed by incubation for 3-5 mins on ice. Then, 1 ml of LB broth was added to the cells and incubated for 1hr at 37 °C in a shaker incubator. Following incubation, the cells were centrifuged at 5000 rpm for 5 min and supernatant was discarded. Next, The pellet was resuspended in 100 µl LB broth and plated onto the LB agar plate containing right antibiotics. The bacterial plates were incubated overnight at 37 °C in an upright position to obtain transformed bacteria in single recombinant colonies.

2.2.12 Plasmid isolation from *E. coli*

The bacterial colony was picked and inoculated in 5-10 ml of LB broth with right antibiotics and incubated for overnight at 37 °C. The following day, the culture was centrifuged at 5000 rpm for 5min, the supernatant was discarded, and pellet was

collected. From the bacterial pellet, the plasmid was isolated using Gene Jet Plasmid Miniprep Kit (Thermo Scientific, Cat No #K0503) according to manufacturer's protocol. In brief, the pellet was resuspended in 250 µl of resuspension buffer and lysed with 250 µl of lysis buffer, followed by adding of 350 µl of neutralization buffer. This solution was mixed well and centrifuged for 10 min at 13000 rpm. The supernatant was loaded into a Gene Jet spin column and centrifuged at 13000 rpm for 1 min. The column was washed twice with 650 µl of wash buffer by centrifuging at 13000 rpm for 1 min. Finally, plasmid DNA was eluted in 35 µl of elution buffer. The plasmid concentration was estimated using Nanodrop and stored at -20 °C for further use.

The largescale plasmid preparations of the *Plasmodium* targeting construct used for electroporation were obtained using the Pure link Hipure plasmid filter maxiprep kit (Invitrogen Cat No#K210016). A detailed description of plasmid isolation procedure is given in the user manual. The plasmid concentration was estimated using Nanodrop and stored at -20°C for further use.

2.2.13 Generation of *PbSIMP (PBANKA_1422900)* knockout construct

2.2.13.1 PCR

PbSIMP knockout (KO) parasites were generated by double homologous recombination method by replacing the endogenous locus with KO construct [275]. To achieve this, pBC-GFP-hDHFR vector was used to generate *PbSIMP* targeting construct. Genomic DNA from *P. berghei* ANKA was used as a template to amplify 615 bp of 5' UTR of *PbSIMP* using *PbSIMP* 5' forward primer (FP1) and *PbSIMP* 5' reverse primer (RP1). A 613bp of 3' UTR of *PbSIMP* was also amplified using *PbSIMP* 3' forward primer (FP2) and *PbSIMP* 3' reverse primer (RP2) (primer sequences provided in table 1). To amplify 5' and 3' fragments of *PbSIMP*, 100µl PCR mix was prepared by adding 1X PCR buffer, 5mM MgCl2, 1mM dNTP mix (Thermo Scientific, Cat No #R72501), 0.25µM FP, 0.25µM RP, 3 units of Taq DNA polymerase (Thermo Scientific, Cat No #11615010) and 50ng genomic DNA and volume was made up to 100µl with nuclease-free water. The reaction mix was kept in a thermal cycler with conditions were as follows: Initial denaturation at 94 °C for 5min for and 94 °C for 30 sec, annealing at 54 °C for 30 sec followed by extension at 72 °C for 1 min. The PCR cycles were repeated 35 times except for initial denaturation with a

final extension at 72 °C for 10 min. After completion of PCR, 2-5µl of amplified product was visualized on 1% agarose gel using UV illuminator that revealed the expected amplicon size. Amplified PCR products were purified by using DNA clean-up and gel extraction kit (Invitrogen, Cat No- K2200-01). The concentration of purified DNA was measured by Nanodrop 2000.

2.2.13.2 Cloning of 5' flanking region of PbSIMP

PCR amplified 5' UTR was purified, and the concentration was quantified by using Nanodrop 2000. 5' amplified product was cloned into pBC-GFP-hDHFR vector. pBC-GFP-hDHFR vector was a generous gift given by Dr. Robert Menard from Pasteur Institute, France. This vector contains two multiple cloning sites (MCS). Location of MCS1 is upstream to the GFP cassette where GFP ORF is flanked with HSP70 promoter and 3'UTR and MCS2 is located downstream of hDHFR cassette where hDHFR ORF is flanked with EF1α promoter and PBDHFR/TS 3' UTR. For cloning of purified 5' part, sample was prepared for double digestion by mixing 3 µL of fast digest buffer (Thermo scientific), 1U of XhoI,1U of ClaI restriction enzymes (MCS1), 1-2 µg of PCR product, and the reaction mix was made up to 30 µL in volume with nuclease-free water. The sample mix was incubated for 3-4hr at 37 °C. Approximately, 2µg of pBC-GFP-hDHFR vector was also digested using the same XhoI and ClaI restriction enzymes and incubated for 3-4hr at 37 °C. After digestion, samples were PCR purified using Gene JET Gel extraction and DNA clean-up Kit (Thermo scientific Cat No #K0831) and the concentration of both digested vector and the PCR product was measured by Nanodrop 2000. Next, Ligation was set up by mixing 1X ligation buffer, purified vector and insert in 1:3 ratio in concentration, 1U of DNA T4 ligase (Thermo scientific) and made up to 20 µl in volume with nuclease-free water. The ligation mixture was kept for incubation at 22 °C for 3 hr and transformed into XL-1 blue MRF competent cells subsequently. After transformation, cells were plated on LB agar plate having (HIMEDIA, Cat N0# CMS218) and tetracycline (Sigma, Cat No# 87128) antibiotics, and incubated at 37°C for overnight. The following day, nearly 10 bacterial colonies were picked and inoculated in fresh LB broth, and colony PCR was performed to screen the positive clones having the insert. After preliminary confirmations, the plasmid was isolated from the positive colony by GeneJET Plasmid Miniprep Kit (Thermo Scientific, Cat No# K0502) and confirmed the presence of 5'

flanking part using restriction double digestion with XhoI and ClaI. Finally, this cloning yielded pBC-GFP-hDHFR-*PbSIMP* KO 5' plasmid.

2.2.13.3 Cloning of 3' flanking region of PbSIMP

Similar to that of 5' flanking region cloning, PCR amplified 3' flanking part was cloned into pBC-GFP-hDHFR-*PbSIMP* KO 5' plasmid using AscI and NotI restriction enzymes that resulted in *PbSIMP* knockout plasmid. Sequencing was done for both 5' and 3' fragments.

2.2.13.4 Release of PbSIMP targeting cassette from knockout plasmid by double restriction Digestion

After the sequence confirmation, *PbSIMP* knockout plasmid was isolated on large scale by Pure link HI pure plasmid filter maxiprep kit (Invitrogen Cat No#K210016) and double digested with XhoI and AscI enzymes to release the targeting cassette consisting of GFP-hDHFR flanked on either side with *PbSIMP* 5' and 3' flanking regions. The gene targeting cassette was gel excised and purified using Gene JET Gel extraction and DNA clean-up Kit (Thermo scientific Cat No #K0831) and concentration was measured by Nanodrop 2000. The digested and purified product was used for transfection to generate *PbSIMP* knockout parasites.

2.2.14 Propagation of *P. berghei ANKA* WT parasite in Swiss Albino mice and Giemsa staining for determination of parasitemia

The *P. berghei ANKA* WT parasites were freshly thawed and intraperitoneally injected into one Swiss albino mouse. The parasitemia was observed by making blood smears by venepuncture of mice tail. The smear was air-dried and fixed in methanol for 5-10 sec. Once methanol was evaporated, smears were stained with 20% Giemsa stain (Sigma, Cat No# GS1L) (v/v in water) for 10 min. The smears were washed with running water and were allowed to air dry. The Giemsa stained blood smears were observed in immersion oil under a light microscope with a 100x objective lens (Nikon). Parasite

stages were observed and identified in infected RBC by their unique morphology. A minimum of 20-25 uniform thin fields were counted which were having approximately 300 RBC and final parasitemia was calculated by the below formula-
Parasitaemia % = sum of infected RBCs / (sum of RBCs per field x sum of counted fields).

2.2.15 In vitro culture of *P. berghei ANKA* asexual stages

Short-term *In vitro* culture of *P. berghei ANKA* blood stages, purification of schizonts, transfection of purified schizonts, and selection of recombinant parasites were followed as described previously [275]. Swiss albino mice were infected with intraperitoneal injection of cryopreserved *P. berghei* ANKA parasites. When parasitemia reached about 1%, blood was collected and passaged to another four donor mice intravenously (i.v.). Donor Mice having 3-5% parasitaemia, and low gametocyte density were anesthetized by ketamine (50mg/ml)/xylazine (20mg/ml) mix. Blood was collected from all four anesthetized mice by cardiac puncture using heparin treated syringes into a 50ml tube containing 0.25ml of 200U/ml Heparin (Sigma, Cat# H3393). After collection, the blood was washed with 10 ml of pre-warmed schizont culture media [RPMI (Lonza BioWhittaker, Cat No# 12-115F) with 20% FBS (Hyclone, Cat No# SH30071.03) and 3.5ml gentamicin (Sigma, Cat No# G1397) for 500ml of media] and RBCs were pelleted down by centrifugation at 200g in a swinging bucket rotor without brake for 8 min at RT. The blood pellet was resuspended in 5ml of pre-warmed schizont culture media and equally distributed into three unvented T75 cell culture flasks (Nunc, Cat No# 156472) containing 20ml of culture media. The T75 flasks were gently aerated with mixture of gas (5% CO2, 5% O2, 90% N2) for 3 min and subsequently incubated at 36.5 °C for 16-18hr with gentle shaking at 40-50rpm in a shaker incubator. During the overnight schizont culture, most of the blood stages transform into schizonts. Following day morning, the quality and quantity of schizonts were measured by making and observing a Giemsa-stained blood smear. The schematic outline of the transfection protocol is shown in Figure 10.

2.2.16 Isolation and purification of schizonts

The mature schizonts were purified using density gradient centrifugation using 60% Nycodenz. Nycodenz was prepared by mixing 27.6g Histodenz powder (Sigma, Cat No #D2158), 300µl of 3Mm KCL, 500 µl of 5mM Tris-HCL, 60 µl of 0.5 mM EDTA and final volume was made up to 100µl with double distilled water. This mixture was autoclaved and stored at 4 °C. 60% Nycodenz was prepared in PBS and warmed for 30 min at 37°C. The schizont culture from T75 flasks was carefully transferred into 50ml falcon tubes, 25ml each tube, and 10ml of 60% nycodenz solution was added gently under the culture suspension. The culture suspension was centrifuged at 380g for 20min at room temperature in a swinging bucket rotor without brake. Mature schizonts were collected from the interface ring between media and pellet with a Pasteur pipette (Fisher Scientific, Cat#13-678). Schizonts were pelleted and washed with 10ml of culture media 2 times by centrifugation at 1500 rpm for 7 min The supernatant was discarded and the schizont pellet was taken for electroporation.

2.2.17 Transfection of *PbSIMP* knockout construct into purified schizonts

PbSIMP KO construct was electroporated in purified schizonts using the Amaxa nucleofector kit (Lonza). For electroporation, nucleofector solution was prepared by mixing 90 µL of mouse T- cell nucleofector solution with 20 µL of supplement and 10 µg of purified *PbSIMP* KO construct. The purified schizont pellet was resuspended in DNA/nucleofector solution. This solution was transferred into a nucleofector cuvette and kept in Amaxa nucleofector device. Electroporation was performed using program U033 (Figure 10). Following electroporation, 100 µL of schizont media was added to the cuvette, transferred to a tube and finally transfected parasites were immediately injected intravenously into Swiss albino mice.

2.2.18 Drug selection of recombinant parasites

After 24 hours of transfection, the parasitemia was observed on Giemsa-stained blood smears made from mice injected with transfected parasites. After confirmation of parasites, mice were orally administered with pyrimethamine drug which was prepared

at 7mg/100ml. While mice were under drug pressure to select recombinant parasites, parasitemia was monitored daily for a period of 5-7 days by making Giemsa-stained blood smears. Initially, parasitemia was deceased gradually, and non-transfected parasites were cleared in blood. The drug-resistant population started to appear after 7 days and parasitemia increased gradually. Following drug selection, the recombinant parasites were collected from mice by retro-orbital bleeding and cryopreserved. From some blood, genomic DNA was isolated to perform genotyping of recombinant parasites. Two independent transfections were done for using *PbSIMP* KO targeting construct.

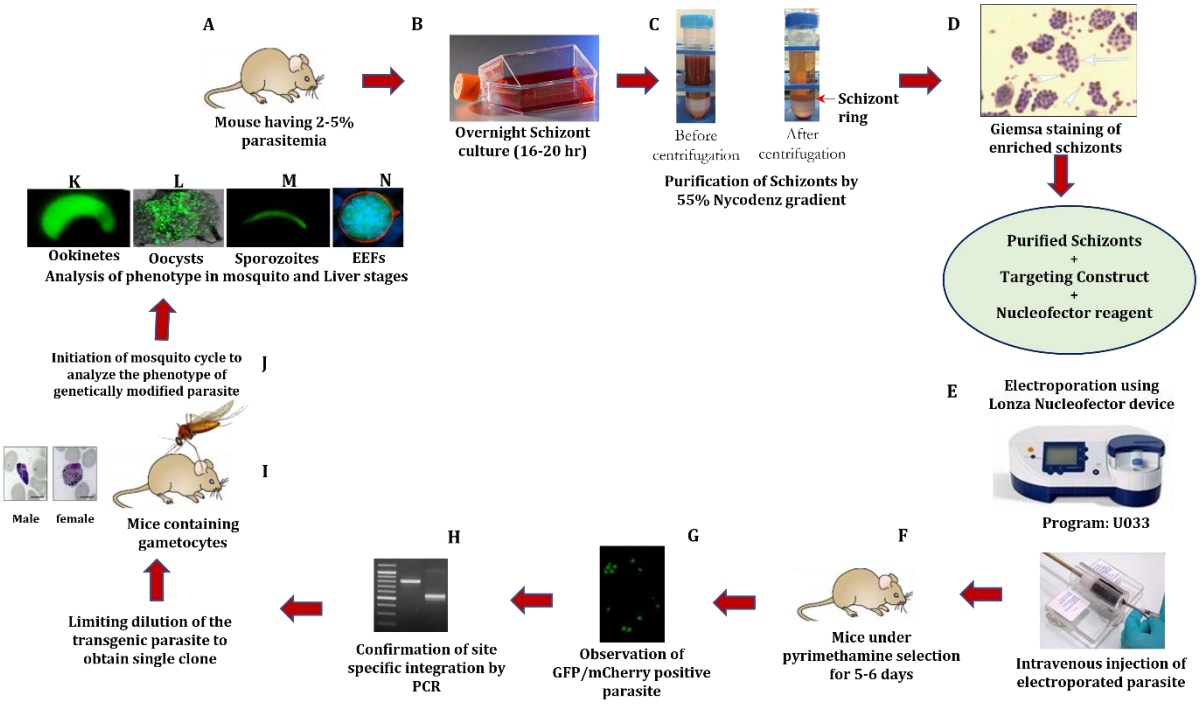


Figure 10. Schematic diagram showing *P. berghei* transfection procedure, drug selection of recombinant parasites, confirmation of target construct site-specific integration and phenotypic characterization of genetically modified parasites. A) Blood was collected from *P. berghei* parasite infected mice having 2-5% parasitemia**. B)** and an in vitro schizont culture was set up overnight. **C)** Next day, the schizonts were enriched by density gradient centrifugation using 60% Nycodenz solution. **D)** Purified schizonts were collected, confirmed by Giemsa staining, and **E)** electroporated with the targeting cassette and transfection mixture using Amexa nucleofector device and immediately intravenously injected into mouse. The mouse was kept on pyrimethamine drug which was administered orally in water for the selection of transfectants. F) following 7 days of drug selection, the parasites were observed for GFP/mCherry fluorescence. G) Genomic DNA of drug-resistant parasites was isolated and correct site-specific integration was confirmed by Diagnostic PCR. H) Limiting dilution was done to obtain single clonal population of successful transfectants and these single clone parasites were injected into mice and

subsequently transmitted to mosquitoes to observe phenotype in stages like K) ookinete, L) oocyst, M) sporozoite, and N) liver stages in the vertebrate host. Images adapted and modified from Janse et al, 2006.

2.2.19 Observation of GFP parasites in the infected blood

When the parasitemia reached to 3-5%, 10µl of blood was collected from infected mice tail by caudal vein puncture and placed in a 1.5 ml microcentrifuge tube having 2U of heparin. The blood was washed with 1XPBS, and the pellet was collected by centrifugation at high speed for 5 sec. The pellet was resuspended in 10µl of 1XPBS and from this 5µl was added on a glass slide and then was covered by a coverslip. The coverslip was sealed with a transparent nail polish and slide were taken to observe GFP fluorescence under a fluorescent microscope (Nikon Eclipse).

2.2.20 Cryopreservation of the *P. berghei* blood-stage parasites

After observing of the GFP parasites in infected blood, the blood was collected in freezing medium containing heparin (10U/ml). The freezing medium was prepared by mixing 9ml of Alsever's solution (Sigma, Cat# A3551) and 1ml of glycerol (Invitrogen, Cat# 15514011). For cryopreservation, two-part of the freezing medium was added to one part of infected blood. After gentle mixing, 250 µL of the mixture of blood and cryopreservative was aliquoted into cryo-vials (Corning, Cat No# CLS430658). The vials were transferred to -20 °C and -80 °C subsequently to allow gradual cooling. After 24h, the vials were stored in liquid nitrogen container for long-term preservation.

2.2.21 Isolation of parasites from infected blood

Approximately, 300 µl of blood was collected from infected mice in a 1.5 ml microcentrifuge tube containing heparin. Blood was centrifuged at 5000 rpm for 8 min at room temperature. The RBC pellet was washed two times in 1X PBS and centrifuged at 5000 rpm for 8 min. The blood pellet was lysed using 300 µl of 0.05% saponin (Sigma, Cat# 47036) (prepared in 1XPBS). The pellet was resuspended and centrifuged at 5000rpm for 8 min. Saponin lysis was repeated two times. After saponin lysis, the parasite pellet was washed twice with 300 µl of 1X PBS by resuspension and centrifugation at 5000 rpm for 8 min. Finally, the supernatant was discarded, and the

parasite pellet was subsequently processed for genomic DNA isolation, RNA isolation, or for making protein lysates.

2.2.22 Genomic DNA isolation from blood-stage parasites

Genomic DNA was extracted from blood stage parasites for genotyping of transfected or clonal lines of parasites and other molecular biology applications such as insert/gene amplification, restriction digestion, and molecular cloning. The parasites pellet was processed for gDNA isolation using the Nucleospin Tissue Kit (MACHEREY-NAGEL). The parasite pellet was resuspended in 200µl of T1 buffer, 25µl of proteinase K (20mg/ml), and 200µl of BT3 buffer. This solution was vortexed and incubated at 70 °C for 15 mins. Followed by incubation, 210 µl of 100% ethanol was added to the solution to allow DNA precipitation and loaded into the nucleon spin column. The spin column was then centrifuged at 12000 rpm for 1 min and flow-through was discarded. Next, the column was washed with 500 µl of BW buffer followed by 650 µl of B5 buffer and centrifuged at 12000 rpm for 1 min. After dry spin, the column was placed into a new microcentrifuge tube and genomic DNA was eluted in 35 µl elution buffer by centrifugation for 1 min at 12000 rpm. The concentration of eluted DNA was measured by Nanodrop 2000 and gDNA was stored at -20°C.

2.2.23 Confirming the stable integration of *PbSIMP* knockout construct in endogenous locus

After obtaining successful transfectants, genomic DNA was isolated and the integration of *PbSIMP* KO construct into parasite endogenous locus was confirmed by performing diagnostic PCRs. For confirmation of 5' integration, diagnostic PCR was done with a set of primers FP3/RP3 where FP3 was designed beyond the site of integration and RP3 primer was designed in GFP reporter cassette. For confirmation of correct 3' integration, FP4 primer was designed within hDHFR cassette and RP4 primer was designed from genomic sequences after the site of integration.

2.2.24 Clonal dilution of *PbSIMP* knockout parasites

Drug-resistant parasites obtained after transfection usually have both the recombinant as well as wild-type parasites that showed resistance to drug selection. To characterize the phenotype of knockout parasites, a homogenous population of recombinant parasites from a single parent is necessary. Towards that, limiting dilution was done to obtain isogenic clones of *PbSIMP* KO parasites. Briefly, 200 µl of cryopreserved transfected parasites were intraperitoneally injected in a mouse. Later, the blood was collected from infected mouse having 0.2-1% parasitemia. A small volume of blood was diluted at 1:10000 in RPMI media and the number of infected and uninfected RBC per µl were counted using hemocytometer. The blood was further diluted to get 0.5 parasite/200 µl in incomplete RPMI medium. A group of 20 mice were intravenously injected with 0.5 parasites/mouse (one parasite per two mice). From 7 days after injection, mice were monitored for infection by Giemsa-stained blood smears. When the parasitemia reached to 3-5% in the positive mice, blood was collected for both genomic DNA isolation and cryopreservation. To confirm if the parasites in the clonal population derived from a single parasite, gDNA was isolated from two different clones obtained from two independent transfections and used for genotyping of single clone population of parasites.

2.2.25 Phenotypic analysis of *Pb*SIMP KO parasites during asexual blood stages

To analyse the asexual propagation rates of *Pb*SIMP KO parasites, approximately $1X10^3$ infected RBC of KO (both C1 and C2) and WT GFP parasites [276] were injected intravenously into a group of 3 female 4-6 week old Swiss albino mice. Parasitemia was monitored daily by making Giemsa stained blood smears for seven days. Parasitemia was determined by microscopic examination of 25 random fields of uniform thin smears.

2.2.26 Generation of pSKC-hDHFR:yFCU plasmid

To generate pSKC-hDHFR:yFCU plasmid, the positive-negative selectable marker cassette (hDHFR:yFCU) was amplified from the plasmid pL1186 [277] using the primers SM-F/SM-R (Table 1). The amplified product was gel purified and digested with SalI/NotI.

The GFP-hDHFR cassettes in pBC-GFP-hDHFR plasmid [276]was replaced with hDHFR:yFCU cassette using SalI/NotI restriction sites to obtain pSKC-hDHFR:yFCU and the plasmid was confirmed by sanger sequencing.

2.2.27 Complementation of *PbSIMP* mutant

For complementation, a GIMO line was generated by targeting *PbSIMP* locus with hDHFR:yFCU positive-negative selectable marker [278]. The 5' and 3' UTR regions of *PbSIMP* were amplified using primers FP1/RP1 and FP2/RP2 respectively. These fragments were cloned into pSKC-hDHFR:yFCU plasmid at *XhoI/SalI* and *NotI*/*AscI* restriction sites respectively. The targeting construct was released from vector backbone using *XhoI and AscI,* gel purified and electroporated into WT *P. berghei* schizonts. The selection of *PbSIMP* GIMO line was performed as described earlier [275]. The correct integration of hDHFR:yFCU cassette was confirmed using primers FP6/RP6 and FP7/ RP7. To generate the complementation construct, *PbSIMP orf* with 5' and 3' homology regions was amplified using the primers FP1/RP2 and gel purified. *PbSIMP* GIMO line was transfected with the purified complementation construct and the integrants were enriched by negative selection using 5-fluorocytosine [275, 278]. Successful replacement was confirmed using primers FP8/RP8 and FP9/RP9. All the primers used are described in Table 1.

2.2.28 Generation of pBC-3XHA-hDHFR localization plasmid

To generate pBC-3XHA-hDHFR, *Pbhsp70* promoter and GFP *orf* of pBC-GFP-hDHFR were replaced with 3XHA oligos annealed *in vitro* (Table 1). Annealed 3XHA oligos yielded dsDNA with overhangs that are compatible to ligate with the DNA digested with restriction enzymes XhoI/BglII. pBC-GFP-hDHFR was digested with XhoI/BglII, and annealed 3XHA oligos were ligated to obtain pBC-3XHA-hDHFR localisation plasmid and sequence was confirmed by sanger sequencing.

2.2.29 Generation of *Pb*SIMP 3XHA transgenic line for studying localization

For generation of *Pb*SIMP 3XHA transgenic line, a 562bp coding region excluding stop codon and a 525 bp 3'UTR were amplified using primers FP10/RP10 and FP11/RP11 respectively. Both the fragments were cloned into pBC-3XHA-hDHFR vector at *Apa1*/*Xho1* and *Not1*/*Asc1* restriction sites respectively. The targeting construct was released from vector back bone using *Apa1* and *Asc1* double digestion and gel purified. The electroporation and selection of transfectants were performed as described earlier [275]. After obtaining successful transfectants, genomic DNA was isolated and the integration of 3XHA-hDHFR cassette was confirmed by using integration specific primers FP12/RP12 and FP13/RP13. The primer sequences are indicated in Table 1.

2.2.30 Breeding of *A. stephensii* mosquitoes

To study the development and infection dynamics of *P. berghei* parasites in the *Anopheles* mosquito vector and mammalian host, laboratory colonies of the *Anopheles stephensi* (*A. stephensii*) mosquitoes were maintained. All stages of *A. stephensii* mosquitoes were reared in an environmental chamber with favourable growth conditions like 27 °C temperature and 80% relative humidity with 12h light/dark cycle. Adult Mosquitoes were fed daily with 10% sucrose solution soaked in sterilized cotton pads. For maintenance of mosquito colony, freshly emerged one-week-old male and female mosquitos were kept in mosquito breeding cages to facilitate mating. Mosquitos were starved for 4-6h by removing sucrose pads and subsequently were allowed to take a 20 min blood meal from a two-month-old New Zealand white male anesthetized rabbit. The rabbit was sedated with a mix of 800 µl of Ketamine (50mg/ml) and 300 µl of xylazine (20mg/ml) injected intramuscularly. Blood meal was given for two consecutive days. On day 2 post blood meal, a water bowl was kept inside the breeding cage for egg laying. The eggs were collected for the next 4 days and shifted environmental chamber. In the chamber, eggs were hatched, and young hatchlings were transferred to plastic trays and were fed with powdered larval food made with low-fat cereal (Kellogg's special) and wheat germ extract (Avees) in the composition of 60:40 ratio. After 7-10 days, the larvae transformed into pupae and pupae were manually collected and placed in a netted cage for the emergence of mosquitoes.

2.2.31 Transmission of *PbSIMP* KO and *P. berghei* WT GFP parasites to *A. stephensii* mosquitoes to study the mosquito stages of parasite

For transmission of infection to mosquitos, netted cages of 400-500 female Anopheles mosquitoes were prepared. Swiss albino mice were infected with either *PbSIMP* KO or WT GFP parasites with intraperitoneal injections. When parasitemia reached to 2-3%, blood was collected and injected into 4–6-week-old SA mice intravenously. Mice were monitored for the gametocytes presence by observing Giemsa-stained blood smears. After confirming the presence of gametocytes in mice, the mice were anesthetized with ketamine/xylazine and kept on top of netted cages. The uninfected female mosquitos were allowed to take 20 min blood meal on sedated mice infected with either *PbSIMP* KO or WT GFP parasites. Two consecutive blood feedings were given with 24h time interval. Blood fed mosquitoes were maintained at 20 °C and 80% RH for 18–22 days to facilitate optimal parasite development in the mosquitos. These mosquitos were fed with 10% sucrose solution on daily basis.

2.2.32 Phenotypic analysis of *Pb*SIMP KO and 3XHA tagged parasites in mosquito

Female *Anopheles stephensi* mosquitoes were allowed to obtain a blood meal from Swiss albino mice carrying 1-2% gametocytes of *PbSIMP* KO and WT GFP line. Two consecutive blood meals were given with 24h time interval. Blood fed mosquitoes were maintained at 20 °C and 80% RH for 18–22 days to facilitate the successful completion of sexual development and for the formation of salivary gland sporozoites. To obtain zygotes and ookinetes, 4-5 mosquitoes were dissected at 2-4h and 16-18h post blood meal respectively. The guts were mechanically disrupted and 2-3µl of sample was spotted on glass slides for performing indirect immunofluorescence assay (IFA). Successful transmission of malaria to *Anopheles* mosquitoes was monitored by observing infected guts and salivary glands for GFP expressing oocysts and sporozoites respectively on day 14 and day 18-20 post blood meal. The sporulation of oocyst was observed at 100X. To assess the morphology of mutant oocyst and salivary gland sporozoites, the infected guts and glands were dissected and mechanically disrupted. The samples were centrifuged at 800 rpm for 3 min. The supernatant containing sporozoites were used for *in vitro* EEF

development and mice infections. Different mosquito stages of *Plasmodium* were visualized using Nikon-AR fluorescent microscope.

2.2.33 *In vitro* EEF development of salivary gland sporozoites

To study *in vitro* exo-erythrocytic form (EEF) or liver stage development, HepG2 (human liver carcinoma) cells that support the complete development of *P. berghei* parasites were used. A 24 well plate (Nunc, Cat No# 142475) was coated with collagen (BD bioscience, Cat# 354236) with a concentration of 10mg/ml overnight. The following day, approximately $2x10^5$ HepG2 cells were seeded and maintained in complete DMEM (cDMEM) with 5% CO2 and at 37 ^oC in a CO2 incubator. After confirming the attainment of a monolayer of HepG2 cells using a Phase contrast microscope, 2×104 sporozoites of WT GFP sporozoites were added to cells, and the plate was centrifuged for 5 min at 1500 rpm using a swing bucket rotor to allow instant attachment of sporozoites to HepG2 cells. The cultures were placed in a CO_2 incubator at 37 ^oC. The cell culture medium was changed after 6h and to avoid any contamination, the culture medium was subsequently replenished every 4 h till 36h time point with cDMEM containing 1x antibiotic and antimycotic solution (Gibco, Cat No#15240062). At 12h, 36h, and 62h time Points, cultures were stopped, coverslip were removed and fixed in 4% formalin solution (Sigma, Cat No# HT5011) and were stored in 4 ^oC till they were taken for immunofluorescence assay.

2.2.34 Immunofluorescence assay

To analyse the morphology of mutant sporozoites and liver stages, IFA was performed as described earlier [279, 280]. The zygotes and ookinetes were stained with anti-p28 antibody (mouse) and immunoreactivity was revealed using goat anti-mouse Alexa 594. The midgut and salivary gland sporozoites were stained with 3D11, a mouse monoclonal antibody [174] specific for *P. berghei* Circumsporozoite protein (CSP) (mouse) and immunoreactivity was revealed using goat anti-mouse Alexa 594. The expression of 3XHA was detected using anti-HA (mouse) antibody procured from abcam (16B12, ab130275) and immunoreactivity was revealed using goat anti-mouse Alexa 594. To study the organisation of the cytoskeletal actin in mutant sporozoites, the *PbSIMP* GIMO

line was used. The mutant sporozoites were stained with FITC conjugated phalloidin (that binds to filamentous actin) and 3D11.

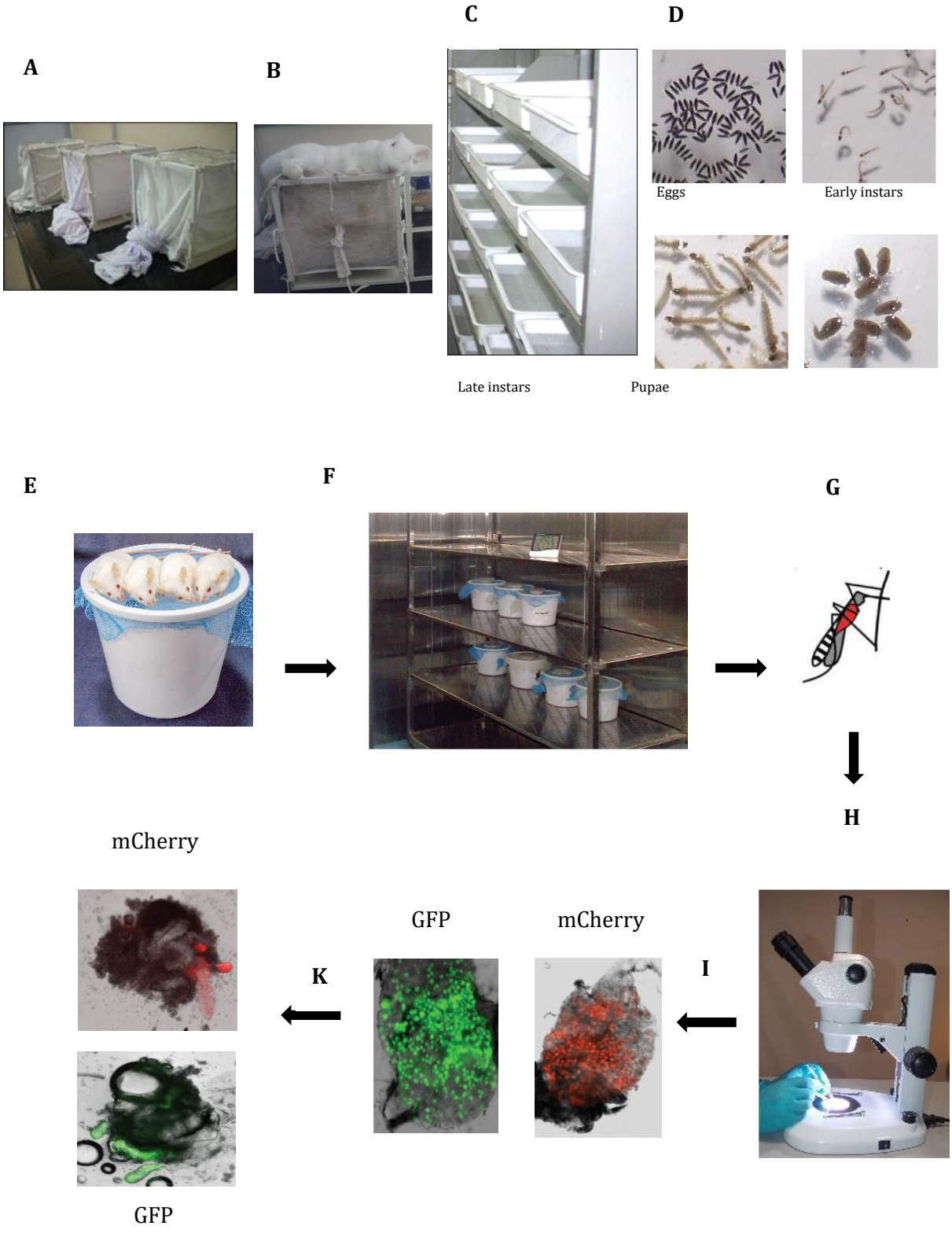


Figure 11. Rearing of *Anopheles* mosquito and maintenance of *P. Berghei* infected mosquito cages. Maintenance of *A. stephensi* colony includes preparation of breeding cages, where pupas are placed in water bowls to emerge into adult mosquitos and mate within 24-36h after they emerge. A) Both male and female

emerged mosquitos are placed in the breeding cage. B) Blood meal is given to mosquitos from an anesthetized rabbit for two successive days at an interval of 24 hours. C) After 36 hr of the second blood meal, water bowl is kept inside the breeding cage for mosquitos to lay eggs. Eggs are collected for next 4 consecutive days and shifted to an environmental chamber maintained at 27 °C with 80% relative humidity. D) Eggs hatch and transform into larvae and finally develop into pupae. E) The pupae are manually collected and placed inside a mosquito cage for the emergence of adult mosquitos. For the preparation of the infection cage, the female mosquitos are collected using a vacuum pump and allowed to feed on infected mice which are positive for *P. berghei* gametocytes. F) The infection cage with fed mosquitos were shifted to an environmental chamber which maintained 21 °C temperature with 80% relative humidity to facilitate the sexual reproduction of *P. berghei* parasites. G) Mosquitos are dissected under a dissection microscope at day14 for midgut oocyst and at day 18 for salivary gland sporozoites post blood meal. H) Both dissected midgut and salivary glands are observed under a fluorescence microscope for oocyst number, sporulation pattern, and sporozoite load in salivary glands respectively.

To study the organization of inner membrane complex (IMC), an IMC marker [281] anti-PIC5 (rabbit polyclonal) antibody was used in combination with 3D11. To confirm the possible orientation of PbSIMP C-terminus, IFA was performed under permeabilized and non-permeabilized conditions. The combination of antibodies used were either anti-HA (mouse) and anti-PIC5 or 3D11 and anti-PIC5. The immunoreactivity of 3D11 and HA was revealed using goat anti-mouse tagged to Alexa 488 and immunoreactivity of PIC5 was revealed using chicken anti-rabbit tagged to Alexa 594. To test the cross reactivity of *Pf*SIMP (C-terminus) mouse antisera on *P. berghei* sporozoites, immunostaining was performed without permeabilization and immunoreactivity was revealed using goat anti-mouse tagged to Alexa 488. The expression of SIMP was analysed during liver stage development (36h) by immunostaining EEFs with *Pf*SIMP mouse antisera and anti-UIS4 (rabbit) antibody (a marker for PVM) [61]. Immunoreactivity was revealed using goat anti-mouse tagged to Alexa 488 and chicken anti-rabbit secondary antibody tagged to Alexa 594. The host and parasite nuclei were stained with DAPI.

2.2.35 Analysis of *in vivo* sporozoite infectivity of *PbSIMP* KO parasites.

To analyze the infectivity of *PbSIMP* KO sporozoites, C57BL/6 mice were intravenously injected with 5×10^3 and 1×10^4 into groups of mice (3–4/group). The parasitemia was

monitored daily from days 3 to 15 post-infection by examining Giemsa-stained tail blood smears. Pre-patency was determined from two independent experiments

2.2.36 Transmission electron microscopy (TEM)

The dissected salivary glands harbouring WT and mutant sporozoites were fixed in 2.5% glutaraldehyde for 2 hours followed by three washes in deionized distilled water. The samples were next treated successively with 2% osmium tetroxide for two hours followed by 2% uranyl acetate for an hour. The sample were extensively washed thrice with deionized distilled water between the two treatments. The samples were dehydrated with series of graded alcohol, followed by treatment with propylene oxide for 20 mins. Epoxy embedding (Sigma) was done as per manufacturer's instructions and incubated at 70°C-80°C for 72 h for complete polymerization. The ultra-thin (30nm) sections were made with diamond knife Leica UC7 ultramicrotome. The sections were mounted on a copper grid and stained with 2% uranyl acetate and counterstained with Reynold's lead citrate. Transmission electron microscopy (JEM 1400, 120 kV, Jeol, Japan) was used for capturing images available at the central instrumentation facility of NIAB Hyderabad.

2.2.37 Expression and purification of *Pf*SIMP protein

*Pf*SIMP was cloned and expressed using pET21a+ vector. Briefly, Rossetta DE3 competent cells were transformed with recombinant pET21a-*Pfsimp* plasmid and induced with 0.5mM IPTG concentration. The culture was incubated and constantly agitated for overnight at 22°C. The cells were harvested by centrifuging at 6000 rpm for 10 minutes at 4°C and processed for the His-tagged purification of *Pf*SIMP through affinity chromatography via Ni-NTA agarose beads [282, 283]. Different imidazole fractions ranging from 10mM to 500mM concentration were used to elute the bound protein from Ni-NTA beads. Imidazole elution fractions were monitored by SDS-PAGE and western blotting for quantification and to check the protein purity. Purified *Pf*SIMP protein was further dialyzed with buffer (100mM Tris, 50mM NaCl and 5% glycerol, pH 8) to eliminate nonspecific proteins.

2.2.38 SDS-PAGE and western blot

Protein samples were boiled in reducing sample buffer and resolved using 10% SDS-PAGE gel. These gels were stained for 2-3 hours at room temperature using staining solution composed of 0.1% (w/v) Coomassie Brilliant Blue, 10% (v/v) acetic acid and 50% (v/v) methanol. This stained gel was destained for 2-3 hours using destaining solution composed of 10% (v/v) acetic acid and 50% (v/v) methanol.

For western blot analysis, first proteins were resolved using 10% SDS-PAGE gel and electro-transferred to nitrocellulose membrane. Non-specific blocking was done with 5% BSA (bovine serum albumin) in TBST (Tris-buffered saline with 0.1% Tween 20) for 1h. After blocking, the membrane was probed with mouse anti-His antibody (Thermo) for 2 h on a rocker at room temperature. Next, the membrane was washed 3 times with TBST and probed with HRP-conjugated goat anti-mouse antibody (Thermo). Membrane was washed three times in TBST and protein bands were visualized using gel documentation system (BioRad).

2.2.39 Generation of *Pf*SIMP polyclonal antibody in mice and rabbit

*Pf*SIMP recombinant protein was purified in large scale and dialyzed for immunization procedure. Female Balb/c mice (5 to 7 weeks old) and New Zealand white rabbit aged 10-16 weeks were used for immunisation. Before immunisation, the naïve mice and rabbit were bled to collect pre-immune sera that were used as a negative control for immunization. Mice and rabbit were intramuscularly primed with purified *Pf*SIMP recombinant protein emulsified with Freund's complete adjuvant (Sigma CFA, F5506-10ML). Two weeks post priming, 3 booster doses were given along with Freud's incomplete adjuvant (sigma IFA, F5881-10ML) at every 2-week interval. The immune sera was collected 10 days after final booster dose.

2.2.40 PIC5 antibody generation in rabbit

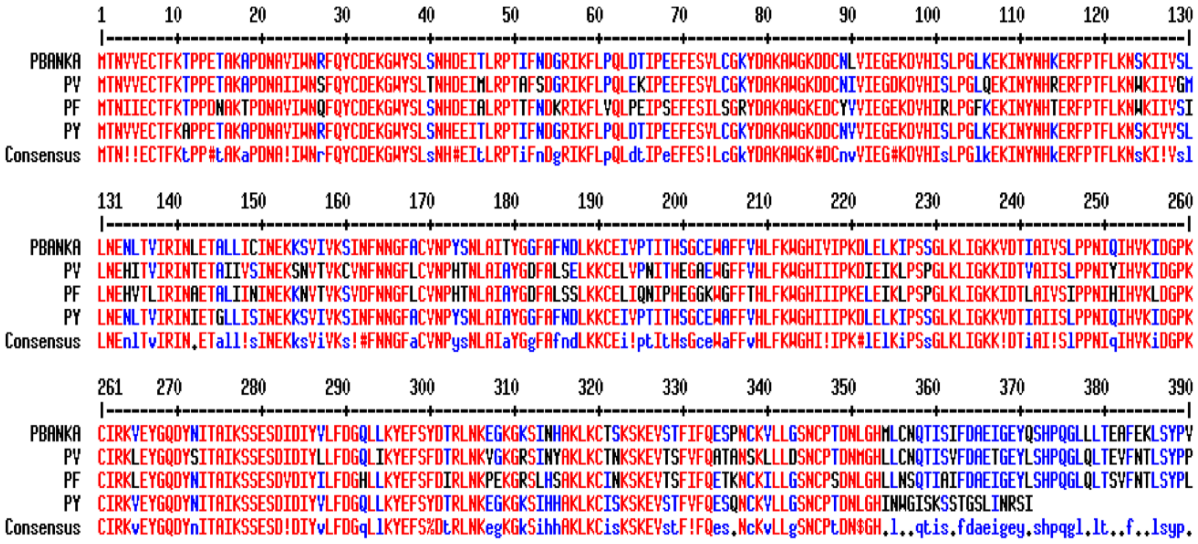
Peptide antisera for PIC5 (PBANKA_1409200) was generated in rabbit essentially following the same immunisation protocol as described above. Two PIC5 peptides (88-EKAIEDAEKALENKESSEN-107 and 129-EENDESVENLENEINEDG-146) were used for immunisation.

2.3 Results

2.3.1 Bioinformatics search reveals that *PbSIMP* is conserved across rodent and human *Plasmodium* species

The PlasmoDB annotates *PBANKA_1422900* as a conserved hypothetical gene. Alignment of *PBANKA_1422900* (*Pb*SIMP) amino acid sequence with other *Plasmodium* orthologues revealed high degree of conservation (Figure 12A). The amino acid identity of *Pb*SIMP (PB) was 96% with *P. yoelli* (PY), and with human parasites, *P. falciparum* (PF) and *P. vivax* (PV), the sequence showed respectively 76% and 81% identity (Figure 12B).

A)



B)

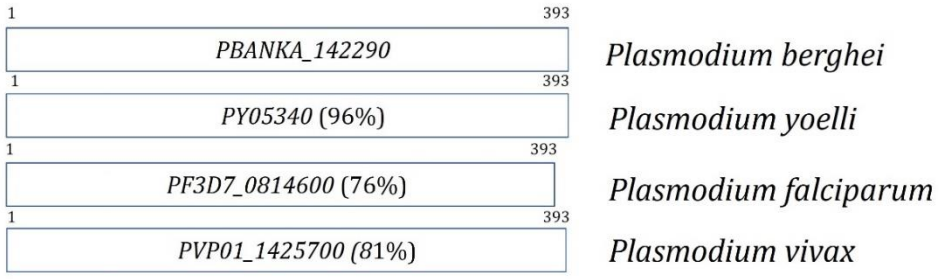


Figure 12. A) Multiple amino acid sequence alignment of Plasmodium SIMP orthologues. P. berghei (PBANKA), P. vivax (PV), P. falciparum (PF) and P. yoelli (PY). Conserved residues are indicated in red. B) Degree of amino acid residue conservation in Plasmodium SIMP orthologs indicated in percentage.

We also analyzed the evolutionary relatedness of *Pb*SIMP. All the *Plasmodium* species infecting rodents formed a separate clade from those infecting aves and primates. Among the primate parasitic species, the human parasites *P. ovale* share a common ancestor with that of the rodent parasites. The human species *P. malariae* and *P. falciparum* share a common ancestor with that of avian species *P. gallinaceum, P. relictum* and those that infect chimps (*P. reichenowi, P. gaboni*) and gorilla (*Plasmodium sp.* gorilla clade G2). The human infecting species *P. vivax* and *P. knowlesi* shares a common ancestor with that of Asian old-world monkeys (*P. inui, P. cynomolgi, P. fragile, P. coatneyi*) (Figure 13).

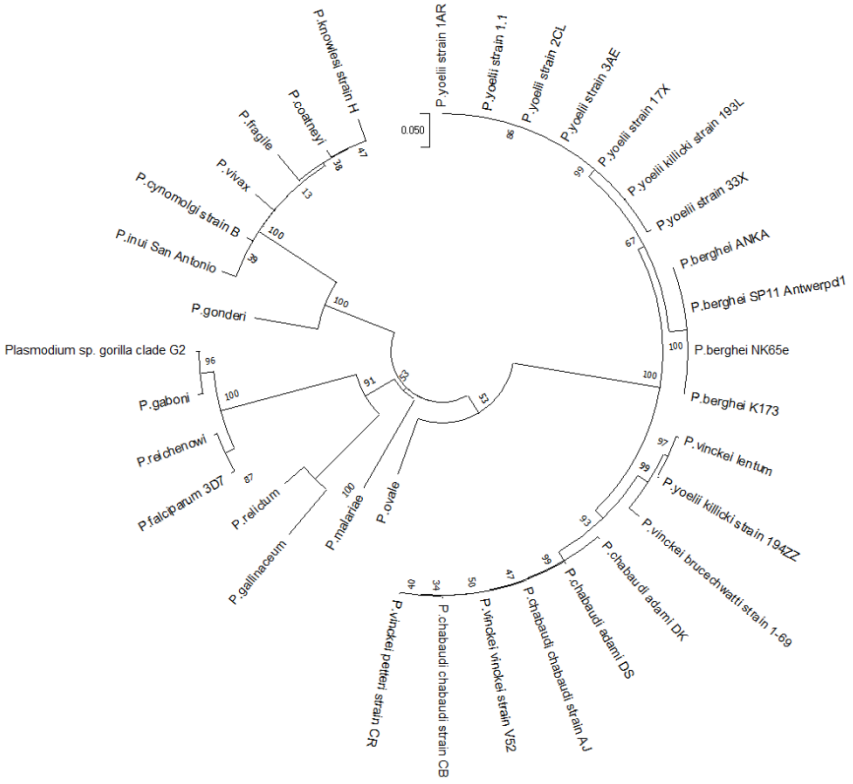


Figure 13. Phylogenetic analysis of PbSIMP with other Plasmodium orthologs. The nucleotide sequences of the PbSIMP and their orthologs were derived and their ancestral states were inferred using the Maximum Likelihood method. All the Plasmodium species infecting the rodents formed a separate clade from those infecting the aves and primates. The percentage of replicate trees in which the associated taxa were clustered together using 1000 bootstraps are shown next to the branches. The evolutionary distance are given in the number of nucleotide substitutions per site as indicated by the scale bar of 0.050.

Since *Pb*SIMP sequence did not have any known functional motifs or domains, we used multiple prediction tools for estimating its cellular localisation. Phobius 1.01 server revealed ~98% probability of the protein being non-cytoplasmic and less than 1% being in transmembrane region (Figure-14A). Predictions for membrane association were also made using the Protscale (Figure-14B), DTU-TMHM 2.0 server (Figure-14C) and Expasy-TMpred (Figure-14D). The Kyte-Doolittle hydropathy plot calculated from Protscale suggested a continuous high hydrophobic score between the amino acid residues 126-253. Further, DTU-TMHM 2.0 server and Expasy-TMpred predicted the presence of membrane-associated domain in the protein mostly between 163-219 amino acid residues (Figure-14E).

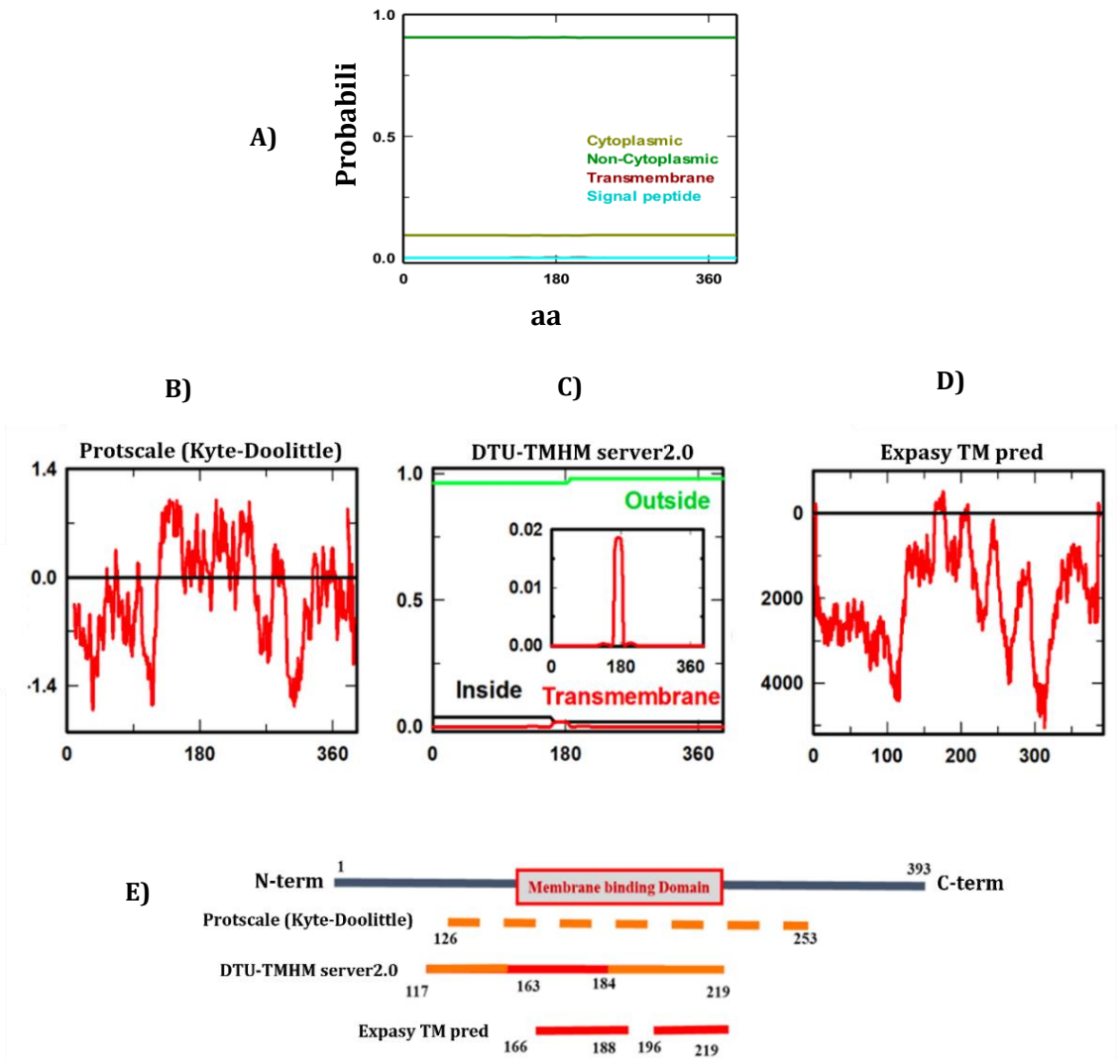
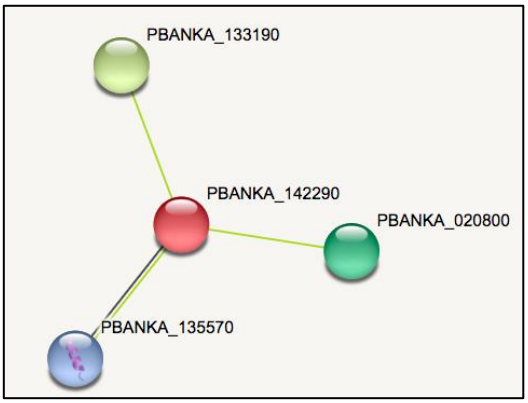


Figure 14. Prediction of cellular localization of PbSIMP. A) Phobius web server output. Posterior probability plot represents, PbSIMP to be a non-cytoplasmic protein. B-D) Prediction of membrane-associated domains. Prediction from Protscale, DTU-TMHM server2.0 and Expasy-TM pred are shown in B,

C and D respectively. (E) Orange line represents the hydrophobic core of the protein, red colour represent the membrane association region obtained from the DTU-TMHM server2.0 and Expasy-TM pred. Kyte-Doolittle plot represents hydrophobic patches in the protein

We next employed STRING database to predict the probable interacting partners for *Pb*SIMP. Our search with the query sequence yielded 3 interacting partners under text mining category that included an RNA helicase (*PBANKA_1331900*), that belongs to the DEAD box helicase family, an adenylyl cyclase-associated protein (CAPS) (*PBANKA_0208000*), and Myosin A (*PBANKA_1355700*) (Figure-15). CAPs are evolutionarily conserved G-actin binding proteins that regulate microfilament turnover and are vital for oocyst development in mosquito [284]. Myosin A is one of the unconventional Class XIV, that are neckless [285].



Your Input:

PBANKA_142290 *annotation not available (393 aa)*

Predicted Functional Partners:

		Neighborhood	Gene Fusion	Cooccurence	Coexpression	Experiments	Databases	Textmining	[Homology]	Score
PBANKA_133190	*RNA helicase-1, putative ; Belongs to the DEAD box helicase family*							•		0.918
PBANKA_020800	*Adenylyl cyclase-associated protein*							•		0.617
PBANKA_135570	*Myosin a, putative; Myosin A ; Belongs to the TRAFAC class myosin-kinesin ATPase superfamily. Myosin family*							•		0.604

Figure 15. Prediction of possible interacting partners of PbSIMP by STRING analysis. STRING analysis showing the possible interaction of PbSIMP with RNA helicase, putative (PBANKA_1331900), Adenylyl cyclase- associated protein (PBANKA_020800) and Myosin A, putative (PBANKA_1355700).

2.3.2 *PbSIMP* maximally expressed in midgut sporozoites

Gene expression analysis of *PbSIMP* across all the parasite stages by quantitative real-time PCR (qRT-PCR) revealed maximal expression in day 14 midgut sporozoites. This analysis concurs with previous studies [269] that demonstrated the high expression of *PbSIMP* in gametocytes and midgut sporozoites. The expression of *PbSIMP* was minimal during liver stage development, merosomes, and in mixed blood stages (Figure-16).

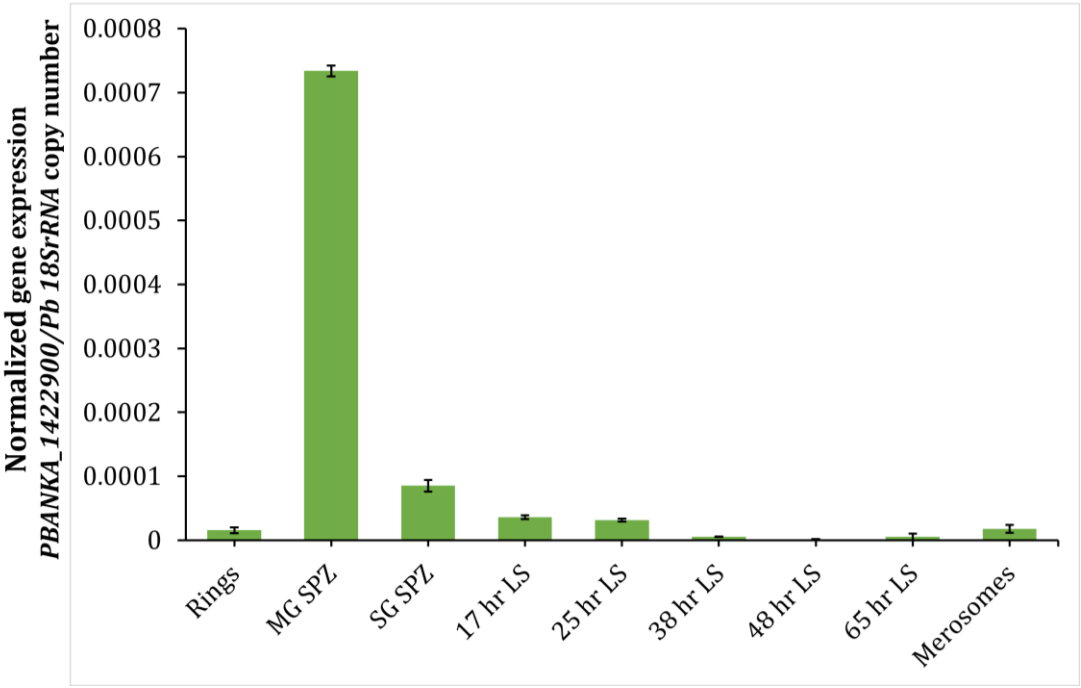


Figure 16. Gene expression analysis. Determination of *PbSIMP* transcript levels across *Plasmodium berghei* life cycle stages by quantitative real time PCR. cDNA samples were generated from different stages as indicated. MBS: mixed blood stages, Mg spz: midgut sporozoites, Sg spz: salivary gland sporozoite stage, liver stages (LS) in hours (h): 17h LS, 25h LS, 38h LS, 48h LS, 65h LS and M: merosomes. The expression values were normalized with *Pb18SrRNA* (internal control gene). Gene expression analysis of *PbSIMP* by real-time PCR reveals maximal expression in the midgut sporozoite stage.

2.3.3 Generation of *PbSIMP* KO parasite line

In order to investigate the functional role of *Pb*SIMP, we generated a knockout by replacing its locus with a targeting construct carrying a GFP and hDHFR drug selection marker (Figure 17A).

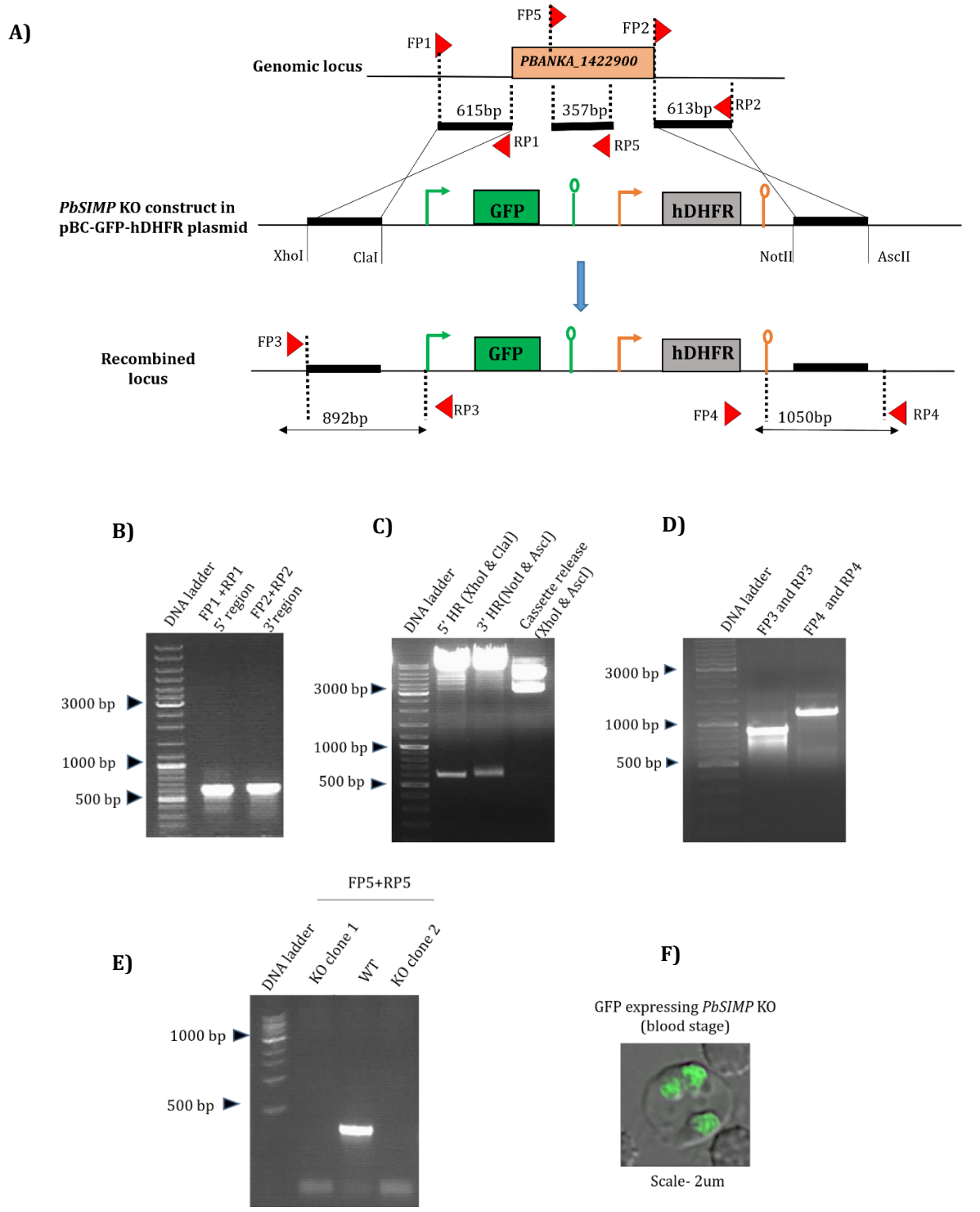


Figure 17. Generation of PbSIMP knockout parasites. A) Strategy for generating PbSIMP KO. PbSIMP 5' and 3' UTR regions used for generating the targeting construct for homologous recombination are indicated as solid lines. Recombined locus shows the replacement of PbSIMP orf with GFP and hDHFR cassettes. B) A 1%agarose gel showing PCR amplified products of 5' and 3' UTR regions for generating the *PbSIMP* KO targeting construct. C) Digestion products of 613 bp of 5' UTR and 615 bp 3' of UTR of PbSIMP following

release with XhoI/ClaI and NotI/AscI respectively and vector was linearized with XhoI/AscI and targeting cassette was gel purified. D) Diagnostic PCRs for confirming correct integration of KO cassette at PbSIMP locus. Primers used for diagnostic PCRs were designed flanking the homology arms used for recombination (as shown in B). E) PCR showing the absence of PbSIMP orf in KO clones from two independent transfections (C1 and C2). F) Merged DIC image showing PbSIMP KO expressing GFP reporter (Scale 5µm).

The 5′ and 3′ regions of *Pb*SIMP were amplified by PCR and cloned in pBC-GFP-hDHFR plasmid (Figure 17B). Correct site-specific integration was confirmed by diagnostic PCR (Figure 17D). Two clones were obtained following limiting dilution of lines from independent transfections. Genotyping of both clones showed the absence of *Pb*SIMP *orf* (Figure 17E) and the recombinants expressed GFP (Figure 17F). The infectivity of mutants was compared with WT GFP line [276] across all life cycle stages.

2.3.4 Blood stage propagation of *PbSIMP* KO parasites:

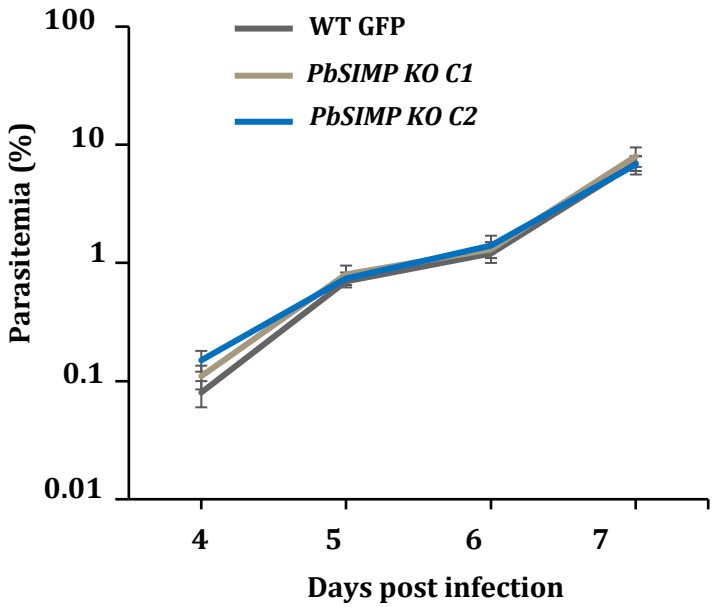


Figure 18. Asexual blood stage propagation. 1X10^3 infected RBCs of WT GFP and *PbSIMP* KO parasites (C1 and C2) were injected intravenously into mice and parasitaemia was monitored daily for 7 days by microscopic observation of Giemsa-stained blood smears.

Asexual propagation was monitored by injecting intravenously, 1×10^3 iRBC of mutant and GFP expressing WT parasites (WT GFP) into a group of mice (5 in each group). Parasitemia was monitored for 7 days post-infection, by making Giemsa-stained blood smears on daily basis. We noted no difference in the growth of mutants as compared to WT GFP (Figure 18) in two independent experiments.

2.3.5 *PbSIMP* KO parasites development in the mosquito vector

The mutants were next analysed in mosquito by initiating a sexual cycle. We noted that the mutants were able to form ookinetes (Figure-19A) and also successfully colonised the mosquito gut wall as evident by presence of oocyst (Figure-19B). Interestingly, the frequency of oocyst/mosquito (Figure-19C), sporulation pattern (Figure-19D), oocyst sporozoites numbers (Figure-19E) and morphology of oocyst sporozoites (Figure-19F) were comparable to WT GFP.

On D18-20 post infection, dissected salivary glands revealed the presence of mutant sporozoites, suggesting their successful colonisation of salivary glands (Figure 20A) and their load was comparable to WT (Figure 20B). However, observing the glands under higher magnifications revealed that the mutants failed to maintain a typical sickle shape structure characteristic of the WT sporozoites (Figure 21A). To analyse the structural alterations associated with the mutant sporozoites, we immunostained sporozoites with 3D11 monoclonal antibody specific for circumsporozoite protein (CSP) [174], a major sporozoite membrane protein. We noted distinct CSP immunoreactivity all along the membrane blebs at multiple foci (Figure 21B), that appeared like extensive membrane detachment when compared to WT sporozoites. Taken together, *Pb*SIMP depletion had a dramatic effect on sporozoite morphology, implying its function in maintenance of the normal sporozoite structural integrity. Owing its unique role, we refer the product of *PBANKA_1422900* as sporozoite structural integrity maintenance protein (*Pb*SIMP).

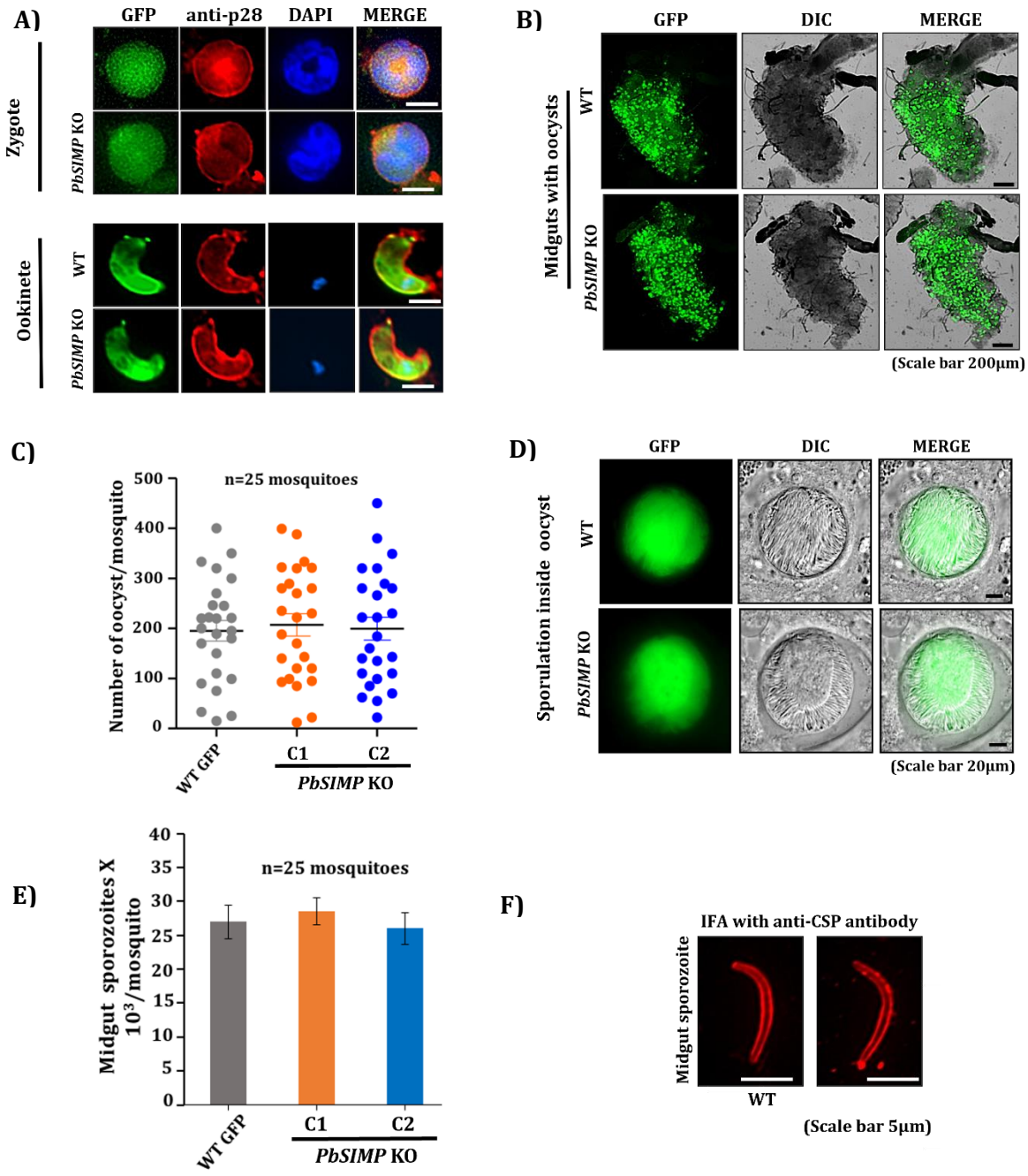


Figure 19: *PbSIMP* does not show any role in sexual stages development, oocyst frequency, sporulation pattern, and structure of oocyst sporozoites. Infection was transmitted to *Anopheles* mosquitoes from mice infected with *PbSIMP* KO and WT GFP parasites to initiate sexual cycle. Mosquito midguts were dissected at 2h and 18-20 h post blood meal to visualize zygotes and ookinetes. A)Anti-p28 staining of zygote (2h) and ookinete (18-20h). Scale bar 5µm. B) Dissected mosquito midguts on day 14 showing oocysts. Scale bar 200µm. C) Dot plot showing quantification of oocyst numbers from individual mosquitoes. D) Sporulation inside oocyst on day 14 post infection. Scale bar 20µm. E) Bar graph showing quantification of midgut sporozoites per infected mosquito. F) CSP staining of midgut sporozoites. Scale bar 5µm.

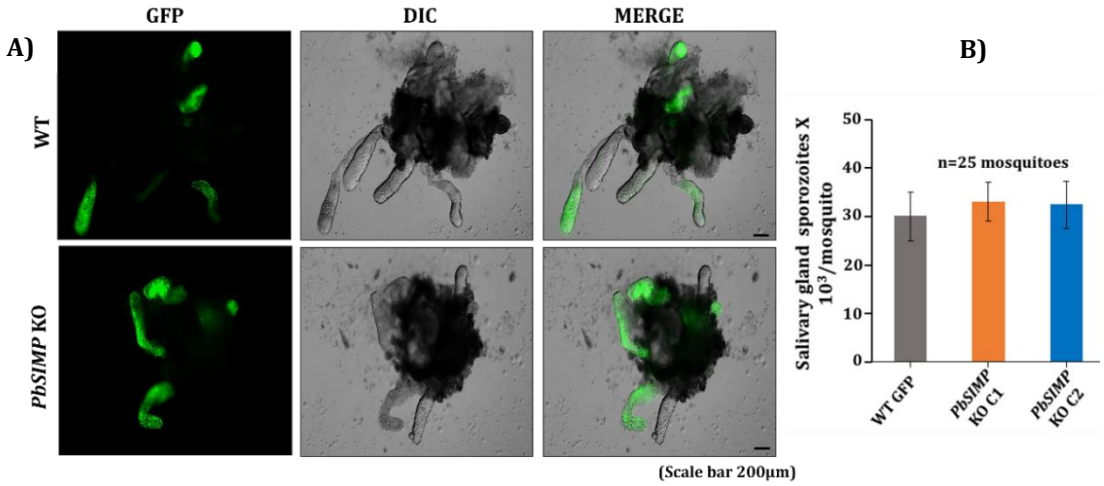


Figure 20. *PbSIMP* KO sporozoites are not defective in invading salivary glands. A) Mosquito salivary glands harbouring sporozoites on day 18 post infection. Scale bar 200µm. B) Bar graph showing quantification of salivary glands sporozoites.

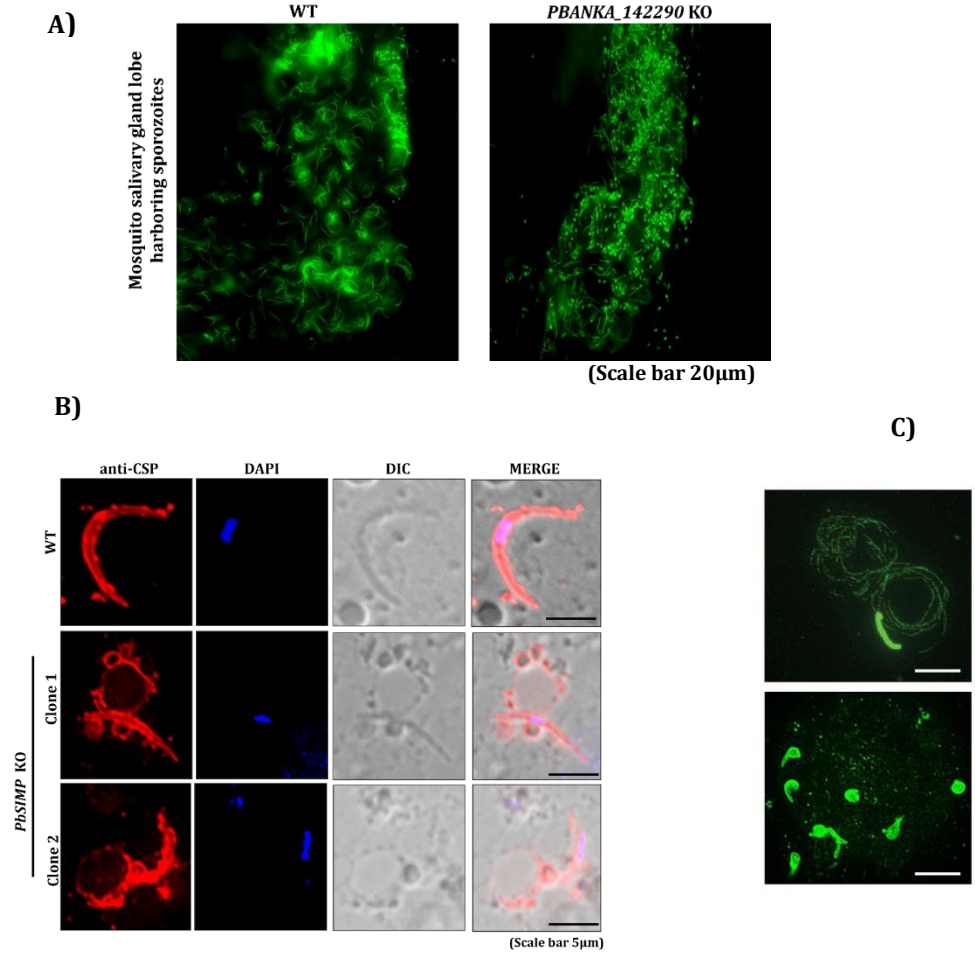


Figure 21. *Pb*SIMP KO sporozoites suffer from loss of regular shape and fail to glide. A) Representative images of salivary glands at higher magnification (20X) Scale bar 20µm. B) CSP staining of salivary gland sporozoites. Sporozoite nuclei were stained with DAPI (Blue). Indirect immunofluorescence

(IFA) were performed for both clones- C1 and C2. Scale bar 5µm. C) Gliding motility of WT and *Pb*SIMP KO sporozoites on glass slide. Scale bar 5µm.

2.3.6 Analysis of prepatency in PbSIMP KO sporozoites

Consistent with loss of regular shape, we noted that the SIMP mutants failed to perform gliding motility (Figure 21C), a pre-requisite for hepatocyte infection. To analyse the transmission ability of *PbSIMP* KO sporozoites to induce infection in the mammalian host, C57BL/6 mice were intravenously infected with two different doses ie. $1X10^4$ and $5X10^3$ sporozoites of either KO or WT GFP and monitored the pre-patent period by examination of Giemsa-stained blood smears. In multiple independent experiments, we noted that in all mice SIMP mutants failed to get rise to blood-stage infection, while WT GFP sporozoites gave a breakthrough blood-stage infection on days 3-3.5 as shown in table (2).

Experiment number	Parasite strain	Numbers of animals used for intravenous injection	Number of sporozoites injected per animal	Number of animals positive for blood stage infection	Pre-patent period
Experiment 1	WT	4	$5X10^3$	3/3	3.5 day
	PbSIMP KO	4	$5X10^3$	0/3	None
Experiment 2	WT	3	$1X10^4$	3/3	3 Days
	PbSIMP KO	3	$1X10^4$	0/3	None

Table 2. Infectivity of *PbSIMP* KO sporozoites in C57BL/6 mice. *PbSIMP* KO sporozoites fail to establish liver stage infection. Different doses of sporozoites in the range of $5X10^3$ to $1x10^4$ were intravenously injected and pre-patency was monitored from day 3 onwards by making Giemsa-stained blood smears. *PbSIMP* KO sporozoites failed to give blood stage infection (as judged till day 15, post infection), while WT sporozoites gave a breakthrough infection by day 3-3.5.

2.3.7 Complementation of PbSIMP depletion

To demonstrate that the observed phenotype was specific to SIMP depletion, we restored the gene function by complementation. Towards this, we generated a *Pb*SIMP GIMO line by replacing *Pb*SIMP locus with a positive-negative selectable marker cassette, hDHFR:yFCU (Figure 22A). The GIMO line was further complemented with copy of *PbSIMP orf* (Figure 22A). The successful integration of GIMO cassette at *PbSIMP* locus and complementation of GIMO locus with *PbSIMP* copy were confirmed by PCR (Figure 22B and C). The *PbSIMP* complemented line produced salivary gland sporozoites similar to WT (Figure 22D).

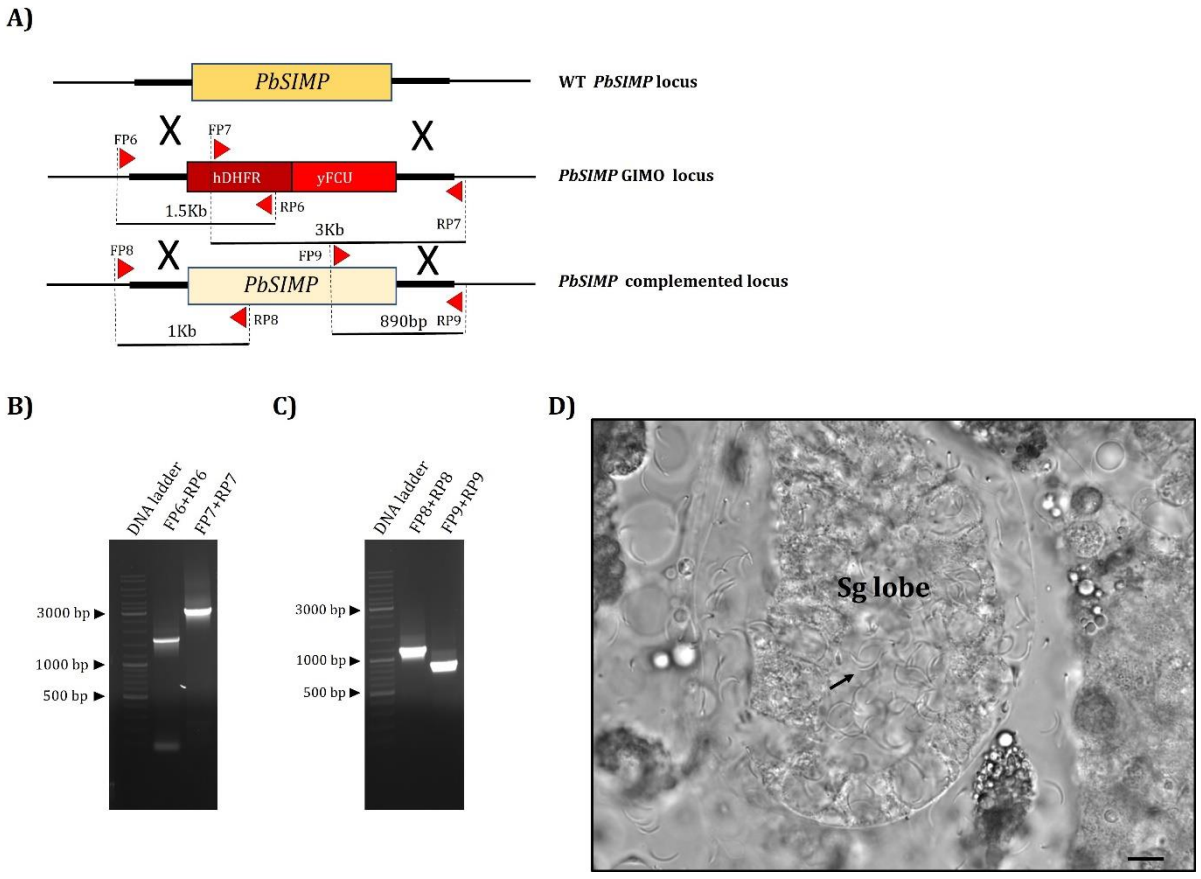


Figure 22. Generation of PbSIMP GIMO line and complementation. (A) Targeting PbSIMP locus (top), with a positive–negative selectable marker (hDHFR:yFCU cassette) for generating PbSIMP GIMO line (middle). PbSIMP GIMO line was further complemented with PbSIMP orf (bottom). Arrows indicate the diagnostic primers to confirm correct integrations in PbSIMP GIMO and complemented lines. Expected PCR product sizes were indicated. (B and C) PCRs for confirming correct integrations of the GIMO cassette and

complementation of PbSIMP orf, respectively. (D) Restoration of salivary gland sporozoite phenotype in complemented line. Salivary gland lobe showing sporozoites with regular shape. Scale bar 10 µm.

2.3.8 *PbSIMP KO* parasites exhibit normal cytoskeletal and IMC organization in salivary gland sporozoites

Since the mutants suffered from extensive structural changes, we next analysed if the cytoskeleton of sporozoite was also altered. *Plasmodium* sporozoites contain monomeric G actin in their cortical region that form transient arrays of F actin to provide linkage substrate for the adaptors of invasins/adhesins [286].

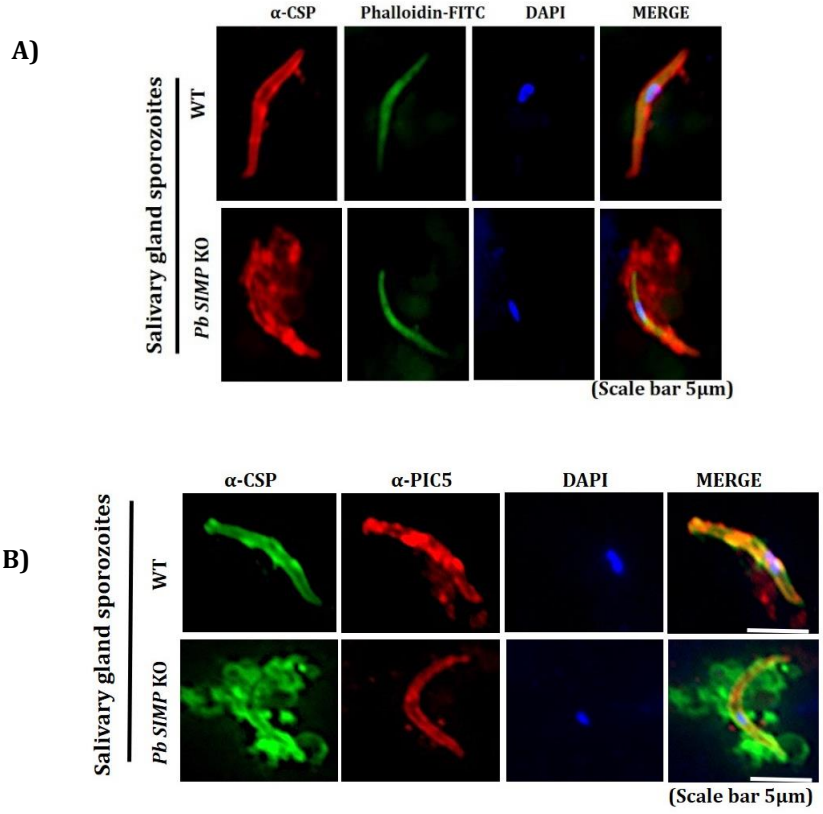


Figure 23. *PbSIMP* depletion does not affect F-actin and IMC organisation. Shown here are immunofluorescence images of midgut and salivary gland sporozoites of both WT and *PbSIMP* KO parasites. A) Staining of salivary gland sporozoites with anti-CSP (mouse) antibody and actin cytoskeletal elements with Phalloidin-FITC. The CSP immunoreactivity was revealed with goat anti mouse Alexa 594. Scale bar 5µm. B) Staining of salivary gland sporozoites with anti-CSP (mouse) antibody and inner membrane complex (IMC) with anti-PIC5 (rabbit) antibody. Immunoreactivity was revealed with goat anti-mouse Alexa flour 488 and chicken anti-rabbit Alexa flour 594. DAPI was used to stain parasite nuclei. Scale bar 5µm.

We stained mutant salivary gland sporozoites with FITC-labelled phalloidin conjugates that binds to short and long filaments of actin. We noted intact F actin staining in mutants similar to WT salivary gland sporozoites (Figure 23A). Thus, structural alterations associated with SIMP mutant did not involve cytoskeletal elements. Since sporozoite motility is dependent on the traction generated by molecular motor that is connected with the inner membrane complex (IMC), we also analysed the organisation of IMC in mutant sporozoites. Immunostaining of PIC5, an IMC marker [281] revealed an intact IMC organisation in mutants (Figure 23B).

2.3.9 The membrane blebbing in *PbSIMP* mutant is not associated with extension of IMC as seen during very early transformation of sporozoite into EEFs.

Towards possible explanation for loss of normal shape in *Pb*SIMP mutant sporozoites, we further analysed the nature of membrane alterations. Normally, when sporozoites transform into EEFs, the IMC dismantles and extends under the membrane until 24 h but later disappears [72].

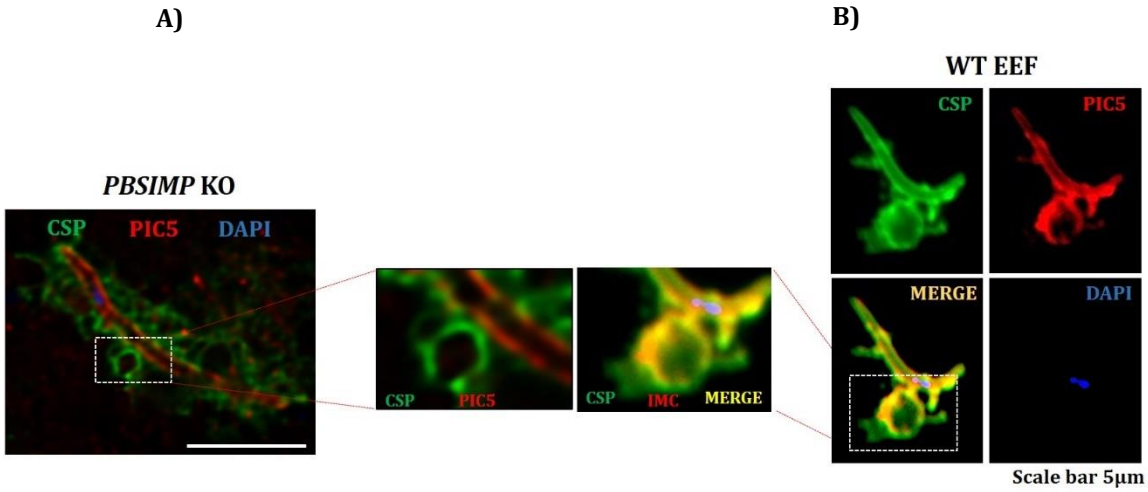


Figure 24. Comparison of IMC organization in PbSIMP mutant sporozoite versus WT early EEF (2-4 h). A-B) Staining of sporozoites and EEFs with anti-CSP (mouse) antibody and IMC with anti-PIC5 (rabbit) antibody. Immunoreactivity was revealed with goat anti-mouse Alexa flour 488 and chicken anti-rabbit Alexa flour 594. DAPI was used to stain parasite nuclei. Scale bar 5µm.

We analysed if the membrane blebs of SIMP mutants have underlying IMC. We immunostained the *Pb*SIMP mutant sporozoites and 4-6 h WT EEFs (structurally reminiscent of the mutant forms) with anti-CSP antibody and anti-PIC5 antibody (Figure 24A and B). We noted that the mutants do not have extensions of IMC under the membrane whereas in transforming WT sporozoites, IMC accompanied the membrane (Figure 24A and B). We conclude that *Pb*SIMP depletion likely leads to loss of contact of sporozoite membrane with underlying IMC. To reiterate the same, we analysed the membrane organisation in mutant sporozoites by TEM. We noted distinct membrane detachment in mutants (Figure-25).

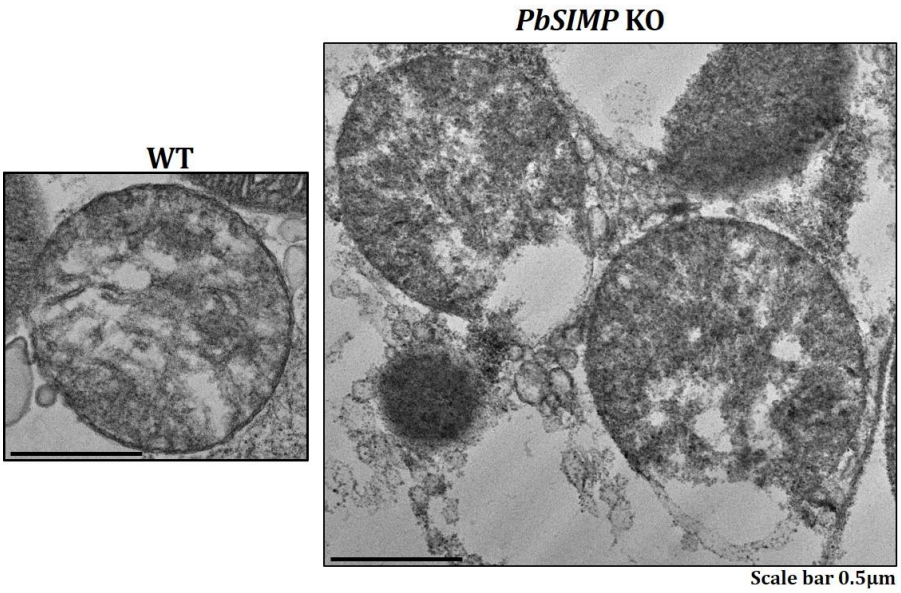


Figure 25. Ultrastructure analysis of *PbSIMP* KO sporozoites reveals membrane detachment. Transmission electron microscopy of sporozoites in cross section. The black arrow indicates membrane detachment in *Pb*SIMP KO sporozoites. Scale bar 0.5µm.

2.3.10 Localization of *PbSIMP*-HA in *Plasmodium berghei* across life cycle stages

Towards demonstrating the cellular localisation of SIMP, we generated a transgenic *P. berghei* line by translationally fusing *PbSIMP orf* with 3X hemagglutinin (HA) tag (Figure 26) and confirmed correct integration by PCR (Figure 26D) and sequencing of recombined locus (Figure 26F&G). The *Pb*SIMP HA transgenic produced normal oocyst and salivary gland sporozoites (Figure 27A). Immunofluorescence assay (IFA) revealed HA expression in gametocytes, ookinetes, oocyst, and salivary gland sporozoites (Figure 27B).

Interestingly, the HA immunoreactivity was majorly localized to gametocyte cytoplasm, however, in ookinetes, oocyst, and salivary gland sporozoites, we noted peripheral/membrane localization. High levels of HA expression in salivary gland sporozoites were consistent with structural alteration in the membrane of PbSIMP mutants (Figure 27C). We also compared the levels of HA signals with that of CSP, a predominant membrane protein and a prime target of protective immune responses on radiation attenuated sporozoites (Figure 27C) (Kumar et al., 2006). HA signal intensity accounted for nearly 50% or more of CSP (Figure 27D). Taken together, we conclude that *Pb*SIMP localizes to sporozoite membrane and has high levels of expression in salivary gland sporozoites.

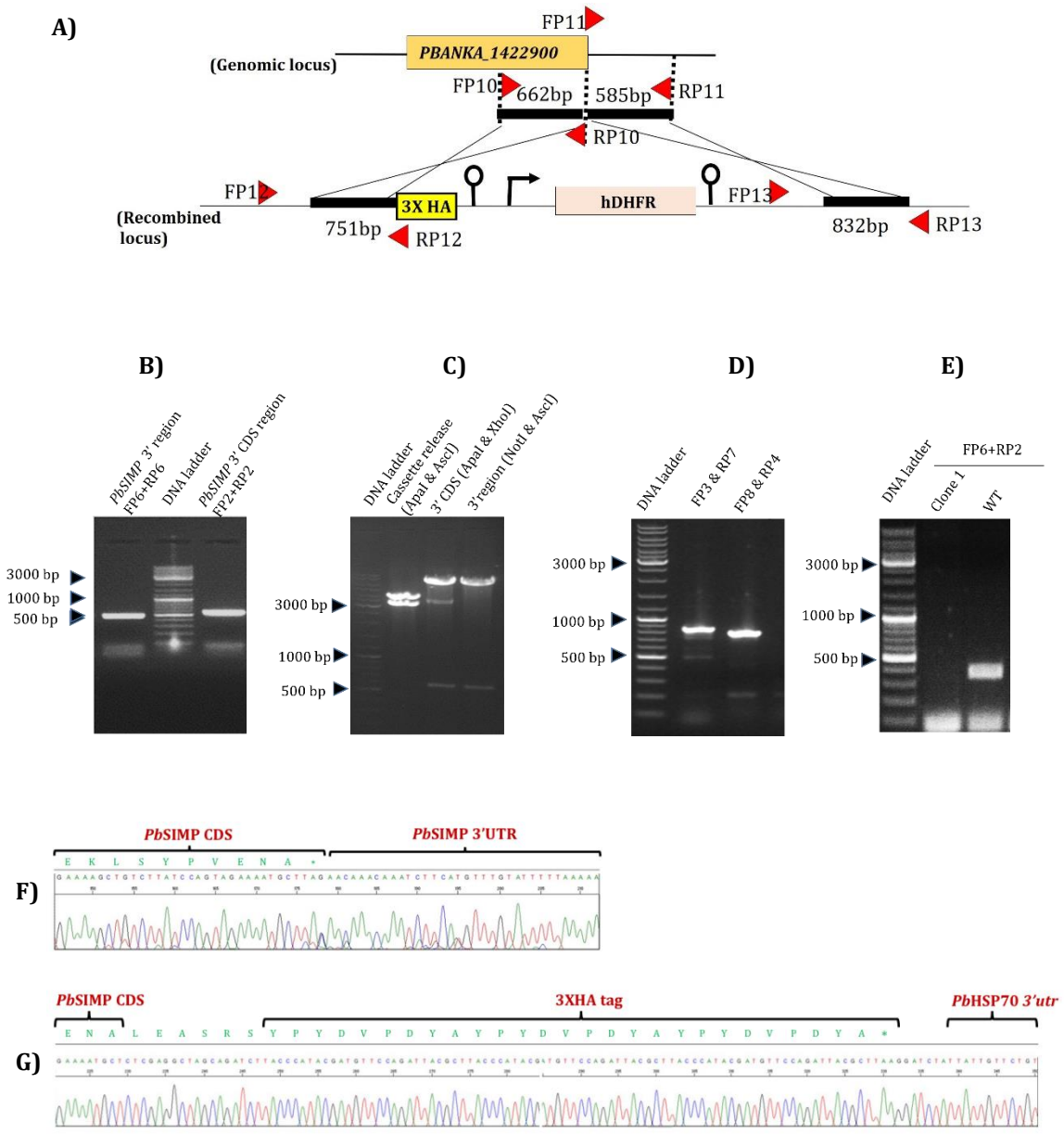


Figure 26. Generation of *PbSIMP*-HA transgenic parasites for expression and localization of sporozoites. A) Strategy for generation of PbSIMP-3XHA transgenic line. 3′ regions of coding sequence and UTR were amplified and cloned in pBC-3XHA-hDHFR to generate the targeting construct. After successful homologous recombination, a 3XHA was introduced in frame to PbSIMP orf. **B)** Amplification of 3′ coding sequence (CDS) and 3′ UTR regions for generating the PbSIMP 3XHA targeting construct. **C)** Digestion products of 662 bp of 3' coding region and 585 bp 3′ of UTR of PbSIMP following release with Apa1/Xho1 and Not1/Asc1respectively and vector was linearized with ApaI/AscI and targeting cassette was gel purified. **D)** Diagnostic PCRs for confirming correct integration of 3XHA epitope tagged to PbSIMP CDS. Primers in red triangles and PCR product sizes are indicated. **E)** Single clone parasite populations were obtained following limiting dilution of drug-resistant parasites. **F-G)** Recombined locus was sequenced and confirmed that *PbSIMP* was in frame with 3XHA.

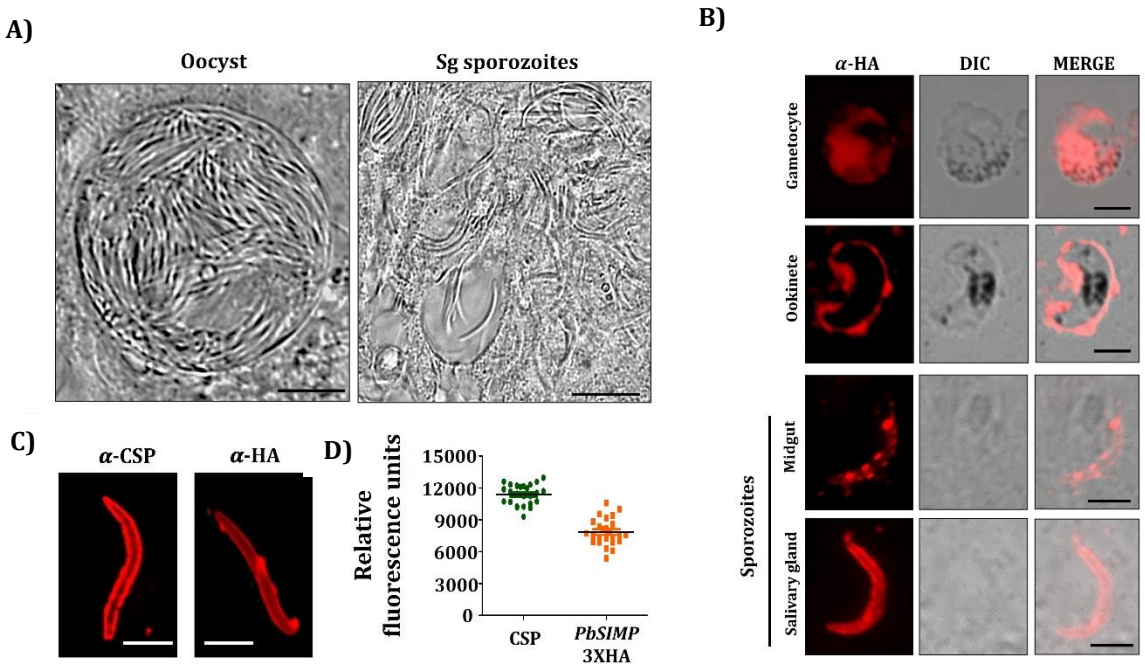


Figure 27. Investigation of *Pb*SIMP 3XHA expression in midgut and salivary gland sporozoite stages. A) *Pb*SIMP 3XHA transgenic line showing normal development of oocyst and salivary gland sporozoites. Scale bar 10 µm. B) Analysis of HA-specific expression in gametocytes, ookinetes, midgut, and salivary gland sporozoites. The HA expression was detected by staining with anti-HA (mouse) primary antibody and revealed with goat anti-mouse Alexa flour 594 secondary antibody. Scale bar 5 µm. C) Immunostaining and quantification HA and CSP of PbSIMP 3XHA tagged salivary gland sporozoites. PbSIMP 3XHA transgenic sporozoites were stained with either anti-HA or anti-CSP antibody and the immunoreactivity was revealed with goat anti-mouse Alexa flour 594. D) Dot plot showing the intensity of immunofluorescence signals from sporozoites. Results are represented as relative fluorescence units. Scale bar 5 µm.

2.3.11 C-terminus of *Pb*SIMP is extracellular

DTU-TMHM 2.0 server and Expasy-TMpred predicted the presence of membrane-associated domain in the protein mostly between 163 and 219 amino acid residues. To investigate the possible orientation of *Pb*SIMP beyond 219 amino acids, we used the *Pb*SIMP C-terminal HA-tagged transgenic line. The transgenic sporozoites were fixed and immunostained for HA and IMC marker-PIC5 under both non-permeabilized and permeabilized conditions (Figure 28A, upper panel). As a positive control, we stained sporozoites with anti-CSP and PIC5 (Figure 28A, lower panel).

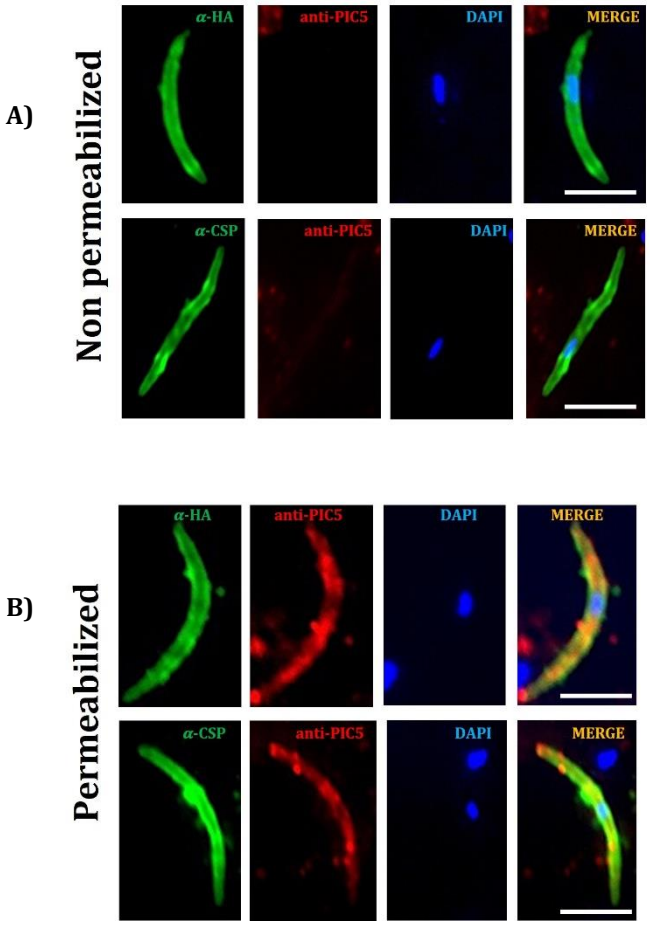


Figure 28. PbSIMP C-terminus region is present extracellularly. A and B) *Pb*SIMP HA transgenic sporozoites were fixed and immunostained with anti-HA (mouse) or anti-CSP (mouse) and anti-PIC5 (rabbit) antibody under (A) non permeabilized and (B) permeabilized condition. The immunoreactivity was revealed with goat anti-mouse tagged to Alexa 488 and chicken anti-rabbit tagged to Alexa 594. Scale bar 5 m. The presence of HA staining on sporozoites without permeabilization suggests that *PbSIMP* C-terminus is extracellular.

As expected, CSP gave a strong positive signal owing to its membrane attachment through its GPI anchor sequence (Figure 28A lower panel). We also noted a very strong signal for HA, suggesting that the C-terminus was indeed extracellular (Figure 28A upper panel). Since PIC5 is an IMC marker that is located underneath the plasma membrane, we used it as a negative control for staining. As expected, we did not see any IMC staining under non-permeabilized conditions (Figure 28A) while IMC showed prominent signals in permeabilized sporozoites (Figure 28B). We conclude that PbSIMP has an extracellular C-terminus, though the precise length of this domain needs to be identified.

2.3.12 SIMP Localization on salivary gland sporozoites and exoerythrocyte stages using *Pf*SIMP antisera

The C-terminus of *Pf*SIMP has 76% identity to *Pb*SIMP (Figure 29A & B). BepiPred software predicted four peptides with a score above 0.62 (Figure 29C), within this region for both *P. berghei* and *P. falciparum* likely, suggesting a probability of being highly immunogenic.

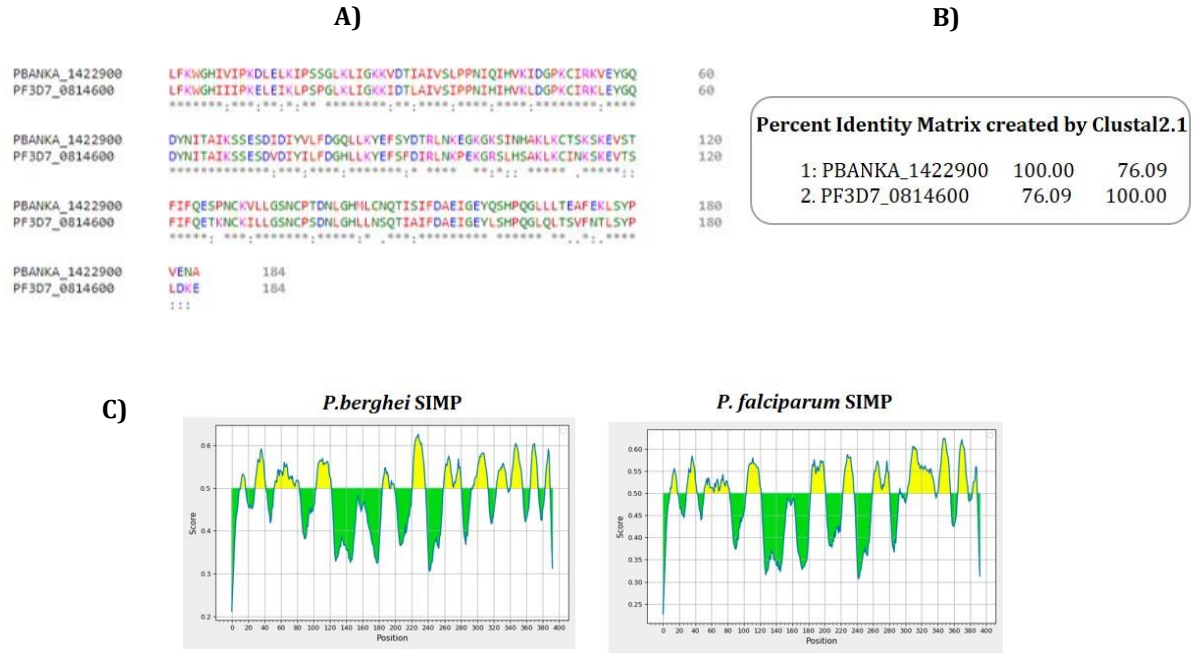


Figure 29. **Prediction of immunogenic epitopes in *Pb*SIMP and *Pf*SIMP by BepiPred analysis.** A) Pairwise amino acid sequence alignment of PbSIMP and PfSIMP C-terminal region. B) Percentage identity matrix of PbSIMP and PfSIMP C-terminal region. C) B cell epitope predictions in PbSIMP and PfSIMP by BepiPred Linear Epitope Predictions 2.0. The annotation of scores were maximum from 220 aa onwards.

We cloned and expressed C-terminal PfSIMP from 201 to 393 amino acids (Figure 30A, B) and generated antisera against purified recombinant. We performed IFA under non-permeabilizing conditions in WT P. berghei sporozoites using antisera against *Pf*SIMP C-terminus. We noted a distinct immunoreactivity on the membrane of midgut and salivary

gland sporozoites (Figure 30C) that concurred with our previous observations. We also analysed the expression of SIMP in in vitro grown P. berghei EEFs.

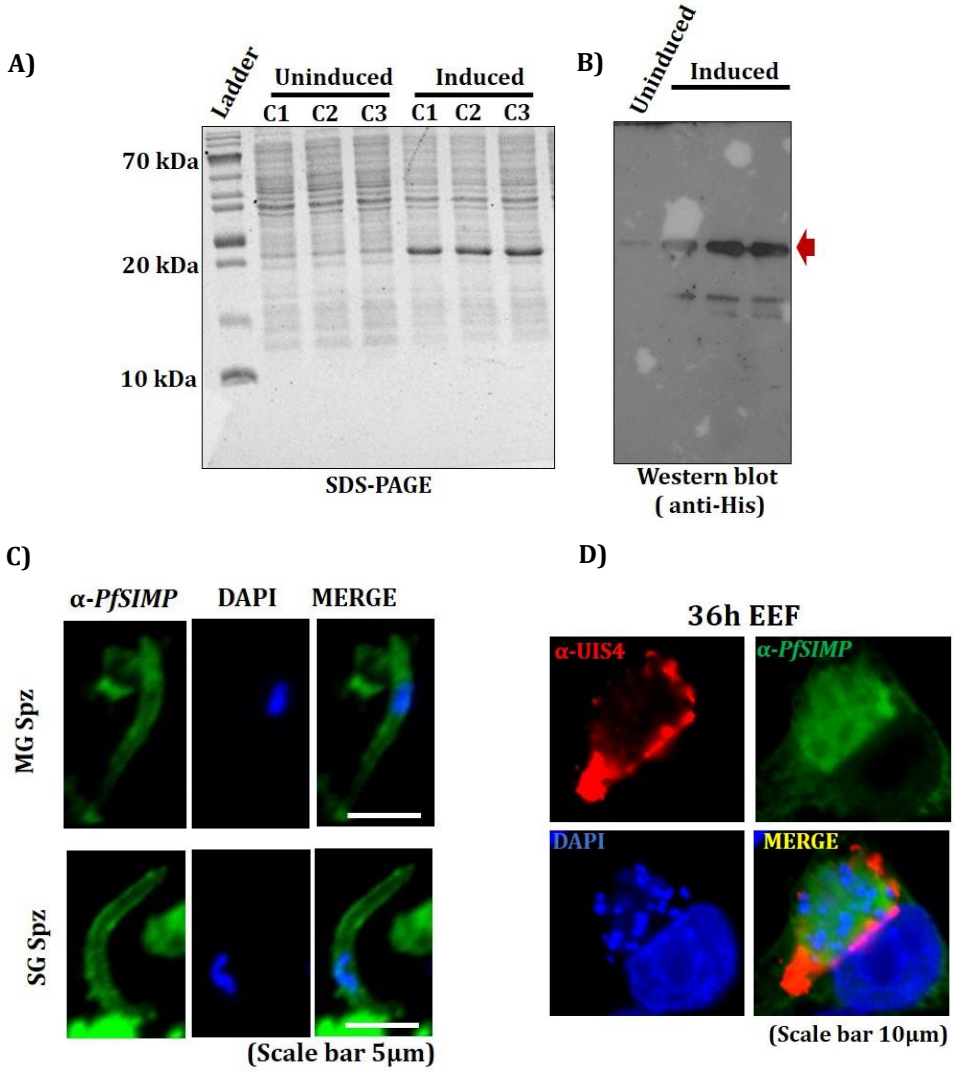


Figure 30. A) SDS-PAGE showing recombinant protein expression of *Pf*SIMP C-terminus. Coomassie-stained SDS-PAGE gel showing *Pf*SIMP expression profile from three clones (C1–C3)under IPTG induced and uninduced conditions. (B) Confirmation of *Pf*SIMP recombinant protein expression by western blotting using anti-His (mouse) antibody under induced and uninduced conditions. Immunoreactivity was revealed with HRP-conjugated anti-mouse secondary antibody. C) Immunoreactivity of *Pf*SIMP C-terminus antibody on non-permeabilized sporozoites. WT *P. berghei* salivary gland sporozoites were fixed and stained with mouse antisera generated against recombinant *Pf*SIMP C-terminus (under non-permeabilized conditions). The immunoreactivity was revealed with goat anti-mouse secondary antibody conjugated to Alexa Fluor 488. The parasite nuclei were stained with DAPI. MG Spz: midgut/oocyst sporozoites, SG Spz: salivary gland sporozoites. Scale bar 5 µm. D) SIMP is detected in the septa of developing EEFs at 36 h. EEFs were immunostained with mouse *Pf*SIMP (c-terminus) antisera and rabbit anti-UIS4 antibody. The

immunoreactivity was revealed with goat anti-mouse Alexa flour 488 and chicken anti-rabbit Alexa flour 594. The host and parasite nuclei were stained with DAPI. Scale bar 10 μm

Interestingly, at 36 h we noted a distinct immunoreactivity in the septa that partitions the daughter merozoites into different compartments (Figure 30D). However, the function of SIMP in liver stages merits additional investigation.

2.4 Discussion

The commitment of *Plasmodium* sporozoites to hepatocytes is an event central to establishment of malaria infection in mammals and hence blocking this process holds great therapeutic potential to prevent clinical malaria. In fact, recent years have seen a surge in defining the protein composition of sporozoite membrane- apparently for 2 important reasons viz., (1) sporozoite proteins act as ligands for hepatocyte membrane, hence their extensive functional characterization may broaden the scope of intervening hepatocyte-sporozoite interactions and (2) the membrane anchored proteins that physically connect to the components of actomyosin molecular motor may serve as additional targets for inhibiting gliding motility, thus tackling the sporozoites at initial stages of infection. In line with such pursuit, we report the functional role of a conserved *Plasmodium* protein-SIMP in maintaining sporozoite shape and hepatocyte infectivity. We demonstrate that SIMP localises to sporozoite membrane, and its C-terminus is highly conserved between *P. berghei* and *P. falciparum* and is likely to be extracellular.

Our *in silico* predictions for probable cellular localisation and membrane association concurred well with genetic evidence that validated the role of SIMP in sporozoite membrane specific function. While functional mapping of precise C-terminus awaits further investigations, the SIMP-HA transgenics nonetheless, reveal the tag to be extracellular, a finding that has significant therapeutic implications by antibody mediated sporozoite neutralisation. Further, the spatiotemporal expression of SIMP during oocyst to salivary gland stages, reiterated the requirement of SIMP primarily in salivary gland sporozoite stage, that also explains why the oocyst sporozoites did not succumb to phenotypic alterations following depletion of SIMP. Such patterns of gene expression concur with independent programs of translational repression implicated in multiple sporozoite specific functions, including invasion of hepatocytes [265].

The link between SIMP depletion and loss of motility may hint to its role as an invasin like protein anchoring the sporozoite plasma membrane with the underlying molecular motor. Members of the TRAP family of protein connect to the molecular motor through an adaptor protein aldolase [210, 261]. Our findings that SIMP mutants fail to glide and infect hepatocytes may point to its likely interaction with Myo A and CAPs as predicted by STRING interactions and concurs with known roles of both interacting

partners in motility related functions viz., CAPs in microfilament turn over [284] and Myosin A in invasion [287]. Nonetheless, our studies of colocalization of SIMP HA with sporozoite membrane marker- TRAP, lack of colocalization of IMC marker-PIC5 with the membrane extensions in mutant sporozoites and distinct membrane detachment in *Pb*SIMP mutants argues to the point that SIMP may anchor sporozoite membrane to underlying molecular motor.

A previous study reported the phenotypic characterization of *Pb*SIMP mutants that was designated as PIMMS22 (Ukegbu *et al.*, 2021). Here the expression of PIMMS22 was demonstrated in gametocyte cytoplasm, ookinete periphery and in permeabilized as well as non-permeabilized midgut sporozoites. The PIMMS22 mutants produced a reduced number of ookinetes that manifested defect in the midgut invasion in *An. coluzzii* mosquitoes. However, in contrast to these findings, we noted no defect in sexual reproduction and oocyst formation in *An. stephensi* mosquitoes. The probable discrepancy can be attributed to the differential susceptibility of *Plasmodium* infections to different *Anopheles* species. A former study detected *Pb*SIMP peptide in the mass spectrometry analysis of *P. falciparum* and *P. yoelii* whole sporozoite lysates [262]. However, our studies provide definitive evidence for its membrane association.

The gross morphology of *Pb*SIMP mutants is reminiscent of the premature sporozoite transformation as seen for other mutants that lack eukaryotic initiation factor-2 alpha kinase (IK2) [288] and Pumilio-2 (Puff2) [289, 290]. The premature transformation of sporozoites in these instances have been attributed to loss of latency in sporozoites resulting from lack of phosphorylation of eIF2-alpha [288] and to possible loss of post transcriptional regulatory mechanism, in the absence of Pumilio-2 [289, 290]. In contrast to the mechanistic underpinning as described for these mutants, the possible EEF-like phenotype observed in our studies is likely due to membrane detachment in the absence of *Pb*SIMP. Further investigations are needed to ascertain physical interaction of *Pb*SIMP with components of molecular motor and if these interactions are mediated by specific adaptor proteins.

2.5 Conclusion

Taken together, our studies show for the first time that *Pb*SIMP is indispensable for producing functionally viable salivary gland sporozoites capable of maintaining regular shape and hence facilitating gliding and invasion of hepatocytes. This is likely possible if SIMP acts as an invasin linking extracellular receptors to molecular motor. Since the extracellular C-terminus of SIMP is highly conserved, antibodies that can effectively target this domain may have therapeutic potential in inhibiting sporozoite invasion. A possibility of such a speculation is both exciting and worth exploring considering the abundance of *Pb*SIMP on sporozoite membrane (nearly 50% or more as compared to CSP). In line with the notion that a vaccine encompassing multiple sporozoite surface antigens will induce better protection, SIMP may be a promising candidate, and can be included in combination with other potent antigens like CSP.

Chapter 3. Functional investigation of *Plasmodium berghei* Serine Repeat Antigen 3 (PbSERA 3)

3.1 Introduction

Current challenges in malaria eradication include the emergence of drug-resistant parasites, insecticide resistance and its effect on malaria transmission. The limitation of present antimalarial chemotherapy calls for a pressing need to identify new and effective antimalarial targets. Malarial proteases are potential targets for vaccine or drug-based therapies.

Proteases are a set of enzymes that catalyse proteolysis, breakdown of proteins by peptide bond hydrolysis into single amino acids or polypeptides. They are involved in numerous biological function such as regulation of protein catabolism and localization, regulation of protein-protein interactions and cell signalling. Protease can be classified into five distinct types depending upon their catalytic activity- serine, cysteine, aspartic, threonine, and metalloprotease [291]. Many infectious microorganisms use protease for their replication, survival and metabolism. Owing to the availability of information on the mechanism of action and active site structures, proteases are attractive targets for drug development. A number of protease inhibitors are now being used for the treatment of human diseases [292].

3.1.1 The role of proteases in *Plasmodium* biology

Plasmodium has a complex multistage life cycle that progresses through diverse host niches and multiple parasite stages. *Plasmodium* has erudite proteolytic machinery which consists of about 115-137 putative proteases expressing all five catalytic groups [293]. By using functional genetics and chemical inhibitors, several *Plasmodium* proteases were identified that participate in the various essential cellular process like invasion, egress, transcriptional regulation, stress response etc. During development *Plasmodium* parasite alternates between the asexual and sexual forms. The cell invasive forms are motile non-replicating forms called zoites, while those maturing within the replication competent parasitophorous vacuole are asexual forms, that upon rupture and exit from the host cell (egress) and establish the further infection [294, 295]. The expression of many specific parasite proteins is necessary to coordinate these cellular activities.

3.1.1.1 *Plasmodium* protease in invasion of host cells

Plasmodium has multiple invasion events during development, viz., the sporozoites invade salivary gland and hepatocytes, merozoites invade erythrocytes and ookinetes invade the mosquito midgut epithelium. *Plasmodium* being an obligate intracellular parasite, the extracellular 'zoites" must invade host cells as zoites are not viable outside the host cells for a long time. Sporozoites and merozoites are biochemically and morphologically different from each other, however, they share a highly conserved invasion machinery.

The secretory apical organelles- micronemes, rhoptries and dense granules facilitate the invasion process by the regulated discharge of surface proteins [90], though, the proteases mediating these processes are still unknown. During merozoite invasion, *Plasmodium* subtilisin-like protease 2 (SUB2) and rhomboids shed the surface adhesins of merozoites [296]. Two rhomboid members PfROM1 and *Pf*ROM4 are well characterized and has been demonstrated to cleave the transmembrane domain of a several adhesins. *Pf*ROM4 is localized to the parasite surface, particularly cleave an adhesin EBA175 which is involved in the sialic acid-dependent invasion pathway [297]. *Pf*ROM1 is localized at the apical end of merozoites [296], and cleaves AMA1 *in vitro* [298]. PbROM1 depletion did not affect asexual blood stages but manifested a defective PV at the hepatic stage [299]. Another key protein for RBC invasion is SUB2, an integral transmembrane protein that is secreted to parasite surface from micronemes [300]. SUB2 causes cleavage of merozoite 1/6/7 complex and AMA1 at the juxtamembrane site [301] and PTRAMP [302]. Attempts for SUB2 gene knockout were unsuccessful, indicating its essential role in blood stage development of the parasite. According to a recent study, SUB2 was also detected in gametocytes, and also released from ookinete during the invasion of midgut epithelial cells, suggesting its role in parasite sexual stage and midgut wall transversal, respectively [303]. TRAP, a sporozoite surface protein could be a potential substrate for rhomboid since mutation at the rhomboid cleavage site resulted in non-motile sporozoites [304]. One more study reported that four *P. berghei* rhomboids (PbROM4, 6, 7 and 8) appear to be essential during blood stages and PbROM3 is essential to sporozoites formation. The potential function of ROM6 to 8 is unknown,

however, it is predicated that ROM6 and ROM7 are localized to the mitochondria and apicoplast, respectively [305].

3.1.1.2 *Plasmodium* protease in egress from host cells

Once development is complete inside the host cell, escape is a necessary step for the parasite to progress through its life cycle. Like hepatic merozoites egress from hepatocytes, merozoites and sporozoites egress respectively from erythrocytes and oocysts [6, 84, 306, 307]. Parasite egress from the host cell is a rapid and tightly regulated process and it begins with initial degradation of PVM followed by RBC/hepatocyte membrane. In various studies, parasite proteases have been shown to be playing a pivotal role in these processes [295]. Before parasite egress, signalling events elicit the release of parasite proteins from exonemes and micronemes into PV and onto the surface of merozoites [119]. PKG, a cyclic-GMP dependent kinase triggers the release of subtilisin-like protease (SUB1) an exonemel protein in the lumen of PV, which processes several substrates that are required for parasite invasion and egress [308]. Serine repeat antigen (SERA) family proteins are known substrates of SUB1 protease. In *P. falciparum,* gene knockout studies demonstrated that *Pf*SERA5 and *Pf*SERA6 are essential and *Pf*SERA2, 3, 7 and 8 are dispensable for the development of asexual blood stages [309]. However, *Pb*SERA5 (also called ECP1) a homolog of *Pf*SERA8, is mainly expressed in sporozoites and disruption of *Pb*SERA5 resulted in a complete block of sporozoite egress from oocyst [187]. In *P. falciparum,* SERA 6 is essential for degradation of RBC membrane [310]. SUB1 KO parasites were unable to rupture PVM and thereby egress from hepatocyte in *P. berghei* [85]. Moreover, in a different study, *P. berghei* conditional knockout of SUB1 showed a defect in the development of schizont and merozoite maturation in hepatocytes, suggesting the different function of SUB1 in liver stages [311]. Another protease DPAP3 is also reported to participate in parasite egress as an inhibitor of DPAP3 prevents the parasite egress [312]. DPAP2 is specifically expressed in gametocytes and knock out of DPAP2 significantly decreases gamete egress [313]. In addition to parasite proteases, the human protease calpain 1 has also been linked in the regulation of parasite egress in *P. falciparum*. Immunodepletion of this calpain 1 prevented parasite egress [314].

3.1.1.3 *Plasmodium* protease in the manipulation of host cells

To replicate and develop within RBCs, parasite extensively modulates their host cell. Renovation of host cells facilitates cytoadherence, nutrient acquisition and immune invasion. *Plasmodium* exports about 10% of its proteome into the RBC across the PVM through the PTEX complex (Plasmodium Translocon for Exported Proteins) [315]. The majority of exported proteins have a protein export element (PEXEL) motif downstream to the secretory signal peptide. A protease plasmepsin V (PM V) in the endoplasmic reticulum recognizes and processes the PEXEL motif of proteins which are directed for export [316, 317].

3.1.1.4 *Plasmodium* protease in the nutrient acquisition

Parasites need a diversity of nutrients to develop inside the host cell. To acquire this, they import proteins into PV from host cytosol and then into food vacuole, a lysosome like- organelle where all imported proteins are processed in to single amino acids. Several different proteases are involved in the hemoglobin degradation, the main protein of RBCs that provide amino acids for protein synthesis of parasite and to create room to grow within the erythrocyte. The proteolytic machinery regulating this consist of three papain-like proteases, falcipains 2A, 2B &3 (FP2a, FP2b and FP3) [318-320], four aspartic proteases, plasmepsins I-IV (PMI, PMII, PM III & PM1V) [321] and metalloprotease falcilysin [322]. These proteases break down hemoglobin into oligopeptides. Several aminopeptidase functions downstream of hemoglobin degradation. Dipeptidyl aminopeptidase (DPAPS), homologs for human cathepsin C, works on smaller oligopeptides and consecutively cleaves N- terminal dipeptides. Three dipeptidyl aminopeptidases (DPAP 1-3) are known in *P. falciparum,* and DPAD1 and DPAP3 are expressed during asexual blood-stage development [323, 324].

3.1.1.5 *Plasmodium* SERA protease

Serine repeat antigens (SERAs) are a multigene family, conserved among all the species of genus *Plasmodium* and tandemly clustered on a single chromosome. SERAs are

highly expressed proteins in *Plasmodium* that are characterized by a central papain-like protease domain. According to their active site residue, SERAs can be categorized into two major clusters: serine-type SERA and cysteine-type SERA. Despite the fact that all *Plasmodium* species encode numerous SERA genes, the number varies. [325, 326]. Complete genome sequence of *Plasmodium* [327, 328] has identified nine (SERA1-9) and five (SERA 1-5) members of SERAs in *P. falciparum* and *P. berghei* respectively.

In *Plasmodium falciparum,* out of 9 SERAs, eight SERA genes (SERA1-8) are tandemly located on chromosome 2 while *Pf*-SERA9 is found on chromosome 9 [309, 329]. *Pf* SERA6-8 has cysteine residue at their canonical active site of the central papain-like protease domain while SERA1-5 and 9 have serine residue [294]. By using a single crossover recombination approach, disruption of SERA2, SERA3, SERA7 and SERA8 was successful. But attempts to delete SERA4, SERA5 and SERA6 failed suggesting a key role of these serine-type SERAs in the erythrocyte cycle [309]. Serine type SERA5 and cysteine-type SERA6 appear to have important roles in *P. falciparum* as they are highly expressed at the late trophozoite and schizont stage and all attempts to disrupt this gene during blood growth were unsuccessful [309, 326]. Previous work has shown extensive proteolytic processing of *Pf*SERA5 by SUB1 just prior to egress and the truncated product of SERA5 could induce antibodies, and that high antibody titers correlate with protection against severe infection [309, 325]. Recent studies show that conditional gene silencing of *Pf*SERA5 or both *Pf*SERA5 and *Pf*SERA4 simultaneously resulted in defect in egress and replication of parasites characterized by premature rupture of host cell and merozoites inability to disseminate efficiently [330]. Furthermore, *Pf*SERA6 null parasites exhibit normal PVM rupture and RBCM poration while RBCM rupture does not occur. It suggests that RBCM rupture and disassembly of RBC cytoskeleton is associated with *Pf*SERA6 dependent proteolytic cleavage [331]. *Plasmodium* SERAs that have important functions during blood stages remain attractive drug targets.

In *P. berghei,* five SERAs (*Pb*SERA1-5) are tandemly aligned on chromosome 3. *Pb*SERA1 and *Pb*SERA2 are serine-type SERA members while *PbSERA3*, 4 and 5 are cysteine-type SERAs. Quantification of the relative transcript abundance for all five SERAs (*Pb*SERA1-5)) using real-time PCR revealed a strongly enhanced expression of fours SERAS (*Pb*SERA1-4) in late liver stages and blood stages but PbSERA5 was predominantly expressed during the oocyst and sporozoites stage [325, 332]. The importance of SERAs in parasite liberation from the host cell was directly supported by

experimental genetics when targeted deletion of *Pb*SERA5 called as ECP1 a homolog of cysteine-type SERA 8 in *P. falciparum*, resulted in motile and viable sporozoites that were not able to egress from oocysts in *Anopheles* mosquito [187]. *Pb*SERA1 and *Pb*SERA2 exhibit differential expression at late stage of merozoite formation and gene knockout (single or double KO) of these genes shows a dispensable role in blood stages [332]. Rodent parasites lacking *Pb*SERA1 and *Pb*SERA2 also showed enhanced expression of cysteine-type *PbSERA3* which suggest the compensatory mechanism and potential functional relationship between distinct SERA subfamilies.

It has been demonstrated that inhibitors against cysteine proteases can block the *Plasmodium berghei* merozoite release in both *Plasmodium* liver stages and blood stages [6, 82, 306, 333]. The liberation of *Plasmodium berghei* merozoites from infected hepatocytes is mediated by cysteine proteases. To find the parasite cysteine proteases that are responsible for egress, the *P. berghei* genome was screened for the cysteine protease encoding genes [334]. Real-time PCR analysis revealed that transcript expression of *PbSERA3* being robustly unregulated in late live stage [334]. This likely suggests a possible role for *PbSERA3* in rupture of PVM to release merozoites into the cytoplasm of the host cell. To corroborate the role of *PbSERA3* in late liver stages, a TAP-tagged *PbSERA3* transgenic was generated against a non-conserved region of the *PbSERA3* and these parasites were used to understand *PbSERA3* processing. Indirect immunofluorescence assay unveiled that *PbSERA3* leaks into the cytoplasm of the host cells during merozoite development. In western blot analysis, processed *PbSERA3* was detected in cell extracts of detached hepatic cells and also schizont infected RBCs [334]. Interestingly, the processing of *PbSERA3* in asexual blood stage schizonts also concurred with the previous observations of PfSERA6 being proteolytically processed by *Pf*SUB1 and the *PbSERA3* being an orthologue of PfSERA6 [335].

Previously it has been demonstrated that E64, a cysteine protease inhibitor blocks merozoite egress from infected RBCs [6, 306]. In order to see the effect of E64 treatment on *Pb*SERA-3 processing, HepG2 cultures 48hpi were treated with E64. In control cells, PbSERA-3 was found in host cell cytoplasm whereas, in E64 treated cells, PbSERA-3 was restricted to the parasite, indicating that PbSERA-3 is indeed inhibited by E64 [334]. The proteolytic processing of proteases is an important process of PVM rupture in the liver-stage parasite.

Multiple attempts to delete *PbSERA3* gene in blood stages were unsuccessful so far, explaining its essential role in blood stages (E.D. Putrianti, F.F. Masduki, and K. Matuschewski, unpubl. data). Since the *PbSERA3* transcript is abundant in late liver stages, the possibility of its role at this stage of life cycle cannot be ruled out. We therefore aimed to characterize the role of *PbSERA3* beyond the blood stages in *P. berghei* life cycle. To achieve this, we employed Flp/FRT-based conditional mutagenesis system to disrupt *PbSERA3* locus in mosquito stage (oocyst) and analysed the SERA3 conditionally silenced sporozoites in liver stages. Interestingly, the sporozoites lacking *PbSERA3* edited locus invaded mosquito salivary glands and the EEFs derived from the mutant sporozoites showed development similar to WT EEFs. However, the late liver stage mutants failed to initiate blood stage infection stages likely suggesting a block in the egress of liver stage merozoites in the absence of *PbSERA3*.

3.2 Materials and methods

Majority of the experiments described in the chapter are similar to those mentioned in Chapter 2. To prevent redundancy, the materials and processes listed below are only explained in brief.

3.2.1 Cloning Vectors

Following plasmids were used for molecular cloning, expression, and genetic manipulation of parasites:

1. pTZ57R/T vector
2. pSKC-TRAP-GFP-2FRT

3.2.2 Primers

Primers used in the construction of *SERA3* cKO plasmid and to study the conditional KO parasites are given in Table 3.

S. No	Primer used for	Primer Name	Primer sequence	Expected product size
1	Generation of *PbSERA3* cKO construct	FP1	CGACCGCGGTATACGTATGTGCAATTAATA	500bp
2		RP1	GGCGTCGACATAAACTTGTTATAGTACAATGT	
3		FP2	GCCCTCGAG TGTTACACAACTAAGGAGAAAA	4556bp
4		RP2	GTAGCGGCCGCATATGTTTATTAAAATTATACA TAACAGAAGAGACA	
5		FP3	GACGGCGCGCC TTTTGAGGTGTGTGCAAATAA	605
6		FP3	CTGCCGCGG TTCCTCTTCAATTGTGTATTAC	
7	Confirmation of *PbSERA3 c*KO	FP4	ATGTAACTTTTGCGCTGTATA	597bp
8		RP4	TACTTTCTAGAGAATAGGAACT	
9		FP5	TACACTTTATGCTTCCGGCT	695bp

10	by integration PCR	RP5	TATTTTTATCCTTTTTCGTCA	
11	Confirmation of *PbSERA3* KO clonal lines	FP6	ACTCCACGTGTTAAAGCATATCG	755bp
12		RP6	TATATGAACTTAAAGACGAATA	
13	Excision specific primers	FP7	GTTGGACTTGATTTTTAAAATG	FP7+RP= 660bp FP8+RP7= 900bp
14		RP7	TTTGCAAGCATAATTAAGATGA	
15		FP8	TTACACACATAAAATGGCTAGTA	
16	*PbSIMP* expression analysis by real time PCR	FP9	TGCAAACGATGAAGTTAGC	148bp
17		RP8	CGAGTAATCCTTGTTTTGG	

3.2.3 Retrieval of *PbSERA3* gene sequence, amino acid sequences, alignment and similarity analysis of *PbSERA* orthologues

Two databases, Plasmodb (www.plasmodb.org) and Sanger's Gene database (http://www.genedb.org/Homepage/*Pb*erghei) were used to retrieve DNA and amino acid sequences of *PbSERA3* (*PBANKA_0304900*) gene. The gene IDS of *PbSERA3* orthologues were also retrieved from these databases which are as follows; *PySERA2*: *Plasmodium yoelii* (rodent) *PY17X_0305600*, PfSERA6: *Plasmodium falciparum* (human) *PF3D7_0207500* and PvSERA: *Plasmodium vivax*(human) *PVX_003800*. To check the homology between these orthologues, the Clustal Omega tool (http://www.ebi.ac.uk/Tools/msa/clustalo/) was used.

3.2.4 Total RNA isolation and cDNA synthesis

To study the gene expression analysis, total RNA was isolated from *P. berghei* parasites at different time points of life cycle stages. For isolation of RNA from the mosquito stages of the parasite, the day 14/15 midguts and day 18/19 salivary glands were obtained by dissecting nearly 50 female *A. stephensii* mosquitos infected with WT *P. berghei* parasites.

These infected midguts and salivary glands tissues were mechanically disrupted by a plastic pestle to release sporozoites. The samples were centrifuged and the supernatant containing sporozoites was taken for RNA isolation. Similarly, HepG2 cells harbouring EEFs at different developmental stages were collected following trypsinization of cells. These infected cells were washed 3 times with sterile PBS and pelleted by centrifugation. For asexual blood stages, WT *P. berghei* blood-stage parasites infected mice were used with 6-8 % parasitemia and the blood from these mice was harvested by cardiac puncture. The blood was lysed by using 0.5% saponin and pelleted at 10,000 rpm at 4°C. This pellet was washed 3 time with RNAse free sterile PBS and the sample was pelleted by centrifugation. RNA was extracted from both the liver stages and blood stages by using PureLink RNA isolation kit (Invitrogen) as per to the manufacturer's protocol. The eluted RNA was quantified using Nanodrop® ND-2000 spectrophotometer. Approximately 2µg of isolated RNA was subsequently processed to generate cDNA.

3.2.5 Expression analysis of *PbSERA3* by quantitative real-time PCR

To quantify the gene expression of *PbSERA3*, the absolute quantification method-Real-time PCR was used. A 148bp fragment of *PbSERA3* was PCR amplified using the primers FP5 and RP5, and further adenylated and ligated in the pTZ57R/T vector. The positive clone was confirmed by sequencing. The gene-specific standards were made from 10^2 to 10^8 copies/µl range by doing log dilution of the positive clone plasmid, following determination of its concentration. Similarly, *Pb 18S rRNA* standards were generated (135bp), that was used as an internal control. For real-time PCR, gene-specific standards and cDNA were generated from different *P. berghei* parasite life cycle stages of were used as a template along 0.25µM each of forward primer and reverse primer of either *PbSERA3* or *Pb 18S rRNA* and SYBR Green super mix. The data was normalized by obtaining the ratio of absolute copy numbers of *PbSERA3* and *Pb 18S rRNA* for each sample.

3.2.6 Construction of the *PbSERA3* conditional silencing vector

Due to the indispensable nature of *PbSERA3* in asexual parasite stage development, a conditional knockout strategy was employed to study the role of *PBSERA*-

3 in oocyst stage, salivary gland sporozoite stage and during the transformation of sporozoite in the hepatocyte. Towards construction of conditional silencing vector of *PbSERA3,* a 500 bp 5' homology region (5' HR) was PCR amplified with *PbSERA3* FP1 and RP1 primer set and cloned in the pSKC-TRAP-GFP-2FRT vector using SacII and SalI restriction enzymes. Next 4556 bp of *PbSERA3* encompassing the promoter and ORF was PCR amplified using FP2/RP2 primer set and cloned in XhoI and NotI of the recombinant pSKC-TRAP-GFP-2FRT vector carrying the 5' UTR region. The vector was further modified by cloning of 605 bp 3' homology region that was amplified using FP3/RP3 primer set and cloned with AscI and SacII restriction enzymes. The final targeting vector consisted of the following genetic elements in tandem- *PbSERA3* 5'UTR, 1st FRT site, promoter+ORF, 3'UTR of TRAP, hDHFR, 2nd FRT site, GFP and PbSERA3 3'UTR. All genetic elements other than the 5'UTR, promotor+ORF and 3'UTR were engineered within the pSKC-TRAP-GFP-2FRT vector. The construct was linearized by digesting it with SacII, and gel purified. The concentration of the gel purified *PbSERA3* conditional targeting vector was determined by using Nanodrop 2000.

3.2.7 Generation of *PbSERA3* conditional silenced parasite

Gel purified targeting vector of *PbSERA3* was electroporated into purified schizonts using Amaxa nucleofector II device following previously optimized program U-033. The conditional silencing construct was electroporated on a TRAP/FLPL parental parasite line, where FLPL (a thermolabile variant of FLP recombinase) expression is under influence of parasite TRAP promoter that is active in the oocyst stage of the parasite.

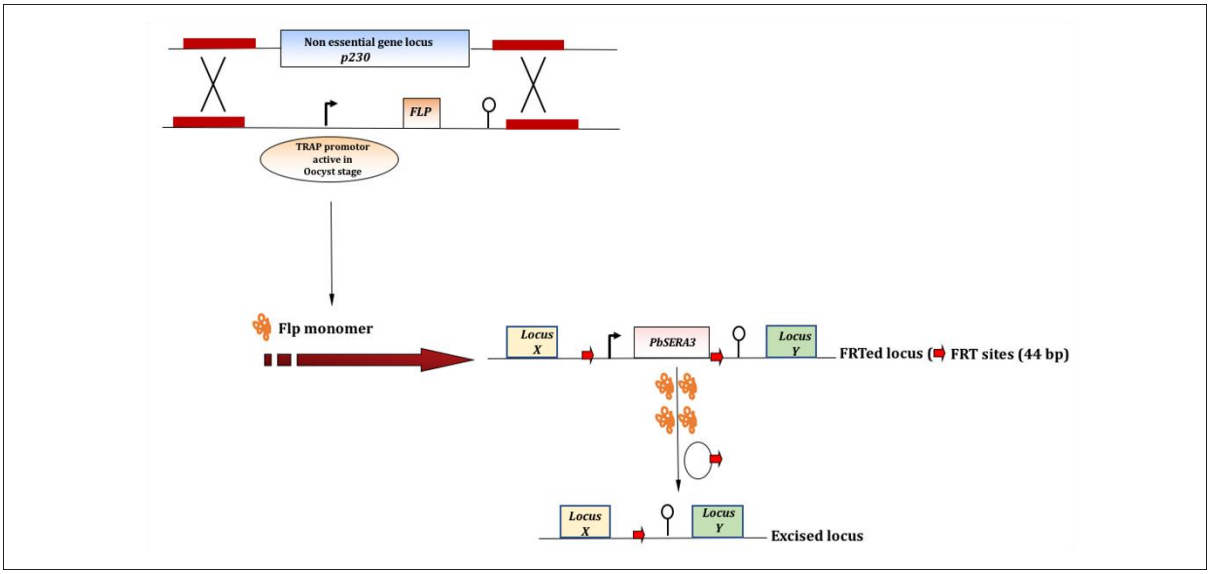


Figure 31. Schematic representation of TRAP/FLPL transgenic line generated by integrating the TRAP promotor sequence (oocyst stage-specific promoter) and FLP recombinase cassette at a dispensable p230 gene locus. For generating the *PbSERA3* conditional KO plasmid, 3 segments were PCR amplified parasite genomic DNA viz., (i) a 500 bp of *PbSERA3* 5' flanking region preceding the promoter, (ii) a 4556 bp of *PbSERA3* promotor+ORF region and (iii) a 605 bp of *PbSERA3* 3' flanking region and cloned respectively at SacII/SalI, XhoI/NotI and AscI/SacII in pSKC-TRAP-GFP-2FRT vector. The targeting vector was linearized with the SacII restriction enzyme. The targeting cassette was gel purified and electroporated into purified schizonts obtained from TRAP/FLPL parental line that express FlpL (a thermolabile variant of FLP recombinase) under the influence of TRAP promoter that is active in the oocyst stages. After successful recombination, the endogenous *PbSERA3* locus was replaced with an engineered SERA3 cassette (Promoter+ORF-TRAP 3'UTR- hDHFR) flanked by FRT sites, the recognition sequences of FlpL recombinase. Upon passing the parasites through mosquito, the sporozoites inside the oocyst undergo excision of FRTed SERA3 locus mediated by FlpL recombinase produced by the activity of TRAP promoter. Excision was confirmed by diagnostic PCR from gDNA of D16 (oocyst sporozoites) and D21 sporozoites (salivary gland sporozoites). The sporozoites lacking *PbSERA3* were further analysed for their ability to infect hepatocytes and transform into EEFs.

The transfected parasites were put on pyrimethamine drug selection and successful recombinant parasites were confirmed for stable site-specific integration of conditional KO cassette by diagnostic PCR. For 5'UTR part integration, diagnostic PCR was done with a set of primers- *PbSERA3* CKO FP4 designed beyond the site of integration and RP4 within the 1st FRT site that amplified 597 bp product from transfected parasites. For 3' region integration, diagnostic PCR was done using a set of primer- *PbSERA3* CKO

FP5/RP5 that were designed within hDHFR/TS promoter and after the site of integration respectively that amplified 695 bp product. After confirming site-specific integration of *PbSERA3* conditional KO cassette in the genome, limiting dilution was done to obtain a single clone population of *PbSERA3* conditional knock-out parasites. Two clones were obtained from two independent transfections.

3.2.8 Growth analysis of *PbSERA3* CKO parasites in blood stages

Approximately 1X10^3 infected RBC of WT GFP or *PbSERA3* cKO parasites (for both clones) were injected intravenously into 4–6-weeks old Swiss albino mice. Parasitemia was monitored daily for 7days to assess the asexual growth kinetics of *PbSERA3* conditional KO parasites by making Giemsa-stained blood smears daily. Asexual blood-stage propagation was analyzed by checking random 25 fields under light microscope.

3.2.9 Transmission of *PbSERA3* conditional KO (cKO) parasites to mosquito to achieve excision of *PbSERA3* locus in mosquito stages

Nearly 1x10^6 infected RBCs of either WT GFP or *PbSERA3* cKO parasites were injected into 4-6 weeks old Swiss albino mice. Following appearance of gametocyte stages in mice, female *A. stephensii* mosquitoes were fed with blood meal for 20min. Followed two consecutive feedings in a span of 24h, the mosquitoes were kept in an environmental chamber at 20^{o}C temperature and 80% humidity till 16 days. Then infected mosquitoes were maintained for 5 more days to 24^{0}C with 80% humidity where the FlpL activity is optimum. TRAP promoter is active from the oocyst stages of the parasite and expresses the FLPL in this stage that excises the endogenous locus flanked by FRT sites. On Day14 post-infection, mosquito midguts were dissected, and oocyst infectivity was observed by using 100x objective lens under fluorescence microscope. On day 21 post blood feed, salivary glands were dissected and observed for sporozoite burden. Both midguts and salivary glands were mechanically crushed and sporozoites were collected. Numbers of sporozoites were counted using hemocytometer. Oocysts and salivary glands harboring sporozoites were observed under an upright fluorescent microscope (Nikon Eclipse). By using NIS software, the images were captured, processed and deconvoluted.

3.2.10 Confirmation of *PbSERA3* FRTed locus excision by PCR

FlpL mediated excision of FRTed locus (*PbSERA3* Promoter+ORF, *TRAP 3' UTR* and *hDHFR* cassette) was confirmed in oocyst and salivary gland sporozoites on day14 and day21 post-infection respectively by diagnostic PCR. The Genomic DNA was isolated from both infected midguts and salivary glands sporozoites. To confirm excision, two different forward primers (FP7and FP8) were used along with one common reverse primer RP7. The FP8 was designed in a region beyond 5'HR and RP7 in the 3'UTR of Hsp70. An amplicon of 900bp was produced with this combination of primers that confirmed excision *PbSERA3* FRTed locus. The FP7 is present before 2nd FRT and when used with common RP7 produced an amplicon size of 600 bp from non-excised *PbSERA3* FRTed locus.

3.2.11 In vitro infectivity of *PbSERA3* conditional KO salivary gland sporozoites

A 24 well plate (Nunc, Cat No# 142475) was coated with collagen (BD bioscience, Cat# 354236) with the concentration of 10mg/ml overnight. The following day, approximately $2x10^5$ HepG2 cells were seeded and maintained in complete DMEM (cDMEM) at 5% CO_2 and 37°C. After confirming the attainment of a monolayer of HepG2 cells using phase contrast microscope, briefly, 2×10^4 sporozoites of either *PbSERA3* conditional KO or WT GFP were added to cells and the plate was centrifuged at 1500 rpm for 5 min. The cultures were maintained at 5% CO_2 and 37°C. The cell culture medium was replenished every 6h with cDMEM containing antibiotics solution (Gibco, Cat No#15240062) to avoid any contamination, till 65 h time point. At 12h, 36h, and 62h time points, coverslips were removed and fixed in 4% formalin solution (Sigma, Cat No# HT5011) and were stored in 4^0C till they were taken for immunofluorescence assay. These fixed cultures were examined for exo-erythrocytic forms (EEFs) by staining EEFs with rabbit anti- UIS4 (parasitophorous vacuolar membrane specific protein) antibody and immunoreactivity was revealed using an anti-rabbit secondary antibody conjugated to Alexa fluor 594.

3.2.12 Assessment of in vivo sporozoite infectivity of *PbSERA3* conditional KO parasites

To determine the pre-patent period of *PbSERA3* conditional KO sporozoites, different doses of mutant sporozoites ($5X10^3$, $1X10^4$, $2X10^4$, $5X10^4$ and $1X10^5$) were intravenously injected in groups of C57BL6 mice (3 mice in each experiment). WT GFP sporozoites were similarly injected that served as controls. Parasitemia was monitored for the next 7 days by examining Giemsa-stained blood smears using light microscope.

3.3 Results

3.3.1 Gene expression analysis of *PbSERA3* revealed maximal expression in 65hr EEF

To analyse the gene expression of *PbSERA3*, gene-specific standards were prepared for *PbSERA3* and *Pb 18S rRNA*. The cDNAs were generated from different stages of parasite and were run alongside standards. Following completion of PCR and data acquisition, the gene expression was expressed as copy numbers of either *PbSERA3* or *Pb18S rRNA*. Normalisation was done by obtaining the ratio of *PbSERA3* copy number versus *Pb 18S rRNA* copy number. The normalised data revealed the highest expression of *PbSERA3* at 65h of liver stage that concurs with a previously published study [334].

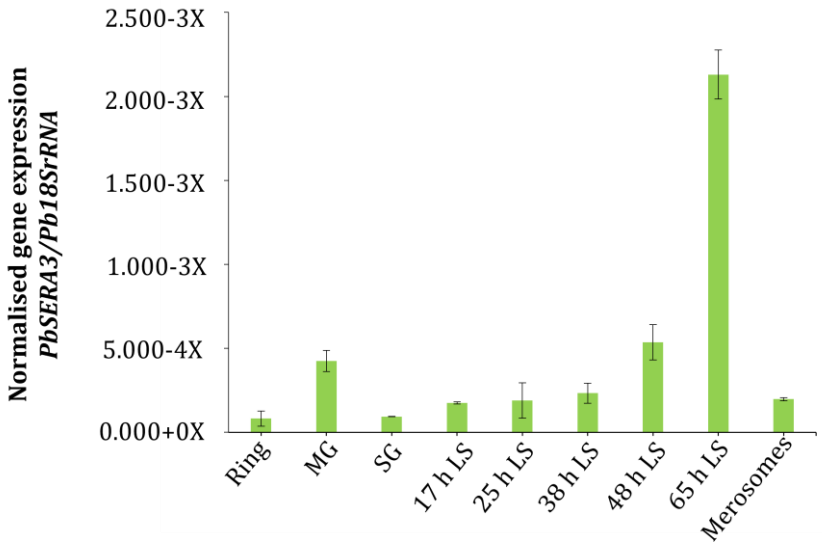


Figure 32. Gene expression analysis. Gene expression analysis of *PbSERA3* by real-time PCR reveals the highest expression at 65h of liver stage. The expression values were normalized with *Pb18SrRNA* (internal control gene) mRNA expression values for respective life cycle stages. Rings (asexual blood stage), MG: (midgut sporozoites), SG: (salivary glands sporozoites). LS: Liver stages: 17h, 25h, 38h, 48h, 65h and merosomes.

3.3.2 Successful integration of *PbSERA3* conditional KO construct at endogenous *PbSERA3* locus by double homologous recombination

A previous studies report that *PbSERA3* locus is refractory to gene manipulation, suggesting that it is highly indispensable. We therefore resorted to generate a *conditional PbSERA3* mutant line using a yeast-based Flp/FRT conditional mutagenesis system [336].

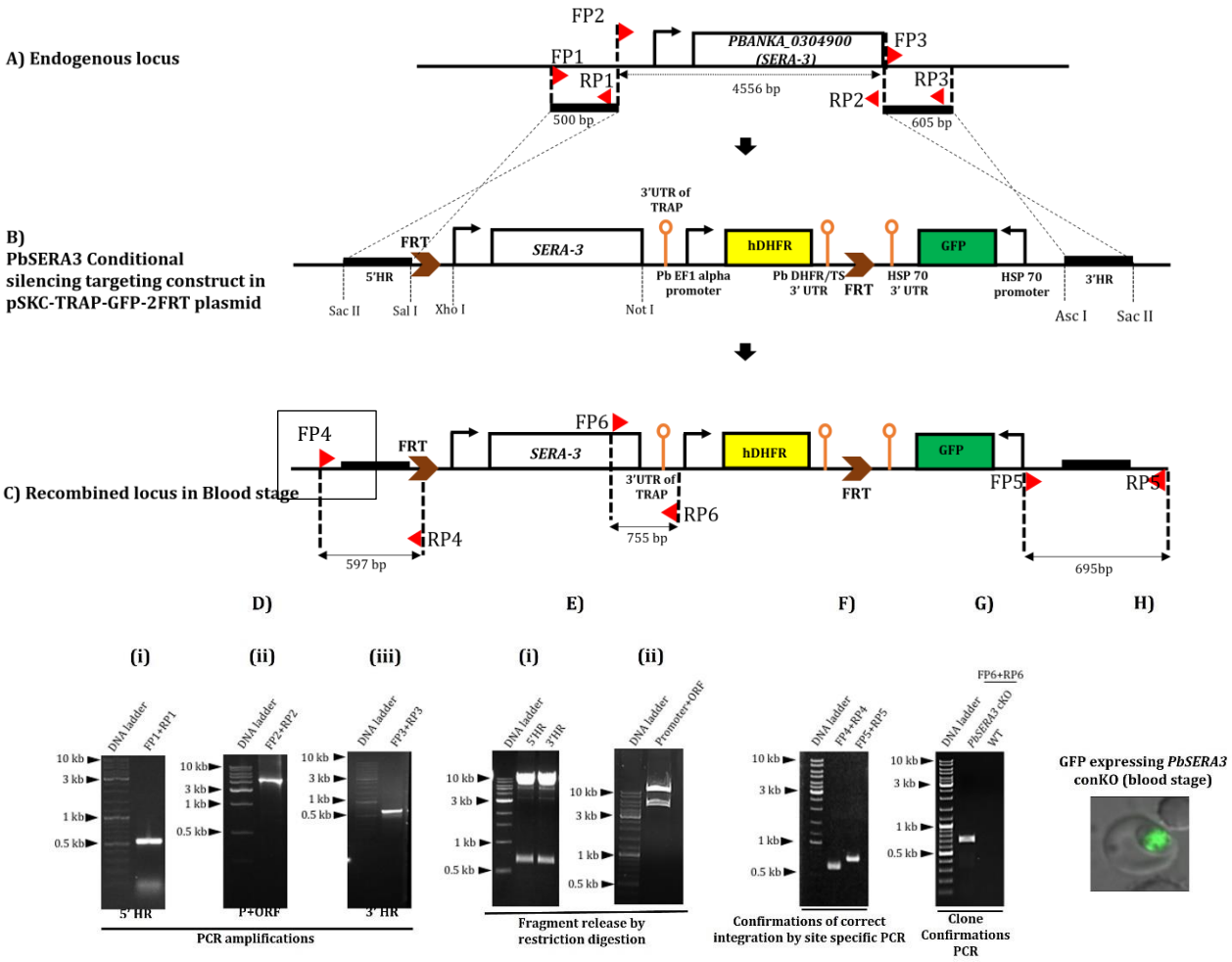


Figure 33. Generation of *PbSERA3* conditional knockout parasites. A) Representation of *PbSERA3* endogenous locus showing *PbSERA3* ORF, 5' and 3'UTRs. B) Elements of the targeting plasmid showing, 500 bp of *PbSERA3* 5' homology region followed by a 4556 bp of *PbSERA3* promotor+ORF, TRAP 3'UTR, hDHFR cassette, GFP cassette and 605 bp of *PbSERA3* 3' flanking region. The first FRT site is present in between *PbSERA3* 5' homology region and promoter+ORF, and the second FRT is after the hDHFR cassette. C) Recombined locus after successful double homologous recombination. In the recombined locus, an FRT site is integrated between *PbSERA3* 5'HR and promoter+ORF. D) (i)1% agarose gels showing PCR amplified products of 500 bp of 5' HR, (ii) 4556 bp of promoter+ORF, and (iii) 605 bp 3' HR of *PbSERA3* using primer set FP1/RP1, FP2/RP2 and FP3/RP3 respectively. E) Digestion products of (i)500 bp of 5' HR, (ii) 4556 bp

of promoter+ORF, and (iii) 605 bp 3' HR of *PbSERA3* following release with SacII/SalI and XhoI/NotI and AscI/SacII respectively F) Diagnostic PCRs showing the confirmation of site-specific integration of targeting cassette using a primer pair, one at beyond the site of integration in endogenous locus and the other within the targeting cassette. Primer sets FP4/RP4, FP5/RP5 yielded 597 bp and 695 bp amplicons that confirm 5' and 3' integration respectively. (G)Drug resistant parasites were clonal diluted and confirmed for single clone population without wild type using FP6/RP6 primers. H) Merged DIC image of *PbSERA3* conditional knockout parasites expressing GFP reporter.

The linearized targeting vector was electroporated in TRAP/FlpL expressing *P.berghei* parasite line and the parasites were intravenously injected into mice. After successful recombination the endogenous *PbSERA3* was replaced with FRTed *SERA3* along with hDHFR and GFP cassette engineered within the transfection plasmid (Figure 33C). The recombinant parasites were selected under drug pressure and correct site-specific integration of targeting construct at *PbSERA3* locus was confirmed by integration PCR using primer sets FP4/RP4 for 5'integration and FP5/RP5 for 3'integration that amplified 597 bp and 695bp respectively (Figure 33F). Limiting dilution was done to obtain a pure clonal population of *PbSERA3* conditional KO line. Two clonal lines of *PbSERA3* conditional KO was obtained from independent transfections and were referred to as C1 and C2. Both clonal lines were checked for absence of any WT *PbSERA3* locus using a primer set FP6/RP6 which amplified product of 755bp (Figure 33G). *PbSERA3* conditional KO clonal lines expressed GFP constitutively (Figure 33H).

3.3.3 *PbSERA3* conditional KO parasites showed normal blood stage propagation

As endogenous *PbSERA3* locus and 3'UTR regions were replaced with FRTed *SERA3* locus and TRAP 3'UTR, we analysed if the recombinant blood stage parasites propagated similar to WT parasites. In this regard, approximately $1X10^3$ infected RBC of either WT or *PbSERA3* conditional KO parasites were injected in a group of 3 mice and parasitemia was monitored for 7 days daily by examining Giemsa-stained blood smears. We noted no difference in the propagation of asexual stages of PbERA3 conditional KO parasites as compared to WT parasites and all asexual stages carrying FRTed locus were viable (Figure 34).

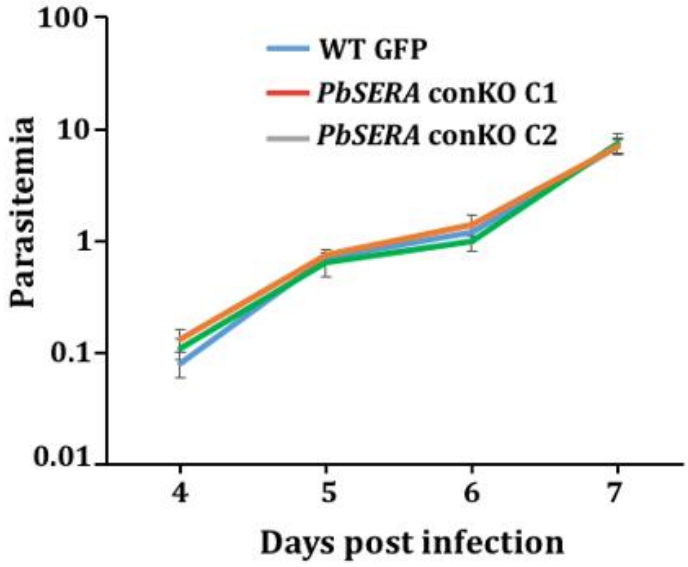


Figure 34. *PbSERA3* conditional KO parasites obtained in TRAP@FlpL line propagated asexually similarly to WT GFP parasites. Asexual blood stage propagation. $1X10^3$ infected RBCs of WT GFP and *PbSERA3* conditional KO parasites (C1 and C2) were injected intravenously into mice and parasitaemia was monitored daily for 7 days by microscopic observation of Giemsa-stained blood smears.

3.3.4 Conditional silencing of *PbSERA3* in mosquito vector

To study the role of SERA3 beyond sexual stages, *PbSERA3* conditional KO parasites were transmitted to *Anopheles* mosquitos. The mosquito midguts were dissected on day 14 and the oocyst burden was analysed. We noted that *PbSERA* conditional KO parasites formed oocyst whose frequency was similar to WT parasites (Figure 35A-B). Further, the sporulation pattern inside the oocyst was also comparable to WT (Figure 35C). Mechanical disruption of oocyst and quantification of oocyst sporozoites also revealed that numbers were comparable to WT (Figure 35D).

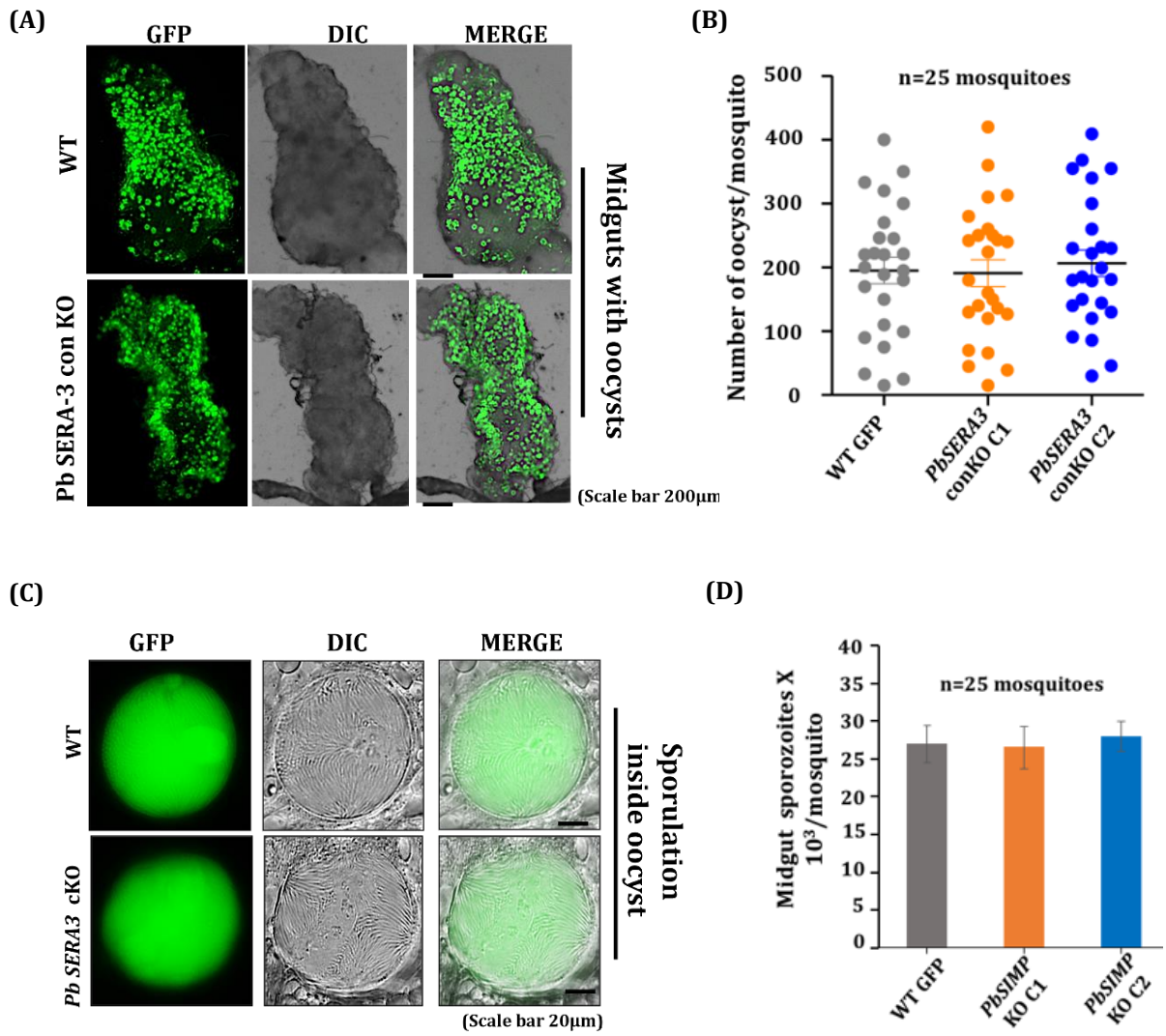


Figure 35. *PbSERA3* cKO parasites produced similar oocyst infectivity to that of WT GFP parasites. Infection was transmitted to *Anopheles* mosquito from mice harboring gametocytes stages of either *PbSERA3* conditional KO or WT GFP parasites to initiate sexual cycle in the mosquito. A) Dissected mosquito midguts on day 14 post-feeding showing oocysts for WT GFP and *PbSERA3* conditional KO parasites at similar rates. B) Dot plot for quantification of oocyst numbers from individual mosquitoes infected either with WT GFP or *PbSERA3* conditional KO parasites. Data represented as Mean+SD. C) Sporulation pattern in a single oocyst from both WT GFP and *PbSERA3* conditional KO parasites. D) Bar graph is drawn for quantification of midgut sporozoites per infected mosquito for WT GFP and *PbSERA3* conditional KO parasites.

To achieve optimal FlpL activity for maximum excision of FRTed locus, mosquitoes harboring the *PbSERA3* cKO parasites were transferred to 25°C from day 16 post blood meal. On day 21, salivary glands were dissected and sporozoites numbers were quantified. We noted *PbSERA3* conditional KO sporozoites numbers were similar to WT GFP sporozoites (Figure 36A-B)

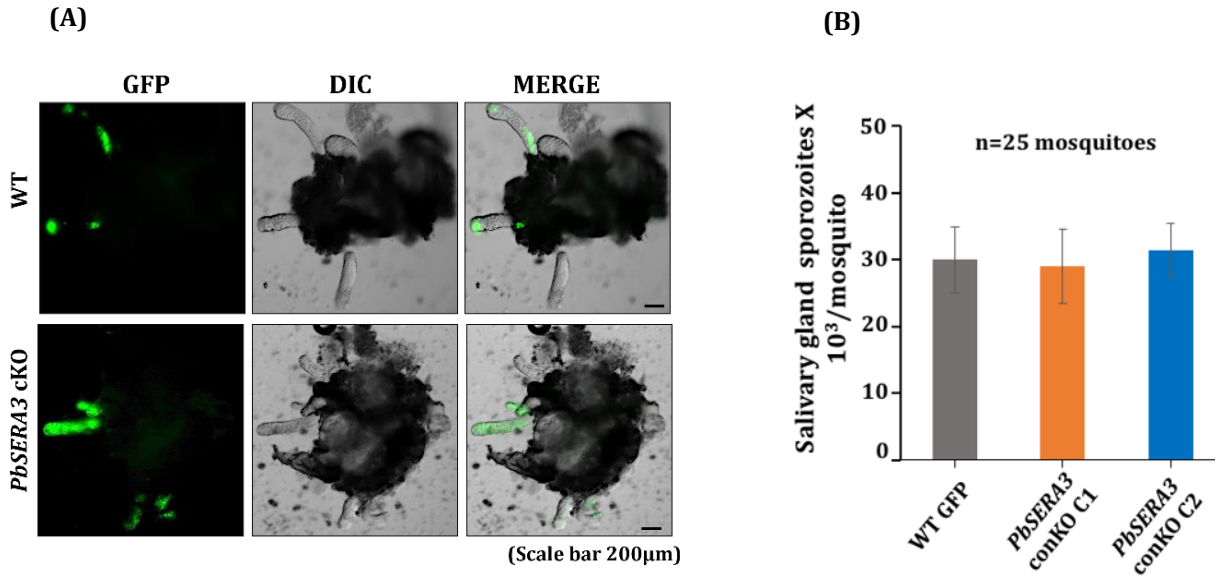


Figure 36. Conditional silencing of *PbSERA3* does not affect salivary gland sporozoite load. A) Representative images of an individual dissected mosquito salivary gland at D21 post blood meal infected with WT GFP or *PbSERA3* conditional KO parasites showing similar sporozoite burden. B) Bar graph for quantification of salivary glands sporozoites per infected mosquito for WT and *PbSERA3* conditional KO parasites showing sporozoites loads were comparable.

3.3.5 Excision PCR for *PbSERA3* cKO sporozoites

Since excision of the FRTed *PbSERA3* locus is expected in the oocyst stages, the genomic DNA was isolated from both infected midguts on D14 and salivary glands on D21. Two two diagnostic primer sets were designed FP7/RP7 and FP8/RP7 as indicated

in the strategy (Figure 37A-B) that amplified a product of 660bp and 900 bp respectively to allow detection of non-excised versus excised PbSERA3 locus.

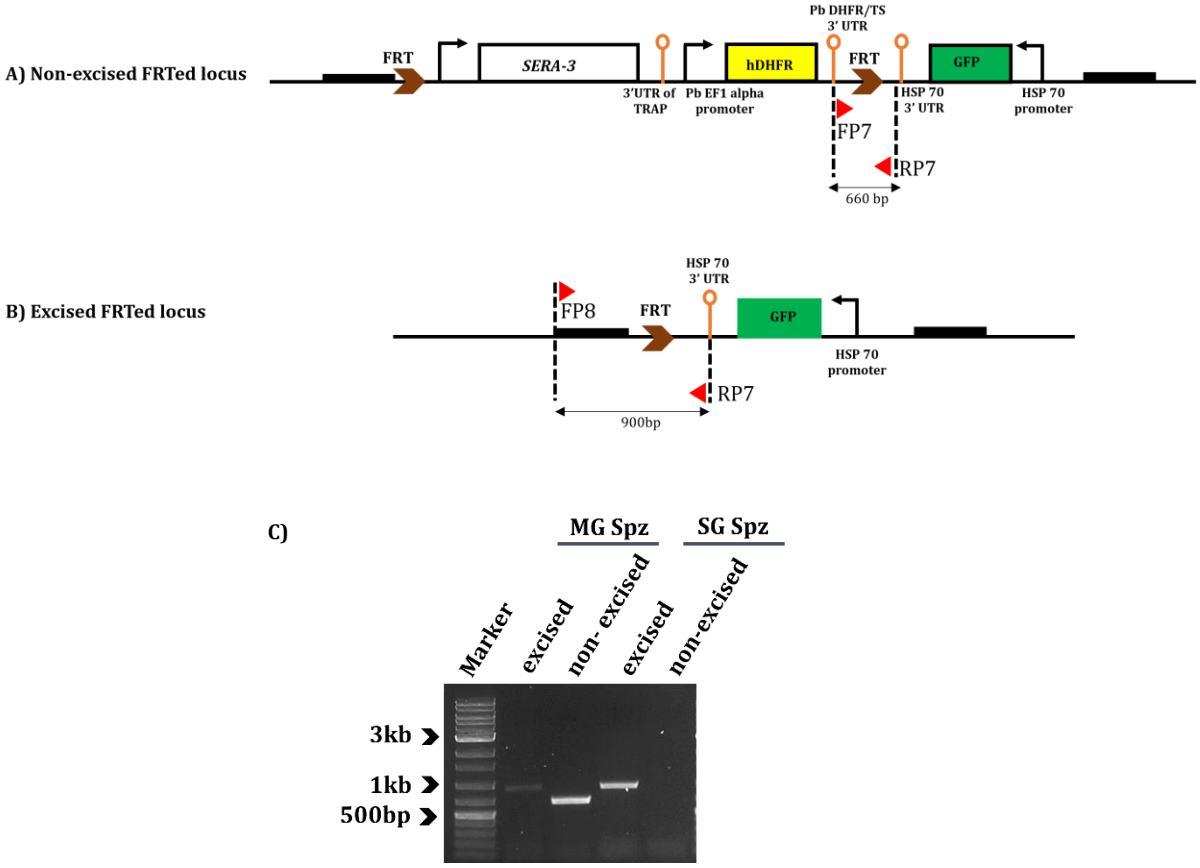


Figure 37. PCR-based confirmation of *PbSERA3* excision in the oocyst and salivary gland sporozoites. A) Schematic diagram of the *PbSERA3* FRTed locus in asexual blood stages before excision. B) Schematic diagram of the *PbSERA3* gene locus after excision. C) Excision-specific PCR analysis of genomic DNA of oocyst and salivary gland sporozoites. On Day 14 and Day 21 genomic DNA was isolated from both oocyst and salivary sporozoites post-infection and analysed using two different primer sets FP7/RP7 and FP8/RP7 as indicated in A & B. A) Product size of 900 bp indicated excision and 660 bp indicated the presence of non-excised parasites. Based on the intensity of the product amplified, the extent of excision was judged. Our results showed partial excision of *PbSERA3* locus in midgut sporozoites by detecting an amplicon size of 900 bp with primers FP8/RP7 while a prominent band corresponding to an amplicon size 660 bp with primers FP7/RP7 confirmed non-excised locus. Near complete excision of *PbSERA3* locus in salivary gland sporozoites was confirmed by same set of primers that gave 900 bp amplicon alone while no amplicon of 660 bp corresponding to non-excised locus was detected.

We noted that in D14 oocyst stage, the locus remained non-excised predominantly, while in salivary glands, the locus was completely excised (Figure 37C). Since no non -excised population of sporozoites were detected in salivary glands, this indicated that *PbSERA3* is not required for sporozoites for salivary glands colonization. These conditionally silenced sporozoites were further used to analyze the role of *PbSERA3* in liver stage development.

3.3.6 *PbSERA3* conditional KO parasites showed normal EEF development as WT GFP parasites

To analyse the development of *PbERA3* conditional KO parasites in the hepatocytes *in vitro,* HepG2 cells were infected with $2x10^4$ salivary gland sporozoites. HepG2 cell cultures were fixed at 12h, 36h and 62 h post-infection. The EEFs derived from sporozoites that have conditionally excised *PbSERA3* locus were analysed by staining them with anti-UIS4 antibody, a marker for PVM [61]. Analysis of EEF growth revealed that EEFs developing from *PbSERA3* excised sporozoites were comparable to WT GFP EEFs both in morphology and development (Figure 38), thus suggesting that *PbSERA3* depletion had no effect on EEF development till 62 h.

3.3.7 Analysis of prepatency in *PbSERA3* KO sporozoites

To analyse the transmission ability of *PbSERA3* conditional KO sporozoites in the mammalian host, C57BL/6 mice were intravenously infected with different doses of salivary gland sporozoites viz., $5x10^3$, $1x10^4$, $5x10^4$ and $1x10^5$ and and monitored the pre-patent period by examination of Giemsa-stained blood smears daily for 15 days. Surprisingly, in all the experiments using *PbSERA3* conditional KO sporozoites, we observed no blood-stage infection, whereas the WT sporozoites became patent on 3-3.5 days (table 4).

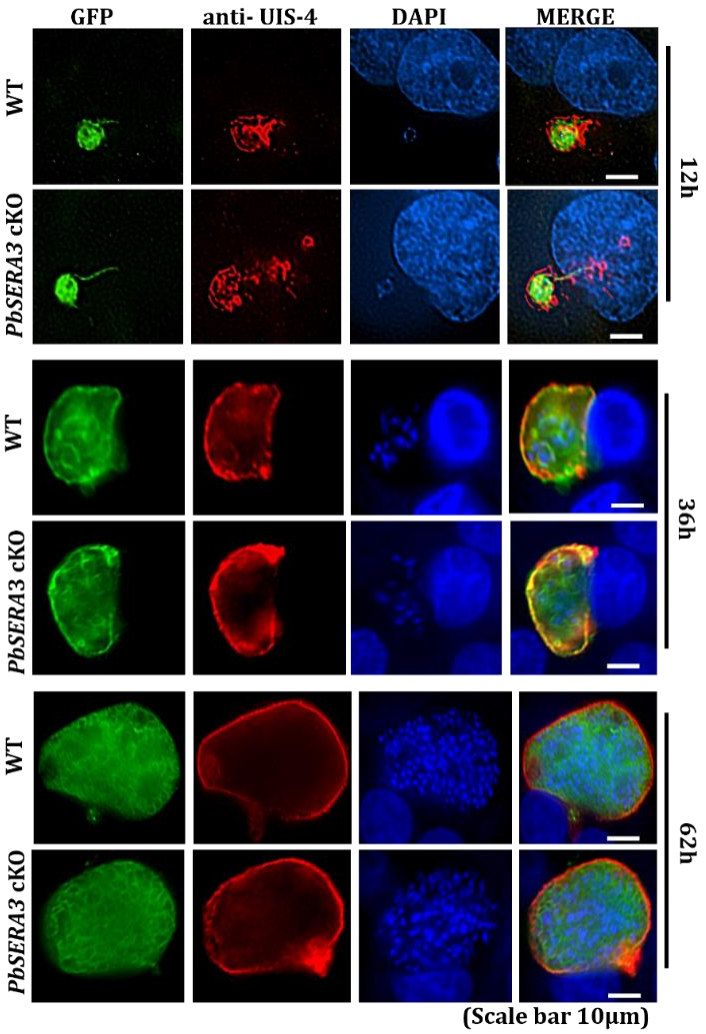


Figure 38. *PbSERA3* is not essential for liver stage development of parasite. On day 21, salivary gland sporozoites were isolated by dissecting infected mosquito. Approximately, $2X10^4$ sporozoites of either WT GFP or *PbSERA3* conditional KO sporozoites were added to HepG2 cell cultures. The cultures were fixed at 12h, 36h and 62h time points. The development of EEFs at different time points was revealed by staining with anti-UIS4 (PVM marker) antibody and DAPI was used to stain nuclei of HepG2 cells and parasites. It was observed that EEFs derived from *PbSERA3* conditional KO sporozoites at all indicated time points were normal as wild-type EEFs.

Experiment number	Parasite strain	Numbers of animals used for intravenous injection	Number of sporozoites injected per animal	Number of animals positive for blood-stage infection	Pre-patent period
Experiment 1	WT	4	$5X10^3$	3/3	3.5 day
	PbSERA3 conditional KO	4	$5X10^3$	0/3	None
Experiment 2	WT	3	$1X10^4$	3/3	3 Days
	PbSERA3 conditional KO	3	$1X10^4$	0/3	None
		3	$5X10^4$	0/3	None
		2	$1X10^5$	0/2	None

Table 4. Infectivity of *PbSERA3* conditional KO sporozoites in C57BL/6 mice. Mice were intravenously inoculated with *PbSERA3* conditional KO or WT sporozoites and pre-patency was monitored from day 3 onwards by making Giemsa-stained blood smears. *PbSERA3* conditional KO sporozoites failed to give blood-stage infection, while WT sporozoites gave a breakthrough infection on days 3-3.5.

3.4 Discussion

Dissemination of parasites from host cells is an obligatory process for continuation of life cycle. Therefore, the egress themes are common at multiple life cycle stages viz., the liver stages, the asexual schizont stages and the oocyst stage. There are multiple evidences that indicate that the mediators of this important biological process are proteases, in particular the SERA family members. *PfSERA5* and *PfSERA6* are essential for merozoite egress from iRBCs. [330, 331]. *PbSERA5* is required for sporozoite egress from oocyst in mosquito midgut.

The Plasmodium parasite, like many obligate intracellular pathogens, has evolved effective molecular strategies for egress from the host cell. So far, all functional characterisations done on the Plasmodium SERA family proteins suggest that these proteases play a important role in parasite egress. To date, *PbSERA1*, *PbSERA2* and *PbSERA4* roles have been tested for their contribution in liver-stage egress which revealed that *PbSERA4* is required for exit from the liver and to initiate blood-stage infection [337].

It has been shown that *PfSERA6* is an essential protease involved in blood-stage parasite egress. The attempts for targeted gene disruption of *PfSERA6* gene [331] or active site Cys644 substitution with an Ala residue [335] were unsuccessful, suggesting that PfSERA6 is indispensable for parasite growth in blood stages. Furthermore, studies on *PbSERA3*, P. berghei ortholog of *PfSERA6* is sensitive to E64, a cysteine protease inhibitor. *PbSERA3* is expressed in late liver stages, released into the host cytoplasm upon rupture of PVM. In the presence of E64, *PbSERA3* is restricted to the parasites and parasites failed to egress from the infected hepatocyte [334]. *PbSERA3* is a 130 kDa precursor protein that undergoes maturation following specific processing by *PbSUB1* in liver stages [85]. It's worth noting that *PfSERA6*, ortholog of the *PbSERA3* in P. falciparum, undergoes an initial cleave by PfSUB1 in blood stages, followed by a second autocatalytic step that is required for RBC rupture thereby merozoite egress. In both *P. falciparum* and *P. knowlesi*, drug-like inhibitors of SERA6 auto-processing prevent parasite egress [338].

Another interesting topic is why these parasites simultaneously express numerous proteases that are very similar. The plausible explanation the expression of many SERA proteins at similar times in both blood stages and liver stages might influence one another's activity. One SERA could, for example, change the function of another by

influencing substrate identification or activation via proteolytic processing. Though this has been suggested for the serine-type SERA proteins, in particular, it is not possible to rule it out for the cysteine-type SERAs.

Till now, functional investigation of PfSERA6 in hepatic stages is not done. Since PfSERA6 is critical for blood-stage development of the parasites and failed gene disruption attempts in the blood stages, we resorted to using P. berghei parasites for functional characterisation of *PbSERA3* (PfSERA6 ortholog) in sporozoite and liver stages. We used a robust conditional silencing system (Cre/lox) and investigated the role of *PbSERA3*. Our studies have showed a likely role of *PbSERA3* in exit from the liver cell to initiate blood-stage infection. Transcription and localization studies of *PbSERA3* revealed that *PbSERA3* is expressed in the late liver stages. Like the egress of blood-stage merozoites, the liberation of merozoites from infected hepatocytes is a well-orchestrated multistep process. Cysteine proteases play a key role in PVM breakdown. Upon PVM disruption, *PbSERA1* and *PbSERA3*-C terminus part were found in the host cytoplasm (Volker T Heussler et al 2008), which suggests the likely role of these proteins in host cell rupture/death. In concordance with these observations, *PbSERA3* conditionally silenced sporozoites failed to initiate break-through infection in mice after administering by both intravenous route and natural transmission by mosquito bite.

The failure of *PbSERA3* knockout parasites to initiate blood-stage infection can be exploited to test its ability to induce an immune response which could give protection to animals from reinfection. Though late-liver stage arresting parasites often confers strong protection against wild-type parasites challenge, it often poses the risk of breakthrough infections. Since depletion of *PbSERA3* protein arrest the parasite at late liver stages, a combination of its deletion with other genes that are involved in EEF growth can ensure the complete attenuation that might be used to produce a safe and efficacious whole parasite vaccine. Given the current focus on malarial molecular targets ideal for drug and vaccine development, we have showed that *PbSERA3* plays a key role in transmission of disease which makes this protease an even more promising therapeutic candidate.

Summary

Summary

In the current study, we investigated the functional role of two *Plasmodium* genes/proteins: (1) PbSIMP, a surface protein that is abundantly expressed in sporozoites, and (2) PbSERA3, a cysteine protease that is required for egress of parasites from infected cell. By using reverse genetics approach, we unravelled previously unknown functions of these proteins that greatly facilitated the understanding of the parasite biology for developing the therapeutic interventions against this deadly disease.

We successfully generated PbSIMP knockout parasites in *Plasmodium berghei* (Pb) and studied the fate of PbSIMP knockout parasites across all life cycle stages of parasite including their cyclical infection between vertebrate host and the female *Anopheles* mosquito. Our findings reveal for the first time that PbSIMP is indispensable to produce functionally viable salivary gland sporozoites that can maintain regular shape, glide, and invade hepatocytes. We observed sporozoite membrane blebbing and loss membrane integrity in the absence of PbSIMP. Since it is required for maintaining membrane integrity and gliding motility of the sporozoites, it is likely possible that SIMP acts as an invasin linking extracellular receptors to molecular motor. Using transgenic PbSIMP HA parasites and anti-HA mouse antibodies, we showed that PbSIMP is a surface protein with C-terminus part of it is extracellular. Since the extracellular C-terminus of SIMP is highly conserved, antibodies that can effectively target this domain may have therapeutic potential in inhibiting sporozoite invasion.

Since PbSERA3 is critical for blood-stages, we generated a conditional mutant of PbSERA3 using a FLP/FRT site specific recombination system. This is a yeast-based recombination system, where FlpL (a thermolabile variant of Flp) is expressed under oocyst specific promoter (TRAP promoter) that allows the excision of Flirted PbSIMP thus leading to its temporal inactivation. PbSERA3 conditional mutants were able to produce functionally viable sporozoites that can infect hepatocytes. *In vitro* studies using PbSERA3 conditional mutant sporozoites revealed that they able to grow till 62h in similar way to WT parasites. However, *PbSERA3* conditional mutants failed to initiate blood stage break through infection upon intravenous injection of sporozoites and natural transmission by mosquito mite. Having shown that the mutant have normal

development till 62h, absence of blood stage infection may likely hint to the role of PbSERA3 in forming merosomes which needs further investigation.

Refrences

1. Marsh, K., *Malaria--a neglected disease?* Parasitology, 1992. **104 Suppl**: p. S53-69.
2. McFadden, G.I., *Plasmodia - don't.* Trends Parasitol, 2012. **28**(8): p. 306.
3. Perkins, S.L., *Malaria's many mates: past, present, and future of the systematics of the order Haemosporida.* J Parasitol, 2014. **100**(1): p. 11-25.
4. Barber, B.E., et al., *World Malaria Report: time to acknowledge Plasmodium knowlesi malaria.* Malar J, 2017. **16**(1): p. 135.
5. Amino, R., et al., *Quantitative imaging of Plasmodium transmission from mosquito to mammal.* Nat Med, 2006. **12**(2): p. 220-4.
6. Salmon, B.L., A. Oksman, and D.E. Goldberg, *Malaria parasite exit from the host erythrocyte: a two-step process requiring extraerythrocytic proteolysis.* Proc Natl Acad Sci U S A, 2001. **98**(1): p. 271-6.
7. Baker, D.A., *Malaria gametocytogenesis.* Mol Biochem Parasitol, 2010. **172**(2): p. 57-65.
8. de Koning-Ward, T.F., P.R. Gilson, and B.S. Crabb, *Advances in molecular genetic systems in malaria.* Nat Rev Microbiol, 2015. **13**(6): p. 373-87.
9. Medica, D.L. and P. Sinnis, *Quantitative dynamics of Plasmodium yoelii sporozoite transmission by infected anopheline mosquitoes.* Infect Immun, 2005. **73**(7): p. 4363-9.
10. Rosenberg, R., et al., *An estimation of the number of malaria sporozoites ejected by a feeding mosquito.* Trans R Soc Trop Med Hyg, 1990. **84**(2): p. 209-12.
11. Kebaier, C., T. Voza, and J. Vanderberg, *Kinetics of mosquito-injected Plasmodium sporozoites in mice: fewer sporozoites are injected into sporozoite-immunized mice.* PLoS Pathog, 2009. **5**(4): p. e1000399.
12. Vaughan, J.A., et al., *Infectivity of Plasmodium berghei sporozoites delivered by intravenous inoculation versus mosquito bite: implications for sporozoite vaccine trials.* Infect Immun, 1999. **67**(8): p. 4285-9.
13. Baldacci, P. and R. Menard, *The elusive malaria sporozoite in the mammalian host.* Mol Microbiol, 2004. **54**(2): p. 298-306.
14. Kappe, S.H., C.A. Buscaglia, and V. Nussenzweig, *Plasmodium sporozoite molecular cell biology.* Annu Rev Cell Dev Biol, 2004. **20**: p. 29-59.
15. Matsuoka, H., et al., *A rodent malaria, Plasmodium berghei, is experimentally transmitted to mice by merely probing of infective mosquito, Anopheles stephensi.* Parasitol Int, 2002. **51**(1): p. 17-23.
16. King, C.A., *Cell surface interaction of the protozoan Gregarina with concanavalin A beads - implications for models of gregarine gliding.* Cell Biol Int Rep, 1981. **5**(3): p. 297-305.
17. Russell, D.G. and R.E. Sinden, *The role of the cytoskeleton in the motility of coccidian sporozoites.* J Cell Sci, 1981. **50**: p. 345-59.
18. Vanderberg, J.P., *Studies on the motility of Plasmodium sporozoites.* J Protozool, 1974. **21**(4): p. 527-37.
19. Pradel, G., S. Garapaty, and U. Frevert, *Proteoglycans mediate malaria sporozoite targeting to the liver.* Mol Microbiol, 2002. **45**(3): p. 637-51.
20. Pradel, G. and U. Frevert, *Malaria sporozoites actively enter and pass through rat Kupffer cells prior to hepatocyte invasion.* Hepatology, 2001. **33**(5): p. 1154-65.
21. Amino, R., et al., *Host cell traversal is important for progression of the malaria parasite through the dermis to the liver.* Cell Host Microbe, 2008. **3**(2): p. 88-96.
22. Ishino, T., et al., *Cell-passage activity is required for the malarial parasite to cross the liver sinusoidal cell layer.* PLoS Biol, 2004. **2**(1): p. E4.
23. Ishino, T., Y. Chinzei, and M. Yuda, *A Plasmodium sporozoite protein with a membrane attack complex domain is required for breaching the liver sinusoidal cell layer prior to hepatocyte infection.* Cell Microbiol, 2005. **7**(2): p. 199-208.
24. Bhanot, P., et al., *A surface phospholipase is involved in the migration of plasmodium sporozoites through cells.* J Biol Chem, 2005. **280**(8): p. 6752-60.

25. Kaiser, K., et al., *A member of a conserved Plasmodium protein family with membrane-attack complex/perforin (MACPF)-like domains localizes to the micronemes of sporozoites.* Mol Biochem Parasitol, 2004. **133**(1): p. 15-26.
26. Myung, J.M., P. Marshall, and P. Sinnis, *The Plasmodium circumsporozoite protein is involved in mosquito salivary gland invasion by sporozoites.* Mol Biochem Parasitol, 2004. **133**(1): p. 53-9.
27. Sultan, A.A., et al., *TRAP is necessary for gliding motility and infectivity of plasmodium sporozoites.* Cell, 1997. **90**(3): p. 511-22.
28. Ancsin, J.B. and R. Kisilevsky, *A binding site for highly sulfated heparan sulfate is identified in the N terminus of the circumsporozoite protein: significance for malarial sporozoite attachment to hepatocytes.* J Biol Chem, 2004. **279**(21): p. 21824-32.
29. Cerami, C., F. Kwakye-Berko, and V. Nussenzweig, *Binding of malarial circumsporozoite protein to sulfatides [Gal(3-SO4)beta 1-Cer] and cholesterol-3-sulfate and its dependence on disulfide bond formation between cysteines in region II.* Mol Biochem Parasitol, 1992. **54**(1): p. 1-12.
30. Cerami, C., et al., *The basolateral domain of the hepatocyte plasma membrane bears receptors for the circumsporozoite protein of Plasmodium falciparum sporozoites.* Cell, 1992. **70**(6): p. 1021-33.
31. Coppi, A., et al., *The Plasmodium circumsporozoite protein is proteolytically processed during cell invasion.* J Exp Med, 2005. **201**(1): p. 27-33.
32. Coppi, A., et al., *Heparan sulfate proteoglycans provide a signal to Plasmodium sporozoites to stop migrating and productively invade host cells.* Cell Host Microbe, 2007. **2**(5): p. 316-27.
33. Menard, R., *The journey of the malaria sporozoite through its hosts: two parasite proteins lead the way.* Microbes Infect, 2000. **2**(6): p. 633-42.
34. Kappe, S.H., et al., *Apicomplexan gliding motility and host cell invasion: overhauling the motor model.* Trends Parasitol, 2004. **20**(1): p. 13-6.
35. Wengelnik, K., et al., *The A-domain and the thrombospondin-related motif of Plasmodium falciparum TRAP are implicated in the invasion process of mosquito salivary glands.* EMBO J, 1999. **18**(19): p. 5195-204.
36. Dundas, K., et al., *Alpha-v-containing integrins are host receptors for the Plasmodium falciparum sporozoite surface protein, TRAP.* Proc Natl Acad Sci U S A, 2018. **115**(17): p. 4477-4482.
37. Silvie, O., et al., *Hepatocyte CD81 is required for Plasmodium falciparum and Plasmodium yoelii sporozoite infectivity.* Nat Med, 2003. **9**(1): p. 93-6.
38. Risco-Castillo, V., et al., *CD81 is required for rhoptry discharge during host cell invasion by Plasmodium yoelii sporozoites.* Cell Microbiol, 2014. **16**(10): p. 1533-48.
39. Risco-Castillo, V., et al., *Malaria Sporozoites Traverse Host Cells within Transient Vacuoles.* Cell Host Microbe, 2015. **18**(5): p. 593-603.
40. Rodrigues, C.D., et al., *Host scavenger receptor SR-BI plays a dual role in the establishment of malaria parasite liver infection.* Cell Host Microbe, 2008. **4**(3): p. 271-82.
41. Yalaoui, S., et al., *Scavenger receptor BI boosts hepatocyte permissiveness to Plasmodium infection.* Cell Host Microbe, 2008. **4**(3): p. 283-92.
42. Kaushansky, A., et al., *Malaria parasites target the hepatocyte receptor EphA2 for successful host infection.* Science, 2015. **350**(6264): p. 1089-92.
43. Langlois, A.C., et al., *Plasmodium sporozoites can invade hepatocytic cells independently of the Ephrin receptor A2.* PLoS One, 2018. **13**(7): p. e0200032.
44. Kaushansky, A. and S.H. Kappe, *Selection and refinement: the malaria parasite's infection and exploitation of host hepatocytes.* Curr Opin Microbiol, 2015. **26**: p. 71-8.
45. Ben Chaabene, R., G. Lentini, and D. Soldati-Favre, *Biogenesis and discharge of the rhoptries: Key organelles for entry and hijack of host cells by the Apicomplexa.* Mol Microbiol, 2021. **115**(3): p. 453-465.

46. Arredondo, S.A., et al., *The Micronemal Plasmodium Proteins P36 and P52 Act in Concert to Establish the Replication-Permissive Compartment Within Infected Hepatocytes.* Front Cell Infect Microbiol, 2018. **8**: p. 413.
47. Bano, N., et al., *Cellular interactions of Plasmodium liver stage with its host mammalian cell.* Int J Parasitol, 2007. **37**(12): p. 1329-41.
48. Baum, J., et al., *A conserved molecular motor drives cell invasion and gliding motility across malaria life cycle stages and other apicomplexan parasites.* J Biol Chem, 2006. **281**(8): p. 5197-208.
49. Gonzalez, V., et al., *Host cell entry by apicomplexa parasites requires actin polymerization in the host cell.* Cell Host Microbe, 2009. **5**(3): p. 259-72.
50. Srinivasan, P., et al., *Binding of Plasmodium merozoite proteins RON2 and AMA1 triggers commitment to invasion.* Proc Natl Acad Sci U S A, 2011. **108**(32): p. 13275-80.
51. Giovannini, D., et al., *Independent roles of apical membrane antigen 1 and rhoptry neck proteins during host cell invasion by apicomplexa.* Cell Host Microbe, 2011. **10**(6): p. 591-602.
52. Silvie, O., et al., *A role for apical membrane antigen 1 during invasion of hepatocytes by Plasmodium falciparum sporozoites.* J Biol Chem, 2004. **279**(10): p. 9490-6.
53. Schussek, S., et al., *Immunization with apical membrane antigen 1 confers sterile infection-blocking immunity against Plasmodium sporozoite challenge in a rodent model.* Infect Immun, 2013. **81**(10): p. 3586-99.
54. Roy, C.R., S.P. Salcedo, and J.P. Gorvel, *Pathogen-endoplasmic-reticulum interactions: in through the out door.* Nat Rev Immunol, 2006. **6**(2): p. 136-47.
55. Ishino, T., Y. Chinzei, and M. Yuda, *Two proteins with 6-cys motifs are required for malarial parasites to commit to infection of the hepatocyte.* Mol Microbiol, 2005. **58**(5): p. 1264-75.
56. Labaied, M., et al., *Plasmodium yoelii sporozoites with simultaneous deletion of P52 and P36 are completely attenuated and confer sterile immunity against infection.* Infect Immun, 2007. **75**(8): p. 3758-68.
57. van Dijk, M.R., et al., *Genetically attenuated, P36p-deficient malarial sporozoites induce protective immunity and apoptosis of infected liver cells.* Proc Natl Acad Sci U S A, 2005. **102**(34): p. 12194-9.
58. Sa, E.C.C., et al., *Plasmodium berghei EXP-1 interacts with host Apolipoprotein H during Plasmodium liver-stage development.* Proc Natl Acad Sci U S A, 2017. **114**(7): p. E1138-E1147.
59. Real, E., et al., *Plasmodium UIS3 sequesters host LC3 to avoid elimination by autophagy in hepatocytes.* Nat Microbiol, 2018. **3**(1): p. 17-25.
60. Mikolajczak, S.A., et al., *L-FABP is a critical host factor for successful malaria liver stage development.* Int J Parasitol, 2007. **37**(5): p. 483-9.
61. Mueller, A.K., et al., *Plasmodium liver stage developmental arrest by depletion of a protein at the parasite-host interface.* Proc Natl Acad Sci U S A, 2005. **102**(8): p. 3022-7.
62. Mueller, A.K., et al., *Genetically modified Plasmodium parasites as a protective experimental malaria vaccine.* Nature, 2005. **433**(7022): p. 164-7.
63. Ishino, T., et al., *LISP1 is important for the egress of Plasmodium berghei parasites from liver cells.* Cell Microbiol, 2009. **11**(9): p. 1329-39.
64. Marti, M., et al., *Targeting malaria virulence and remodeling proteins to the host erythrocyte.* Science, 2004. **306**(5703): p. 1930-3.
65. Hiller, N.L., et al., *A host-targeting signal in virulence proteins reveals a secretome in malarial infection.* Science, 2004. **306**(5703): p. 1934-7.
66. Hugel, F.U., G. Pradel, and U. Frevert, *Release of malaria circumsporozoite protein into the host cell cytoplasm and interaction with ribosomes.* Mol Biochem Parasitol, 1996. **81**(2): p. 151-70.
67. Frevert, U., et al., *Malaria circumsporozoite protein inhibits protein synthesis in mammalian cells.* EMBO J, 1998. **17**(14): p. 3816-26.

68. Singh, A.P., et al., *Plasmodium circumsporozoite protein promotes the development of the liver stages of the parasite.* Cell, 2007. **131**(3): p. 492-504.
69. Ingmundson, A., et al., *The exported Plasmodium berghei protein IBIS1 delineates membranous structures in infected red blood cells.* Mol Microbiol, 2012. **83**(6): p. 1229-43.
70. Jaijyan, D.K., H. Singh, and A.P. Singh, *A Sporozoite- and Liver Stage-expressed Tryptophan-rich Protein Plays an Auxiliary Role in Plasmodium Liver Stage Development and Is a Potential Vaccine Candidate.* J Biol Chem, 2015. **290**(32): p. 19496-511.
71. Orito, Y., et al., *Liver-specific protein 2: a Plasmodium protein exported to the hepatocyte cytoplasm and required for merozoite formation.* Mol Microbiol, 2013. **87**(1): p. 66-79.
72. Kaiser, K., N. Camargo, and S.H. Kappe, *Transformation of sporozoites into early exoerythrocytic malaria parasites does not require host cells.* J Exp Med, 2003. **197**(8): p. 1045-50.
73. Hegge, S., et al., *Key factors regulating Plasmodium berghei sporozoite survival and transformation revealed by an automated visual assay.* FASEB J, 2010. **24**(12): p. 5003-12.
74. Vaughan, A.M. and S.H.I. Kappe, *Malaria Parasite Liver Infection and Exoerythrocytic Biology.* Cold Spring Harb Perspect Med, 2017. **7**(6).
75. Sturm, A., et al., *Alteration of the parasite plasma membrane and the parasitophorous vacuole membrane during exo-erythrocytic development of malaria parasites.* Protist, 2009. **160**(1): p. 51-63.
76. Vial, H.J. and M.L. Ancelin, *Malarial lipids. An overview.* Subcell Biochem, 1992. **18**: p. 259-306.
77. Ralph, S.A., et al., *Tropical infectious diseases: metabolic maps and functions of the Plasmodium falciparum apicoplast.* Nat Rev Microbiol, 2004. **2**(3): p. 203-16.
78. Vaughan, A.M., et al., *Type II fatty acid synthesis is essential only for malaria parasite late liver stage development.* Cell Microbiol, 2009. **11**(3): p. 506-20.
79. Mota, M.M. and A. Rodriguez, *Plasmodium yoelii: efficient in vitro invasion and complete development of sporozoites in mouse hepatic cell lines.* Exp Parasitol, 2000. **96**(4): p. 257-9.
80. Baer, K., et al., *Release of hepatic Plasmodium yoelii merozoites into the pulmonary microvasculature.* PLoS Pathog, 2007. **3**(11): p. e171.
81. Vaughan, A.M., et al., *Complete Plasmodium falciparum liver-stage development in liver-chimeric mice.* J Clin Invest, 2012. **122**(10): p. 3618-28.
82. Sturm, A., et al., *Manipulation of host hepatocytes by the malaria parasite for delivery into liver sinusoids.* Science, 2006. **313**(5791): p. 1287-90.
83. Graewe, S., et al., *Hostile takeover by Plasmodium: reorganization of parasite and host cell membranes during liver stage egress.* PLoS Pathog, 2011. **7**(9): p. e1002224.
84. Sturm, A. and V. Heussler, *Live and let die: manipulation of host hepatocytes by exoerythrocytic Plasmodium parasites.* Med Microbiol Immunol, 2007. **196**(3): p. 127-33.
85. Tawk, L., et al., *A key role for Plasmodium subtilisin-like SUB1 protease in egress of malaria parasites from host hepatocytes.* J Biol Chem, 2013. **288**(46): p. 33336-46.
86. Falae, A., et al., *Role of Plasmodium berghei cGMP-dependent protein kinase in late liver stage development.* J Biol Chem, 2010. **285**(5): p. 3282-8.
87. Dvorak, J.A., et al., *Invasion of erythrocytes by malaria merozoites.* Science, 1975. **187**(4178): p. 748-50.
88. Weiss, G.E., et al., *Revealing the sequence and resulting cellular morphology of receptor-ligand interactions during Plasmodium falciparum invasion of erythrocytes.* PLoS Pathog, 2015. **11**(2): p. e1004670.
89. Gilson, P.R. and B.S. Crabb, *Morphology and kinetics of the three distinct phases of red blood cell invasion by Plasmodium falciparum merozoites.* Int J Parasitol, 2009. **39**(1): p. 91-6.
90. Cowman, A.F. and B.S. Crabb, *Invasion of red blood cells by malaria parasites.* Cell, 2006. **124**(4): p. 755-66.

91. Goel, V.K., et al., *Band 3 is a host receptor binding merozoite surface protein 1 during the Plasmodium falciparum invasion of erythrocytes.* Proc Natl Acad Sci U S A, 2003. **100**(9): p. 5164-9.
92. Preiser, P., et al., *The apical organelles of malaria merozoites: host cell selection, invasion, host immunity and immune evasion.* Microbes Infect, 2000. **2**(12): p. 1461-77.
93. Paul, A.S., E.S. Egan, and M.T. Duraisingh, *Host-parasite interactions that guide red blood cell invasion by malaria parasites.* Curr Opin Hematol, 2015. **22**(3): p. 220-6.
94. Riglar, D.T., et al., *Super-resolution dissection of coordinated events during malaria parasite invasion of the human erythrocyte.* Cell Host Microbe, 2011. **9**(1): p. 9-20.
95. Tham, W.H., J. Healer, and A.F. Cowman, *Erythrocyte and reticulocyte binding-like proteins of Plasmodium falciparum.* Trends Parasitol, 2012. **28**(1): p. 23-30.
96. Orlandi, P.A., F.W. Klotz, and J.D. Haynes, *A malaria invasion receptor, the 175-kilodalton erythrocyte binding antigen of Plasmodium falciparum recognizes the terminal Neu5Ac(alpha 2-3)Gal- sequences of glycophorin A.* J Cell Biol, 1992. **116**(4): p. 901-9.
97. Singh, S., et al., *Distinct external signals trigger sequential release of apical organelles during erythrocyte invasion by malaria parasites.* PLoS Pathog, 2010. **6**(2): p. e1000746.
98. Gao, X., et al., *Triggers of key calcium signals during erythrocyte invasion by Plasmodium falciparum.* Nat Commun, 2013. **4**: p. 2862.
99. Tham, W.H., et al., *Plasmodium falciparum Adhesins Play an Essential Role in Signalling and Activation of Invasion into Human Erythrocytes.* PLoS Pathog, 2015. **11**(12): p. e1005343.
100. Egan, E.S., et al., *Malaria. A forward genetic screen identifies erythrocyte CD55 as essential for Plasmodium falciparum invasion.* Science, 2015. **348**(6235): p. 711-4.
101. Chen, L., et al., *An EGF-like protein forms a complex with PfRh5 and is required for invasion of human erythrocytes by Plasmodium falciparum.* PLoS Pathog, 2011. **7**(9): p. e1002199.
102. Reddy, K.S., et al., *Multiprotein complex between the GPI-anchored CyRPA with PfRH5 and PfRipr is crucial for Plasmodium falciparum erythrocyte invasion.* Proc Natl Acad Sci U S A, 2015. **112**(4): p. 1179-84.
103. Crosnier, C., et al., *Basigin is a receptor essential for erythrocyte invasion by Plasmodium falciparum.* Nature, 2011. **480**(7378): p. 534-7.
104. Volz, J.C., et al., *Essential Role of the PfRh5/PfRipr/CyRPA Complex during Plasmodium falciparum Invasion of Erythrocytes.* Cell Host Microbe, 2016. **20**(1): p. 60-71.
105. Patel, S.D., et al., *Plasmodium falciparum merozoite surface antigen, PfRH5, elicits detectable levels of invasion-inhibiting antibodies in humans.* J Infect Dis, 2013. **208**(10): p. 1679-87.
106. Alexander, D.L., et al., *Plasmodium falciparum AMA1 binds a rhoptry neck protein homologous to TgRON4, a component of the moving junction in Toxoplasma gondii.* Eukaryot Cell, 2006. **5**(7): p. 1169-73.
107. Alexander, D.L., et al., *Identification of the moving junction complex of Toxoplasma gondii: a collaboration between distinct secretory organelles.* PLoS Pathog, 2005. **1**(2): p. e17.
108. Richard, D., et al., *Interaction between Plasmodium falciparum apical membrane antigen 1 and the rhoptry neck protein complex defines a key step in the erythrocyte invasion process of malaria parasites.* J Biol Chem, 2010. **285**(19): p. 14815-22.
109. Besteiro, S., et al., *Export of a Toxoplasma gondii rhoptry neck protein complex at the host cell membrane to form the moving junction during invasion.* PLoS Pathog, 2009. **5**(2): p. e1000309.
110. Besteiro, S., J.F. Dubremetz, and M. Lebrun, *The moving junction of apicomplexan parasites: a key structure for invasion.* Cell Microbiol, 2011. **13**(6): p. 797-805.
111. Harvey, K.L., et al., *Insights and controversies into the role of the key apicomplexan invasion ligand, Apical Membrane Antigen 1.* Int J Parasitol, 2014. **44**(12): p. 853-7.
112. Koch, M. and J. Baum, *The mechanics of malaria parasite invasion of the human erythrocyte - towards a reassessment of the host cell contribution.* Cell Microbiol, 2016. **18**(3): p. 319-29.

113. Yap, A., et al., *Conditional expression of apical membrane antigen 1 in Plasmodium falciparum shows it is required for erythrocyte invasion by merozoites.* Cell Microbiol, 2014. **16**(5): p. 642-56.
114. Egan, T.J., *Haemozoin formation.* Mol Biochem Parasitol, 2008. **157**(2): p. 127-36.
115. Dahl, E.L. and P.J. Rosenthal, *Multiple antibiotics exert delayed effects against the Plasmodium falciparum apicoplast.* Antimicrob Agents Chemother, 2007. **51**(10): p. 3485-90.
116. Scherf, A., J.J. Lopez-Rubio, and L. Riviere, *Antigenic variation in Plasmodium falciparum.* Annu Rev Microbiol, 2008. **62**: p. 445-70.
117. Petter, M., et al., *Expression of P. falciparum var genes involves exchange of the histone variant H2A.Z at the promoter.* PLoS Pathog, 2011. **7**(2): p. e1001292.
118. Dvorin, J.D., et al., *A plant-like kinase in Plasmodium falciparum regulates parasite egress from erythrocytes.* Science, 2010. **328**(5980): p. 910-2.
119. Collins, C.R., et al., *Malaria parasite cGMP-dependent protein kinase regulates blood stage merozoite secretory organelle discharge and egress.* PLoS Pathog, 2013. **9**(5): p. e1003344.
120. Das, S., et al., *Processing of Plasmodium falciparum Merozoite Surface Protein MSP1 Activates a Spectrin-Binding Function Enabling Parasite Egress from RBCs.* Cell Host Microbe, 2015. **18**(4): p. 433-44.
121. Taylor, L.H., D. Walliker, and A.F. Read, *Mixed-genotype infections of the rodent malaria Plasmodium chabaudi are more infectious to mosquitoes than single-genotype infections.* Parasitology, 1997. **115 (Pt 2)**: p. 121-32.
122. Janse, C.J., et al., *Plasmodium berghei: in vivo generation and selection of karyotype mutants and non-gametocyte producer mutants.* Exp Parasitol, 1992. **74**(1): p. 1-10.
123. Alano, P., et al., *Plasmodium falciparum: parasites defective in early stages of gametocytogenesis.* Exp Parasitol, 1995. **81**(2): p. 227-35.
124. Kafsack, B.F., et al., *A transcriptional switch underlies commitment to sexual development in malaria parasites.* Nature, 2014. **507**(7491): p. 248-52.
125. Sinha, A., et al., *A cascade of DNA-binding proteins for sexual commitment and development in Plasmodium.* Nature, 2014. **507**(7491): p. 253-257.
126. Brancucci, N.M.B., et al., *Heterochromatin protein 1 secures survival and transmission of malaria parasites.* Cell Host Microbe, 2014. **16**(2): p. 165-176.
127. Coleman, B.I., et al., *A Plasmodium falciparum histone deacetylase regulates antigenic variation and gametocyte conversion.* Cell Host Microbe, 2014. **16**(2): p. 177-186.
128. Filarsky, M., et al., *GDV1 induces sexual commitment of malaria parasites by antagonizing HP1-dependent gene silencing.* Science, 2018. **359**(6381): p. 1259-1263.
129. Eksi, S., et al., *Plasmodium falciparum gametocyte development 1 (Pfgdv1) and gametocytogenesis early gene identification and commitment to sexual development.* PLoS Pathog, 2012. **8**(10): p. e1002964.
130. Hawking, F., M.E. Wilson, and K. Gammage, *Evidence for cyclic development and short-lived maturity in the gametocytes of Plasmodium falciparum.* Trans R Soc Trop Med Hyg, 1971. **65**(5): p. 549-59.
131. Gautret, P. and A. Motard, *Periodic infectivity of Plasmodium gametocytes to the vector. A review.* Parasite, 1999. **6**(2): p. 103-11.
132. Dearnley, M., et al., *Reversible host cell remodeling underpins deformability changes in malaria parasite sexual blood stages.* Proc Natl Acad Sci U S A, 2016. **113**(17): p. 4800-5.
133. Dearnley, M.K., et al., *Origin, composition, organization and function of the inner membrane complex of Plasmodium falciparum gametocytes.* J Cell Sci, 2012. **125**(Pt 8): p. 2053-63.
134. Farfour, E., et al., *The extravascular compartment of the bone marrow: a niche for Plasmodium falciparum gametocyte maturation?* Malar J, 2012. **11**: p. 285.
135. Billker, O., et al., *The roles of temperature, pH and mosquito factors as triggers of male and female gametogenesis of Plasmodium berghei in vitro.* Parasitology, 1997. **115 (Pt 1)**: p. 1-7.

136. Billker, O., et al., *Calcium and a calcium-dependent protein kinase regulate gamete formation and mosquito transmission in a malaria parasite.* Cell, 2004. **117**(4): p. 503-14.
137. Kuehn, A. and G. Pradel, *The coming-out of malaria gametocytes.* J Biomed Biotechnol, 2010. **2010**: p. 976827.
138. McRobert, L., et al., *Gametogenesis in malaria parasites is mediated by the cGMP-dependent protein kinase.* PLoS Biol, 2008. **6**(6): p. e139.
139. Bansal, A., et al., *PfCDPK1 is critical for malaria parasite gametogenesis and mosquito infection.* Proc Natl Acad Sci U S A, 2018. **115**(4): p. 774-779.
140. Bansal, A., et al., *Plasmodium falciparum Calcium-Dependent Protein Kinase 2 Is Critical for Male Gametocyte Exflagellation but Not Essential for Asexual Proliferation.* mBio, 2017. **8**(5).
141. Rangarajan, R., et al., *A mitogen-activated protein kinase regulates male gametogenesis and transmission of the malaria parasite Plasmodium berghei.* EMBO Rep, 2005. **6**(5): p. 464-9.
142. Tewari, R., et al., *An atypical mitogen-activated protein kinase controls cytokinesis and flagellar motility during male gamete formation in a malaria parasite.* Mol Microbiol, 2005. **58**(5): p. 1253-63.
143. Hitz, E., et al., *PfMAP-2 is essential for male gametogenesis in the malaria parasite Plasmodium falciparum.* Sci Rep, 2020. **10**(1): p. 11930.
144. Mair, G.R., et al., *Regulation of sexual development of Plasmodium by translational repression.* Science, 2006. **313**(5787): p. 667-9.
145. Janse, C.J., et al., *Rapid repeated DNA replication during microgametogenesis and DNA synthesis in young zygotes of Plasmodium berghei.* Trans R Soc Trop Med Hyg, 1986. **80**(1): p. 154-7.
146. Thompson, J., C.J. Janse, and A.P. Waters, *Comparative genomics in Plasmodium: a tool for the identification of genes and functional analysis.* Mol Biochem Parasitol, 2001. **118**(2): p. 147-54.
147. van Dijk, M.R., et al., *A central role for P48/45 in malaria parasite male gamete fertility.* Cell, 2001. **104**(1): p. 153-64.
148. van Dijk, M.R., et al., *Three members of the 6-cys protein family of Plasmodium play a role in gamete fertility.* PLoS Pathog, 2010. **6**(4): p. e1000853.
149. Eksi, S., et al., *Malaria transmission-blocking antigen, Pfs230, mediates human red blood cell binding to exflagellating male parasites and oocyst production.* Mol Microbiol, 2006. **61**(4): p. 991-8.
150. Targett, G.A., et al., *Plasmodium falciparum sexual stage antigens: immunogenicity and cell-mediated responses.* Immunol Lett, 1990. **25**(1-3): p. 77-81.
151. Sinden, R.E., et al., *The biology of sexual development of Plasmodium: the design and implementation of transmission-blocking strategies.* Malar J, 2012. **11**: p. 70.
152. Sinden, R.E., R.H. Hartley, and L. Winger, *The development of Plasmodium ookinetes in vitro: an ultrastructural study including a description of meiotic division.* Parasitology, 1985. **91 (Pt 2)**: p. 227-44.
153. Reininger, L., et al., *A NIMA-related protein kinase is essential for completion of the sexual cycle of malaria parasites.* J Biol Chem, 2005. **280**(36): p. 31957-64.
154. Reininger, L., et al., *An essential role for the Plasmodium Nek-2 Nima-related protein kinase in the sexual development of malaria parasites.* J Biol Chem, 2009. **284**(31): p. 20858-68.
155. Huber, M., E. Cabib, and L.H. Miller, *Malaria parasite chitinase and penetration of the mosquito peritrophic membrane.* Proc Natl Acad Sci U S A, 1991. **88**(7): p. 2807-10.
156. Deligianni, E., et al., *Essential role of Plasmodium perforin-like protein 4 in ookinete midgut passage.* PLoS One, 2018. **13**(8): p. e0201651.
157. Siden-Kiamos, I., et al., *Stage-specific depletion of myosin A supports an essential role in motility of malarial ookinetes.* Cell Microbiol, 2011. **13**(12): p. 1996-2006.
158. Tomas, A.M., et al., *P25 and P28 proteins of the malaria ookinete surface have multiple and partially redundant functions.* EMBO J, 2001. **20**(15): p. 3975-83.

159. Matuschewski, K. and H. Schuler, *Actin/myosin-based gliding motility in apicomplexan parasites.* Subcell Biochem, 2008. **47**: p. 110-20.
160. Meissner, M., D. Schluter, and D. Soldati, *Role of Toxoplasma gondii myosin A in powering parasite gliding and host cell invasion.* Science, 2002. **298**(5594): p. 837-40.
161. Morrissette, N.S. and L.D. Sibley, *Cytoskeleton of apicomplexan parasites.* Microbiol Mol Biol Rev, 2002. **66**(1): p. 21-38; table of contents.
162. Gaskins, E., et al., *Identification of the membrane receptor of a class XIV myosin in Toxoplasma gondii.* J Cell Biol, 2004. **165**(3): p. 383-93.
163. Bergman, L.W., et al., *Myosin A tail domain interacting protein (MTIP) localizes to the inner membrane complex of Plasmodium sporozoites.* J Cell Sci, 2003. **116**(Pt 1): p. 39-49.
164. Dessens, J.T., et al., *CTRP is essential for mosquito infection by malaria ookinetes.* EMBO J, 1999. **18**(22): p. 6221-7.
165. Ishino, T., et al., *A calcium-dependent protein kinase regulates Plasmodium ookinete access to the midgut epithelial cell.* Mol Microbiol, 2006. **59**(4): p. 1175-84.
166. Hillyer, J.F., C. Barreau, and K.D. Vernick, *Efficiency of salivary gland invasion by malaria sporozoites is controlled by rapid sporozoite destruction in the mosquito haemocoel.* Int J Parasitol, 2007. **37**(6): p. 673-81.
167. Meis, J.F., et al., *A scanning electron microscopic study of the sporogonic development of Plasmodium falciparum in Anopheles stephensi.* Acta Trop, 1992. **50**(3): p. 227-36.
168. Aly, A.S., A.M. Vaughan, and S.H. Kappe, *Malaria parasite development in the mosquito and infection of the mammalian host.* Annu Rev Microbiol, 2009. **63**: p. 195-221.
169. Hamilton, A.J., C.S. Davies, and R.E. Sinden, *Expression of circumsporozoite proteins revealed in situ in the mosquito stages of Plasmodium berghei by the Lowicryl-immunogold technique.* Parasitology, 1988. **96 (Pt 2)**: p. 273-80.
170. Posthuma, G., et al., *Immunogold localization of circumsporozoite protein of the malaria parasite Plasmodium falciparum during sporogony in Anopheles stephensi midguts.* Eur J Cell Biol, 1988. **46**(1): p. 18-24.
171. Canning, E.U. and R.E. Sinden, *The organization of the ookinete and observations on nuclear division in oocysts of Plasmodium berghei.* Parasitology, 1973. **67**(1): p. 29-40.
172. Terzakis, J.A., H. Sprinz, and R.A. Ward, *The transformation of the Plasmodium gallinaceum oocyst in Aedes aegypti mosquitoes.* J Cell Biol, 1967. **34**(1): p. 311-26.
173. Thathy, V., et al., *Levels of circumsporozoite protein in the Plasmodium oocyst determine sporozoite morphology.* EMBO J, 2002. **21**(7): p. 1586-96.
174. Yoshida, N., et al., *Hybridoma produces protective antibodies directed against the sporozoite stage of malaria parasite.* Science, 1980. **207**(4426): p. 71-3.
175. Cochrane, A.H., et al., *Monoclonal antibodies identify the protective antigens of sporozoites of Plasmodium knowlesi.* Proc Natl Acad Sci U S A, 1982. **79**(18): p. 5651-5.
176. Tsuji, M., G. Corradin, and F. Zavala, *Monoclonal antibodies recognize a processing dependent epitope present in the mature CS protein of various plasmodial species.* Parasite Immunol, 1992. **14**(5): p. 457-69.
177. Menard, R., et al., *Circumsporozoite protein is required for development of malaria sporozoites in mosquitoes.* Nature, 1997. **385**(6614): p. 336-40.
178. Wang, Q., H. Fujioka, and V. Nussenzweig, *Exit of Plasmodium sporozoites from oocysts is an active process that involves the circumsporozoite protein.* PLoS Pathog, 2005. **1**(1): p. e9.
179. Baton, L.A. and L.C. Ranford-Cartwright, *Spreading the seeds of million-murdering death: metamorphoses of malaria in the mosquito.* Trends Parasitol, 2005. **21**(12): p. 573-80.
180. Lavazec, C., et al., *Analysis of mutant Plasmodium berghei parasites lacking expression of multiple PbCCp genes.* Mol Biochem Parasitol, 2009. **163**(1): p. 1-7.
181. Pradel, G., et al., *A multidomain adhesion protein family expressed in Plasmodium falciparum is essential for transmission to the mosquito.* J Exp Med, 2004. **199**(11): p. 1533-44.

182. Trueman, H.E., et al., *Functional characterization of an LCCL-lectin domain containing protein family in Plasmodium berghei.* J Parasitol, 2004. **90**(5): p. 1062-71.
183. Raine, J.D., et al., *Female inheritance of malarial lap genes is essential for mosquito transmission.* PLoS Pathog, 2007. **3**(3): p. e30.
184. Tremp, A.Z., et al., *Plasmodium berghei LAPs form an extended protein complex that facilitates crystalloid targeting and biogenesis.* J Proteomics, 2020. **227**: p. 103925.
185. Khater, E.I., R.E. Sinden, and J.T. Dessens, *A malaria membrane skeletal protein is essential for normal morphogenesis, motility, and infectivity of sporozoites.* J Cell Biol, 2004. **167**(3): p. 425-32.
186. Kudryashev, M., et al., *Structural basis for chirality and directional motility of Plasmodium sporozoites.* Cell Microbiol, 2012. **14**(11): p. 1757-68.
187. Aly, A.S. and K. Matuschewski, *A malarial cysteine protease is necessary for Plasmodium sporozoite egress from oocysts.* J Exp Med, 2005. **202**(2): p. 225-30.
188. Engelmann, S., O. Silvie, and K. Matuschewski, *Disruption of Plasmodium sporozoite transmission by depletion of sporozoite invasion-associated protein 1.* Eukaryot Cell, 2009. **8**(4): p. 640-8.
189. Mastan, B.S., et al., *Plasmodium berghei plasmepsin VIII is essential for sporozoite gliding motility.* Int J Parasitol, 2017. **47**(5): p. 239-245.
190. Klug, D. and F. Frischknecht, *Motility precedes egress of malaria parasites from oocysts.* Elife, 2017. **6**.
191. Pimenta, P.F., M. Touray, and L. Miller, *The journey of malaria sporozoites in the mosquito salivary gland.* J Eukaryot Microbiol, 1994. **41**(6): p. 608-24.
192. Mueller, A.K., et al., *Invasion of mosquito salivary glands by malaria parasites: prerequisites and defense strategies.* Int J Parasitol, 2010. **40**(11): p. 1229-35.
193. Sterling, C.R., M. Aikawa, and J.P. Vanderberg, *The passage of Plasmodium berghei sporozoites through the salivary glands of Anopheles stephensi: an electron microscope study.* J Parasitol, 1973. **59**(4): p. 593-605.
194. Golenda, C.F., W.H. Starkweather, and R.A. Wirtz, *The distribution of circumsporozoite protein (CS) in Anopheles stephensi mosquitoes infected with Plasmodium falciparum malaria.* J Histochem Cytochem, 1990. **38**(4): p. 475-81.
195. Barreau, C., et al., *Plasmodium gallinaceum: sporozoite invasion of Aedes aegypti salivary glands is inhibited by anti-gland antibodies and by lectins.* Exp Parasitol, 1995. **81**(3): p. 332-43.
196. Brennan, J.D., et al., *Anopheles gambiae salivary gland proteins as putative targets for blocking transmission of malaria parasites.* Proc Natl Acad Sci U S A, 2000. **97**(25): p. 13859-64.
197. Touray, M.G., et al., *Developmentally regulated infectivity of malaria sporozoites for mosquito salivary glands and the vertebrate host.* J Exp Med, 1992. **175**(6): p. 1607-12.
198. Nagasawa, H., et al., *Localization of circumsporozoite protein of Plasmodium ovale in midgut oocysts.* Infect Immun, 1987. **55**(12): p. 2928-32.
199. Sidjanski, S.P., J.P. Vanderberg, and P. Sinnis, *Anopheles stephensi salivary glands bear receptors for region I of the circumsporozoite protein of Plasmodium falciparum.* Mol Biochem Parasitol, 1997. **90**(1): p. 33-41.
200. Tewari, R., D. Rathore, and A. Crisanti, *Motility and infectivity of Plasmodium berghei sporozoites expressing avian Plasmodium gallinaceum circumsporozoite protein.* Cell Microbiol, 2005. **7**(5): p. 699-707.
201. do Rosario, V.E., et al., *Plasmodium falciparum: administration of anti-sporozoite antibodies during sporogony results in production of sporozoites which are not neutralized by human anti-circumsporozoite protein vaccine sera.* Trans R Soc Trop Med Hyg, 1989. **83**(3): p. 305-7.

202. Warburg, A., et al., *Plasmodium gallinaceum: antibodies to circumsporozoite protein prevent sporozoites from invading the salivary glands of Aedes aegypti.* Exp Parasitol, 1992. **75**(3): p. 303-7.
203. Matuschewski, K., et al., *Plasmodium sporozoite invasion into insect and mammalian cells is directed by the same dual binding system.* EMBO J, 2002. **21**(7): p. 1597-606.
204. Kappe, S., et al., *Conservation of a gliding motility and cell invasion machinery in Apicomplexan parasites.* J Cell Biol, 1999. **147**(5): p. 937-44.
205. Robson, K.J., et al., *A highly conserved amino-acid sequence in thrombospondin, properdin and in proteins from sporozoites and blood stages of a human malaria parasite.* Nature, 1988. **335**(6185): p. 79-82.
206. Rogers, W.O., et al., *Characterization of Plasmodium falciparum sporozoite surface protein 2.* Proc Natl Acad Sci U S A, 1992. **89**(19): p. 9176-80.
207. Ishino, T., et al., *Rhoptry neck protein 2 expressed in Plasmodium sporozoites plays a crucial role during invasion of mosquito salivary glands.* Cell Microbiol, 2019. **21**(1): p. e12964.
208. Kariu, T., et al., *MAEBL is essential for malarial sporozoite infection of the mosquito salivary gland.* J Exp Med, 2002. **195**(10): p. 1317-23.
209. Thompson, J., et al., *Plasmodium cysteine repeat modular proteins 1-4: complex proteins with roles throughout the malaria parasite life cycle.* Cell Microbiol, 2007. **9**(6): p. 1466-80.
210. Combe, A., et al., *TREP, a novel protein necessary for gliding motility of the malaria sporozoite.* Int J Parasitol, 2009. **39**(4): p. 489-96.
211. Steinbuechel, M. and K. Matuschewski, *Role for the Plasmodium sporozoite-specific transmembrane protein S6 in parasite motility and efficient malaria transmission.* Cell Microbiol, 2009. **11**(2): p. 279-88.
212. Mikolajczak, S.A., et al., *Distinct malaria parasite sporozoites reveal transcriptional changes that cause differential tissue infection competence in the mosquito vector and mammalian host.* Mol Cell Biol, 2008. **28**(20): p. 6196-207.
213. Santos, J.M., et al., *Malaria parasite LIMP protein regulates sporozoite gliding motility and infectivity in mosquito and mammalian hosts.* Elife, 2017. **6**.
214. Frischknecht, F., et al., *Imaging movement of malaria parasites during transmission by Anopheles mosquitoes.* Cell Microbiol, 2004. **6**(7): p. 687-94.
215. Franke-Fayard, B., et al., *A Plasmodium berghei reference line that constitutively expresses GFP at a high level throughout the complete life cycle.* Mol Biochem Parasitol, 2004. **137**(1): p. 23-33.
216. Vanderberg, J.P. and U. Frevert, *Intravital microscopy demonstrating antibody-mediated immobilisation of Plasmodium berghei sporozoites injected into skin by mosquitoes.* Int J Parasitol, 2004. **34**(9): p. 991-6.
217. Frevert, U., et al., *Intravital observation of Plasmodium berghei sporozoite infection of the liver.* PLoS Biol, 2005. **3**(6): p. e192.
218. Vanderberg, J.P., *Development of infectivity by the Plasmodium berghei sporozoite.* J Parasitol, 1975. **61**(1): p. 43-50.
219. Lindner, S.E., et al., *Transcriptomics and proteomics reveal two waves of translational repression during the maturation of malaria parasite sporozoites.* Nat Commun, 2019. **10**(1): p. 4964.
220. Mota, M.M., J.C. Hafalla, and A. Rodriguez, *Migration through host cells activates Plasmodium sporozoites for infection.* Nat Med, 2002. **8**(11): p. 1318-22.
221. Siau, A., et al., *Temperature shift and host cell contact up-regulate sporozoite expression of Plasmodium falciparum genes involved in hepatocyte infection.* PLoS Pathog, 2008. **4**(8): p. e1000121.
222. Collins, F.H. and S.M. Paskewitz, *Malaria: current and future prospects for control.* Annu Rev Entomol, 1995. **40**: p. 195-219.
223. Warrell DA, H.G., *Essential Malariology.* 2002.

224. Karunaweera, N.D., et al., *The paroxysm of Plasmodium vivax malaria.* Trends Parasitol, 2003. **19**(4): p. 188-93.
225. Langhorne, J., et al., *Immunity to malaria: more questions than answers.* Nat Immunol, 2008. **9**(7): p. 725-32.
226. Bruneel, F., et al., *The clinical spectrum of severe imported falciparum malaria in the intensive care unit: report of 188 cases in adults.* Am J Respir Crit Care Med, 2003. **167**(5): p. 684-9.
227. Blumberg, L., et al., *Predictors of mortality in severe malaria: a two year experience in a non-endemic area.* Anaesth Intensive Care, 1996. **24**(2): p. 217-23.
228. Kattenberg, J.H., et al., *Systematic review and meta-analysis: rapid diagnostic tests versus placental histology, microscopy and PCR for malaria in pregnant women.* Malar J, 2011. **10**: p. 321.
229. Abba, K., et al., *Rapid diagnostic tests for diagnosing uncomplicated non-falciparum or Plasmodium vivax malaria in endemic countries.* Cochrane Database Syst Rev, 2014(12): p. CD011431.
230. Moody, A., *Rapid diagnostic tests for malaria parasites.* Clin Microbiol Rev, 2002. **15**(1): p. 66-78.
231. Harvey, B., J.S. Remington, and A.J. Sulzer, *IgM malaria antibodies in a case of congenital malaria in the United States.* Lancet, 1969. **1**(7590): p. 333-5.
232. Doderer, C., et al., *A new ELISA kit which uses a combination of Plasmodium falciparum extract and recombinant Plasmodium vivax antigens as an alternative to IFAT for detection of malaria antibodies.* Malar J, 2007. **6**: p. 19.
233. White, N.J., *Qinghaosu (artemisinin): the price of success.* Science, 2008. **320**(5874): p. 330-4.
234. Wells, T.N., J.N. Burrows, and J.K. Baird, *Targeting the hypnozoite reservoir of Plasmodium vivax: the hidden obstacle to malaria elimination.* Trends Parasitol, 2010. **26**(3): p. 145-51.
235. Winzeler, E.A. and M.J. Manary, *Drug resistance genomics of the antimalarial drug artemisinin.* Genome Biol, 2014. **15**(11): p. 544.
236. Pluess, B., et al., *Indoor residual spraying for preventing malaria.* Cochrane Database Syst Rev, 2010(4): p. CD006657.
237. Crompton, P.D., et al., *A prospective analysis of the Ab response to Plasmodium falciparum before and after a malaria season by protein microarray.* Proc Natl Acad Sci U S A, 2010. **107**(15): p. 6958-63.
238. Nussenzweig, R.S., et al., *Protective immunity produced by the injection of x-irradiated sporozoites of plasmodium berghei.* Nature, 1967. **216**(5111): p. 160-2.
239. Laurens, M.B., *RTS,S/AS01 vaccine (Mosquirix): an overview.* Hum Vaccin Immunother, 2020. **16**(3): p. 480-489.
240. Stoute, J.A., et al., *A preliminary evaluation of a recombinant circumsporozoite protein vaccine against Plasmodium falciparum malaria. RTS,S Malaria Vaccine Evaluation Group.* N Engl J Med, 1997. **336**(2): p. 86-91.
241. Duffy, P.E. and J. Patrick Gorres, *Malaria vaccines since 2000: progress, priorities, products.* NPJ Vaccines, 2020. **5**(1): p. 48.
242. Datoo, M.S., et al., *Efficacy of a low-dose candidate malaria vaccine, R21 in adjuvant Matrix-M, with seasonal administration to children in Burkina Faso: a randomised controlled trial.* Lancet, 2021. **397**(10287): p. 1809-1818.
243. Ashley, E.A., et al., *Spread of artemisinin resistance in Plasmodium falciparum malaria.* N Engl J Med, 2014. **371**(5): p. 411-23.
244. Barr, P.J., et al., *Recombinant Pfs25 protein of Plasmodium falciparum elicits malaria transmission-blocking immunity in experimental animals.* J Exp Med, 1991. **174**(5): p. 1203-8.
245. Gozar, M.M., V.L. Price, and D.C. Kaslow, *Saccharomyces cerevisiae-secreted fusion proteins Pfs25 and Pfs28 elicit potent Plasmodium falciparum transmission-blocking antibodies in mice.* Infect Immun, 1998. **66**(1): p. 59-64.

246. Shimp, R.L., Jr., et al., *Development of a Pfs25-EPA malaria transmission blocking vaccine as a chemically conjugated nanoparticle.* Vaccine, 2013. **31**(28): p. 2954-62.
247. Wu, Y., et al., *Transfection of Plasmodium falciparum within human red blood cells.* Proc Natl Acad Sci U S A, 1995. **92**(4): p. 973-7.
248. Carlton, J.M., et al., *Genome sequence and comparative analysis of the model rodent malaria parasite Plasmodium yoelii yoelii.* Nature, 2002. **419**(6906): p. 512-9.
249. Carlton, J., J. Silva, and N. Hall, *The genome of model malaria parasites, and comparative genomics.* Curr Issues Mol Biol, 2005. **7**(1): p. 23-37.
250. Janse, C.J., et al., *Conserved location of genes on polymorphic chromosomes of four species of malaria parasites.* Mol Biochem Parasitol, 1994. **68**(2): p. 285-96.
251. Rich, S.M. and F.J. Ayala, *Progress in malaria research: the case for phylogenetics.* Adv Parasitol, 2003. **54**: p. 255-80.
252. Kooij, T.W., et al., *A Plasmodium whole-genome synteny map: indels and synteny breakpoints as foci for species-specific genes.* PLoS Pathog, 2005. **1**(4): p. e44.
253. Gueirard, P., et al., *Development of the malaria parasite in the skin of the mammalian host.* Proc Natl Acad Sci U S A, 2010. **107**(43): p. 18640-5.
254. Matuschewski, K., *Getting infectious: formation and maturation of Plasmodium sporozoites in the Anopheles vector.* Cell Microbiol, 2006. **8**(10): p. 1547-56.
255. Daher, W. and D. Soldati-Favre, *Mechanisms controlling glideosome function in apicomplexans.* Curr Opin Microbiol, 2009. **12**(4): p. 408-14.
256. Boucher, L.E. and J. Bosch, *The apicomplexan glideosome and adhesins - Structures and function.* J Struct Biol, 2015. **190**(2): p. 93-114.
257. Heintzelman, M.B., *Gliding motility in apicomplexan parasites.* Semin Cell Dev Biol, 2015. **46**: p. 135-42.
258. Bosch, J., et al., *Structure of the MTIP-MyoA complex, a key component of the malaria parasite invasion motor.* Proc Natl Acad Sci U S A, 2006. **103**(13): p. 4852-7.
259. Green, J.L., et al., *Compositional and expression analyses of the glideosome during the Plasmodium life cycle reveal an additional myosin light chain required for maximum motility.* J Biol Chem, 2017. **292**(43): p. 17857-17875.
260. Santos, J.M., et al., *Apicomplexan cytoskeleton and motors: key regulators in morphogenesis, cell division, transport and motility.* Int J Parasitol, 2009. **39**(2): p. 153-62.
261. Jewett, T.J. and L.D. Sibley, *Aldolase forms a bridge between cell surface adhesins and the actin cytoskeleton in apicomplexan parasites.* Mol Cell, 2003. **11**(4): p. 885-94.
262. Lindner, S.E., et al., *Total and putative surface proteomics of malaria parasite salivary gland sporozoites.* Mol Cell Proteomics, 2013. **12**(5): p. 1127-43.
263. Swearingen, K.E., et al., *Interrogating the Plasmodium Sporozoite Surface: Identification of Surface-Exposed Proteins and Demonstration of Glycosylation on CSP and TRAP by Mass Spectrometry-Based Proteomics.* PLoS Pathog, 2016. **12**(4): p. e1005606.
264. Swearingen, K.E., et al., *Proteogenomic analysis of the total and surface-exposed proteomes of Plasmodium vivax salivary gland sporozoites.* PLoS Negl Trop Dis, 2017. **11**(7): p. e0005791.
265. Bogale, H.N., et al., *Transcriptional heterogeneity and tightly regulated changes in gene expression during Plasmodium berghei sporozoite development.* Proc Natl Acad Sci U S A, 2021. **118**(10).
266. Coppi, A., et al., *The malaria circumsporozoite protein has two functional domains, each with distinct roles as sporozoites journey from mosquito to mammalian host.* J Exp Med, 2011. **208**(2): p. 341-56.
267. Yang, A.S.P., et al., *AMA1 and MAEBL are important for Plasmodium falciparum sporozoite infection of the liver.* Cell Microbiol, 2017. **19**(9).
268. Labaied, M., N. Camargo, and S.H. Kappe, *Depletion of the Plasmodium berghei thrombospondin-related sporozoite protein reveals a role in host cell entry by sporozoites.* Mol Biochem Parasitol, 2007. **153**(2): p. 158-66.

269. Otto, T.D., et al., *A comprehensive evaluation of rodent malaria parasite genomes and gene expression.* BMC Biol, 2014. **12**: p. 86.
270. Kall, L., A. Krogh, and E.L. Sonnhammer, *Advantages of combined transmembrane topology and signal peptide prediction--the Phobius web server.* Nucleic Acids Res, 2007. **35**(Web Server issue): p. W429-32.
271. Elisabeth Gasteiger, C.H., Alexandre Gattiker, S'everine Duvaud, Marc R. Wilkins, Ron D. Appel, Amos Bairoch, *Protein Identification and Analysis Tools on the ExPASy Server*. The Proteomics Protocols Handbook. Springer Protocols Handbooks. 2005: Humana Press.
272. Hofmann, K. and W. Stoffel. *Tmbase-A database of membrane spanning protein segments*. 1993.
273. Krogh, A., et al., *Predicting transmembrane protein topology with a hidden Markov model: application to complete genomes.* J Mol Biol, 2001. **305**(3): p. 567-80.
274. Szklarczyk, D., et al., *STRING v10: protein-protein interaction networks, integrated over the tree of life.* Nucleic Acids Res, 2015. **43**(Database issue): p. D447-52.
275. Janse, C.J., J. Ramesar, and A.P. Waters, *High-efficiency transfection and drug selection of genetically transformed blood stages of the rodent malaria parasite Plasmodium berghei.* Nat Protoc, 2006. **1**(1): p. 346-56.
276. Al-Nihmi, F.M., et al., *A Novel and Conserved Plasmodium Sporozoite Membrane Protein SPELD is Required for Maturation of Exo-erythrocytic Forms.* Sci Rep, 2017. **7**: p. 40407.
277. Ponzi, M., et al., *Egress of Plasmodium berghei gametes from their host erythrocyte is mediated by the MDV-1/PEG3 protein.* Cell Microbiol, 2009. **11**(8): p. 1272-88.
278. Lin, J.W., et al., *A novel 'gene insertion/marker out' (GIMO) method for transgene expression and gene complementation in rodent malaria parasites.* PLoS One, 2011. **6**(12): p. e29289.
279. Jillapalli, R., et al., *A Plasmodium berghei putative serine-threonine kinase 2 (PBANKA_0311400) is required for late liver stage development and timely initiation of blood stage infection.* Biol Open, 2019. **8**(8).
280. Togiri, J., et al., *Plasmodium berghei sporozoite specific genes- PbS10 and PbS23/SSP3 are required for the development of exo-erythrocytic forms.* Mol Biochem Parasitol, 2019. **232**: p. 111198.
281. Wichers, J.S., et al., *Identification of novel inner membrane complex and apical annuli proteins of the malaria parasite Plasmodium falciparum.* Cell Microbiol, 2021. **23**(9): p. e13341.
282. Porath, J., et al., *Metal chelate affinity chromatography, a new approach to protein fractionation.* Nature, 1975. **258**(5536): p. 598-9.
283. Walker, P.A., et al., *Efficient and rapid affinity purification of proteins using recombinant fusion proteases.* Biotechnology (N Y), 1994. **12**(6): p. 601-5.
284. Hliscs, M., et al., *Structure and function of a G-actin sequestering protein with a vital role in malaria oocyst development inside the mosquito vector.* J Biol Chem, 2010. **285**(15): p. 11572-83.
285. Matuschewski, K., et al., *Identification of the class XIV myosins Pb-MyoA and Py-MyoA and expression in Plasmodium sporozoites.* Mol Biochem Parasitol, 2001. **112**(1): p. 157-61.
286. Schmitz, S., et al., *Malaria parasite actin polymerization and filament structure.* J Biol Chem, 2010. **285**(47): p. 36577-85.
287. Robert-Paganin, J., et al., *Plasmodium myosin A drives parasite invasion by an atypical force generating mechanism.* Nat Commun, 2019. **10**(1): p. 3286.
288. Zhang, M., et al., *The Plasmodium eukaryotic initiation factor-2alpha kinase IK2 controls the latency of sporozoites in the mosquito salivary glands.* J Exp Med, 2010. **207**(7): p. 1465-74.
289. Gomes-Santos, C.S., et al., *Transition of Plasmodium sporozoites into liver stage-like forms is regulated by the RNA binding protein Pumilio.* PLoS Pathog, 2011. **7**(5): p. e1002046.
290. Muller, K., K. Matuschewski, and O. Silvie, *The Puf-family RNA-binding protein Puf2 controls sporozoite conversion to liver stages in the malaria parasite.* PLoS One, 2011. **6**(5): p. e19860.

291. Rawlings, N.D. and A.J. Barrett, *Evolutionary families of peptidases.* Biochem J, 1993. **290 (Pt 1)**: p. 205-18.
292. Drag, M. and G.S. Salvesen, *Emerging principles in protease-based drug discovery.* Nat Rev Drug Discov, 2010. **9**(9): p. 690-701.
293. Cai, H., et al., *Proteases in malaria parasites - a phylogenomic perspective.* Curr Genomics, 2011. **12**(6): p. 417-27.
294. Blackman, M.J., *Proteases in host cell invasion by the malaria parasite.* Cell Microbiol, 2004. **6**(10): p. 893-903.
295. Blackman, M.J., *Malarial proteases and host cell egress: an 'emerging' cascade.* Cell Microbiol, 2008. **10**(10): p. 1925-34.
296. Baker, R.P., R. Wijetilaka, and S. Urban, *Two Plasmodium rhomboid proteases preferentially cleave different adhesins implicated in all invasive stages of malaria.* PLoS Pathog, 2006. **2**(10): p. e113.
297. O'Donnell, R.A., et al., *Intramembrane proteolysis mediates shedding of a key adhesin during erythrocyte invasion by the malaria parasite.* J Cell Biol, 2006. **174**(7): p. 1023-33.
298. Srinivasan, P., I. Coppens, and M. Jacobs-Lorena, *Distinct roles of Plasmodium rhomboid 1 in parasite development and malaria pathogenesis.* PLoS Pathog, 2009. **5**(1): p. e1000262.
299. Vera, I.M., et al., *Plasmodium protease ROM1 is important for proper formation of the parasitophorous vacuole.* PLoS Pathog, 2011. **7**(9): p. e1002197.
300. Harris, P.K., et al., *Molecular identification of a malaria merozoite surface sheddase.* PLoS Pathog, 2005. **1**(3): p. 241-51.
301. Howell, S.A., et al., *A single malaria merozoite serine protease mediates shedding of multiple surface proteins by juxtamembrane cleavage.* J Biol Chem, 2003. **278**(26): p. 23890-8.
302. Green, J.L., et al., *Plasmodium thrombospondin related apical merozoite protein (PTRAMP) is shed from the surface of merozoites by PfSUB2 upon invasion of erythrocytes.* Mol Biochem Parasitol, 2006. **150**(1): p. 114-7.
303. Suarez-Cortes, P., et al., *Comparative Proteomics and Functional Analysis Reveal a Role of Plasmodium falciparum Osmiophilic Bodies in Malaria Parasite Transmission.* Mol Cell Proteomics, 2016. **15**(10): p. 3243-3255.
304. Ejigiri, I., et al., *Shedding of TRAP by a rhomboid protease from the malaria sporozoite surface is essential for gliding motility and sporozoite infectivity.* PLoS Pathog, 2012. **8**(7): p. e1002725.
305. Lin, J.W., et al., *Loss-of-function analyses defines vital and redundant functions of the Plasmodium rhomboid protease family.* Mol Microbiol, 2013. **88**(2): p. 318-38.
306. Wickham, M.E., J.G. Culvenor, and A.F. Cowman, *Selective inhibition of a two-step egress of malaria parasites from the host erythrocyte.* J Biol Chem, 2003. **278**(39): p. 37658-63.
307. Orfano, A.S., et al., *Species-specific escape of Plasmodium sporozoites from oocysts of avian, rodent, and human malarial parasites.* Malar J, 2016. **15**(1): p. 394.
308. Yeoh, S., et al., *Subcellular discharge of a serine protease mediates release of invasive malaria parasites from host erythrocytes.* Cell, 2007. **131**(6): p. 1072-83.
309. Miller, S.K., et al., *A subset of Plasmodium falciparum SERA genes are expressed and appear to play an important role in the erythrocytic cycle.* J Biol Chem, 2002. **277**(49): p. 47524-32.
310. Thomas, J.A., et al., *Development and Application of a Simple Plaque Assay for the Human Malaria Parasite Plasmodium falciparum.* PLoS One, 2016. **11**(6): p. e0157873.
311. Suarez, C., et al., *The malarial serine protease SUB1 plays an essential role in parasite liver stage development.* PLoS Pathog, 2013. **9**(12): p. e1003811.
312. Arastu-Kapur, S., et al., *Identification of proteases that regulate erythrocyte rupture by the malaria parasite Plasmodium falciparum.* Nat Chem Biol, 2008. **4**(3): p. 203-13.
313. Tanaka, T.Q., et al., *Plasmodium dipeptidyl aminopeptidases as malaria transmission-blocking drug targets.* Antimicrob Agents Chemother, 2013. **57**(10): p. 4645-52.
314. Chandramohanadas, R., et al., *Apicomplexan parasites co-opt host calpains to facilitate their escape from infected cells.* Science, 2009. **324**(5928): p. 794-7.

315. Gilson, P.R., et al., *Host cell remodelling in malaria parasites: a new pool of potential drug targets.* Int J Parasitol, 2017. **47**(2-3): p. 119-127.
316. Klemba, M. and D.E. Goldberg, *Characterization of plasmepsin V, a membrane-bound aspartic protease homolog in the endoplasmic reticulum of Plasmodium falciparum.* Mol Biochem Parasitol, 2005. **143**(2): p. 183-91.
317. Russo, I., et al., *Plasmepsin V licenses Plasmodium proteins for export into the host erythrocyte.* Nature, 2010. **463**(7281): p. 632-6.
318. Shenai, B.R., et al., *Characterization of native and recombinant falcipain-2, a principal trophozoite cysteine protease and essential hemoglobinase of Plasmodium falciparum.* J Biol Chem, 2000. **275**(37): p. 29000-10.
319. Sijwali, P.S., et al., *Expression and characterization of the Plasmodium falciparum haemoglobinase falcipain-3.* Biochem J, 2001. **360**(Pt 2): p. 481-9.
320. Singh, N., et al., *Plasmodium falciparum: biochemical characterization of the cysteine protease falcipain-2'.* Exp Parasitol, 2006. **112**(3): p. 187-92.
321. Liu, J., et al., *The role of Plasmodium falciparum food vacuole plasmepsins.* J Biol Chem, 2005. **280**(2): p. 1432-7.
322. Eggleson, K.K., K.L. Duffin, and D.E. Goldberg, *Identification and characterization of falcilysin, a metallopeptidase involved in hemoglobin catabolism within the malaria parasite Plasmodium falciparum.* J Biol Chem, 1999. **274**(45): p. 32411-7.
323. Klemba, M., I. Gluzman, and D.E. Goldberg, *A Plasmodium falciparum dipeptidyl aminopeptidase I participates in vacuolar hemoglobin degradation.* J Biol Chem, 2004. **279**(41): p. 43000-7.
324. Wang, F., et al., *Biochemical characterization of Plasmodium falciparum dipeptidyl aminopeptidase 1.* Mol Biochem Parasitol, 2011. **175**(1): p. 10-20.
325. Arisue, N., et al., *Phylogeny and evolution of the SERA multigene family in the genus Plasmodium.* J Mol Evol, 2007. **65**(1): p. 82-91.
326. McCoubrie, J.E., et al., *Evidence for a common role for the serine-type Plasmodium falciparum serine repeat antigen proteases: implications for vaccine and drug design.* Infect Immun, 2007. **75**(12): p. 5565-74.
327. Gardner, M.J., et al., *Chromosome 2 sequence of the human malaria parasite Plasmodium falciparum.* Science, 1998. **282**(5391): p. 1126-32.
328. Gardner, M.J., et al., *Genome sequence of the human malaria parasite Plasmodium falciparum.* Nature, 2002. **419**(6906): p. 498-511.
329. Aoki, S., et al., *Serine repeat antigen (SERA5) is predominantly expressed among the SERA multigene family of Plasmodium falciparum, and the acquired antibody titers correlate with serum inhibition of the parasite growth.* J Biol Chem, 2002. **277**(49): p. 47533-40.
330. Collins, C.R., et al., *The Plasmodium falciparum pseudoprotease SERA5 regulates the kinetics and efficiency of malaria parasite egress from host erythrocytes.* PLoS Pathog, 2017. **13**(7): p. e1006453.
331. Thomas, J.A., et al., *Publisher Correction: A protease cascade regulates release of the human malaria parasite Plasmodium falciparum from host red blood cells.* Nat Microbiol, 2018. **3**(4): p. 523.
332. Putrianti, E.D., et al., *The Plasmodium serine-type SERA proteases display distinct expression patterns and non-essential in vivo roles during life cycle progression of the malaria parasite.* Cell Microbiol, 2010. **12**(6): p. 725-39.
333. Li, J., et al., *Differential localization of processed fragments of Plasmodium falciparum serine repeat antigen and further processing of its N-terminal 47 kDa fragment.* Parasitol Int, 2002. **51**(4): p. 343-52.
334. Schmidt-Christensen, A., et al., *Expression and processing of Plasmodium berghei SERA3 during liver stages.* Cell Microbiol, 2008. **10**(8): p. 1723-34.

335. Ruecker, A., et al., *Proteolytic activation of the essential parasitophorous vacuole cysteine protease SERA6 accompanies malaria parasite egress from its host erythrocyte.* J Biol Chem, 2012. **287**(45): p. 37949-63.
336. Combe, A., et al., *Clonal conditional mutagenesis in malaria parasites.* Cell Host Microbe, 2009. **5**(4): p. 386-96.
337. Putrianti, E.D., et al., *A Plasmodium cysteine protease required for efficient transition from the liver infection stage.* PLoS Pathog, 2020. **16**(9): p. e1008891.
338. Tan, M.S.Y., et al., *Autocatalytic activation of a malarial egress protease is druggable and requires a protein cofactor.* EMBO J, 2021. **40**(11): p. e107226.

Publications

Publications from thesis:

1. A Conserved Plasmodium Structural Integrity Maintenance Protein (SIMP) is associated with sporozoite membrane and is essential for maintaining shape and infectivity. **Singh D**, Patri S, Narahari V, Segireddy RR, Dey S, Saurabh A, Macha V, Prabhu NP, Srivastava A, Kolli SK, Kumar KA. **Mol Microbiol**. 2022 Mar 17. doi: 10.1111/mmi.14894)PMID: 35301756.

* A microcommenty is published in Molecular Microbiology (**https://doi.org/10.1111/mmi.14910**) on the above-mentioned manuscript. The commentary highlights the importance of these findings in the context of developing a pre-erythrocytic vaccine based on SIMP.

Other publications:

1. Surface expressed Plasmodium circumsporozoite protein (CSP) modulatescellular flexibility and motility. Aditya Prasad Patra, Vrushali Pathak, Segireddy Rameswara Reddy , Aditya Chhatre, Crismita Dmello, Satya Narayan, **Dipti Singh** , Kumar KA, Sri Rama Koti Ainavarapu, and Shobhona Sharma. **bioRxiv preprint** doi: https://doi.org/10.1101/2021.08.04.455043.

2. Plasmodium berghei sporozoite specific genes- PbS10 and PbS23/SSP3 are required for the development of exo-erythrocytic forms. Togiri J, Segireddy RR, Mastan BS, **Singh D**, Kolli SK, Ghosh A, Al-Nihmi FMA, Maruthi M, Choudhary HH, Dey S, Mishra S, Kumar KA. **Mol Biochem Parasitol**. 2019 Jun 26;232:111198. doi:10.1016/j.molbiopara.2019.111198.

3. Biochemical and physiological investigations on adenosine 5' monophosphate deaminase from *Plasmodium* spp. Nagappa LK, **Singh D**, Dey S, Kumar KA, Balaram H. **Mol Microbiol**. 2019 Aug;112(2):699-717. doi: 10.1111/mmi.14313. Epub 2019 Jul 5.

4. Modulation of host cell SUMOylation facilitates efficient development of Plasmodium berghei and Toxoplasma gondii. Maruthi M, **Singh D**, Reddy SR, Mastan BS, Mishra S, Kumar KA. **Cell Microbiol.** 2017 Jul;19(7). doi: 10.1111/cmi.12723. Epub 2017 Feb 20.

Check for updates

Received: 30 December 2021 | Revised: 7 March 2022 | Accepted: 8 March 2022

DOI: 10.1111/mmi.14894

RESEARCH ARTICLE

WILEY

A conserved *Plasmodium* structural integrity maintenance protein (SIMP) is associated with sporozoite membrane and is essential for maintaining shape and infectivity

Dipti Singh[1] | Smita Patri[1] | Veeda Narahari[1] | Rameswara R. Segireddy[1] | Sandeep Dey[1] | Archi Saurabh[2] | Macha Vijay[3] | N. Prakash Prabhu[2] | Anand Srivastava[3] | Surendra Kumar Kolli[1] | Kota Arun Kumar[1]

[1]Department of Animal Biology, School of Life Sciences, University of Hyderabad, Hyderabad, India

[2]Department of Biotechnology & Bioinformatics, School of Life Sciences, University of Hyderabad, Hyderabad, India

[3]National Institute of Animal Biotechnology, Hyderabad, India

Correspondence
Surendra Kumar Kolli and Kota Arun Kumar, Department of Animal Biology, School of Life Sciences, University of Hyderabad, Gachibowli, Hyderabad, Telangana – 500046, India.
Email: skk@uohyd.ac.in and kaksl@uohyd.ac.in

Funding information
Department of Biotechnology, Ministry of Science and Technology, India, Grant/Award Number: BT/PR2495/BRB/10/950/2011

Abstract

Plasmodium sporozoites are extracellular forms introduced during mosquito bite that selectively invade mammalian hepatocytes. Sporozoites are delimited by a cell membrane that is linked to the underlying acto-myosin molecular motor. While membrane proteins with roles in motility and invasion have been well studied, very little is known about proteins that maintain the sporozoite shape. We demonstrate that in *Plasmodium berghei (Pb)* a conserved hypothetical gene, *PBANKA_1422900* specifies sporozoite structural integrity maintenance protein (SIMP) required for maintaining the sporozoite shape and motility. Sporozoites lacking SIMP exhibited loss of regular shape, extensive membrane blebbing at multiple foci, and membrane detachment. The mutant sporozoites failed to infect hepatocytes, though the altered shape did not affect the organization of cytoskeleton or inner membrane complex (IMC). Interestingly, the components of IMC failed to extend under the membrane blebs likely suggesting that SIMP may assist in anchoring the membrane to IMC. Endogenous C-terminal HA tagging localized SIMP to membrane and revealed the C-terminus of the protein to be extracellular. Since SIMP is highly conserved among *Plasmodium* species, these findings have important implications for utilizing it as a novel sporozoite-specific vaccine candidate.

KEYWORDS
gliding motility, inner membrane complex, *Plasmodium*, sporozoites

1 | INTRODUCTION

The life cycle of *Plasmodium* in mammalian host starts with the bite of a female *Anopheles* mosquito that delivers sporozoites in the skin of the vertebrate host (Gueirard et al., 2010). The sporozoites make their way to the liver, where they transform into exoerythrocytic forms. Following exoerythrocytic schizogony, first-generation merozoites are packaged in membrane-bound structures called merosomes (Sturm et al., 2006) that are extruded into sinusoids. Rupture of merosome releases parasites into the bloodstream, which initiates an erythrocytic cycle. In RBC, the parasites replicate asexually and go through a series of transformations resulting in rings, trophozoites, schizonts, and gametocytes.

Gametocytes are sexual forms and the terminal stages of the parasite in the mammalian host. These forms enter gut of a female *Anopheles* mosquito during a blood meal. Sexual reproduction occurs in the lumen of gut, resulting in a zygote that transforms into motile ookinete. The ookinete breaches midgut epithelium and settles on

 © 2022 John Wiley & Sons Ltd.

the hemocoel side of the gut and further develops into an oocyst. Sporozoites develop within the oocyst and upon maturation are released into the hemocoel. The sporozoites make their way to the salivary glands and are ready to infect a new host when mosquitoes take a blood meal (Matuschewski, 2006).

Sporozoites are eukaryotic cells that are delimited by a trilamellar pellicle consisting of plasma membrane and two closely opposed inner membranes called inner membrane complex (IMC) (Bergman et al., 2003). Alveolins are a class of proteins that make up the subpellicular network, present on the cytoplasmic side of IMC, and provide mechanical strength to the cell (Khater et al., 2004; Mann & Beckers, 2001). Sporozoites move using a substrate-dependent motility called gliding motility (Kappe et al., 2004)—a cell movement that is dependent on coordinated and well-orchestrated interaction between a macromolecular complex—the glideosome, actin, a glideosome-associated protein, and transmembrane proteins (Daher & Soldati-Favre, 2009). Glideosome is a molecular complex whose core consists of Myosin A (MyoA), which belongs to class XIV and mainly functions in regulating gliding motility and host cell invasion (Boucher & Bosch, 2015; Heintzelman, 2015; Meissner et al., 2002). Structurally, the MyoA lacks a tail domain, but its neck region binds two light chains—a myosin tail domain interacting protein (MTIP) and an essential light chain (Bosch et al., 2006; Green et al., 2017). MTIP links MyoA to glideosome and inner membrane complex. Post-translational modifications lead to assembly of the molecular complex following Ca^{2+} signaling and the energy required for sporozoite movement is likely produced by the relocation of glycolytic enzymes in close proximity of glideosome (Daher & Soldati-Favre, 2009). Microtubules present beneath IMC provide mechanical support to sporozoites (Santos et al., 2009). The invasins bind to substratum or host cell receptors on the extracellular side and to the components of actomyosin motor toward cytoplasmic side of sporozoite using adaptors proteins, for example, glycolytic enzymes like aldolase (Jewett & Sibley, 2003). This linkage transduces the force through cell membrane allowing continuous forward movement of sporozoites concomitant with rearward traction of parasite–substrate interactions (Matuschewski & Schuler, 2008).

Sporozoites move from their site of deposition, breach multiple biological barriers, attach, or commit to a suitable host cell, and infect by forming a replication-competent organelle, the parasitophorous vacuole (PV). The aforementioned activities of sporozoite are a function of a highly organized apical complex. This complex consists of a set of cytoskeletal structures—apical rings, microtubules, and specialized secretory organelles—micronemes, rhoptries, and dense granules (Santos et al., 2009). An arsenal of proteins that also serve as bonafide markers, sort to these compartments and assist in mediating all sporozoite-specific functions. As sporozoite surface proteins interact with hepatocytes, they have immense potential for therapeutic intervention. The past decade has seen a surge in defining sporozoite membrane composition using high-throughput mass spectrometry approaches (Lindner et al., 2013; Swearingen et al., 2016, 2017). Most noteworthy, these investigations reiterated that invasion and signaling related proteins are membrane resident (Lindner et al., 2013, Swearingen et al., 2016, 2017), IMC components can access the extracellular side of the plasma membrane and the major surface proteins of sporozoite—the CSP and TRAP bear potential glycosylation sites in their TSR (thrombospondin type 1 repeat) motif (Swearingen et al., 2016). Additionally, several proteins that constitute the glideosome and others that regulate transcription and translation are phosphorylated (Swearingen et al., 2017). More recently, it has been documented that during maturation in salivary glands, the sporozoites temporally regulate protein expression by two overlapping, and independent programs of translational repression (Bogale et al., 2021). This allows precise expression of genes that mediate one or more functions highly specific for oocyst egress or invasion of salivary glands and hepatocytes.

While most sporozoite membrane proteins achieve one or more functions specific to hepatocyte commitment (Coppi et al., 2011; Yang et al., 2017), motility (Combe et al., 2009; Sultan et al., 1997) and invasion (Labaied et al., 2007; Sultan et al., 1997), not much is known about proteins that maintain the sporozoite shape and structure. A previous study has demonstrated the role of PBANKA_1422900 (designated as PIMMS22) in the transmission stages of *P. berghei* (Ukegbu et al., 2021) and the protein was identified in sporozoite proteome analysis (Lindner et al., 2019). In the current study, we show that *PBANKA_1422900*—a hypothetical gene encodes SIMP that localizes to sporozoite membrane and is required for maintaining sporozoite shape and infectivity. Importantly, we demonstrate that the C-terminus of SIMP is highly conserved between *Pb* and *Pf*, and is extracellular, a finding that has immense potential for developing therapeutic sporozoite vaccine.

2 | RESULTS AND DISCUSSION

The PlasmoDB annotates *PBANKA_1422900* as a conserved hypothetical gene. Alignment of *PBANKA_1422900* (*Pb*SIMP) amino acid sequence with other *Plasmodium* orthologues revealed a high degree of conservation (Figure S1a). The amino acid identity of *Pb*SIMP (PBANKA) was 96% with *P. yoelli* (PY), and with human parasites, *P. falciparum* (PF) and *P. vivax* (PV), the sequence showed, respectively, 76% and 81% identity (Figure S1b). We also analyzed the evolutionary relatedness of *Pb*SIMP. All the *Plasmodium* species infecting rodents formed a separate clade from those infecting aves and primates. Among the primate parasitic species, the human parasites *P. ovale* share a common ancestor with that of the rodent parasites. The human species *P. malariae* and *P. falciparum* share a common ancestor with that of avian species *P. gallinaceum*, *P. relictum*, and those that infect chimps (*P. reichenowi*, *P. gaboni*) and gorilla (*Plasmodium sp.* gorilla clade G2). The human infecting species *P. vivax* and *P. knowlesi* shares a common ancestor with that of Asian old world monkeys (*P. inui*, *P. cynomolgi*, *P. fragile*, and *P. coatneyi*) (Figure S2).

Since *Pb*SIMP sequence did not have any known functional motifs or domains, we used multiple prediction tools for estimating its cellular localization. Phobus 1.01 server revealed ~98% probability of the protein being non-cytoplasmic and less than 1% being in

transmembrane region (Figure S3a). Predictions for membrane association were also made using the Protscale (Figure S3b), DTU-TMHM 2.0 server (Figure S3c), and Expasy-TMpred (Figure S3d). The Kyte-Doolittle hydropathy plot calculated from Protscale suggested a continuous high hydrophobic score between the amino acid residues 126–253. Further, DTU-TMHM 2.0 server and Expasy-TMpred predicted the presence of membrane-associated domain in the protein mostly between 163–219 amino acid residues (Figure S3e).

We next employed STRING database to predict the probable interacting partners for *Pb*SIMP. Our search with the query sequence yielded 3 interacting partners under the text mining category that included an RNA helicase (*PBANKA_1331900*), that belongs to the DEAD box helicase family, an adenylyl cyclase-associated protein (CAPS) (*PBANKA_0208000*), and Myosin A (*PBANKA_1355700*) (Figure S4). CAPs are evolutionarily conserved G-actin binding proteins that regulate microfilament turnover and are vital for oocyst development in mosquitoes (Hliscs et al., 2010). Myosin A is one of the unconventional Class XIV, that are neckless (Matuschewski et al., 2001).

Expression analysis revealed the highest transcription of *Pb*SIMP at oocyst stages (D14) likely suggesting a role at this stage or in salivary gland stage (Figure 1a). In order to investigate the functional role of *Pb*SIMP, we generated a knockout by replacing its locus with a targeting construct carrying a GFP and hDHFR drug selection marker (Figure 1b). The 5′ and 3′ regions of *Pb*SIMP were amplified by PCR and cloned in pBC-GFP-hDHFR plasmid (Figure 1c). Correct site-specific integration was confirmed by diagnostic PCR (Figure 1d). Two clones were obtained following limiting dilution of lines from independent transfections. Genotyping of both clones showed the absence of *Pb*SIMP *orf* (Figure 1e) and the recombinants expressed GFP (Figure 1f). The infectivity of mutants was compared with WT GFP line (Al-Nihmi et al., 2017) across all life cycle stages. Asexual propagation was monitored by injecting intravenously, 1×10^3 iRBC of mutant and GFP expressing WT parasites (WT GFP) into a group of mice (5 in each group). Parasitemia was monitored for 7 days post-infection, by making Giemsa-stained blood smears on daily basis. We noted no difference in the growth of mutants as compared to WT GFP (Figure 2a) in two independent experiments. The mutants were next analyzed in the mosquito by initiating a sexual cycle. We noted that the mutants were able to form zygotes, ookinetes (Figure 2b) and also successfully colonized the mosquito gut wall as evident by the presence of oocysts (Figure 2c). Interestingly, the frequency of oocyst/mosquito (Figure 2d), sporulation pattern (Figure 2e), oocyst sporozoites numbers (Figure 2f),

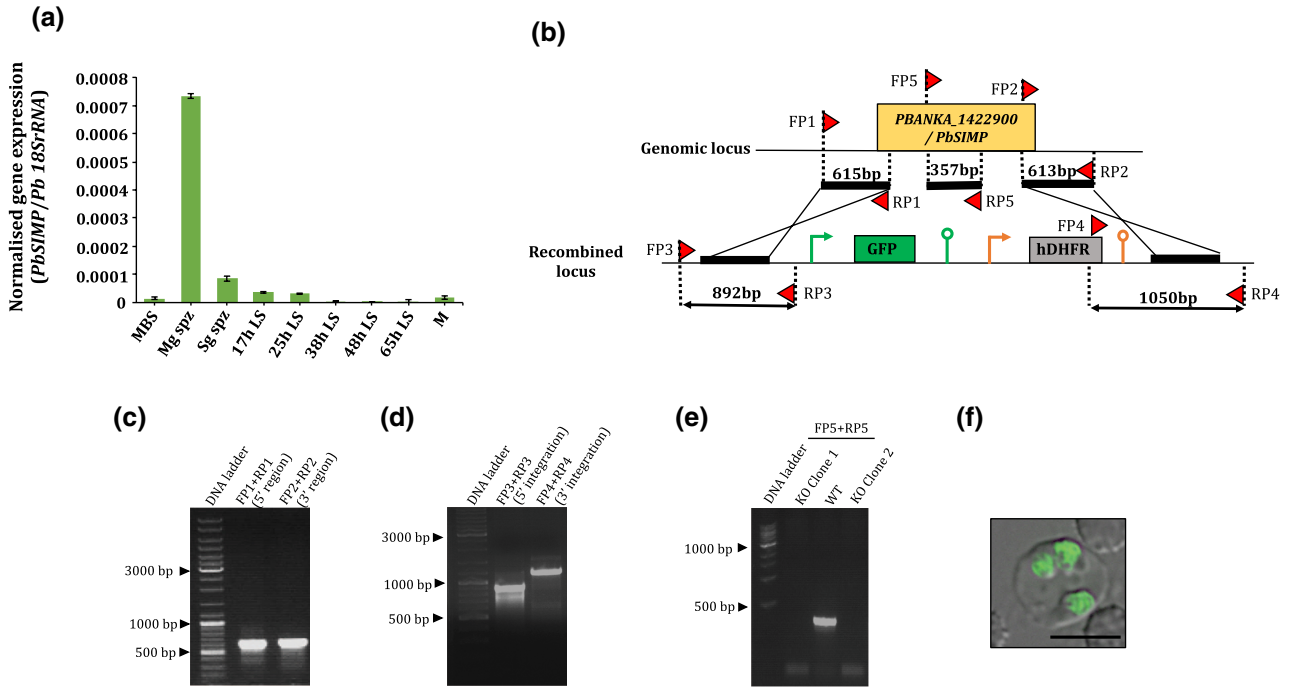


FIGURE 1 Gene expression analysis, generation of *PbSIMP* KO construct, and genotypic characterization of KO line. (a) Gene expression analysis. Determination of *PbSIMP* transcript levels across *Plasmodium berghei* life cycle stages by quantitative real-time PCR. cDNA samples were generated from different stages as indicated. MBS: mixed-blood stages, Mg spz: midgut sporozoites, Sg spz: salivary gland sporozoite stage, liver stages (LS) in hours (h): 17 h LS, 25 h LS, 38 h LS, 48 h LS, 65 h LS and M: merosomes. The expression values were normalized with *Pb18SrRNA* (internal control gene). (b) Strategy for generating *PbSIMP* KO. *Pb*SIMP 5′ and 3′ UTR regions used for generating the targeting construct for homologous recombination are indicated as solid lines. Recombined locus shows the replacement of *Pb*SIMP *orf* with GFP and hDHFR cassettes. Primers in red triangles (see Table S1 for primer sequences) and PCR product sizes are indicated. (c) Amplification of 5′ and 3′ UTR regions for generating the *Pb*SIMP KO targeting construct. (d) Diagnostic PCRs for confirming correct integration of KO cassette at *PbSIMP* locus. Primers used for diagnostic PCRs were designed flanking the homology arms used for recombination (as shown in b). (e) PCR showing the absence of *Pb*SIMP orf in KO clones from two independent transfections (C1 and C2). (f) Merged DIC image of asexual blood stage showing *PbSIMP* KO expressing GFP reporter (scale bar 5 μm)

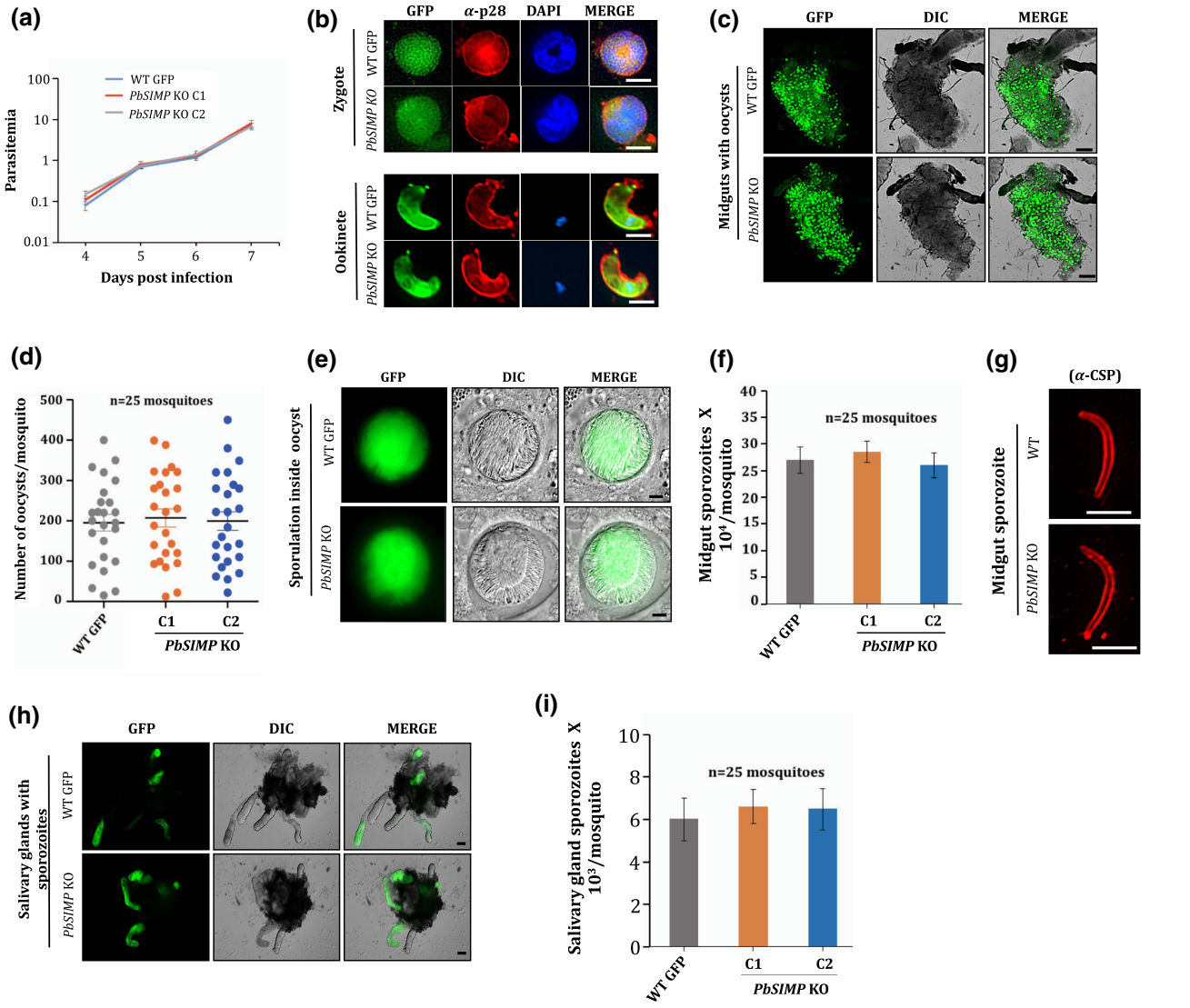


FIGURE 2 Phenotypic characterization of *PbSIMP* KO. (a) Asexual blood stage propagation. 1×10^3 infected RBCs of WT GFP and *PbSIMP* KO parasites (C1 and C2) were injected intravenously into mice and parasitemia was monitored daily for 7 days by microscopic observation of Giemsa-stained blood smears. (b) *PbSIMP* is dispensable for sexual stages of *P. berghei*. Infection was transmitted to *Anopheles* mosquitoes from mice infected with *PbSIMP* KO and WT GFP parasites to initiate sexual cycle. Mosquito midguts were dissected at 2 h and 18–20 h post-blood meal to visualize zygotes and ookinetes. Anti-p28 staining of zygote (2 h) and ookinete (18–20 h). Scale bar 5 μm. (c) Dissected mosquito midguts on day 14 showing oocysts. Scale bar 200 μm. (d) Dot plot showing quantification of oocyst numbers from individual mosquitoes. (e) Sporulation inside oocyst on day 14 post-infection. Scale bar 20 μm. (f) Bar graph showing quantification of midgut sporozoites per infected mosquito. (g) CSP staining of midgut sporozoites. Scale bar 5 μm. (h) Mosquito salivary glands harboring sporozoites on day 18 post-infection. Scale bar 200 μm. (i) Bar graph showing quantification of salivary glands sporozoites

and morphology of oocyst sporozoites (Figure 2g) was comparable to WT GFP. On D18-20 post-infection, dissected salivary glands revealed the presence of mutant sporozoites, suggesting their successful colonization of salivary glands (Figure 2h) and their load was comparable to WT (Figure 2i). However, observing the glands under higher magnifications revealed that the mutants failed to maintain a typical sickle shape structure characteristic of the WT sporozoites (Figure 3a). To analyze the structural alterations associated with the mutant sporozoites, we immunostained sporozoites with 3D11 monoclonal antibody specific for circumsporozoite protein (CSP) (Yoshida et al., 1980), a major sporozoite membrane protein. We noted distinct CSP immunoreactivity all along the membrane blebs at multiple foci (Figure 3b), that appeared like extensive membrane detachment when compared to WT sporozoites. Taken together, *Pb*SIMP depletion had a dramatic effect on sporozoite morphology, implying its function in the maintenance of the normal sporozoite structural integrity. Owing to its unique role, we refer to the product of *PBANKA_1422900* as sporozoite structural integrity maintenance protein (*Pb*SIMP).

Consistent with loss of regular shape, we noted that the SIMP mutants failed to perform gliding motility (Figure 3c), a pre-requisite for hepatocyte infection. These observations were further reiterated

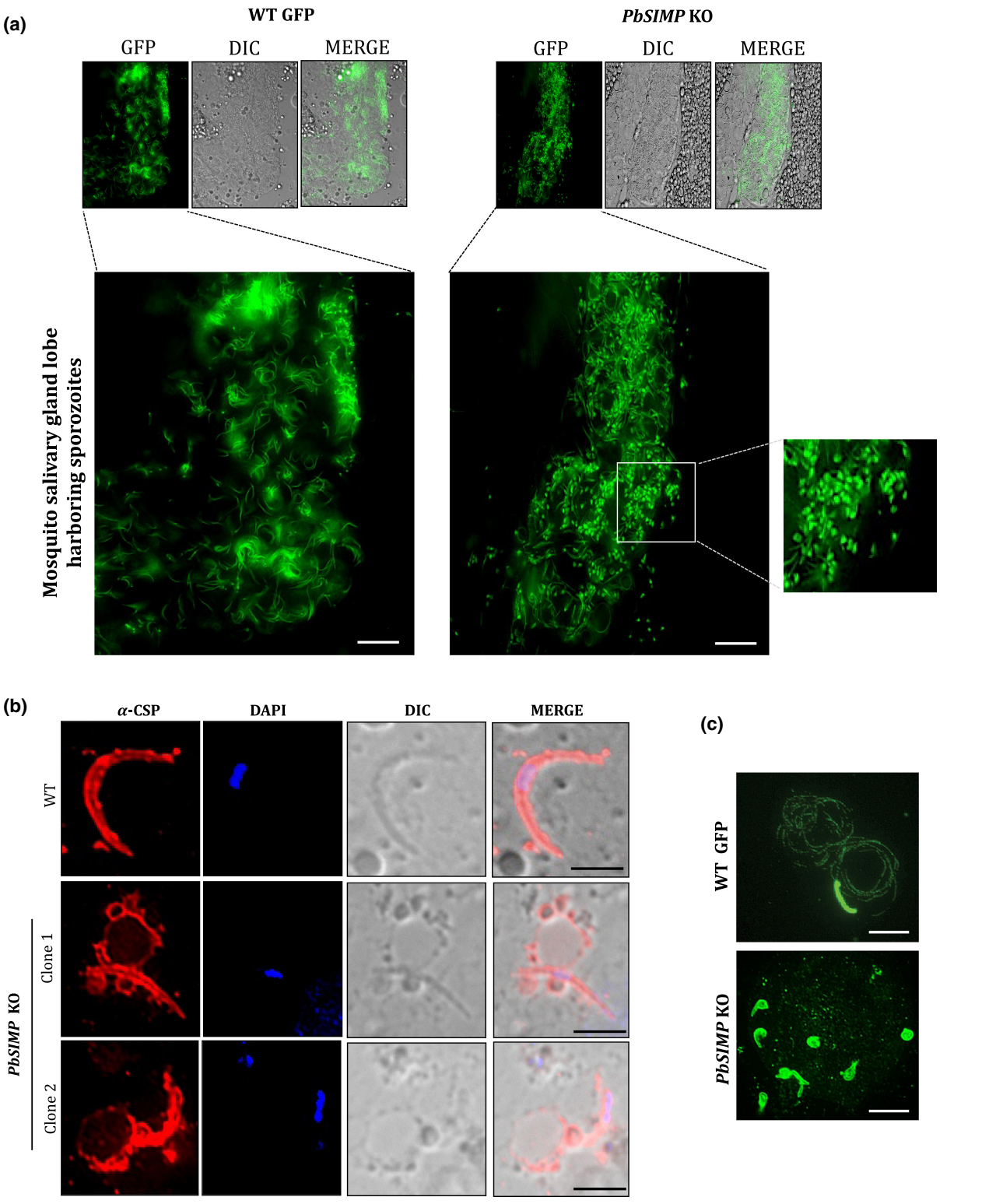


FIGURE 3 *Pb*SIMP KO sporozoites suffer from loss of regular shape and fail to glide. (a) Representative images of salivary glands at higher magnification (20×). Scale bar 20 μm. (b) CSP staining of salivary gland sporozoites. Sporozoite nuclei were stained with DAPI (Blue). Indirect immunofluorescence (IFA) was performed for both clones—C1 and C2. Scale bar 5 μm. (c) Gliding motility of WT and *Pb*SIMP KO sporozoites on glass slide. Scale bar 5 μm

by the inability of the mutant sporozoites to initiate blood-stage infection in mice that were intravenously injected with either 5×10^3 or 1×10^4 sporozoites (Table 1). Loss of motility in mutant sporozoite pointed to a likely association of *Pb*SIMP with molecular motor and concurred with STRING predictions, though the precise nature of interaction awaits further investigations.

TABLE 1 Analysis of pre-patency in *PbSIMP* KO sporozoites

Exp. No.	Parasite strain	No. of animals used for i.v. injection	No. of sporozoites injected per animal	No. of animals positive for blood-stage breakthrough	Pre-patency period (days)
1	WT	4	5×10^3	4/4	3.5
	PbSIMP KO	4	5×10^3	0/4	N/A
2	WT	3	1×10^4	3/3	3
	PbSIMP KO	3	1×10^4	0/3	N/A

Note: Pre-patent period: Defined as time required for the appearance of blood stage infection following exposure to sporozoites.

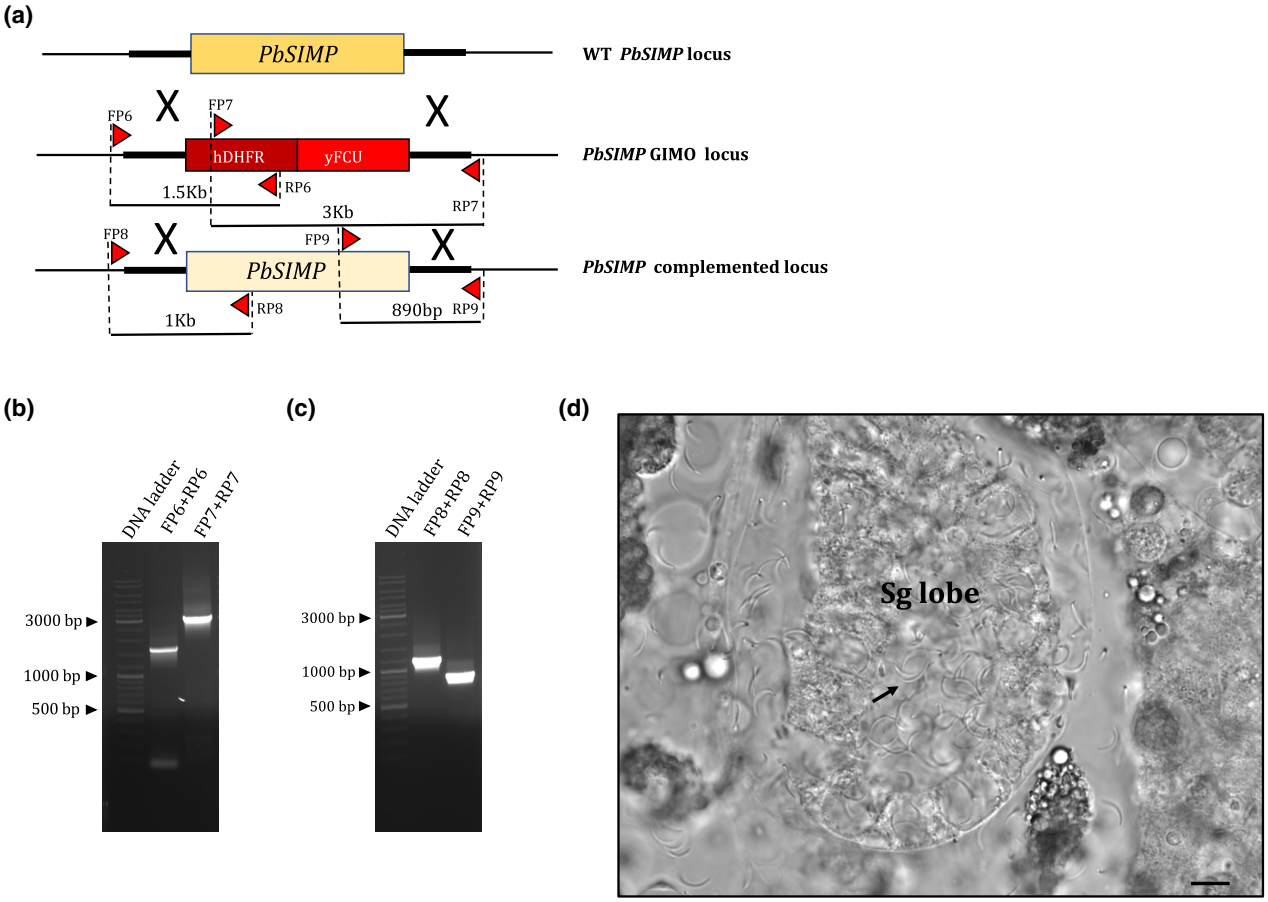


FIGURE 4 Generation of *Pb*SIMP GIMO line and complementation. (a) Targeting *PbSIMP* locus (top), with a positive–negative selectable marker (hDHFR:yFCU cassette) for generating *Pb*SIMP GIMO line (middle). *Pb*SIMP GIMO line was further complemented with *PbSIMP orf* (bottom). Arrows indicate the diagnostic primers to confirm correct integrations in *Pb*SIMP GIMO and complemented lines. Expected PCR product sizes were indicated. (b and c) PCRs for confirming correct integrations of the GIMO cassette and complementation of *PbSIMP orf*, respectively. (d) Restoration of salivary gland sporozoite phenotype in complemented line. Salivary gland lobe showing sporozoites with regular shape. Scale bar 10 μm

To demonstrate that the observed phenotype was specific to SIMP depletion, we restored the gene function by complementation. Toward this, we generated a *Pb*SIMP GIMO line by replacing the *Pb*SIMP locus with a positive–negative selectable marker cassette, hDHFR:yFCU (Figure 4a). The GIMO line was further complemented with a copy of *PbSIMP orf* (Figure 4a). The successful integration of GIMO cassette at *PbSIMP* locus and complementation of GIMO locus with *PbSIMP* copy was confirmed by PCR (Figure 4b,c). The *PbSIMP* complemented line produced salivary gland sporozoites similar to WT (Figure 4d) and were motile (data not shown).

Since the mutants suffered from extensive structural changes, we next analyzed if the cytoskeleton of sporozoite was also altered. *Plasmodium* sporozoites contain monomeric G actin in their cortical region that form transient arrays of F actin to provide linkage substrate for the adaptors of invasins/adhesins (Schmitz et al., 2010). We stained mutant salivary gland sporozoites with FITC-labeled phalloidin conjugates that bind to short and long filaments of actin. We noted intact F actin staining in mutants similar to WT salivary gland sporozoites (Figure 5a). Thus, structural alterations associated with SIMP mutant did not involve cytoskeletal

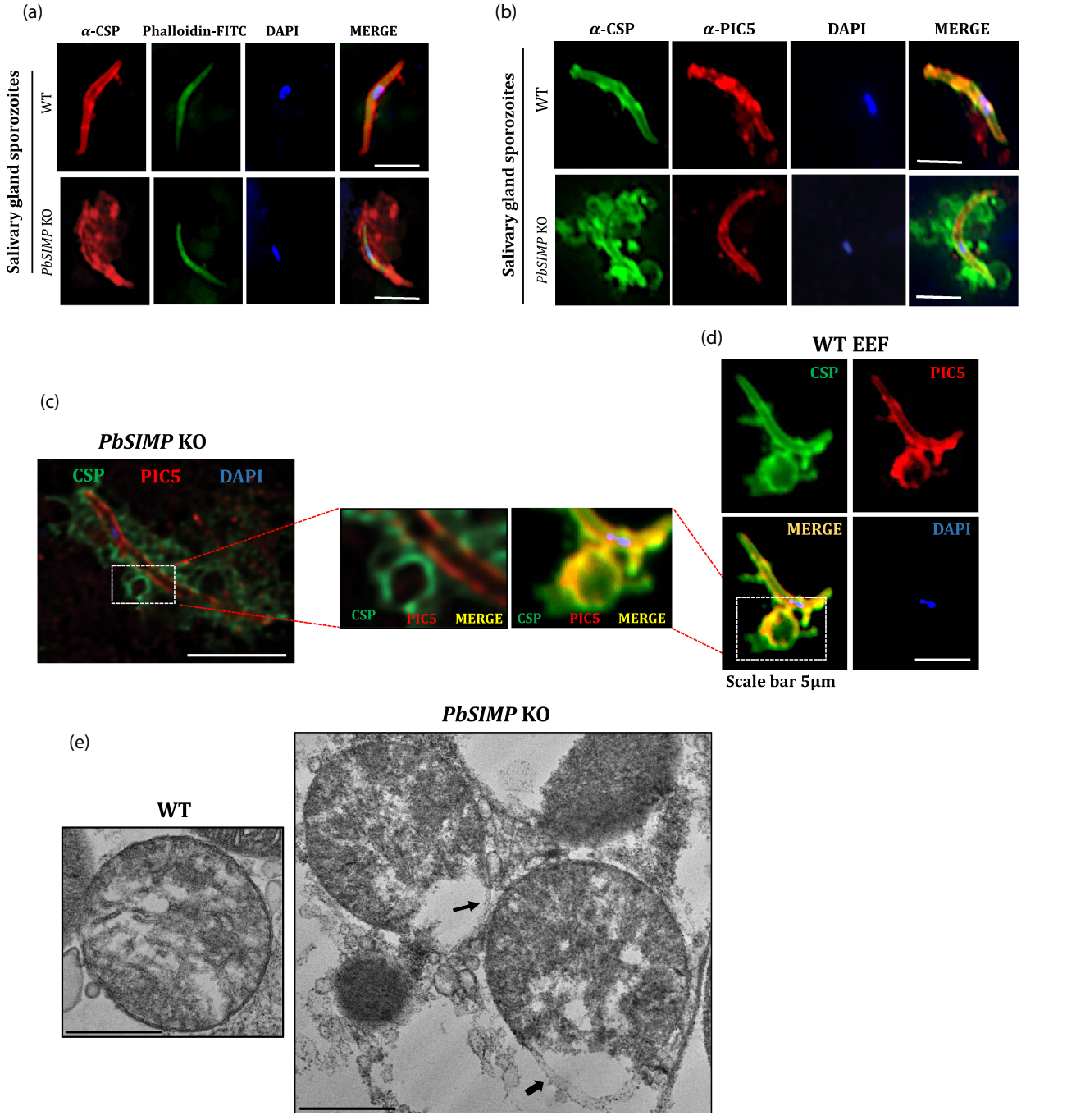


FIGURE 5 SIMP mutant sporozoites have normal cytoskeletal and IMC organization. (a) Staining of salivary gland sporozoites with anti-CSP (mouse) antibody and actin cytoskeletal elements with Phalloidin-FITC. The CSP immunoreactivity was revealed with goat anti-mouse Alexa 594. Scale bar 5 µm. (b) Staining of salivary gland sporozoites with anti-CSP (mouse) antibody and inner membrane complex (IMC) with anti-PIC5 (rabbit) antibody. Immunoreactivity was revealed with goat anti-mouse Alexa flour 488 and chicken anti-rabbit Alexa flour 594. DAPI was used to stain parasite nuclei. Scale bar 5 µm. (c and d) Comparison of IMC organization in *Pb*SIMP mutant sporozoite versus WT early EEF (2–4 h). Staining of sporozoites and EEFs with anti-CSP (mouse) antibody and IMC with anti-PIC5 (rabbit) antibody. Immunoreactivity was revealed with goat anti-mouse Alexa flour 488 and chicken anti-rabbit Alexa flour 594. DAPI was used to stain parasite nuclei. Scale bar 5 µm. (e) Transmission electron microscopy of sporozoites in cross section. The black arrow indicates membrane detachment in *Pb*SIMP KO sporozoites. Scale bar 0.5 µm

elements. Since sporozoite motility is dependent on the traction generated by a molecular motor that is connected with the inner membrane complex (IMC), we also analyzed the organization of IMC in mutant sporozoites. Immunostaining of PIC5, an IMC marker (Wichers et al., 2021) revealed an intact IMC organization in mutants (Figure 5b).

Toward a possible explanation for loss of normal shape in *Pb*SIMP mutant sporozoites, we further analyzed the nature of membrane alterations. Normally, when sporozoites transform into EEFs, the IMC dismantles and extends under the membrane until 24 h but later disappears (Kaiser et al., 2003). We analyzed if the membrane blebs of SIMP mutants have underlying IMC. We immunostained the *Pb*SIMP mutant sporozoites and 4–6 h WT EEFs (structurally reminiscent of the mutants forms) with anti-CSP antibody and anti-PIC5 antibody (Figure 5c,d). We noted that the mutants do not have extensions of IMC under the membrane, whereas in transforming WT sporozoites, IMC accompanied the membrane (Figure 5c,d). We conclude that *Pb*SIMP depletion likely leads to loss of contact of sporozoite membrane with underlying IMC. To reiterate the same, we analyzed the membrane organization in mutant sporozoites by TEM. We noted distinct membrane detachment in mutants (Figure 5e).

Toward demonstrating the cellular localization of SIMP, we generated a transgenic *P. berghei* line by translationally fusing *PbSIMP orf* with 3X hemagglutinin (HA) tag (Figure 6a) and confirmed correct integration by PCR (Figure 6b) and sequencing of a recombined locus (Figure S7d,e). The *Pb*SIMP HA transgenic produced normal oocyst and salivary gland sporozoites (Figure 6c). Immunofluorescence assay (IFA) revealed HA expression in gametocytes, ookinetes, oocyst, and salivary gland sporozoites (Figure 6d). Interestingly, the HA

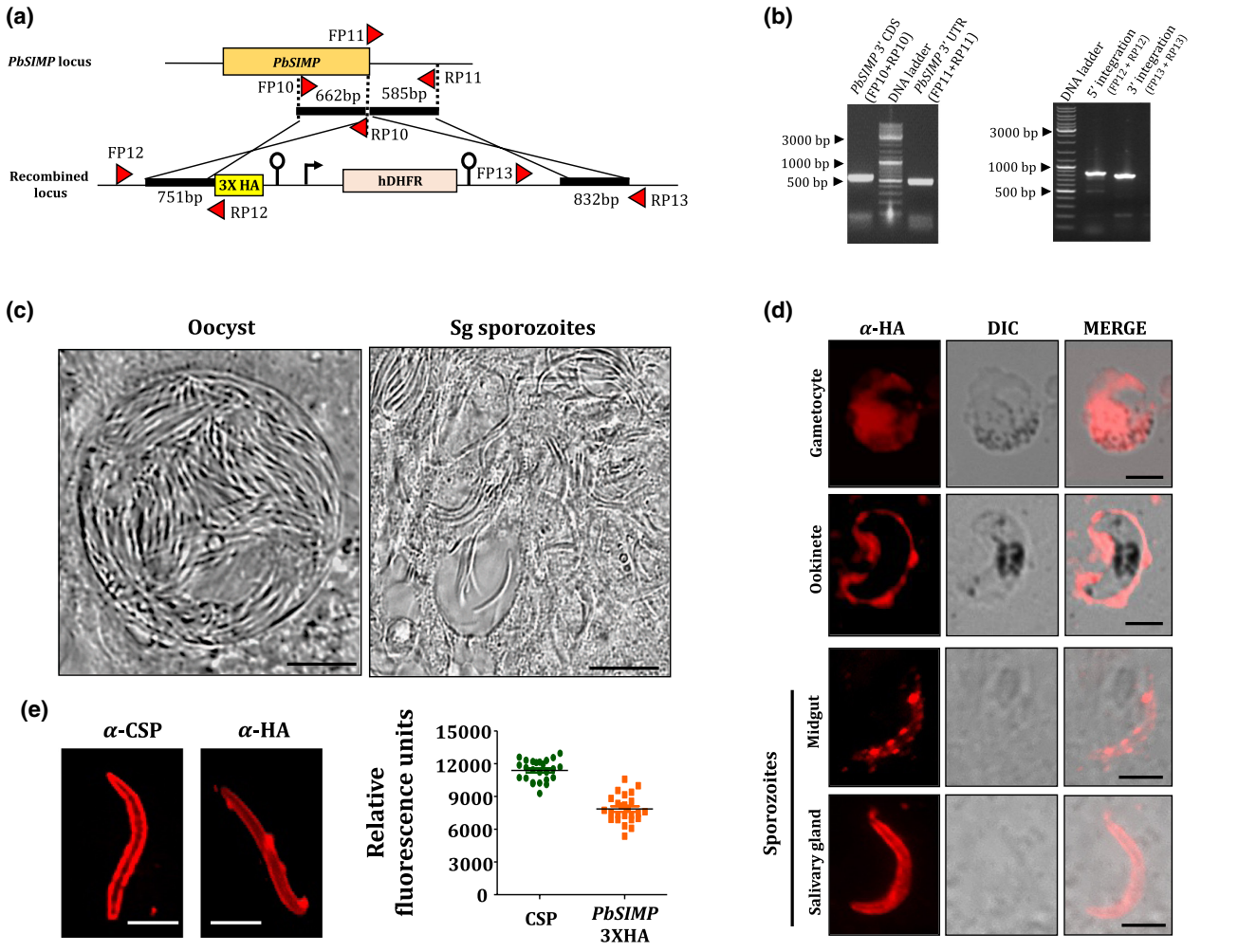


FIGURE 6 Generation of *Pb*SIMP HA transgenic line and investigating the epitope expression in midgut and salivary gland sporozoite stages. (a) Strategy for generation of *PbSIMP*-3XHA transgenic line. 3′ regions of coding sequence and UTR were amplified and cloned in pBC-3XHA-hDHFR to generate the targeting construct. After successful homologous recombination, a 3XHA was introduced in frame to *PbSIMP orf*. (b) Amplification of 3′ coding sequence (CDS) and 3′ UTR regions for generating the *Pb*SIMP 3XHA targeting construct (left panel). Diagnostic PCRs for confirming correct integration of 3XHA epitope tagged to *PbSIMP* CDS (right panel). Primers in red triangles and PCR product sizes are indicated. (c) *PbSIMP* 3XHA transgenic line showing normal development of oocyst and salivary gland sporozoites. Scale bar 10 μm. (d) Analysis of HA-specific expression in gametocytes, ookinetes, midgut, and salivary gland sporozoites. The HA expression was detected by staining with anti-HA (mouse) primary antibody and revealed with goat anti-mouse Alexa flour 594 secondary antibody. Scale bar 5 μm. (e) Immunostaining and quantification HA and CSP of *Pb*SIMP 3XHA tagged salivary gland sporozoites. *PbSIMP* 3XHA transgenic sporozoites were stained with either anti-HA or anti-CSP antibody and the immunoreactivity was revealed with goat anti-mouse Alexa flour 594 (left panel). Dot plot showing the intensity of immunofluorescence signals from sporozoites. Results are represented as relative fluorescence units (right panel). Scale bar 5 μm

immunoreactivity was majorly localized to gametocyte cytoplasm, however, in ookinetes, oocyst, and salivary gland sporozoites, we noted peripheral/membrane localization. High levels of HA expression in salivary gland sporozoites were consistent with structural alteration in the membrane of *Pb*SIMP mutants (Figure 6d). We also compared the levels of HA signals with that of CSP, a predominant membrane protein and a prime target of protective immune responses on radiation attenuated sporozoites (Kumar et al., 2006). HA signal intensity accounted for nearly 50% or more of CSP (Figure 6e). Taken together, we conclude that *Pb*SIMP localizes to sporozoite membrane and has high levels of expression in salivary gland sporozoites.

DTU-TMHM 2.0 server and Expasy-TMpred predicted the presence of membrane-associated domain in the protein mostly between 163 and 219 amino acid residues. To investigate the possible orientation of *Pb*SIMP beyond 219 amino acids, we used the *Pb*SIMP C-terminal HA-tagged transgenic line. The transgenic sporozoites were fixed and immunostained for HA and IMC marker-PIC5 under both non-permeabilized and permeabilized conditions (Figure 7a, upper panel). As a positive control, we stained sporozoites with anti-CSP and PIC5 (Figure 7a, lower panel). As expected, CSP gave a strong positive signal owing to its membrane attachment through its GPI anchor sequence (Figure 7a lower panel). We also noted a very strong signal for HA, suggesting that the C-terminus was indeed extracellular (Figure 7a upper panel). Since PIC5 is an IMC marker that is located underneath the plasma membrane, we used it as a negative control for staining. As expected, we did not see any IMC staining under non-permeabilized conditions (Figure 7a) while IMC showed prominent signals in permeabilized sporozoites (Figure 7b). We conclude that *Pb*SIMP has an extracellular C-terminus, though the precise length of this domain needs to be identified.

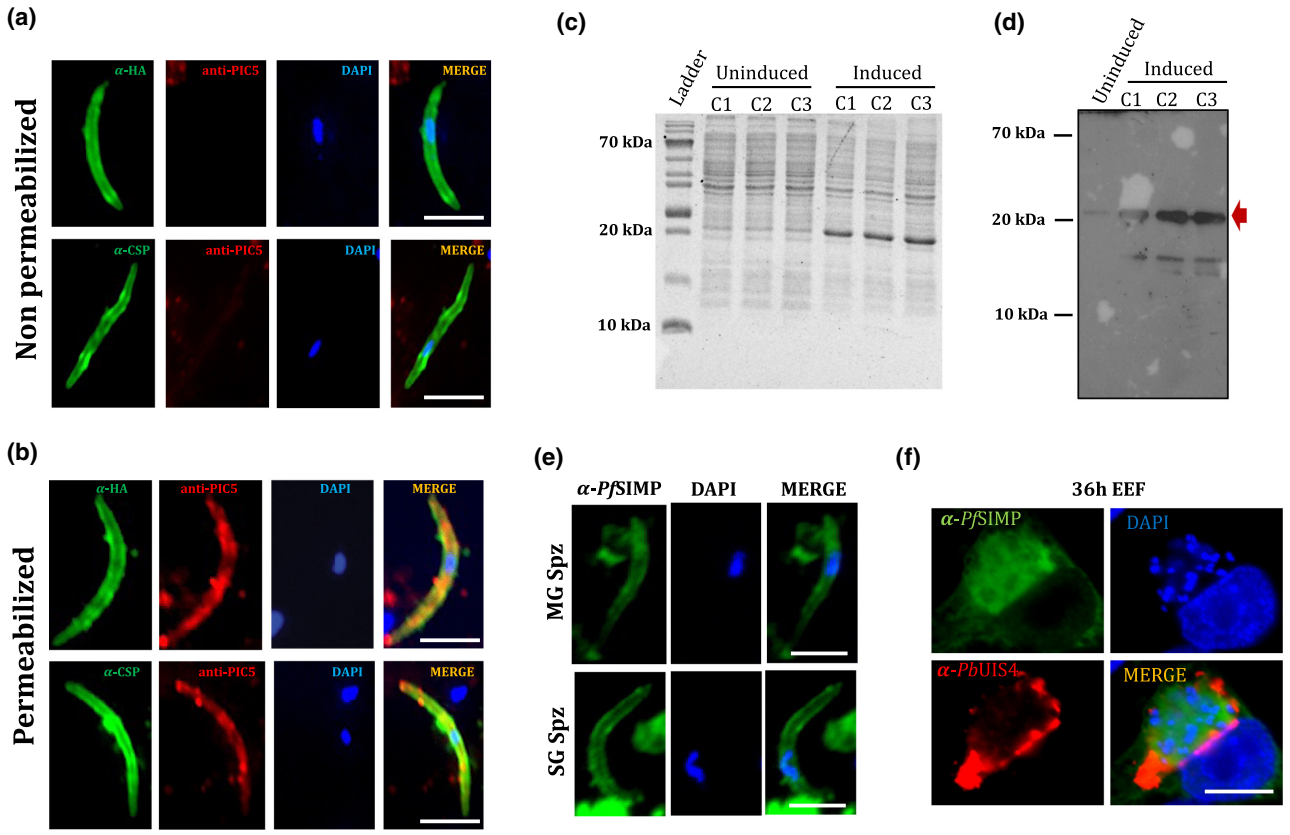


FIGURE 7 C-terminus of *Pb*SIMP is extracellular. (a and b) *Pb*SIMP HA transgenic sporozoites were fixed and immunostained with anti-HA (mouse) or anti-CSP (mouse) and anti-PIC5 (rabbit) antibody under (a) non-permeabilized and (b) permeabilized conditions. The immunoreactivity was revealed with goat anti-mouse tagged to Alexa 488 and chicken anti-rabbit tagged to Alexa 594. Scale bar 5 μm. (c) SDS-PAGE showing recombinant protein expression of *Pf*SIMP C-terminus. Coomassie-stained SDS-PAGE gel showing *Pf*SIMP expression profile from three clones (C1–C3) under IPTG induced and uninduced conditions. (d) Confirmation of *Pf*SIMP recombinant protein expression by western blotting using anti-His (mouse) antibody under induced and uninduced conditions. Immunoreactivity was revealed with HRP-conjugated anti-mouse secondary antibody. (e) Immunoreactivity of *Pf*SIMP C-terminus antibody on non-permeabilized sporozoites. WT *P. berghei* salivary gland sporozoites were fixed and stained with mouse antisera generated against recombinant *Pf*SIMP C-terminus (under non-permeabilized conditions). The immunoreactivity was revealed with goat anti-mouse secondary antibody conjugated to Alexa Fluor 488. The parasite nuclei were stained with DAPI. MG Spz: midgut/oocyst sporozoites, SG Spz: salivary gland sporozoites. Scale bar 5 μm. (f) SIMP is detected in the septa of developing EEFs at 36 h. EEFs were immunostained with mouse *Pf*SIMP (c-terminus) antisera and rabbit anti-UIS4 antibody. The immunoreactivity was revealed with goat anti-mouse Alexa flour 488 and chicken anti-rabbit Alexa flour 594. The host and parasite nuclei were stained with DAPI. Scale bar 10 μm

The C-terminus of *Pf*SIMP has 76% identity to *Pb*SIMP (Figure S5a,b). BepiPred software predicted four peptides with a score above 0.62 (Figure 5c), within this region for both *P. berghei* and *P. falciparum* likely, suggesting a probability of being highly immunogenic. We cloned and expressed C-terminal *Pf*SIMP from 201 to 393 amino acids (Figure 7c,d) and generated antisera against purified recombinant. We performed IFA under non-permeabilizing conditions in WT *P. berghei* sporozoites using antisera against *Pf*SIMP C-terminus. We noted a distinct immunoreactivity on the membrane of midgut and salivary gland sporozoites (Figure 7e) that concurred with our previous observations (Figure 6e). We also analyzed the expression of SIMP in in vitro grown *P. berghei* EEFs. Interestingly, at 36 h we noted a distinct immunoreactivity in the septa that partitions the daughter merozoites into different compartments (Figure 7f). However, the function of SIMP in liver stages merits additional investigation.

The commitment of *Plasmodium* sporozoites to hepatocytes is an event central to the establishment of malaria infection in mammals and hence blocking this process holds great therapeutic potential to prevent clinical malaria. In fact, recent years have seen a surge in defining the protein composition of sporozoite membrane—apparently for two important reasons viz., (1) sporozoite proteins act as ligands for hepatocyte membrane, hence their extensive functional characterization may broaden the scope of intervening hepatocyte-sporozoite interactions and (2) the membrane-anchored proteins that physically connect to the components of actomyosin molecular motor may serve as additional targets for inhibiting gliding motility, thus tackling the sporozoites at initial stages of infection. In line with such pursuit, we report the functional role of a conserved *Plasmodium* protein-SIMP in maintaining sporozoite shape and hepatocyte infectivity. We demonstrate that SIMP localizes to the sporozoite membrane, and its C-terminus is highly conserved between *P. berghei* and *P. falciparum* and is likely to be extracellular.

Our in silico predictions for probable cellular localization and membrane association concurred well with genetic evidence that validated the role of SIMP in sporozoite membrane-specific function. While functional mapping of precise C-terminus awaits further investigations, the SIMP-HA transgenics nonetheless, reveal the tag to be extracellular, a finding that has significant therapeutic implications by antibody-mediated sporozoite neutralization. Further, the spatiotemporal expression of SIMP during oocyst to salivary gland stages, reiterated the requirement of SIMP primarily in salivary gland sporozoite stage, which also explains why the oocyst sporozoites did not succumb to phenotypic alterations following depletion of SIMP. Such patterns of gene expression concur with independent programs of translational repression implicated in multiple sporozoite-specific functions, including invasion of hepatocytes (Bogale et al., 2021). SIMP manifests translational repression in the sexual stages of *P. berghei* (Mair et al., 2006). However, our gene expression analysis and epitope tagging showed no translational repression in oocyst and salivary gland sporozoite stages as documented earlier in *P. falciparum* and *P. yoelii* (Lindner et al., 2019).

The link between SIMP depletion and loss of motility may hint at its role as an invasin-like protein anchoring the sporozoite plasma membrane with the underlying molecular motor. Members of the TRAP family of protein connect to the molecular motor through an adaptor protein aldolase (Combe et al., 2009; Jewett & Sibley, 2003). Our findings that SIMP mutants fail to glide and infect hepatocytes may point to its likely interaction with Myo A and CAPs as predicted by STRING interactions and concurs with known roles of both interacting partners in motility-related functions viz., CAPs in microfilament turn over (Hliscs et al., 2010) and Myosin A in invasion (Robert-Paganin et al., 2019). Nonetheless, our studies of colocalization of SIMP HA with sporozoite membrane marker—TRAP, lack of colocalization of IMC marker-PIC5 with the membrane extensions in mutant sporozoites and distinct membrane detachment in *Pb*SIMP mutants argues to the point that SIMP may anchor sporozoite membrane to underlying molecular motor.

A previous study reported the phenotypic characterization of *Pb*SIMP mutants that was designated as PIMMS22 (Ukegbu et al., 2021). Here the expression of PIMMS22 was demonstrated in gametocyte cytoplasm, ookinete periphery, and in permeabilized as well as non-permeabilized midgut sporozoites. The PIMMS22 mutants produced a reduced number of ookinetes that manifested defect in the midgut invasion in *Anopheles coluzzii* mosquitoes. However, in contrast to these findings, we noted no defect in sexual reproduction and oocyst formation in *Anopheles stephensi* mosquitoes. The probable discrepancy can be attributed to the differential susceptibility of *Plasmodium* infections to different *Anopheles* species. A former study detected *Pb*SIMP peptide in the mass spectrometry analysis of *P. falciparum* and *P. yoelii* whole sporozoite lysates (Lindner et al., 2013). However, our studies provide definitive evidence for its membrane association.

The gross morphology of *Pb*SIMP mutants is reminiscent of the premature sporozoite transformation as seen for other mutants that lack eukaryotic initiation factor-2 alpha kinase (IK2) (Zhang et al., 2010) and Pumilio-2 (Puff2) (Gomes-Santos et al., 2011; Muller et al., 2011). The premature transformation of sporozoites in these instances has been attributed to loss of latency in sporozoites resulting from lack of phosphorylation of eIF2-alpha (Zhang et al., 2010) and to possible loss of post-transcriptional regulatory mechanism, in the absence of Pumilio-2 (Gomes-Santos et al., 2011, Muller et al., 2011). In contrast to the mechanistic underpinning as described for these mutants, the possible EEF-like phenotype observed in our studies is likely due to membrane detachment in the absence of *Pb*SIMP. Further investigations are needed to ascertain the physical interaction of *Pb*SIMP with components of molecular motor and if these interactions are mediated by specific adaptor proteins (Figure 8).

3 | CONCLUSIONS

Taken together, our studies show for the first time that *Pb*SIMP is indispensable for producing functionally viable salivary gland

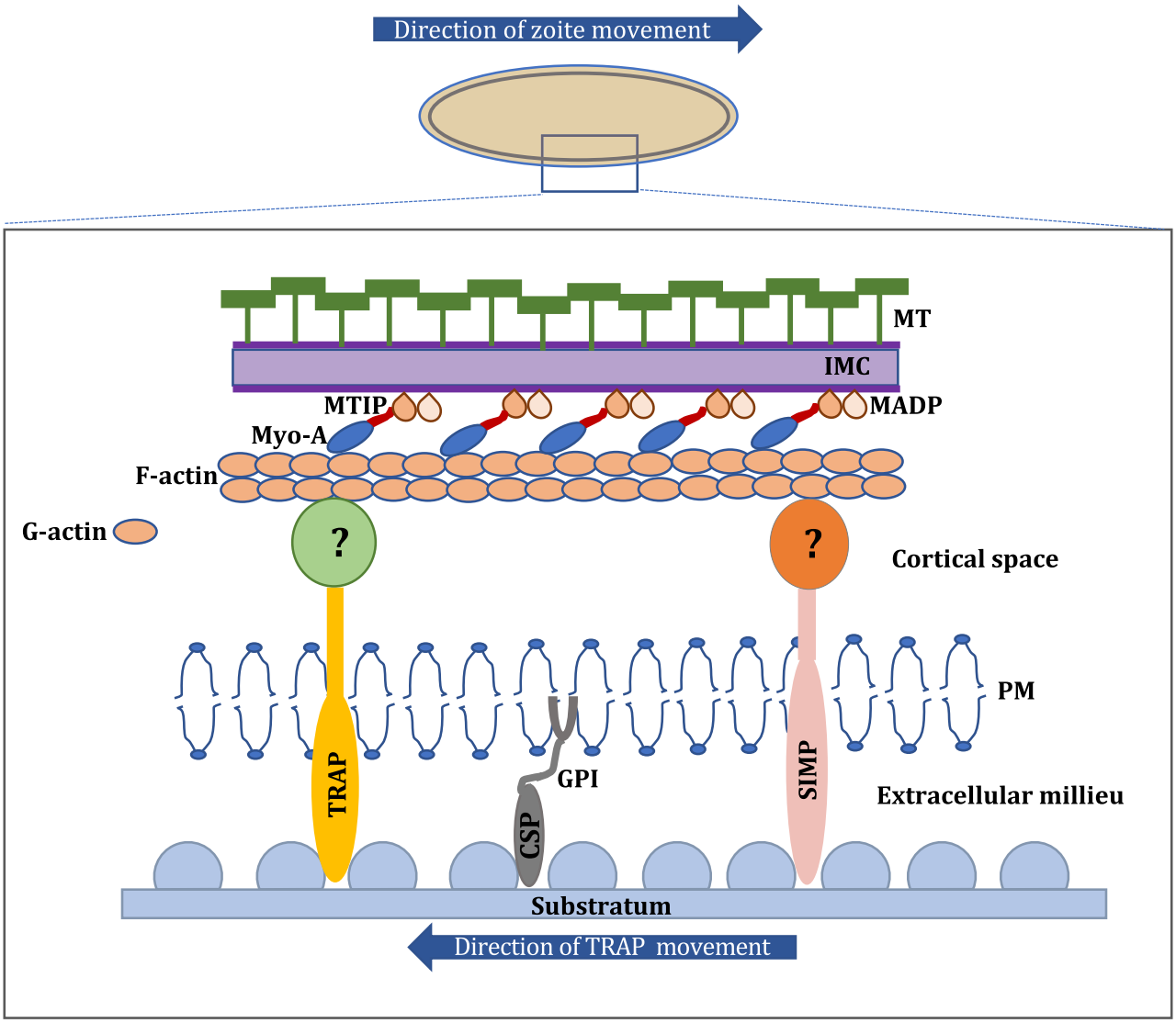


FIGURE 8 A schematic model of sporozoite plasma membrane with newly identified protein SIMP. The sporozoite membrane is shown with known markers like CSP (attached by GPI anchor sequence) and TRAP (attached through transmembrane domain). In the current study, we show *Pb*SIMP as a novel protein associated with the sporozoite membrane through its predicted membrane-binding/transmembrane domain, exposing the C-terminus extracellularly. The association of *Pb*SIMP N-terminus to molecular motor is speculative. MT: Microtubule, IMC: Inner membrane complex, MTIP: Myosin A tail domain interacting protein, MADP: myosin A docking protein, PM: plasma membrane, GPI: glycosylphosphatidylinositol, CSP: circumsporozoite protein, TRAP: thrombospondin-related anonymous protein, SIMP: structural integrity maintenance protein

sporozoites capable of maintaining regular shape and hence facilitating gliding and invasion of hepatocytes. This is likely possible if SIMP acts as an invasin linking extracellular receptors to molecular motor. Since the extracellular C-terminus of SIMP is highly conserved, antibodies that can effectively target this domain may have therapeutic potential in inhibiting sporozoite invasion. A possibility of such a speculation is both exciting and worth exploring considering the abundance of *Pb*SIMP on sporozoite membrane (nearly 50% or more as compared to CSP). In line with the notion that a vaccine encompassing multiple sporozoite surface antigens will induce better protection, SIMP may be a promising candidate and can be included in combination with other potent antigens like CSP.

4 | MATERIALS AND METHODS

4.1 | Experimental animals and parasite lines

Six- to eight-week-old female BALB/c, Swiss albino, or C57BL/6 mice were purchased from National Institute of Nutrition (NIN), Hyderabad, India, and used for all animal experiments. All animal experiments were approved by Institutional Animal Ethical Committee and were in accordance with the CPCSEA guidelines. *Plasmodium* cycles were initiated by asexual propagation of WT GFP, *Pb*SIMP *KO* line, *Pb*SIMP-complemented line, and *Pb*SIMP 3XHA tagged line in Swiss Albino mice or BALB/c mice. To obtain the mosquito stages of *Plasmodium*, female *Anopheles* mosquitoes were allowed to obtain a

blood meal from gametocyte-positive mice carrying respective parasite lines. For analysis of pre-patency, C57BL/6 mice were infected with WT GFP and *Pb*SIMP KO sporozoites by intravenous route.

4.2 | Phylogenetic analysis

The nucleotide sequence of *Pb*SIMP was used as query for searching homologs in NCBI. The sequences were subjected to multiple sequence alignment using the MUSCLE method, and the aligned sequences were used to generate the phylogenetic trees. Care was taken to consider only those sequences that were translated in frame with reference to the standard genetic code. The phylogenetic tree was generated using the Maximum Likelihood method and General Time Reversible model. The rates of substitution were analyzed using the gamma distribution model.

4.3 | Prediction of cellular localization of *Pb*SIMP

The cellular localization probability *PbSIMP* was estimated using Phobus 1.01 server (Kall et al., 2007). Phobus uses a hidden Markov model (HMM) approach to calculate the localization probabilities. Protscale (Elisabeth Gasteiger et al., 2005) was used to calculate the Kyte-Doolittle hydropathy plot. For Kyte-Doolittle prediction, window size 19 was used. Expasy-TMpred and DTU-TMHM 2.0 were used to predict the transmembrane nature of the protein. Expasy-TMpred is based on TMbase (Hofmann & Stoffel, 1993), a database for naturally occurring transmembrane proteins, while DTU-TMHM 2.0 utilizes a hidden Markov model (Krogh et al., 2001) to predict the transmembrane topology. For an unbiased prediction, multiple tools were selected.

4.4 | Cell lines

HepG2 cell lines were procured from National Centre for Cell Science (NCCS), Pune, India. Cells were maintained in complete Dulbecco's modified Eagle's medium (DMEM)(Gibco) containing 25 mM HEPES, 2 mM L-glutamine, and 4.5 g/L glucose supplemented with 10% fetal bovine serum (FBS) (Gibco), 1× antibiotic antimycotic (Gibco).

4.5 | Retrieval and alignment of *Pb*SIMP and its orthologs

DNA and protein sequences of *P. berghei* SIMP and its orthologues were retrieved from PlasmoDB (www.plasmodb.org). Primers were designed based on the sequence information provided on these databases. MULTALIN (http://multalin.toulouse.inra.fr/multalin/) tool was used to check SIMP protein homology among *P. berghei*, *P. yoelii*, and *P. chabaudi* which are rodent *Plasmodium* strains, and *P. falciparum* (human strain).

4.6 | Gene expression analysis

Total RNA was isolated from mixed blood stages, day 14 midgut sporozoites, days 18–20 salivary gland sporozoites, in vitro liver stages at various time points (17 h, 25 h, 38 h, 48 h, and 65 h) and merosomes. For preparing RNA from midgut and salivary gland sporozoites, nearly 150–200 mosquitos were dissected. The dissected guts and salivary glands were mechanically disrupted by crushing with a plastic pestle. To obtain RNA from liver stages, HepG2 cells were infected with salivary gland sporozoites and lysed at different points as mentioned above. RNA from mixed blood stages was obtained from mouse infected with WT *P. berghei*. All samples were lysed in Trizol (Invitrogen, Cat# 15596026) and RNA was extracted using PureLink RNA mini kit (Life technologies, Cat# 12183018A) following the manufacturer's instructions. The cDNA synthesis was performed in 20 µl volume that contained 2 µg total RNA and 2 µl each of 10× PCR buffer, 2.5 mM dNTPs (Invitrogen, cat# R72501), 5 mM MgCl2, 2.5 mM random hexamers (Applied Biosystems, cat# N8080127), 1.5 units RNAse inhibitor (Applied Biosystems, N8080119), and 1.5 units MuLV reverse transcriptase (Applied Biosystems, cat# AM2682). Gene expression of *Pb*SIMP across all life cycle stages was measured by real-time PCR using the absolute quantification method. Gene-specific standard was generated by amplifying a 148 bp product from *Pb*SIMP *orf* using primers mentioned in Table 1. The product was cloned into a TA vector. The standard for *Pb18S rRNA* was similarly made, which was used as internal control (Al-Nihmi et al., 2017). The normalized gene expression values were calculated by taking the ratio of *Pb*SIMP and *Pb18SrRNA*.

4.7 | Generation of knockout parasites

PbSIMP knockout (KO) parasites were generated by the double homologous recombination method by replacing the endogenous locus with the KO construct (Janse et al., 2006). The KO targeting construct carried a 615 bp of 5′ upstream homology region and 613 bp of 3′ downstream homology region of *PbSIMP*. The 5′ and 3′ regions were amplified from *P. berghei* genomic DNA using primers FP1/RP1 and FP2/RP2. These amplified 5′ and 3′ products were cloned into the pBC-GFP-hDHFR vector at *Xho*I/*Cla*I and *Not*I/*Asc*I sites, respectively. Targeting cassette was released from vector using *Xho*I and *Asc*I digestion and gel purified. Two independent transfections were performed using the method described earlier (Janse et al., 2006). Briefly, 5 µg of DNA was added to purified schizonts and mixed with amaxa nucleofector solution (VPA-1006). Electroporation was performed by using program U-033. The electroporated schizonts were intravenously injected into mice. Twenty-four hours post-transfection, mice were kept on pyrimethamine selection for 8–12 days. Following successful selection, recombinant GFP expressing KO parasites were obtained. Genomic DNA was isolated from transfectants, and correct integration of KO targeting cassette at *PbSIMP* locus was confirmed

by integration PCR using primers indicated in Table S1. Limiting dilution was performed to obtain single clone population. Two clones (C1 and C2), one from each independent transfection were confirmed for the absence of *PbSIMP orf* by PCR using primers indicated in Table S1. These clones were used for phenotypic characterization across all life cycle stages.

4.8 | Generation of pSKC-hDHFR:yFCU plasmid

To generate pSKC-hDHFR:yFCU plasmid, the positive–negative selectable marker cassette (hDHFR:yFCU) was amplified from the plasmid pL1186 (Ponzi et al., 2009) using the primers SM-F/SM-R (Table S1). The amplified product was gel purified and digested with *Sal*I/*Not*I. The GFP-hDHFR cassettes in pBC-GFP-hDHFR (Figure S6a) plasmid (Al-Nihmi et al., 2017) was replaced with hDHFR:yFCU cassette (Figure S6b) using *Sal*I/*Not*I restriction sites to obtain pSKC-hDHFR:yFCU (Figure S6c) and the plasmid was confirmed by sanger sequencing.

4.9 | Complementation of *PbSIMP* mutant

For complementation, a GIMO line was generated by targeting *PbSIMP* locus with hDHFR:yFCU positive–negative selectable marker (Lin et al., 2011). The 5′ and 3′ UTR regions of *PbSIMP* were amplified using primers FP1/RP1 and FP2/RP2, respectively. These fragments were cloned into pSKC-hDHFR:yFCU plasmid at *Xho*I/*Sal*I and *Not*I/*Asc*I restriction sites, respectively. The targeting construct was released from vector backbone using *Xho*I *and Asc*I, gel purified and electroporated into WT *P. berghei* schizonts. The selection of *PbSIMP* GIMO line was performed as described earlier (Janse et al., 2006). The correct integration of hDHFR:yFCU cassette was confirmed using primers FP6/RP6 and FP7/ RP7. To generate the complementation construct, *PbSIMP orf* with 5′ and 3′ homology regions was amplified using the primers FP1/RP2 and gel purified. *PbSIMP* GIMO line was transfected with the purified complementation construct and the integrants were enriched by negative selection using 5-fluorocytosine (Janse et al., 2006; Lin et al., 2011). Successful replacement was confirmed using primers FP8/RP8 and FP9/RP9. All the primers used are described in Table S1.

4.10 | Generation of pBC-3XHA-hDHFR localization plasmid

To generate pBC-3XHA-hDHFR, *Pbhsp70* promoter, and *gfp orf* of pBC-GFP-hDHFR (Figure S7a) were replaced with 3XHA oligos annealed in vitro (Figure S7b and Table S1). Annealed 3XHA oligos yielded dsDNA with overhangs that are compatible to ligate with the DNA digested with restriction enzymes *Xho*I/*Bgl*II. pBC-GFP-hDHFR was digested with *Xho*I/*Bgl*II, and annealed 3XHA oligos were ligated to obtain pBC-3XHA-hDHFR (Figure S7c) localization plasmid and sequence was confirmed by sanger sequencing.

4.11 | Generation of *Pb*SIMP 3XHA transgenic line for studying localization

For generation of *Pb*SIMP 3XHA transgenic line, a 562 bp coding region excluding stop codon and a 525 bp 3′UTR were amplified using primers FP10/RP10 and FP11/RP11, respectively. Both the fragments were cloned into the pBC-3XHA-hDHFR vector at *Apa*I/*Xho*I and *Not*I/*Asc*I restriction sites, respectively. The targeting construct was released from vector backbone using *Apa*I and *Asc*I double digestion and gel purified. The electroporation and selection of transfectants were performed as described earlier (Janse et al., 2006). After obtaining successful transfectants, genomic DNA was isolated, and the integration of 3XHA-hDHFR cassette was confirmed by using integration-specific primers FP12/RP12 and FP13/RP13. The primer sequences are indicated in Table S1.

4.12 | Phenotypic analysis of *Pb*SIMP KO parasites during asexual blood stages

To analyze the asexual propagation rates of *Pb*SIMP KO parasites, approximately 1×10^3 infected RBC of KO (both C1 and C2) and WT GFP parasites (Al-Nihmi et al., 2017) were injected intravenously into a group of three female 4- to 6-week-old Swiss albino mice. Parasitemia was monitored daily by making Giemsa-stained blood smears for 7 days. Parasitemia was determined by microscopic examination of 25 random fields of uniform thin smears.

4.13 | Phenotypic analysis of *Pb*SIMP KO and 3XHA tagged parasites in mosquito

Female *Anopheles stephensi* mosquitoes were allowed to obtain a blood meal from Swiss albino mice carrying 1%–2% gametocytes of *PbSIMP* KO and WT GFP line. Two consecutive blood meals were given at 24 h time interval. Blood-fed mosquitoes were maintained at 20°C and 80% RH for 18–22 days to facilitate the successful completion of sexual development and for the formation of salivary gland sporozoites. To obtain zygotes and ookinetes, four to five mosquitoes were dissected at 2–4 h and 16-18 h post-blood meal, respectively. The guts were mechanically disrupted and 2–3 µl of sample was spotted on glass slides for performing indirect immunofluorescence assay (IFA). Successful transmission of malaria to *Anopheles* mosquitoes was monitored by observing infected guts and salivary glands for GFP expressing oocysts and sporozoites, respectively, on day 14 and days 18–20 post-blood meal. The mosquito midguts and salivary glands were dissected in incomplete RPMI-1640 (Gibco, Cat# 21875034) The sporulation of oocyst was observed at 100×. To assess the morphology of mutant oocyst and salivary gland sporozoites, the infected guts, and glands were dissected and mechanically disrupted. The samples were centrifuged at 800 rpm for 3 min. The supernatant containing sporozoites was

used for in vitro EEF development and mice infections. Different mosquito stages of *Plasmodium* were visualized using Nikon-AR fluorescent microscope.

4.14 | Analysis of *Pb*SIMP KO sporozoite infectivity

To analyze the infectivity of *Pb*SIMP KO sporozoites, C57BL/6 mice were intravenously injected with 5×10^3 and 1×10^4 into groups of mice (3–4/group). The parasitemia was monitored daily from days 3 to 15 post-infection by examining Giemsa-stained tail blood smears. Pre-patency was determined from two independent experiments.

4.15 | Indirect immunofluorescence assay

To analyze the morphology of mutant sporozoites and liver stages, IFA was performed as described earlier (Jillapalli et al., 2019; Togiri et al., 2019). The zygotes and ookinetes were stained with anti-p28 antibody (mouse) and immunoreactivity was revealed using goat anti-mouse Alexa 594. The midgut and salivary gland sporozoites were stained with 3D11, a mouse monoclonal antibody (Yoshida et al., 1980) specific for *P. berghei* Circumsporozoite protein (CSP) (mouse) and immunoreactivity was revealed using goat anti-mouse Alexa 594. *PbSIMP* expression was analyzed in gametocyte, ookinete, oocyst, and salivary gland sporozoite stages using 3XHA tagged line. HA immunoreactivity was detected using anti-HA (mouse) antibody procured from abcam (16B12, ab130275), and immunoreactivity was revealed using goat anti-mouse Alexa 594. To study the organization of the cytoskeletal actin in mutant sporozoites, the *Pb*SIMP GIMO line was used. The mutant sporozoites were stained with FITC conjugated phalloidin (that binds to filamentous actin) and 3D11. To study the organization of the inner membrane complex (IMC), an IMC marker (Wichers et al., 2021) anti-PIC5 (rabbit polyclonal) antibody was used in combination with 3D11. To confirm the possible orientation of the *Pb*SIMP C-terminus, IFA was performed under permeabilized and non-permeabilized conditions. The combination of antibodies used was either anti-HA (mouse) and anti-PIC5 or 3D11 and anti-PIC5. The immunoreactivity of 3D11 and HA was revealed using goat anti-mouse tagged to Alexa 488 and immunoreactivity of PIC5 was revealed using chicken anti-rabbit tagged to Alexa 594. To test the cross reactivity of *Pf*SIMP (C-terminus) mouse antisera on *P. berghei* sporozoites, immunostaining was performed without permeabilization, and immunoreactivity was revealed using goat anti-mouse tagged to Alexa 488. The expression of SIMP was analyzed during liver stage development (36 h) by immunostaining EEFs with *Pf*SIMP mouse antisera and anti-UIS4 (rabbit) antibody (a marker for PVM) (Mueller et al., 2005). Immunoreactivity was revealed using goat anti-mouse tagged to Alexa 488 and chicken anti-rabbit secondary antibody tagged to Alexa 594. The host and parasite nuclei were stained with DAPI.

4.16 | TEM

The dissected salivary glands harboring WT and mutant sporozoites were fixed in 2.5% glutaraldehyde for 2 h followed by three washes in deionized distilled water. The samples were next treated successively with 2% osmium tetroxide for 2 h followed by 2% uranyl acetate for an hour. The sample was extensively washed thrice with deionized distilled water between the two treatments. The samples were dehydrated with series of graded alcohol, followed by treatment with propylene oxide for 20 min. Epoxy embedding (Sigma) was done as per manufacturer's instructions and incubated at 70–80°C for 72 h for complete polymerization. The ultra-thin (30 nm) sections were made with diamond knife Leica UC7 ultramicrotome. The sections were mounted on a copper grid and stained with 2% uranyl acetate and counterstained with Reynold's lead citrate. Transmission electron microscopy (JEM 1400, 120 kV, Jeol, Japan) was used for capturing images available at the central instrumentation facility of NIAB Hyderabad.

4.17 | Expression and purification of *Pf*SIMP protein

*Pf*SIMP was cloned and expressed using pET21a + vector. Briefly, Rossetta DE3 competent cells were transformed with recombinant pET21a-*Pfsimp* plasmid and induced with 0.5 mM IPTG concentration. The culture was incubated and constantly agitated overnight at 22°C. The cells were harvested by centrifuging at 6000 rpm for 10 min at 4°C and processed for the His-tagged purification of *Pf*SIMP through affinity chromatography via Ni-NTA agarose beads (Porath et al., 1975; Walker et al., 1994). Different imidazole fractions ranging from 10 mM to 500 mM concentration were used to elute the bound protein from Ni-NTA beads. Imidazole elution fractions were monitored by SDS-PAGE and western blotting for quantification and to check the protein purity. Purified *Pf*SIMP protein was further dialyzed with buffer (100 mM Tris, 50 mM NaCl, and 5% glycerol, pH 8) to eliminate nonspecific proteins.

4.18 | Generation of *Pf*SIMP polyclonal antibody in mice and rabbit

*Pf*SIMP recombinant protein was purified in large scale and dialyzed for immunization procedure. Female Balb/c mice (5–7 weeks old) and New Zealand white rabbit aged 10–16 weeks were used for immunization. Before immunization, the naïve mice and rabbit were bled to collect pre-immune sera that was used as a negative control for immunization. Mice and rabbit were intramuscularly primed with purified *Pf*SIMP recombinant protein emulsified with Freund's complete adjuvant (Sigma CFA, F5506-10ML). Two weeks post-priming, three booster doses were given along with Freud's incomplete adjuvant (sigma IFA, F5881-10ML) at every 2-week interval. The immune sera was collected 10 days after final booster dose.

4.19 | PIC5 antibody generation in rabbit

Peptide antisera for PIC5 (PBANKA_1409200) was generated in rabbit essentially following the same immunization protocol as described above. Two PIC5 peptides (88-EKAIEDAEKALENKESSEN-107 and 129-EENDESVENLENEINEDG-146) were used for immunization.

ACKNOWLEDGMENTS

KAK acknowledges financial assistance from DBT (BT/PR2495/BRB/10/950/2011) for procuring fluorescent microscope. We thank K. Tejaswi Naidu for his help in phylogenetic analysis.

CONFLICT OF INTEREST

The authors declare that they have no conflicts of interest with the contents of this article.

AUTHOR CONTRIBUTIONS

KAK, DS, and SKK conceived the project. DS and SKK generated plasmid constructs. DS performed gene expression analysis and generated KO line, GIMO line, and 3XHA expressing transgenic line. VN generated the complemented line. Recombinant PfSIMP protein expression and antibody generation in mice and rabbit were done by SP. PIC5 antibody generation in mice and rabbits were done by SD. All *P. berghei* mosquito infection cycles were maintained by DS and RRS. IFAs were done by DS. Midgut and salivary gland sporozoite dissections were done by KAK. MC and AS assisted in TEM experiments and analysis. AS and NPP performed in silico analysis. Microscopy was done by DS, SD, and KAK. Manuscript was written by KAK, DS, and SKK with input from all the authors.

DATA AVAILABILITY STATEMENT

The data that support the findings of this study are available from the corresponding author upon reasonable request.

ORCID

Surendra Kumar Kolli https://orcid.org/0000-0001-6125-0036

Kota Arun Kumar https://orcid.org/0000-0002-9451-2917

REFERENCES

Al-Nihmi, F.M., Kolli, S.K., Reddy, S.R., Mastan, B.S., Togiri, J., Maruthi, M. et al. (2017) A novel and conserved *Plasmodium* sporozoite membrane protein SPELD is required for maturation of Exo-erythrocytic forms. *Scientific Reports*, *7*, 40407.

Bergman, L.W., Kaiser, K., Fujioka, H., Coppens, I., Daly, T.M., Fox, S. et al. (2003) Myosin a tail domain interacting protein (MTIP) localizes to the inner membrane complex of *Plasmodium* sporozoites. *Journal of Cell Science*, *116*, 39–49.

Bogale, H.N., Pascini, T.V., Kanatani, S., Sa, J.M., Wellems, T.E., Sinnis, P. et al. (2021) Transcriptional heterogeneity and tightly regulated changes in gene expression during *Plasmodium berghei* sporozoite development. *Proceedings of the National Academy of Sciences of the United States of America*, *118*(10), e2023438118.

Bosch, J., Turley, S., Daly, T.M., Bogh, S.M., Villasmil, M.L., Roach, C. et al. (2006) Structure of the MTIP-MyoA complex, a key component of the malaria parasite invasion motor. *Proceedings of the National Academy of Sciences of the United States of America*, *103*, 4852–4857.

Boucher, L.E. & Bosch, J. (2015) The apicomplexan glideosome and adhesins—structures and function. *Journal of Structural Biology*, *190*, 93–114.

Combe, A., Moreira, C., Ackerman, S., Thiberge, S., Templeton, T.J. & Menard, R. (2009) TREP, a novel protein necessary for gliding motility of the malaria sporozoite. *International Journal for Parasitology*, *39*, 489–496.

Coppi, A., Natarajan, R., Pradel, G., Bennett, B.L., James, E.R., Roggero, M.A. et al. (2011) The malaria circumsporozoite protein has two functional domains, each with distinct roles as sporozoites journey from mosquito to mammalian host. *The Journal of Experimental Medicine*, *208*, 341–356.

Daher, W. & Soldati-Favre, D. (2009) Mechanisms controlling glideosome function in apicomplexans. *Current Opinion in Microbiology*, *12*, 408–414.

Elisabeth Gasteiger, C.H., Gattiker, A., Duvaud, S.'e., Wilkins, M.R., Appel, R.D. & Bairoch, A. (2005) *Protein identification and analysis tools on the ExPASy server*. Totowa, NJ: Humana Press.

Gomes-Santos, C.S., Braks, J., Prudencio, M., Carret, C., Gomes, A.R., Pain, A. et al. (2011) Transition of *Plasmodium* sporozoites into liver stage-like forms is regulated by the RNA binding protein Pumilio. *PLoS Pathogens*, *7*, e1002046.

Green, J.L., Wall, R.J., Vahokoski, J., Yusuf, N.A., Ridzuan, M.A.M., Stanway, R.R. et al. (2017) Compositional and expression analyses of the glideosome during the *Plasmodium* life cycle reveal an additional myosin light chain required for maximum motility. *The Journal of Biological Chemistry*, *292*, 17857–17875.

Gueirard, P., Tavares, J., Thiberge, S., Bernex, F., Ishino, T., Milon, G. et al. (2010) Development of the malaria parasite in the skin of the mammalian host. *Proceedings of the National Academy of Sciences of the United States of America*, *107*, 18640–18645.

Heintzelman, M.B. (2015) Gliding motility in apicomplexan parasites. *Seminars in Cell & Developmental Biology*, *46*, 135–142.

Hliscs, M., Sattler, J.M., Tempel, W., Artz, J.D., Dong, A., Hui, R. et al. (2010) Structure and function of a G-Actin sequestering protein with a vital role in malaria oocyst development inside the mosquito vector. *The Journal of Biological Chemistry*, *285*, 11572–11583.

Hofmann, K. & Stoffel, W. (1993) TMbase-a database of membrane spanning proteins segments. *Biological Chemistry Hoppe-Seyler*, *347*, 167.

Janse, C.J., Ramesar, J. & Waters, A.P. (2006) High-efficiency transfection and drug selection of genetically transformed blood stages of the rodent malaria parasite *Plasmodium berghei*. *Nature Protocols*, *1*, 346–356.

Jewett, T.J. & Sibley, L.D. (2003) Aldolase forms a bridge between cell surface adhesins and the Actin cytoskeleton in apicomplexan parasites. *Molecular Cell*, *11*, 885–894.

Jillapalli, R., Narwal, S.K., Kolli, S.K., Mastan, B.S., Segireddy, R.R., Dey, S. et al. (2019) A plasmodium berghei putative serine-threonine kinase 2 (PBANKA_0311400) is required for late liver stage development and timely initiation of blood stage infection. *Biology Open*, *8*(8), bio042028.

Kaiser, K., Camargo, N. & Kappe, S.H. (2003) Transformation of sporozoites into early exoerythrocytic malaria parasites does not require host cells. *The Journal of Experimental Medicine*, *197*, 1045–1050.

Kall, L., Krogh, A. & Sonnhammer, E.L. (2007) Advantages of combined transmembrane topology and signal peptide prediction—the Phobius web server. *Nucleic Acids Research*, *35*, W429–W432.

Kappe, S.H., Buscaglia, C.A., Bergman, L.W., Coppens, I. & Nussenzweig, V. (2004) Apicomplexan gliding motility and host cell invasion: overhauling the motor model. *Trends in Parasitology*, *20*, 13–16.

Khater, E.I., Sinden, R.E. & Dessens, J.T. (2004) A malaria membrane skeletal protein is essential for normal morphogenesis, motility, and infectivity of sporozoites. *The Journal of Cell Biology*, *167*, 425–432.

Check for updates

Received: 28 March 2022 | Revised: 12 April 2022 | Accepted: 12 April 2022

DOI: 10.1111/mmi.14910

COMMENTARY

WILEY

A conserved malaria parasite protein required for maintenance of sporozoite cell shape and transmission

Johannes T. Dessens[1] | Eva Hesping[2]

[1]Department of Infection Biology, Faculty of Infectious and Tropical Diseases, London School of Hygiene & Tropical Medicine, London, UK

[2]Division of Infectious Diseases and Immune Defence, Walter and Eliza Hall Institute of Medical Research, Parkville, Victoria, Australia

Correspondence
Johannes T. Dessens, Department of Infection Biology, Faculty of Tropical and Infectious Diseases, London School of Hygiene & Tropical Medicine, Keppel Street, London WC1E 7HT, UK.
Email: johannes.dessens@lshtm.ac.uk

Funding information
Biotechnology and Biological Sciences Research Council, Grant/Award Number: BB/V006428; Medical Research Council, Grant/Award Number: MR/P021611

Abstract

Malaria parasites are transmitted by mosquitoes and a substantial part of the parasite's complex life cycle takes place inside the insect. Parasite transmission starts with the uptake of parasite stages called gametocytes from the vertebrate host with the blood meal of a female vector mosquito, completing several weeks later with the injection of parasite stages called sporozoites into the vertebrate host by mosquito bite. The sporozoites form in their thousands inside ookinete-derived oocysts situated on the abluminal side of the mosquito midgut epithelium by a process of cell division known as sporogony. After their formation, sporozoites egress from the oocyst into the haemolymph, invade the salivary glands and mature to become infective to the vertebrate. This MicroCommentary reviews recent reports describing a conserved plasma membrane-associated protein of *Plasmodium berghei*, PBANKA_1422900, and its role in maintaining the shape and structural integrity of sporozoites in salivary glands and during inoculation into the vertebrate host. Combined results from three separate studies provide mechanistic insights into how this protein achieves structural maintenance of the sporozoite, and how in turn this promotes the sporozoite's ability to overcome several physical obstacles and allow it to establish infection in the vertebrate.

Plasmodium sporozoites are responsible for malaria transmission from the insect to the vertebrate host, and to do so must invade the salivary glands of the insect, pass through the salivary ducts, cross the skin and blood vessels to reach and ultimately infect the liver cells (Amino et al., 2006; Hopp et al., 2021; Figure 1). To achieve this, sporozoites have a slender concave-convex shape and possess specialised secretory organelles (i.e., micronemes and rhoptries) and a unique cortical structure called the pellicle that facilitates invasion and motility (Gubbels & Duraisingh, 2012). The pellicle is defined by a double membrane layer named the inner membrane complex (IMC) that is located directly underneath the plasma membrane (Ferreira et al., 2020). A viscoelastic, subpellicular network (SPN) of intermediate filaments is located at the cytoplasmic side of the IMC (Mann & Beckers, 2001). The SPN is tightly associated with the IMC and forms an internal cytoskeletal basket that supports the IMC membranes and provides tensile strength and flexibility to the cell (Khater et al., 2004; Mann & Beckers, 2001; Tremp et al., 2008; Tremp & Dessens, 2011). The SPN and IMC separate the main cytosol from a smaller cortical cytoplasm that contains the molecular machinery that drives sporozoite motility. The latter relies on an actinomyosin motor system that is situated in the space between the plasma membrane and the IMC. The molecular motor and its auxiliary proteins are linked to cell surface adhesins via actin filaments and bridging proteins, and are internally anchored into the IMC (Frenal et al., 2010). Invasion of the salivary glands and infection of the vertebrate host require distinct sporozoite protein repertoires, the expression of which is temporally regulated by programmes of translational repression (Bogale et al., 2021; Lindner et al., 2019). However, many apicomplexan zoite proteins associated with motility and vertebrate infection remain to be characterised (Harding & Frischknecht, 2020). In this MicroCommentary, we review three related studies on one sporozoite protein in the malaria parasite

 © 2022 John Wiley & Sons Ltd.

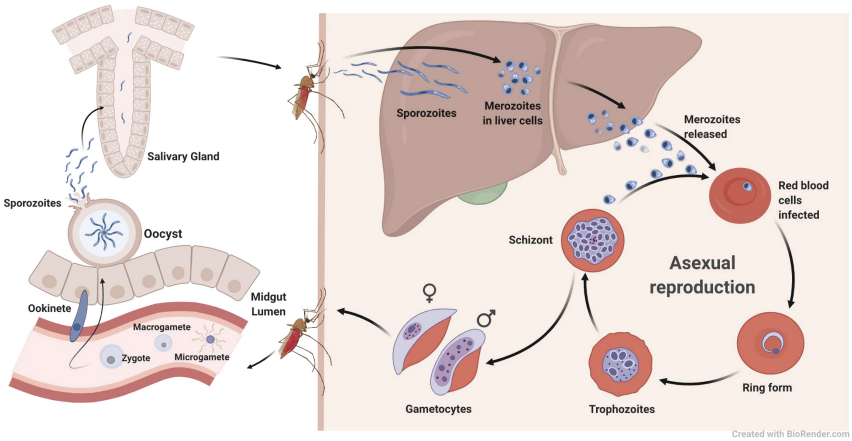


FIGURE 1 Malaria parasite life cycle

Plasmodium berghei, PBANKA_1422900, that has a critical role in maintaining sporozoite shape, integrity and infectivity.

In a study by Singh and colleagues reported in this issue (Singh et al., 2022), the protein PBANKA_1422900 is named Structural Integrity Maintenance Protein (SIMP). The authors demonstrate by gene disruption that SIMP is dispensable for asexual, sexual, ookinete, oocyst and sporozoite stage development. However, SIMP-depleted sporozoites, albeit able to colonise the salivary glands in numbers comparable to wild-type parasites, are not infective to the mouse and unable to establish blood-stage infections after intravenous injection of sporozoites. Singh et al. (2022) go on to investigate why SIMP knockout sporozoites are non-infectious. By using circumsporozoite protein (CSP) immunostaining, they show that salivary gland-resident SIMP-depleted sporozoites have an abnormal shape that is characterised by the presence of multiple plasma membrane 'blebs', and further show that these sporozoites display highly reduced gliding motility on glass slides, which is a likely cause of their infectivity loss. These shape and motility phenotypes were reversed in parasites where SIMP function is restored by complementation (Singh et al., 2022). Further cellular investigation of SIMP-depleted sporozoites indicates that they possess an intact cytoskeleton (using phalloidin/actin staining), as well as an intact IMC organisation using immunostaining of the IMC marker PIC5. PIC5 immunostaining also revealed that the IMC does not underlie the plasma membrane blebs indicating that SIMP depletion leads to loss of contact between the plasma membrane and IMC (Figure 2). This conclusion is indeed supported by their transmission electron microscopic examination of SIMP-depleted salivary gland sporozoites (Singh et al., 2022).

The authors further investigate the localisation of SIMP by generating a transgenic line expressing SIMP fused at its carboxy terminus to a triple haemagglutinin (HA) tag, which allowed them to show by immunostaining that the protein is expressed in gametocytes, ookinetes, sporozoites and liver stages. They show that, in ookinetes and sporozoites, SIMP is predominantly located at the cell periphery, consistent with their in silico predictions that SIMP, while not possessing any clear known functional domains or motifs, has a potential central hydrophobic membrane-associated domain. Moreover, sporozoites expressing HA-tagged SIMP immunostained under both

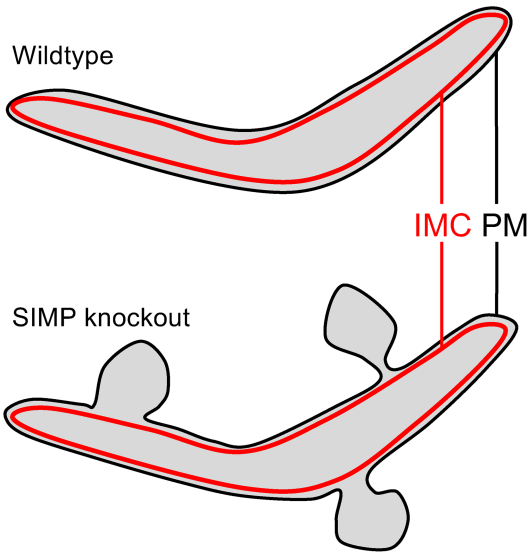


FIGURE 2 Cartoon of *plasmodium berghei* wildtype and SIMP-depleted (SIMP knockout) salivary gland sporozoites depicting the plasma membrane (PM) and inner membrane complex (IMC). Depletion of PBANKA_1422900 causes detachment of the PM from the IMC resulting in a gradual loss of sporozoite shape, structural integrity and infectivity

non-permeabilised and permeabilised conditions, in sharp contrast to PIC5 that only immunostained under permeabilised conditions. The latter observations strongly indicate that the carboxy terminus of SIMP is in fact extracellular. This notion was corroborated by showing that immunostaining with antibodies raised against the carboxy-terminal part of SIMP also does not require sporozoite permeabilisation (Singh et al., 2022).

We obtain further insight into the role of PBANKA_1422900 from a second study in which the protein is named 'concavin' (Kehrer et al., 2022). Kehrer and colleagues use carboxy-terminal GFP tagging of the protein combined with immunofluorescence to show its expression in gametocytes, ookinetes, sporozoites and liver stages. The localisation of concavin in ookinetes and sporozoites is shown to be predominantly peripheral, however, immunostaining with anti-GFP antibodies only worked on permeabilised cells leading the

authors to conclude that the protein remains intracellular. Further analyses show that the protein is not associated with the SPN protein PHIL1, but co-localises with CSP, collectively pointing to an association with the cytosolic side of the plasma membrane. Kehrer et al. go on to demonstrate that concavin-depleted salivary gland sporozoites over time obtain abnormal shape and display reduced motility (Kehrer et al., 2022). Via electron microscopy and array tomography the authors further show dissociation between the IMC and plasma membrane in concavin-depleted sporozoites.

Concavin-depleted sporozoites are still able to infect mice after mosquito bite, albeit with lower efficacy and increased prepatent periods (Kehrer et al., 2022), indicating that sporozoite infectivity to mice is reduced, but not abolished. The authors go on to show that the reduction in infectivity is not caused by a failure to infect hepatocytes, but rather by reduced efficacy of the sporozoites getting through the narrow salivary ducts, combined with a reduced efficacy to traverse the skin, suggesting that the deformed concavin-depleted sporozoites are having trouble entering and moving through confined spaces (Kehrer et al., 2022). Moreover, they show that a proportion of these sporozoites 'disintegrate' while migrating through the skin. Based on these collective observations, the authors postulate that concavin rivets the plasma membrane to the IMC thereby maintaining the shape of the sporozoite (Kehrer et al., 2022).

A third study of PBANKA_1422900, here named PIMMS22 (Ukegbu et al., 2021), is broadly consistent, demonstrating similar expression and subcellular localisation profiles of the protein as well as a loss of sporozoite infectivity to the mouse in PIMMS22-depleted parasite lines. However, the sporozoite-associated phenotype of PIMMS22-depleted parasites was not investigated in any depth, the study instead focused on an ookinete-associated loss-of-function phenotype (Ukegbu et al., 2021). The authors show that PIMMS22-depleted ookinetes display reduced infectivity as evidenced by significant (4- to 17-fold) reductions in the number of oocysts developing compared to their wild-type counterparts. Ukegbu and colleagues go on to show that PIMMS22 knockout ookinetes have normal motility, ruling out that impaired locomotion is the cause of their infectivity loss (Ukegbu et al., 2021). Instead, the authors conclude that PIMMS22-depleted ookinetes are impaired in midgut invasion as well as ookinete-to-oocyst transition. The findings of this study (Ukegbu et al., 2021) differ from the other two studies where no marked effect on ookinete infectivity was observed (Kehrer et al., 2022; Singh et al., 2022). As distinct mosquito species were used in assessing parasite development, this discrepancy is explained by differences in susceptibility of *Anopheles* species to *Plasmodium* infection (Singh et al., 2022). Indeed, several ookinete surface molecules have been reported as having roles in evading the insect's innate complement-like immune responses to parasite infection (Molina-Cruz et al., 2013; Ukegbu et al., 2017, 2020) and this result raises the prospect that PIMMS22, too, could play a role in this aside from its role in sporozoite infectivity.

The importance of sporozoite shape for infectivity to the mouse has been demonstrated with other pellicle proteins that are required for normal sporozoite shape and motility, for example the SPN-resident alveolin IMC1h (Coghlan et al., 2019; Tremp & Dessens, 2011; Volkmann et al., 2012). IMC1h-depleted sporozoites have reduced motility and cannot infect mice via natural mosquito bite or via subcutaneous needle injection, but they can establish infections after intravenous needle injection (Volkmann et al., 2012). Moreover, IMC1h null mutant sporozoites display normal hepatocyte infection rates in vitro (Volkmann et al., 2012), as is indeed the case for concavin null mutants (Kehrer et al., 2022). The identified role of PBANKA_1422900 in maintaining sporozoite shape and integrity further supports the notion that traversal of the dermis constitutes a major bottleneck for sporozoite infection of the vertebrate host.

What remains somewhat puzzling is why depletion of protein PBANKA_1422900 has no discernible effect on ookinete shape or motility, even though the protein appears to have the same subcellular localisation as it does in sporozoites. One explanation is that the protein has an entirely different function in ookinetes, something that the Ukegbu et al study (Ukegbu et al., 2021) might be alluding to. It is also possible that the life span of ookinetes simply is not long enough for their cell shape to be impacted by the absence of the protein. Contrary to sporozoites, which constitute the final life stage in the insect and live for many days, ookinetes quickly transform into oocysts after crossing the mosquito midgut epithelium. It would be interesting to investigate if there is a longer-term effect on the shape or integrity of cultured ookinetes depleted of PBANKA_1422900.

There is still discrepancy whether PBANKA_1422900 has an extracellular part or not. While the studies by Singh et al (Singh et al., 2022) and by Ukegbu et al. (2021) support an extracellular localisation of at least part of the protein, the Kehrer et al study (Kehrer et al., 2022) does not. This is relevant in the context of several malaria intervention strategies. First, malaria vaccine based on immunodominant sporozoite antigen like CSP (Kumar et al., 2006) target the sporozoite's ability to establish parasite infection after mosquito bite (Cowman et al., 2016). The relatively abundant PBANKA_1422900, if indeed extracellular, could be a valuable addition to the list of urgently needed new malaria vaccine candidates (Matuschewski, 2017). In addition, given its potential surface expression on ookinetes, transmission-blocking vaccines could be generated based on PBANKA_1422900. This type of vaccine target gametocyte and/or ookinete surface proteins via antibodies taken up by the mosquito with its *Plasmodium*-infected blood meal to block parasite development in the midgut (Delves et al., 2018). Thus, further scrutiny of the potential extracellular nature of this protein is warranted.

ACKNOWLEDGEMENTS

This research was funded in whole, or in part, by the United Kingdom Medical Research Council [Grant reference MR/P021611] and UK Biotechnology and Biological Sciences Research Council [Grant reference BB/V006428].

DATA AVAILABILITY STATEMENT

Data sharing is not applicable to this article as no new data were created or analyzed in this study.

Molecular & Biochemical Parasitology 232 (2019) 111198

Contents lists available at ScienceDirect

Molecular & Biochemical Parasitology

journal homepage: www.elsevier.com/locate/molbiopara

Plasmodium berghei sporozoite specific genes- *PbS10* and *PbS23/SSP3* are required for the development of exo-erythrocytic forms

Jyothi Togiri[a,1], Rameswara Reddy Segireddy[a,1], Babu S. Mastan[a], Dipti Singh[a], Surendra Kumar Kolli[a], Ankit Ghosh[b], Faisal Mohammed Abdul Al-Nihmi[a], Mulaka Maruthi[a], Hadi Hasan Choudhary[b], Sandeep Dey[a], Satish Mishra[b], Kota Arun Kumar[a,*]

[a] Department of Animal Biology, School of Life Sciences, University of Hyderabad, Hyderabad, 500046, India
[b] Division of Parasitology, CSIR-Central Drug Research Institute, Lucknow, 226031, India

ARTICLE INFO

Keywords:
Malaria
Plasmodium
Sporozoites
Exo-erythrocytic forms

ABSTRACT

Plasmodium sporozoites are infective forms of the parasite to mammalian hepatocytes. Sporozoite surface or secreted proteins likely play an important role in recognition, invasion and successful establishment of hepatocyte infection. By approaches of reverse genetics, we report the functional analysis of two *Plasmodium berghei* (*Pb*) sporozoite specific genes- *PbS10* and *PbS23/SSP3* that encode for proteins with a putative signal peptide. The expression of both genes was high in oocyst and salivary gland sporozoite stages as compared to other life cycle stages and *PbS23/SSP3* protein was detected in salivary gland sporozoites. Both mutants were indistinguishable to wild-type parasites with regard to asexual growth in RBC, ability to complete sexual reproduction and form sporozoites in vector host. While the sporozoite stage of both mutants were able to glide and invade hepatocytes normally in vitro and in vivo, *PbS10* mutants suffered growth attenuation at an early stage while *PbS23/SSP3* mutants manifested defect during late exo-erythrocytic form maturation. Interestingly, both mutants gave rare breakthrough infections, suggesting that while both were critical for liver stage development, their depletion did not completely abrogate blood stage infection. These findings have important implications for weakening sporozoites by multiple gene attenuation towards the generation of a safe whole organism vaccine.

1. Introduction

Malaria is a deadly infectious disease caused by a protozoan parasite that belongs to the genus *Plasmodium.* The parasite kills nearly half a million people each year, mostly young children in sub-Saharan Africa [1]. These parasites have a complex life cycle that alternates between a mammalian host and a female *Anopheles* mosquito. Infection to the mammalian host is initiated when infected mosquito injects sporozoites into the skin while obtaining a blood meal [2]. The injected sporozoites glide through several cellular barriers using an actin-myosin based molecular motor present beneath its plasma membrane [3]. This movement referred to as gliding motility facilitates the sporozoite to reach the blood vessels. Once inside the capillaries, the sporozoites are selectively arrested in the liver sinusoids. Within the liver, the sporozoites actively migrate through few hepatocytes prior to the productive invasion, characterized by invagination of hepatocyte plasma membrane and formation of a parasitophorous vacuole (PV) [4]. Within the PV, the sporozoite transforms into exo-erythrocytic forms (EEFs) or liver stages and undergo several rounds of asexual replication producing few thousand hepatic merozoites. Upon complete maturation of EEFs, the hepatic merozoites are packaged in host cell-derived membrane-bound structures called merosomes [5]. The merosomes facilitate the delivery of the hepatic merozoites into the blood and initiate an erythrocytic cycle (EC). During the EC, the parasites transform within the RBC into different forms like the rings, trophozoites and schizonts. The rapid multiplication of parasites at this stage is associated with all clinical manifestations of malaria. The schizonts contain 16–32 merozoites and upon egress from RBC, reinitiate the EC or alternatively form sexually dimorphic stages called the gametocytes. The gametocytes are the terminal stages of the parasite in the vertebrate host and undergo further development only in the gut of the female *Anopheles* mosquito. When a mosquito ingests these gametocytes during a blood meal, the male and female gametes emerge from respective gametocytes. The gametes fuse and form a zygote. The zygote transforms into a

* Corresponding author.
E-mail address: kaksl@uohyd.ernet.in (K.A. Kumar).
[1] These authors contributed equally for the work.

https://doi.org/10.1016/j.molbiopara.2019.111198
Received 18 January 2019; Received in revised form 17 June 2019; Accepted 23 June 2019
Available online 26 June 2019
0166-6851/ © 2019 Elsevier B.V. All rights reserved.

motile ookinete that passes through the midgut epithelium and attaches on the hemocoel side of the gut. Here it develops into an oocyst over a period of 12–14 days and harbours several thousand sporozoites. Upon rupture of oocyst, the sporozoites are released into the mosquito hemocoel that further enter and colonize the salivary glands.

One of the obligatory steps towards the establishment of malaria infection in mammalian host involves attachment of sporozoites to hepatocytes, prior to the invasion. As blocking this process holds enormous potential in preventing clinical malaria, identification and functional investigation of sporozoite surface proteins have fueled great interest in the recent past [6,7]. Sporozoite surface proteins perform a myriad range of functions that together mediate multiple aspects of infection. Till date, the most extensively studied sporozoite surface proteins are circumsporozoite protein (CSP) and Thrombospondin related anonymous protein (TRAP) that play a crucial role in hepatocyte infection. Both CSP and TRAP are secretory proteins, embedded in sporozoite plasma membrane respectively by a GPI anchor and transmembrane domain [7]. The role of CSP begins in oocyst, being essential for sporulation [8] and mediates the navigation of sporozoites within mosquito from hemocoel to salivary glands and in the mammalian host to liver by changing its conformation [9]. TRAP is physically engaged with the molecular motor with its cytoplasmic tail facilitating sporozoite gliding, invasion, and infectivity [10]. Another well-studied sporozoite surface protein is Apical membrane protein-1 (AMA-1) that has both signal peptide and transmembrane domains [11]. Secretory proteins like TRAP and AMA-1 are stored in specialized apical vesicles at the anterior end of the sporozoite, referred to as micronemes and are discharged following contact of sporozoite with host cells [11]. Antibodies against CSP [12,13], and AMA-1 [11], effectively block the entry of sporozoites into hepatocytes reducing the incidence of liver infection. Therefore, investigating the role of other sporozoite surface proteins in hepatocyte interaction or their requirement for intrahepatic development may help in intervening the parasite life cycle.

A previous study has identified 25 sporozoite specific genes (S genes) in a suppression subtractive hybridization (SSH) screen performed between two invasive stages of *Plasmodium yoellii*- the merozoite and sporozoite stages [14]. Of these, 12 genes encoded for proteins with the putative signal peptide (SP). In addition to CSP and TRAP, the high expression of other genes is consistent with their roles in establishing infection in mosquito and the mammalian host. For example, S3/UIS4 and S7/UIS3 referred to as UIS genes (upregulated in infective sporozoites) [15] are required for completion of EEF development [16,17]. S4/CelTOS and S13/PLP1 are micronemal proteins that aid respectively in cell traversal [18,19], and membrane wounding activity [20] required for sporozoites to reach hepatocytes [21]. S5/SIAP-1 is sporozoite invasion-associated protein that facilitates sporozoite egress from oocyst and migration to salivary glands [22]. S16 is dispensable to parasite with no obvious phenotype at any stage [23]. S21 or thrombospondin-related sporozoite protein (TRSP) possesses at its N- terminal end a thrombospondin type 1 repeat, as found in CSP and TRAP, and facilitates in cell-cell interactions and cell guidance [24]. S23/SSP3, is a conserved sporozoite surface protein with a putative type 1 transmembrane domain. In *Plasmodium yoelii*, S23 is expressed both in midgut and salivary gland sporozoite stages with cytoplasmic and surface localisation respectively and is required for sporozoite gliding motility [25].

In the current study, we report the functional role of two *P. berghei* (*Pb*) genes- *PbS10* and *PbS23/SSP3* by generating mutants. Both *PbS10* and *PbS23/SSP3* showed maximal expression during oocyst and salivary gland sporozoite stage respectively and *PbS23/SSP3* protein was detected in salivary gland sporozoites. Inspite of high expression levels in sporozoite stages, both *PbS23/SSP3* and *PbS10* were required only for EEF development, while other sporozoite specific functions like gliding motility, invasion and infectivity remained unaffected.

2. Materials and methods

2.1. Experimental animals, parasite lines, mosquitoes, and cell lines

Six to eight weeks old female Swiss albino (SA) mice were procured from National Institute of Nutrition NIN, Hyderabad, India and used for asexual blood stage propagation, mosquito feedings, and sporozoite production. C57BL/6 mice (6–8 week old) were used to determine the pre patent period in mutant parasites. All experiments using the animals were in accordance to the regulations of the institutional animal ethics committee. Wild-type *Plasmodium berghei ANKA* strain was used for generating both *PbS10* and *PbS23/SSP3* mutants and cycled between SA mice and *Anopheles stephensi* (*A. stephensi*) mosquitoes. Adult mosquitoes were maintained at 28 °C temperature, 80% humidity and fed on 10% sucrose solution. For initiation of sexual cycle in the mosquito, 5 days old mosquitoes were blood fed on SA mice infected with either WT or either of the mutant parasites. The infected mosquitoes were maintained at 20 °C temperature and 80% humidity with 12/12 light and dark cycle. Infected mosquitoes were dissected on day 14 and on day 18 to 20 post blood meal to observe the oocyst and salivary glands sporozoites respectively. Human liver hepatocellular cell lines (HepG2) were used for studying the development of EEFs (liver stage parasites) and the cells were maintained in DMEM medium (Gibco, Cat #11965-118) supplemented with 1X antibiotic and antimycotic (Gibco, Cat # 15240062) and 10% Fetal bovine serum (Gibco, Cat # 10270-106)

2.2. Analysis of PbS10 and PbS23/SSP3 transcripts levels across all life cycle stages

Total RNA was isolated from mosquito midgut sporozoites (day 14 oocyst), D18-20 salivary gland sporozoites, different time points during in vitro EEF development like 16 h, 25 h, 42 h, 50 h and 65 h and mixed blood stages. To obtain RNA from mosquito stage sporozoites, nearly 100 infected midguts and salivary glands were dissected. For obtaining liver stage samples, HepG2 cultures infected with sporozoites and cells were lysed at different time points as specified above. RNA was extracted from all samples using Trizol (Invitrogen, Cat# 15596026), followed by treatment with DNAse I (Ambion). The samples were passed through an RNeasy cleanup column (Qiagen Cat # 74,204). The cDNA was synthesized from 2 µg total RNA in a 20 µL reaction mixture containing 2 µL of 10X PCR buffer, 1 µL of dNTPs (2.5 mM each) (Invitrogen, cat # R72501), 1 µL of random hexamers (Applied Biosystems, cat # N8080127), 1 µL of RNase inhibitor (Applied Biosystems, N8080119, 1 µL of MuLV reverse transcriptase (Applied Biosystems, cat # AM2682). Real-time PCR was carried out in a 10 µl reaction volume that contained 1XSYBR Green PCR Master Mix (Bio Rad) and 0.25 µM gene-specific primers and 1 µl of cDNA sample from each stage. Real-time PCR was performed using the Eppendorf Realplex 2 qPCR machine using absolute quantification method. Gene-specific standards were generated for both *PbS10* and *PbS23/SSP3* by amplifying 145 bp and 141 bp fragment using primers indicated in Table 1. Expression of *PbS10* and *PbS23/SSP3* was normalised to the expression of *Pb18SrRNA*, a housekeeping gene [26]. The normalized gene expression values were calculated by taking the ratio of *PbS10* or *PbS23/SSP3* and *Pb18SrRNA*.

2.3. Targeted disruption and deletion of PbS10 and PbS23/SSP3

PbS10 and *PbS23/SSP3* mutants were generated by gene disruption (GD) and deletion (KO) methods respectively by double homologous recombination strategy [27]. For the generation of *Pb*S10 gene disruption construct, two homology fragments 5′ (507 bp) and 3′ (530 bp) were amplified using primer pairs FP1/RP1 and FP2/RP2 respectively. 5′ and 3′ fragments were cloned into pBC-GFP-hDHFR vector at *Xho*I/

Table 1
List of primers used in this study.

S.No	Primers used for	Primer designation	Primer sequence	Expected product size (bp)
1	Generation of *PbS10* GD construct	FP1	AGACTCGAGATGAATAAACTATATGCTTG	507
2		RP1	TAAATCGATTTTTCGGTTTTTTCTTTTTCT	
3		FP2	ACAGCGGCCGCTCGTATAGGAAATAAAGAAAA	530
4		RP2	GAAGGCGCGCCTTATTCCATAGCAAACTTGT	
5	Confirmation of *PbS10* gene disruption by integration PCR	FP3	ATAGAAGGTCAAAATGAATGA	1231
6		RP3	TTCCGCAATTTGTTGTACATA	
7		FP4	GTTGTCTCTTCAATGATTCATAAATAG	1719
8		RP4	TAGAGGTATTAGAATCATGTCA	
9	Confirming the *PbS10* GD clonal lines	FP5	AACTGAATACTAACAAAATTT	668
10		RP5	TTTTTGCTAAAATATGTTCAA	
11	Generation of *PbS23/SSP3* KO construct	FP6	AGTCTCGAGACACTTATTTTATCATATTA	573
12		RP6	ATAATCGATTTTTAATAGCGTGATGTAA	
13		FP7	ATAGCGGCCGCTTCCATAAAACATCAAAATA	523
14		RP7	ACTGGCGCGCCAACATGATTCGCACAAAA	
15	Confirmation of *PbS23/SSP3* gene deletion by integration PCR	FP8	TATAACCCAAATGCTTCG	773
16		RP8	TTCCGCAATTTGTTGTACATA	
17		FP9	GTTGTCTCTTCAATGATTCATAAATAG	646
18		RP9	TATTGTACTATAAATTGTATAG	
19	Confirming the *PbS23/SSP3* gene deleted clonal lines	FP10	ACATTTAAACAACAATATCC	525
20		RP10	TTTAATATTTGTATCGTAAGA	
21	*PbS23/SSP3*-3XHA localisation construct	FP11	TACGGGCCCACATTTAAACAACAATATCC	528
22		RP11	ACACTCGAGTTTAATATTTGTATCGTAAGA	
23		FP12	ATAGCGGCCGCTTCCATAAAACATCAAAATA	530
24		RP12	ACTGGCGCGCCAACATGATTCGCACAAAA	
25	Conformation of *PbS23/SSP3* HA integration	FP13	TGAAACAATTGGACAAATTTA	732
26		RP13	GATCCTTAAGCGTAATCTGGAACATCG	
27		FP14	GTTGTCTCTTCAATGATTCATAAATAG	737
28		RP14	ATAGCGACAAGTTGCTTTTTT	
29	*PbS10* expression analysis by real time PCR	FP15	ACATGAATCCCAAGAAAATGAT	145
30		RP15	AACTAATTTCCCTTCTGTTTCT	
31	*PbS23/SSP3* expression analysis by real time PCR	FP16	GAGCATGAAATAGGAAAT	141
32		RP16	ATATATTGGCACAATGCTAT	
33	*Pb18S rRNA* expression analysis by real time PCR	FP17	AAGCATTAAATAAAGCGAATACATCCTTAC	134
34		RP17	GGAGATTGGTTTTGACGTTTATGT	
35	*GAPDH* expression analysis by real time PCR	FP18	CCTCAACTACATGGTTTACAT	122
36		RP18	GCTCCTGGAAGATGGTGATG	

*Cla*I and *Not*I/*Asc*I respectively. Similarly, *PbS23/SSP3* KO construct was generated by amplifying 573 bp for 5′ and 531 bp for 3′ fragments using primers FP6/RP6 and FP7/RP7 respectively. Both targeting constructs was released by *Xho*I and *Asc*I digestion and gel purified. Nearly 5–6 µg of DNA was added to amaxa nucleofector solution and electroporated into schizont using program U-033 as described earlier [28]. Two independent transfections were performed with each targeting construct. Mice were kept on pyrimethamine drug pressure for 24 h post-transfection to select recombinant parasites [28]. Following drug selection, the recombinant parasites were obtained where GFP expression was driven by PbHSP70 promotor. Blood was collected from mice harbouring recombinant parasites derived from two independent transfections for each mutant. Genomic DNA was isolated from different transfected populations and the stable integration of GFP-hDHFR cassette was confirmed by integration specific PCR. The sequence information of primers used in generation of targeting constructs are indicated in Table 1.

2.4. Generation of PbS23/SSP3 HA transgenic line

For the generation of *PbS23/SSP3* HA transgenic line, two homology fragments of 528 bp and 530 bp were amplified using primer pairs FP11/RP11 and FP12/RP12 respectively. The 528bp and 530bp fragments corresponded respectively to the region preceding stop codon and the 3′ UTR of *PbS23/SSP3*. The 528bp and 530bp fragments and were cloned into pBC-3XHA-hDHFR vector at *Apa1/Xho1* and *Not1/Asc1* restriction sites respectively. The targeting construct was released by *Apa1* and *Asc*I digestion and gel purified. The electroporation and selection of *PbS23/SSP3* 3XHA transgenic was done as described above [28]. Genomic DNA was isolated from different transfected populations and the stable integration of 3XHA-hDHFR cassette was confirmed by integration specific PCR. The sequence information of primers used in generation of targeting constructs are indicated in Table 1.

2.5. Phenotypic analysis of PbS10 GD and PbS23/SSP3 KO mutants during asexual blood stages

Approximately 10^3 infected RBC (iRBC) of two cloned lines of either mutants and WT GFP parasites [26] were injected intravenously (i.v.) in 4–6 week old SA mice. Parasitemia was monitored daily by making Giemsa-stained blood smears. Parasitemia was determined by checking 25 random fields of uniform thin smears under a light microscope.

2.6. Phenotypic analysis of PbS10 GD and PbS23/SSP3 KO mutants in A. stephensi

Female *A. stephensi* mosquitoes were used to study the developmental stages of both mutants. Four to five SA mice were injected intravenously with 10^6 iRBC of either mutants or WT parasites. When the parasitemia reached around 5%, all gametocyte positive mice were anesthetized and exposed to *A. stephensi* mosquito bites. Two successive blood meals were given with 24 h time interval. The blood-fed mosquitoes were maintained at 20^0 C temperature and 80% RH. Post blood meal on days 14 and 18–20, midguts and salivary glands were dissected and analysed respectively for the presence of oocyst and sporozoites under a fluorescent microscope. Infected midguts containing oocyst and salivary gland containing sporozoites were disrupted using a plastic pestle and sporozoites were partially purified from mosquito debris by

spinning at 800 rpm for 3 min in an Eppendorf centrifuge (Cat# 5430R). The sporozoite numbers were estimated using a hemocytometer.

2.7. Monitoring gliding motility in PbS10 GD and PbS23/SSP3 KO mutant sporozoites

Day 18 post blood meal, the mosquitoes salivary glands harbouring either mutants and WT GFP sporozoites were dissected in medium containing DMEM and 10% FBS. The glands were disrupted using a plastic pestle. The released sporozoites were spotted on a clean glass slide and a cover slip was gently placed over it and sealed. The slides were observed at 100X magnification using a Nikon AR fluorescent microscope and the video recording of the sporozoite gliding was performed in the bright field using the Ni-S elements soft ware.

2.8. Cell traversal and invasion assays for PbS10 GD and PbS23/SSP3 KO mutant sporozoites

Approximately 2×10^4 sporozoites of either mutants and WT were added to monolayer of HepG2 cells in the presence of dextran (Texas Red, 10,000 MW, Neutral, Invitrogen) in 24 well plates. Plates were centrifuged at 1500 rpm for 4 min [4] and incubated for 1 h at 37^0C in a CO_2 incubator to allow the sporozoites to glide and perform cell traversal activity. The cells were washed with PBS for removal of excess dextran. The dextran positive cells were counted using a fluorescent microscope and plotted in the graph. Host cell invasion by sporozoites was analysed by double staining [29]. To quantify in vitro invasion, approximately 2×10^4 sporozoites were added on to a monolayer of HepG2 cells and incubated for 2 h. The cells were subsequently fixed in 4% formalin solution. The extracellular sporozoites were stained with 3d11, an anti-CSP repeat specific monoclonal antibody [30] and immunoreactivity was revealed by anti-mouse secondary antibody conjugated to Alexa Fluor 594. To assess sporozoite infectivity, 25 random fields were counted and the number of GFP expressing sporozoites (total) and the number of sporozoites positive for CSP immunoreactivity (extracellular sporozoites, red) was enumerated per field. The sporozoite infection rate was calculated by using the formula- the number of GFP expressing sporozoites per field - number of sporozoites stained red per field/ number of GFP expressing sporozoites per field. The data was represented in values relative to WT sporozoites.

2.9. In vitro development of PbS10 GD and PbS23/SSP3 KO mutants sporozoites

Approximately 2×10^5 HepG2 cells were seeded on cover slips that were previously coated with 10 mg/ml concentration of collagen (Corning, Cat# 354,236) for 4 h. After attaining 70–80 percent confluency, 2×10^4 sporozoites of either mutants and WT GFP were added and centrifuged at 1500 rpm for 4 min. The cultures were maintained at 37°C in a CO_2 incubator for 3 days to allow EEF development. At 12 h, 36 h and 62 h time points, the cover slips were removed from 24 well plates and fixed in 4% formalin solution and stained for UIS4, a marker for parasitophorous vacuolar membrane [17]. DAPI was used for staining the nuclei.

2.10. In vivo infectivity of PbS10 GD and PbS23/SSP3 KO sporozoites by intravenous route and mosquito bite

C57BL/6 mice were used to assess the transmission ability of both mutants. A group of 3–6 C57BL/6 mice were intravenously (i.v) injected with 5×10^3 sporozoites of either mutants and WT GFP. The parasitemia was monitored daily from day 3 post infection by examination of Giemsa-stained blood smears. To assess the *in vivo* infection competence of both mutants for hepatocytes, 1×10^4 sporozoites were injected through an i.v., route in a group of 3–4 mice and total RNA was isolated from infected liver at 14 h post infection. cDNA was generated from 2 µg of RNA and was used as a template for qRT PCR to quantify parasite specific *18S rRNA* transcripts using primer set FP17 and RP17. The expression of *GAPDH* was analysed in parallel as reference gene using primer set FP18 and RP18. Gene specific standards were generated for both *Pb18S rRNA* and *GAPDH* by cloning respectively the PCR products generated using primers FP17/RP17 and FP18/RP18 in pTZ57R/T vector. Both standards were subjected to log dilution to establish a dymanic range from 10^2 to 10^6 copies per reaction. The amounts of parasite-derived 18S rRNA copies were determined from a standard curve, generated with known amounts of 18S rRNA plasmid. The gene expression was read as plasmid equivalents and the parasite liver load was expressed as normalised values obtained by taking the ratio of *Pb18S rRNA* to *GAPDH*.

To assess the ability of both mutant sporozoites to infect liver following their delivery through mosquito bite, 2 independent bite experiments were performed for each mutant. In each bite experiment, 12–15 mosquitoes were used that were harbouring either of the mutant sporozoite in their salivary glands. Following bite experiment, all blood meal positive mosquitoes were dissected and observed under fluorescent microscope to confirm the presence GFP expressing mutant sporozoites. Nearly 85% of all blood meal positive mosquitoes were positive for salivary gland sporozoites.

3. Results

3.1. PbS10 and PbS23/SSP3 are single copy genes unique to Plasmodium and encode for proteins with signal sequence

PbS10 and *PbS23/SSP3* were identified in SSH screen between salivary gland sporozoites versus merozoites and encode secretory proteins having a predicted molecular mass of 66.7 kDa and 50.4 kDa respectively. A BLAST search of PlasmoDB by using *Pb*S10 and *Pb*S23/SSP3 as query showed that these are single copy genes having single homologs in the other *Plasmodium* species. Sequence identity between amino acid sequences of *Pb*S10 (PBANKA_100250), *Py*S10: *Plasmodium yoelii* (rodent) PY01067, *Pf*S10: *Plasmodium falciparum* (human) PF3D7_0404800, *Pv*S10: *Plasmodium vivax* (human) PVX_001000; and *Pb*S23/SSP3 (PBANKA_142520), PyS23: *Plasmodium yoelii* (PY01796), *Pf*S23: *Plasmodium falciparum* (PF3D7_0812300), *Pv*S23: *Plasmodium vivax* (PVX_123155) was analysed using BLASTP tool of the NCBI database of "non-redundant protein sequences". The amino acid sequence similarity between PbS10 and *Pb*S23/SSP3 as compared to other Plasmodium orthologues is shown in Supp Fig. 1A and 1B respectively. No homologs were identified with this tool in any other species indicating that *Pb*S10 and *Pb*S23/SSP3 are unique to *Plasmodium*. Similarity searches of conserved domain database (http://www.ncbi.nlm.nih.gov/Structure/cdd/wrpsb.cgi) and Pfam (http://pfam.xfam.org/) by using *Pb*S10 and *PbS23/SSP3* as query did not find any conserved domains. *Pb*S10 and *PbS23/SSP3* sequences were analysed for the presence of signal peptide and transmembrane domains by using multiple tools like TMHMM, DAS, TMpred, TopPred2 that confirmed that both *Pb*S10 and *PbS23/SSP3* have a signal peptide at N-terminus and *PbS23/SSP3* has a transmembrane domain at C-terminus. *PbS23/SSP3* has 13 conserved cysteine resides in which 12 are in the ectodomain and 1 in transmembrane domain [25]. The percentage of amino acid sequence identity of *Pb*S10 and *Pb*S23/SSP3 to other orthologues- *P. yoelli* (*Py*), *P. falciparum* (*Pf*) and *P. vivax* (*Pv*) are indicated in supplementary Fig. 1A and B. Sequence alignment of *Pb*S23/SSP3 with other indicated orthologues is shown in supplementary Fig. 1C. The conserved cysteine residues across all *Plasmodium* orthologues are indicated inside the box.

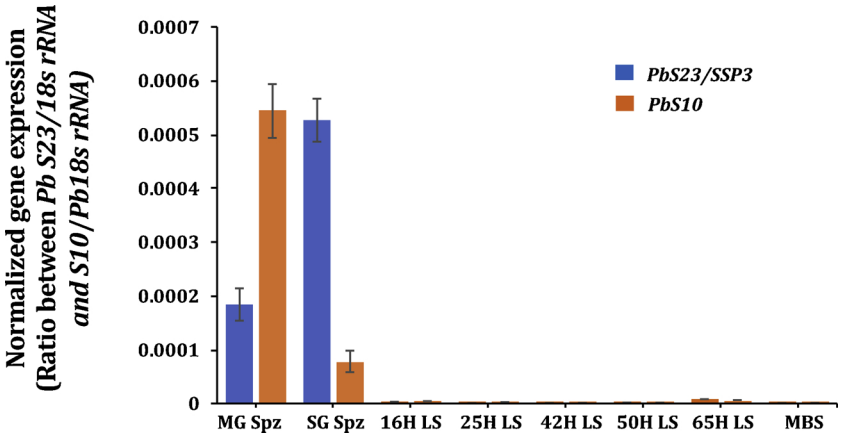


Fig. 1. Analysis of *PbS10* and *PbS23/SSP3* transcripts levels by quantitative real-time PCR. cDNA samples were generated from different life cycle stages of *P. berghei* (*Pb*) as indicated. Midgut sporozoites (MG Spz), salivary gland sporozoite (SG Spz), liver stages (LH) at 16 h, 25 h, 42 h, 50 h, 65 h and mixed blood stages (MBS). The transcript copy numbers were normalized to *Pb18S rRNA*.

3.2. PbS10 and PbS23/SSP3 show high expression in sporozoite stages of the mosquito

Quantitative real-time PCR analysis revealed maximal expression of *PbS10* in midgut oocyst stages followed by salivary gland sporozoite stage. However, the expression of *PbS23/SSP3* was maximal in salivary gland sporozoite stages followed by midgut oocyst stages. These data concur with the previous studies [14] that demonstrated the differential expression of S genes in salivary gland sporozoite. The expression of both *PbS10* and *PbS23/SSP3* was minimal during different time points of liver stage development and in mixed blood stages (Fig. 1).

3.3. Generation of PbS10 GD and PbS23/SSP3 KO mutants

Genomic DNA was isolated from drug-resistant parasites obtained following transfection with *PbS10* GD and *PbS23/SSP3* KO constructs. The endogenous locus and gene disruption strategy for *PbS10* is shown in Fig. 2A and B. For confirming correct 5′ integration of *PbS10* GD construct at endogenous locus, primer set FP3/RP3 was used. The primer FP3 was specific to a region upstream to the site of integration at 5′ region of ORF and primer RP3 was designed within the *PbHSP70* promotor region of GFP cassette. The product that was amplified using this primer set yielded 1,231 bp (Fig. 2C). The 3′ integration was confirmed using primer set FP4/RP4. The primer FP4 was specific to 3′ regulatory region of *hDHFR* cassette and primer RP4 was specific to a region downstream to integration site. A product size of 1,719 bp confirmed correct integration (Fig. 2C). Clonal lines of *PbS10* GD were confirmed for the absence of WT locus using primer set FP5/RP5 that specifically amplified a product of 668 bp within the ORF from WT parasites and not the clonal *PbS10* GD mutants (Fig. 2D). The correct integration of *PbS23/SSP3* KO was similarly confirmed as described for *PbS10* GD mutants. The endogenous locus and gene KO strategy for *PbS23/SSP3* is shown in Fig. 3A and B respectively. Primer sets FP8/RP8 and FP9/RP9 was used to confirm correct integration at 5′ and 3′

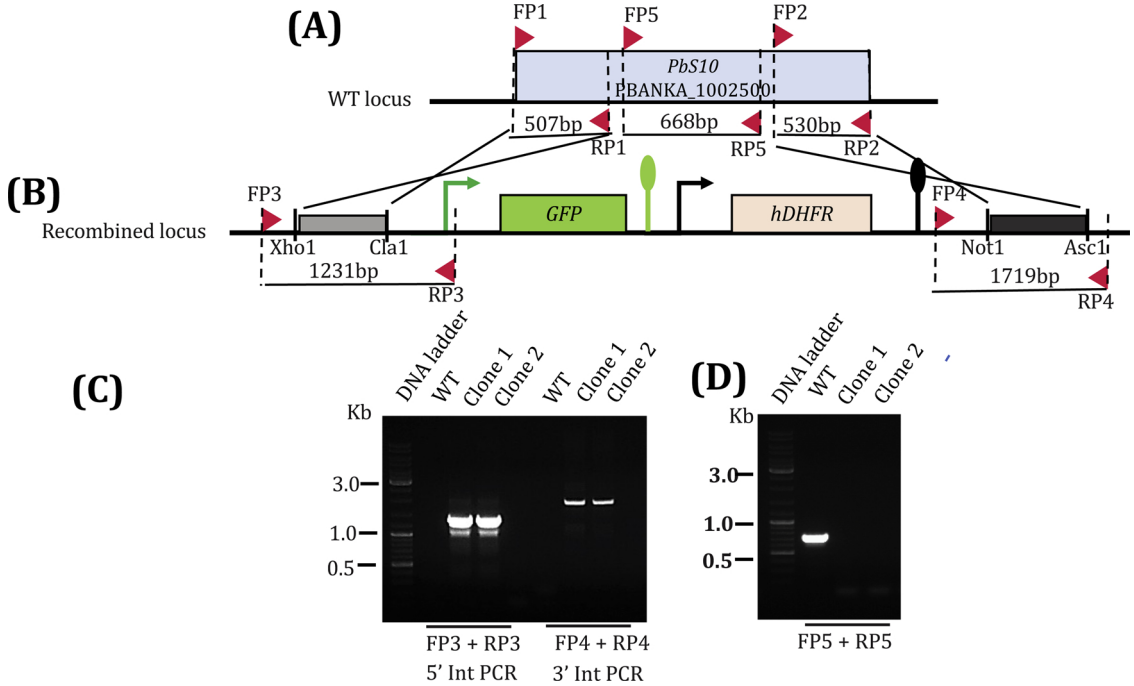


Fig. 2. *PbS10* gene disruption (GD) strategy and genotypic characterization of *PbS10* mutants. (A) Schematic of *PbS10* locus and its disruption by a GFP-hDHFR *PbS10* construct. The disruption construct carried 5′ region and 3′ region within the *PbS10* ORF that flanked respectively the GFP and drug selection marker human dihydrofolate reductase (hDHFR). The 5′ and 3′ regions within the *PbS10* ORF were amplified respectively by using primer sets FP1, RP1 and FP2, RP2. (B) Recombined *PbS10* locus containing GFP and hDHFR cassette. (C) Diagnostic PCR for confirmation of *PbS10* disruption. The correct 5′ and 3′ integration was confirmed using primer sets FP3, RP3 and FP4, RP4 respectively that yielded expected products in two independent clones- 1 and 2 but not WT. Primer set FP5, RP5 amplified a product with in the *PbS10* ORF from WT but not from the *PbS10* gene disrupted clones indicating a homogeneous population.

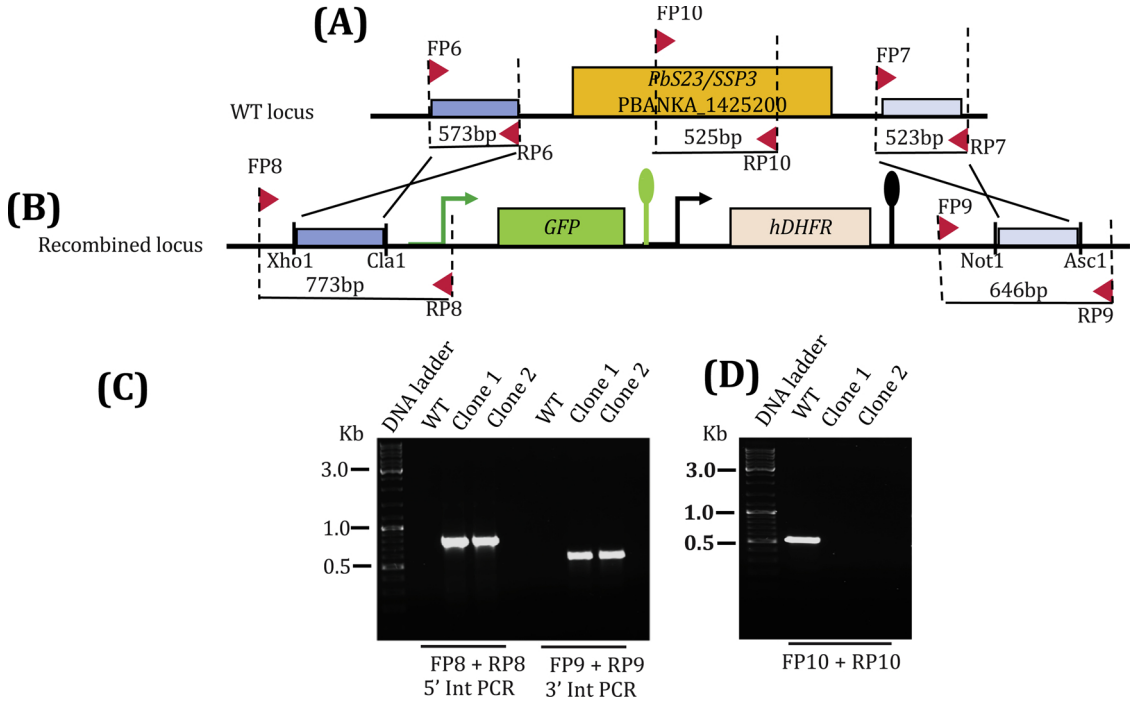


Fig. 3. *PbS23/SSP3* gene knockout (KO) strategy and genotypic characterization of *PbS23/SSP3* mutants. (A) Schematic of *PbS23/SSP3* locus and its replacement by a GFP-hDHFR *PbS23/SSP3* KO construct. The KO construct carried 5′ and 3′ UTR regions of *PbS23/SSP3* flanking respectively the GFP and drug selection marker hDHFR. The 5′ and 3′ UTR regions were amplified respectively by using primer sets FP6, RP6 and FP7, RP7. (B) Recombined *PbS23/SSP3* locus containing GFP and hDHFR cassette. (C) Diagnostic PCR for confirmation of *PbS23/SSP3* replacement. The correct 5′ and 3′ integration was confirmed using primer sets FP8, RP8 and FP9, RP9 respectively that yielded expected products in two independent clones- 1 and 2 but not WT. Primer set FP10, RP10 amplified a product with in the *PbS23/SSP3* ORF from WT but not from the *PbS10* gene disrupted clones indicating a homogeneous population.

end respectively that yielded products of 773 bp and 646 bp (Fig. 3C). The primer set FP10/RP10 yielded 525 bp product from WT parasites but not from *PbS23/SSP3* KO confirming the establishment of *PbS23/SSP3* KO clonal lines (Fig. 3D).

3.4. Generation of PbS23/SSP3-3XHA transgenic line

To localize *PbS23/SSP3*, a *PbS23/SSP3* HA transgenic was generated by appending a C -terminal HA tag to *PbS23/SSP3* protein. The endogenous locus of *PbS23/SSP3* is shown in Fig. 4A and the recombined locus is shown in Fig. 4B. To confirm correct integration of *PbS23/SSP3*-3XHA construct at endogenous locus, primer sets FP13/RP13 and FP14/RP14 was used that yielded respectively 732 bp and 737 bp products only from two clonal lines of *PbS23/SSP3*-3XHA transgenic and not the WT parasites (Fig. 4C).

3.5. PbS10 GD and PbS23/SSP3 KO mutants do not manifest any defect in during asexual blood stage propagation

Approximately 200 µl of infected blood having ˜3% parasitemia of either mutants and WT GFP were intravenously injected into different groups of mice. The asexual growth of the parasites was monitored by observing Giemsa-stained blood smears made on a daily basis. No difference was noted in the growth of both *PbS10* GD and *PbS23/SSP3* KO mutants as compared to WT GFP parasites (Fig. 5A).

3.6. PbS10 GD and PbS23/SSP3 KO mutants undergo normal development in A. stephensi

An exception amongst functionally characterized “S” genes having a role other than in sporozoite specific functions was noted for S4 that is required for the mosquito infections [18]. These findings prompted us to investigate if S10 and S23 likely played any role in the transmission stages. We, therefore, analysed the stages that immediately followed sexual reproduction. Mosquitoes were allowed to obtain blood meal from mice harbouring either of the mutant parasites and WT GFP. The mosquitoes were dissected at 8 h and 16–18 h post blood meal. The samples corresponding to these time points were stained with anti-p28 antibody [31] to reveal the retort and ookinete stages (Fig. 5B). We noted that both mutants were able to generate these stages with frequency similar to WT GFP parasites that further corroborated with the frequency of oocyst on infected midguts (Fig. 5C and D). We noted no difference in the sporulation pattern inside oocyst (Fig. 5E) as well as the gross oocyst sporozoite numbers per mosquito in both mutants as compared to WT GFP (Fig. 5F). We next analysed the ability of both mutants to reach the mosquito salivary glands. Whole mounts of dissected salivary glands, when observed under fluorescent microscope, revealed successful colonisation by both the sporozoite mutants (Fig. 5G) that did not differ in numbers as compared to WT GFP sporozoites (Fig. 5H). We conclude that *Pb*S10 and *Pb*S23/SSP3 is not required for the development of *P. berghei* in mosquito stages.

3.7. PbS10 GD and PbS23/SSP3 KO mutants exhibit normal sporozoite gliding motility, cell traversal and infectivity

The movement of salivary gland sporozoites for either mutants when observed under 100X magnification revealed gliding pattern that was similar to WT sporozoites. Live video recording of the sporozoite gliding motility for both mutants and WT were done by using Ni-S elements software (Supp movie 1 (WT sporozoite), Supp movie 2 (*PbS10* GD mutant sporozoite) and Supp movie 3 (*PbS23/SSP3* KO mutant sporozoite). The ability of both mutants to traverse through the HepG2 cells was comparable to WT sporozoites as quantified by the frequency of texas-red dextran positive cells (Fig. 6A) [32]. The sporozoite inside out assay for quantification of in vitro sporozoite infectivity revealed that both mutants invaded HepG2 cells with

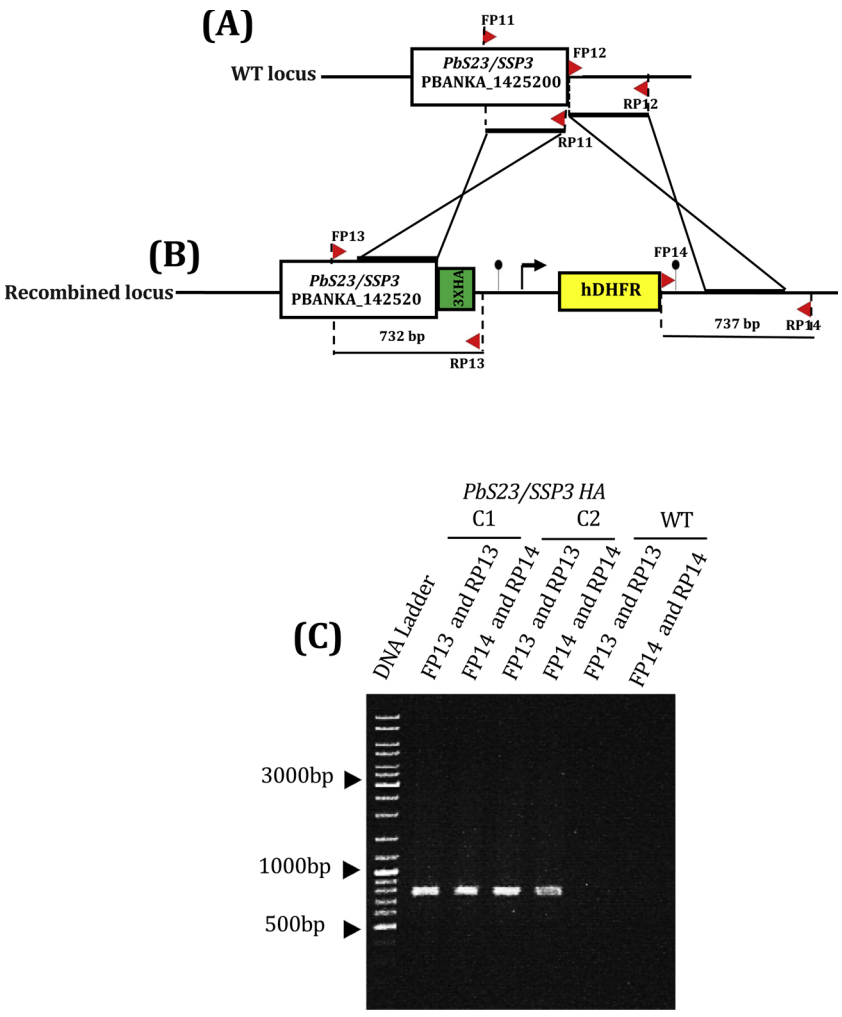


Fig. 4. Strategy for generation of *PbS23/SSP3* 3XHA transgenic line and its genotypic characterization (A) Schematic of *PbS23/SSP3* locus and appending a 3XHA tag using a 3XHA-hDHFR targeting construct. The 3′UTR of PbHSP70 was engineered downstream to HA tag. The targeting construct carried last 500 bp of *PbS23/SSP3* ORF and endogenous 3′ UTR of *PbS23/SSP3* flanking respectively the 3XHA tag and drug selection marker hDHFR. The last 500 bp of *PbS23/SSP3* ORF and 3′ UTR regions were amplified respectively by using primer sets FP11, RP11, and FP12, RP12. (B) Recombined *PbS23/SSP3* locus containing 3XHA in tandem to *PbS23/SSP3* ORF followed by the hDHFR cassette. (C) Diagnostic PCR for confirming correct integration of 3XHA-hDHFR targeting construct by using primer sets FP13, RP13, and FP14, RP14 respectively that yielded expected products in two independent clones- 1 and 2 but not WT.

efficiency comparable to WT sporozoites (Fig. 6B). We further quantified the frequency of EEFs for both mutants. At 12 h and 36 h time points, there was no difference in the frequency of EEFs between both mutants and WT. However, at 62 h time point, there was a dramatic reduction in the frequency of *PbS10* GD EEFs that mostly appeared degenerating, while the *PbS23/SSP3* KO EEF frequency was nearly similar to WT (Fig. 6C). We conclude that *Pb*S10 and *Pb*S23/SSP3 are not required for gliding motility, cell traversal, hepatocyte infection and initiation of sporozoite transformation into EEFs.

3.8. PbS10 GD and PbS23/SSP3 KO mutant sporozoites show block during early and late EEF development in vitro

PbS10 GD and *PbS23/SSP3* KO mutants manifested no defect in their growth until 12 h time point (Fig. 7A). However, beyond this time point ie., at 36 h *PbS10* GD mutants did not show any appreciable growth as compared to *PbS23/SSP3* KO and WT GFP parasites (Fig. 7B). For *PbS23/SSP3* KO mutants, we did not notice any significant difference in EEF size both at 36 h and 62 h time points as compared to WT EEFs as revealed by UIS4 staining (Fig. 7B and C). We performed quantification of EEF size for both mutants by observing 20 random fields at 12 h, 36 h and 62 h (Fig. 7D). Additionally we noted, a significant reduction in the formation of hepatic merozoites in *PbS23/SSP3* KO mutants as revealed by DAPI staining (Fig. 7E). Taken together, our observations revealed a critical requirement of *Pb*S10 during early liver stage development beyond 12 h while the *Pb*S23/SSP3 depletion affected the development of late liver stages.

3.9. PbS10 GD and PbS23/SSP3 KO mutant sporozoites infect hepatocytes in vivo normally but give rise to rare breakthrough infections

The in vivo infection of C57Bl6 mice with 1×10^4 sporozoites of both mutants followed by the analysis of the parasite specific 18SrRNA copy number in the liver revealed that both mutants were unaffected in their potential to commit hepatocyte infection (Fig. 8). In other independent experiments, we monitored the prepatency in the mouse that was infected intravenously with 5×10^3 sporozoites of either mutants and WT. We observed that *PbS10* GD mutant sporozoite yielded no infection in the majority of the animals tested in 3 independent experiments. We noted 1/5 and 1/6 mice became positive for blood stage infection in two independent groups while in one group none of the 3 mice tested were positive for infection till day 15 (Table 2). Interestingly the mice that became positive for infection showed a prepatency of D8-D9 that corroborated with the drastic growth defect beyond 12 h under in vitro conditions. Surprisingly, *PbS23/SSP3* KO mutants also were unable to initiate timely patency considering their in vitro growth characteristics similar to WT. In 3 independent experiments, 1/6, 1/6 and 1/5 mice became positive for blood stage infection. The positive mice showed prepatent period of day 5–6 (Table 2). This suggested that *PbS23/SSP3* KO mutants were comparatively less severely attenuated than *PbS10* GD mutant. We further tested the ability of both mutant sporozoites obtained from rare breakthrough infections for their ability to reinfect mice. We again observed rare breakthrough infections similar to our primary infection studies as reported in Table 2 (data not shown).

We also tested the infectivity of both sporozoite mutants by

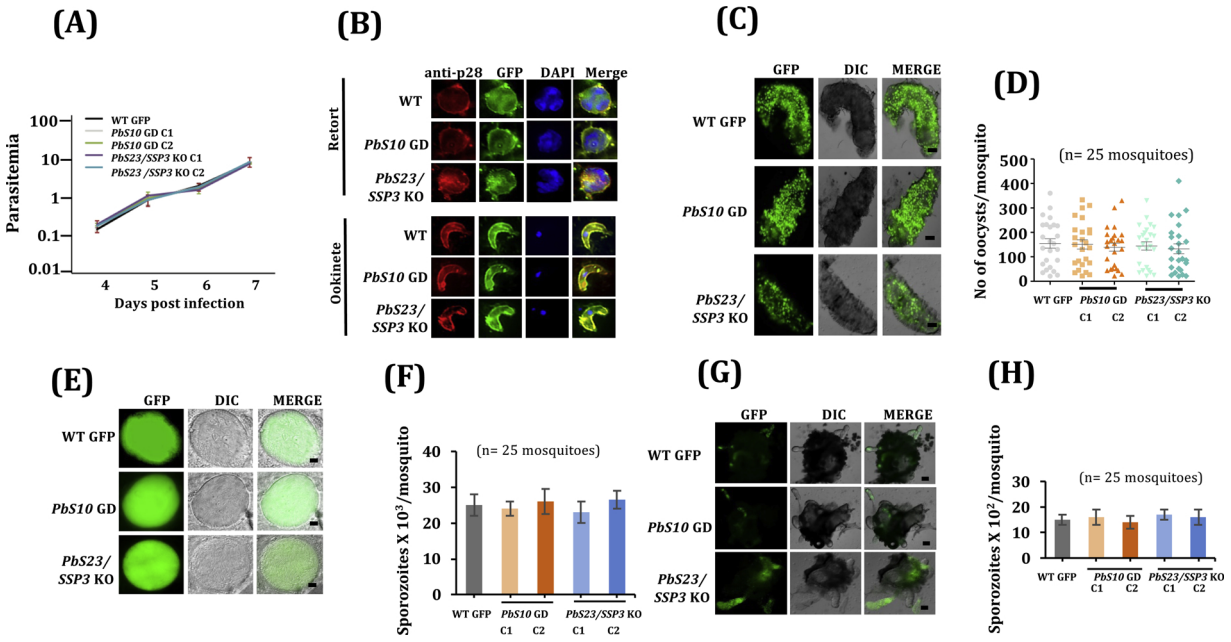


Fig. 5. Phenotypic characterization of *PbS10* GD and *PbS23/SSP3* KO mutants in asexual and mosquito stages. (A) Asexual blood stage propagation was normal in both clones 1 and 2 for *PbS10* GD and *PbS23/SSP3* KO mutants. BALB/c mice (n = 3) were injected with 1×10^3 infected RBC by the intravenous route. The parasitemia was monitored by microscopic observation of Giemsa-stained blood smears. The graph shows the values of mean ± S.D. Three independent experiments were performed and data for one of the representative experiments is shown. (B–H) Mosquito stages of *PbS10* GD and *PbS23/SSP3* KO mutants. Female *Anopheles* mosquito were allowed to obtain blood meal from mice harbouring gametocyte stages of *PbS10* GD and *PbS23/SSP3* KO mutants. Following blood meal, the mosquito guts were dissected at 2 h (zygote) and 16 h (ookinete) time points. Both samples were stained with anti-p28 antibody, a marker for zygote and ookinete and immunoreactivity was revealed using Alexaflor 594 anti-mouse secondary antibody. (B) Both *PbS10* GD and *PbS23/SSP3* KO mutants were able to form zygote and ookinetes. Scale bar 5 µm. (C) Representative image of day 14 midguts showing oocyst burden in *PbS10* GD and *PbS23/SSP3* KO mutants. Scale bar 20 µm. (D) Quantification of *PbS10* GD and *PbS23/SSP3* KO mutant oocysts per mosquito from clone 1 and 2, n = 25. Two independent experiments were performed, one with each clone. Shown are the mean ± S.D. from one experiment. (E) Oocyst showing normal sporulation pattern in *PbS10* GD and *PbS23/SSP3* KO mutants. Scale bar 20 µm. (F) Quantification of *PbS10* GD and *PbS23/SSP3* KO mutant oocysts sporozoites per mosquito from clone 1 and 2, n = 25. Two independent experiments were performed, one with each clone. Shown are the mean ± S.D. from one experiment. (G) Representative images of dissected mosquito salivary glands harbouring *PbS10* GD and *PbS23/SSP3* KO mutant sporozoites. Scale bar 200 µm. (H) Quantification of *PbS10* GD and *PbS23/SSP3* KO mutant salivary gland sporozoites per mosquito from clone 1 and 2, n = 25. Two independent experiments were performed, one with each clone. Shown are the mean ± S.D. from one experiment.

mosquito bite (Table 3). In two independent bite experiments performed for *PbS23/SSP3* mutants (n = 5 per group), none of the mice became positive for infection till D15 post infection, as judged by observing Giemsa stained smears. Of the two independent bite experiments performed for *PbS10* GD mutants (n = 5 per group), one group of mice completely failed to produce blood stage infection. However, in the second group, 1 mice became positive on D12. Taken together, the ability of both mutants to reach hepatocytes in vivo, with efficiency similar to WT sporozoites, but failing to cause to a timely prepatent period establishes the role of both *Pb*S10 and *Pb*S23/SSP3 in EEF development.

3.10. *PbS23/SSP3 is detected in salivary gland sporozoite stages*

The staining of *PbS23/SSP3*-3XHA with an anti-HA antibody followed by revealing its immunoreactivity with anti-rabbit secondary antibody conjugated Alexaflour 594 confirmed expression in salivary gland sporozoites. 3d11, a monoclonal antibody specific for the repeat region of *P. berghei* CSP was used as a marker for sporozoite stage. The CSP immunoreactivity was revealed by using anti-mouse secondary antibody conjugated Alexafluor 488. The specificity of anti-HA antibody towards *PbS23/SSP3*-3XHA transgenic sporozoites was confirmed by lack of its immunoreactivity towards WT sporozoites (Fig. 9). Parasite nuclei was stained with DAPI.

4. Discussion

In the current study, we analysed the functional role of *PbS23/SSP3* and *PbS10* for its probable role in sporozoite specific functions, viz., gliding, hepatocyte infection and EEF development. Maximal expression of both genes during oocyst and salivary gland sporozoite stage as compared to the mixed blood stage or developing EEF stages was consistent with earlier studies [14] that reported enrichment of both transcripts in *P. yoelli* salivary gland stage. However we show for the first time in *P. berghei*, a more robust expression of *PbS10* in oocyst stages and maximal expression of *PbS23/SSP3* in salivary gland sporozoite stage. Further, our studies also confirmed the presence of *PbS23/SSP3* protein in salivary gland sporozoites consistent with earlier reports in *P. yoelii* documenting the cellular distribution of S23/SSP2 in endoplasmic reticulum of oocyst sporozoites and an exclusive membrane localization in salivary gland sporozoite stages [25]. Interestingly, several conserved cysteine residues have been identified in Py23 that are typical of the 6 cysteine protein family [25]. The members of this family have been shown to localise either to micronemes or parasite surface and aid in cell-cell interactions [33,34], [35]. Our studies show that these cysteine residues are also highly conserved in PbS23/SSP3 protein (Supp Fig. 1C). While the known sporozoite microneme resident 6-cysteine proteins like P52 and P36 have been implicated in hepatocyte infection [34,36,37], the lack of invasion deficient phenotype in *PbS23/SSP3* mutants clearly rules out the role of these conserved cysteine residues in cell-cell communication.

In contrast to the gliding defect associated with the *PyS23* KO sporozoites [25], we observed normal gliding for *PbS23/SSP3* KO mutant sporozoites as judged by in vitro gliding assays and infectivity studies. The discrepancy is not surprising, given other instances where orthologous gene mutants within rodent species of *Plasmodium* may

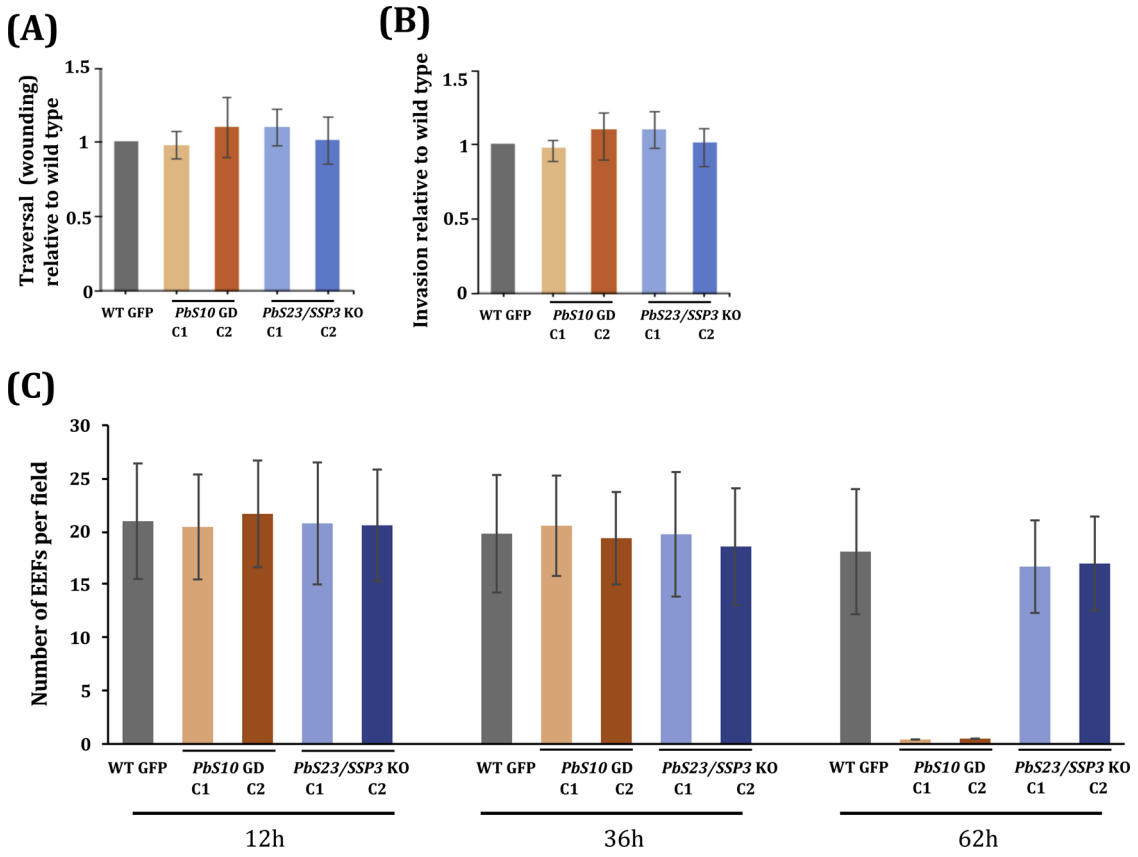


Fig. 6. *PbS10* GD and *PbS23/SSP3* KO mutant sporozoites exhibit normal cell traversal activity and infectivity in HepG2 cells. (A) Cell traversal assay for WT and *PbS10 GD and PbS23/SSP3* KO mutant sporozoites (clones C1 and C2) in the presence of rhodamine-labeleddextran. The frequency of cells positive for rhodamine-labeled dextran was nearly the same is both clonal lines of *PbS10 GD and PbS23/SSP3* KO mutant as compared to WT. (B) Quantification of intracellular infectivity of *PbS10* GD *and PbS23/SSP3* KO mutant sporozoites by inside-out assay. Equal numbers (2×10^4) sporozoites of WT GFP and *PbS10 GD and PbS23/SSP3* KO mutant sporozoites (clones C1 and C2) were added to monolayers of HepG2 cells. One hour later, the cultures were fixed and the extracellular sporozoites were stained with anti-CSP monoclonal antibody 3D11 and the immunoreactivity was revealed using anti-mouse secondary antibody conjugated to Alexa Fluor. The slides were observed under a Nikon AR fluorescent microscope and in each field, the total number of sporozoites (GFP positive) and a number of extracellular sporozoites (Red fluorescence) were counted and the invasion efficiency relative to WT was obtained. (C) Quantification of EEF frequency in HepG2 cells at 12 h post invasion. WT, *PbS10* GD and *PbS23/SSP3* KO sporozoites were added to monolayers of HepG2 cells and incubated for 12 h. The cultures were fixed and stained with anti-UIS-4 antibody, a marker for the PVM. The number of EEFs were quantified by randomly observing 25 field. For each mutant, two independent experiments were done with clones C1 and C2.

have a varying phenotype. For example, in *P. yoelii*, FAS-II was shown to be essential and parasites lacking FabB/F failed to complete liver stage development and did not initiate blood stage infection in BALB/c mice [38]. However, *P. berghei* parasites lacking FabI were though attenuated severely, yet initiated a normal blood stage infection in C57BL/6 mice [39,40]. Also, while PyS23 mutants manifested no obvious defect in EEF development and initiated a timely blood stage infection, the *PbS23/SSP3* mutants were unable to cause blood stage infection in the majority of mice though the in vitro development of liver stages did not differ from WT as judged by UIS4 staining pattern. These observations together with the delay in prepatency in mice that rarely become positive for infection indicated a block in late liver stage. A likely explanation for the inability to develop blood stage infection in the absence of any noticeable defect in EEF size may likely indicate compromised schizogony as noted in the pattern of nuclear staining of *PbS23/SSP3* mutants. While more direct evidence for role of PbS23/SSP3 in regulating liver stage schizogony as speculated in this study is lacking, the manifestation of varying phenotypes for rodent mutants in different host backgrounds merits more detailed investigation.

The requirement of *Pb*S10 for progression of EEF growth beyond 12 h was also evident in vivo, as the pre patent period associated with the mutant was D8-9. Despite severe attenuation, the rare breakthrough infections following delivery of sporozoites by i.v., or mosquito bite was unexpected of *PbS10* GD mutants. A likely explanation is that these mutants may not be completely deficient in intracellular growth in vivo, owing to a conducive intrahepatic niche as compared to HepG2 cells. Importantly, the delay in patency during rare and infrequent breakthrough infections coincided with the respective degree of growth arrest viz., D8-12 for *PbS10* GD mutants and D5 for *PbS23/SSP3* KO mutants.

While the most recent studies on sporozoite surface proteome are comprehensive [6,7], not all sporozoite proteins bearing putative SP were detected in these data sets. A likely explanation for this may be a relatively low abundance of such proteins or perhaps their translation at later time point following sporozoite transformation. Consistent with the former notion, more than 50% of genes that are highly transcribed in the sporozoite stage as detected by more than one transcriptomic approaches [15,41], were not translated at this stage both in *P. falciparum* and *P. yoelli* [6] implying that many of these gene products are only essential for liver stage development. Infact, the exclusive role of both *PbS10* and *PbS23/SSP3* in liver stage development is similar to previously characterised *S3/UIS4* and *S7/UIS3* genes. The arrest of *S7/UIS3* and *S3/UIS4* mutants during liver stage development paved way for using these mutants as whole organism vaccines that yeilded sterile immunity [16,17]. In our study, while both mutants gave rise to rare break through infections, none the less, the fact that sporozoites are

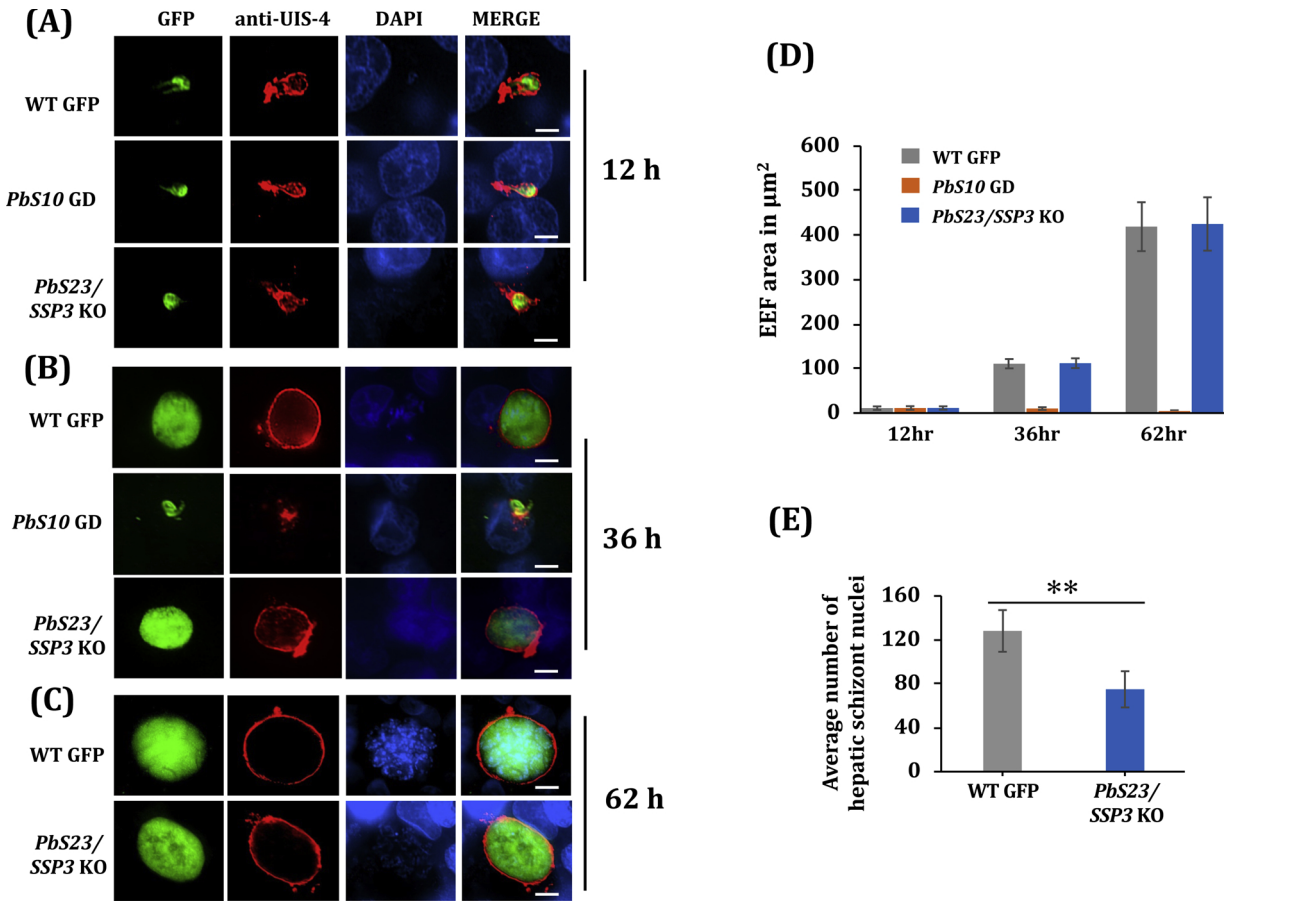


Fig. 7. *PbS10* GD and *PbS23/SSP3* KO mutants show respectively early and late growth arrest in HepG2 cells. *PbS10* GD and *PbS23/SSP3* KO mutant sporozoites were added to HepG2 cultures and fixed at 12 h, 36 h, and 62 h. The cultures were stained with an anti-UIS4 antibody specific for the parasitophorous vacuolar membrane and the immunoreactivity was revealed using anti-rabbit secondary antibody conjugated to Alexa Fluor 594. DAPI staining was performed to visualise the host and parasite nuclei. EEFs at (A) 12 h, (B) 36 h and (C) 62 h time point. (D) Measurement of EEF size at indicated time points in WT, *PbS10* GD and *PbS23/SSP3* KO lines. The data was generated for single clones of *PbS10* GD and *PbS23/SSP3* KO (E) Hepatic schizogony was enumerated by counting the DAPI positive parasite nuclei that showed significant reduction in *PbS23/SSP3* mutants as compared to WT (**$p < 0.0022$).

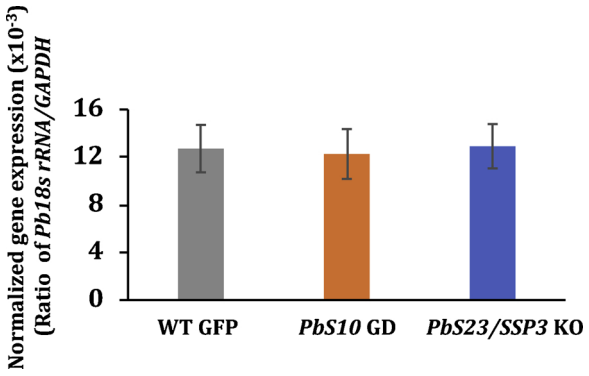


Fig. 8. Quantification of in vivo sporozoite infectivity in *PbS10* GD and *PbS23/SSP3* KO mutants. A group of 3–4 C57Bl6 mice were intravenously injected with 1×10^4 sporozoites of WT or *PbS10* GD and *PbS23/SSP3* KO mutants. Fourteen hours post infection, parasite burden was evaluated in mice livers by measuring the *P. berghei* specific 18S rRNA copy number by qRT-PCR. The gene expression values were normalized by taking ratio of *Pb18S rRNA* and *GAPDH* plasmid equivalents.

drastically altered in their capacity to initiate a timely blood stage infection may still hold potential to further weaken the sporozoites by generating double mutants of *PbS10* and *PbS23/SSP3*. Infact *Plasmodium* mutants that completely resist break though infections were obtained by multiple gene attenuation [42] and may have additional safety benefits in terms of greater mitigation of their viability as compared to single gene mutants.

The role of secretory proteins during liver stage development may have additional functions in modulating host responses. For example, S2/CSP is introduced into the host cell cytoplasm and it shuttles to the nucleus to alter the host gene expression in favour of the parasite growth [43]. Likewise, S7/UIS3 was shown to interact with liver fatty acid binding protein (L-FABP) and may likely sequester host proteins for the favourable growth of EEFs [44]. In this context, the failure of both *PbS10* GD and *PbS23/SSP3* KO mutants to complete EEF development may likely suggest their inability to possibly manipulate the hepatocytes, in a yet to be identified manner. Taken together, we report the role of *Pb*S10 and *Pb*S23/SSP3 in liver stage development. It will be interesting to test whether targeting the orthologues of *Pb*S10 and *PbS23/SSP3* in other human malarial parasites will yield similar phenotypes.

Summary statement

Plasmodium berghei sporozoite secretory proteins PbS10 and PbS23/SSP3 are required for liver stage development and not for a commitment to hepatocyte infection.

Table 2
Analysis of prepatent period for *PbS10* GD and *PbS23/SSP3* KO sporozoite mutants.

Group	Experiment number	Number of sporozoites injected	Number of mice positive/no of mice infected	Prepatent period
WT	1	5×10^3	3/3	D3
PbS10 GD mutant		5×10^3	1*/5	D8
WT	2	5×10^3	3/3	D3
PbS10 GD mutant		5×10^3	1*/6	D9
WT	3	5×10^3	3/3	D3
PbS10 GD mutant		5×10^3	0/3	NA
WT	1	5×10^3	3/3	D3
PbS23/SSP3 KO mutant		5×10^3	1*/6	D5
WT	2	5×10^3	3/3	D3
PbS23/SSP3 KO mutant		5×10^3	1*/6	D5
WT	3	5×10^3	3/3	D3
PbS23/SSP3 KO mutant		5×10^3	1*/5	D6

Table 3
Analysis of prepatent period for *PbS10* GD and *PbS23/SSP3* KO sporozoite mutants by mosquito bite.

Group	Experiment number	Number of mice used for bite	Number of mice positive/no of mice infected	Prepatent period in days (D)
WT	1	3	3/3	D3.5
PbS10 GD mutant		5	0/5	ND
WT	2	3	3/3	D3.5
PbS10 GD mutant		5	1*/5	D12 for one mice*
***PbS23/SSP3* KO mutant**				
WT	1	3	3/3	D3.5
PbS23/SSP3 KO mutant		5	0/5	ND
WT	2	3	3/3	D3.5
PbS23/SSP3 KO mutant		5	0/5	ND

*Indicates the mice that became positive for blood stage infection. ND: Not detected.

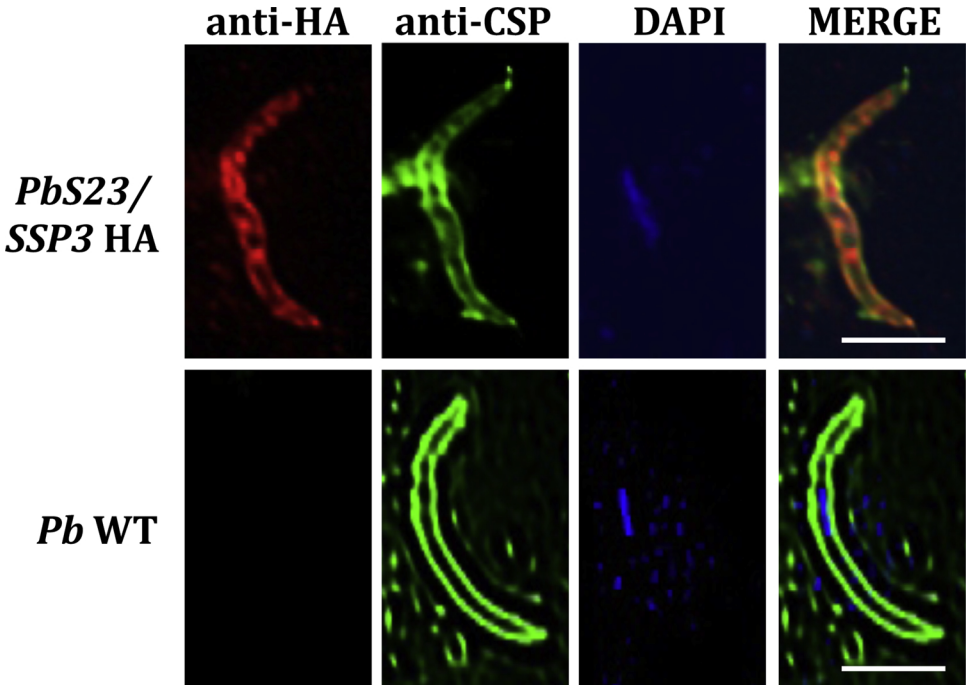


Fig. 9. Localisation of *Pb*S23/*SSP3*-3XHA in salivary gland sporozoites. *PbS23/SSP3*-3XHA transgenic line (Clone 1) was propagated in mouse and transmitted to female *Anopheles* mosquitoes. Day 18 salivary gland sporozoites were obtained and stained both with anti-HA rabbit antibody and 3d11, a mouse monoclonal antibody specific for the CSP. The immunoreactivity was revealed by using respectively an anti-rabbit Alexaflour 594 and anti-mouse Alexaflour 488 secondary antibodies. DAPI was used to stain the parasite nuclei. Top panel is *Pb*S23/SSP3-3XHA sporozoite. Lower panel is WT sporozoite. Scale bar 5 µm.

Acknowledgments

We thank Dr. Robert Menard (Institute Pasteur) for the pBC-GFP-hDHFR plasmid. We thank Dr. Photini Sinnis (Johns Hopkins University) for UIS4 antibody and Dr. Oliver Billiker (Wellcome Sanger Institute) for the p28 antibody. JT, RRS MM and AG were supported by Council of Scientific and Industrial Research (CSIR), Government of India. SKK and HHC were supported by CSIR-UCG (University Grants Commission), Government of India. BSM was supported by Department of Biotechnology (DBT), Government of India. KAK acknowledges the financial support from Department of Science and Technology (DST), Government of India (SR/SO/HS-122/2008) and DBT (BT/PR2495/BRB/10/950/2011). SM acknowledges DBT Ramalingaswami Fellowship grant (GAP0142).

Appendix A. Supplementary data

Supplementary material related to this article can be found, in the

Check for updates

Molecular Microbiology (2019) 112(2), 699–717

doi:10.1111/mmi.14313
First published online 5 July 2019

Biochemical and physiological investigations on adenosine 5′ monophosphate deaminase from *Plasmodium spp.*

Lakshmeesha Kempaiah Nagappa,[1†] Dipti Singh,[2†] Sandeep Dey,[2] Kota Arun Kumar[2*] and Hemalatha Balaram[1*]

[1] *Molecular Biology and Genetics Unit, Jawaharlal Nehru Centre for Advanced Scientific Research (JNCASR), Bengaluru, India.*

[2] *Department of Animal Biology, School of Life Sciences, University of Hyderabad, Hyderabad, India.*

Summary

The interplay between ATP generating and utilizing pathways in a cell is responsible for maintaining cellular ATP/energy homeostasis that is reflected by Adenylate Energy Charge (AEC) ratio. Adenylate kinase (AK), that catalyzes inter-conversion of ADP, ATP and AMP, plays a major role in maintaining AEC and is regulated by cellular AMP levels. Hence, the enzymes AMP deaminase (AMPD) and nucleotidases, which catabolize AMP, indirectly regulate AK activity and in-turn affect AEC. Here, we present the first report on AMPD from *Plasmodium*, the causative agent of malaria. The recombinant enzyme expressed in *Saccharomyces cerevisiae* was studied using functional complementation assay and residues vital for enzyme activity have been identified. Similarities and differences between *Plasmodium falciparum* AMPD (PfAMPD) and its homologs from yeast, *Arabidopsis* and humans are also discussed. The AMPD gene was deleted in the murine malaria parasite *P. berghei* and was found to be dispensable during all stages of the parasite life cycle. However, when episomal expression was attempted, viable parasites were not obtained, suggesting that perturbing AMP homeostasis by over-expressing AMPD might be lethal. As AMPD is known to be allosterically modulated by ATP, GTP and phosphate, allosteric activators of PfAMPD could be developed as anti-parasitic agents.

Abbreviations: ADSS, adenylosuccinate synthetase; ASL, adenylosuccinate lyase; GMPS, guanosine monophosphate synthetase; HGXPRT, hypoxanthine-guanine-xanthine phosphoribosyltransferase; IMPDH, inosine monophosphate dehydrogenase; ISN1, inosine monophosphate specific nucleotidase; PNP, purine nucleoside phosphorylase; IFA, immunofluorescence assay; EEFs, exo-erythrocytic forms.

Accepted 22 May, 2019. *For correspondence: E-mail: kaksl@uohyd.ernet.in (K.A. Kumar); Tel. (+91) 40 23134530; Fax (+91) 40 23010120 and E-mail: hb@jncasr.ac.in (H. Balaram); Tel. (+91) 80 22082812; Fax (+91) 80 22082766.†Have contributed equally to this work.

Introduction

Malaria caused by the parasitic protozoan *Plasmodium* is one of the deadliest diseases causing 445,000 deaths per annum worldwide (WHO, 2017). Although the PlasmoDB database is replete with information on the genome and proteome of the organism, most proteins are uncharacterized or have putative status (Bahl *et al.*, 2002, 2003; Aurrecoechea *et al.*, 2008). This inadequacy of proper understanding of the biochemistry of the organism has been a major impediment to the efforts put forth towards mitigation of this menacing disease. With genetic manipulation being highly challenging in *P. falciparum*, understanding the physiological significance of these uncharacterized/putative proteins becomes a non-trivial task (de Koning-Ward *et al.*, 2000). As the parasite is completely dependent on the salvage of precursors (predominantly hypoxanthine) for its purine nucleotide bio-synthesis (Downie *et al.*, 2008), the enzymes involved in this pathway have been sought after as potential drug targets. Although many enzymes of the purine nucleotide metabolism in *Plasmodium* have been studied in great detail (Hypoxanthine-guanine-xanthine phosphoribosyltransferase (HGXPRT), adenylosuccinate synthetase (ADSS), adenylosuccinate lyase (ASL), purine nucleoside phosphorylase) (Jayalakshmi *et al.*, 2002; Eaazhisai *et al.*, 2004; Madrid *et al.*, 2008; Bulusu *et al.*, 2009; Mehrotra *et al.*, 2010; Roy *et al.*, 2015a,b), a few more remain uncharacterized (AMPD, IMP dehydrogenase, IMP-specific nucleotidase and other purine nucleotidases). Through this study, we add further knowledge to the existing understanding of this protozoan

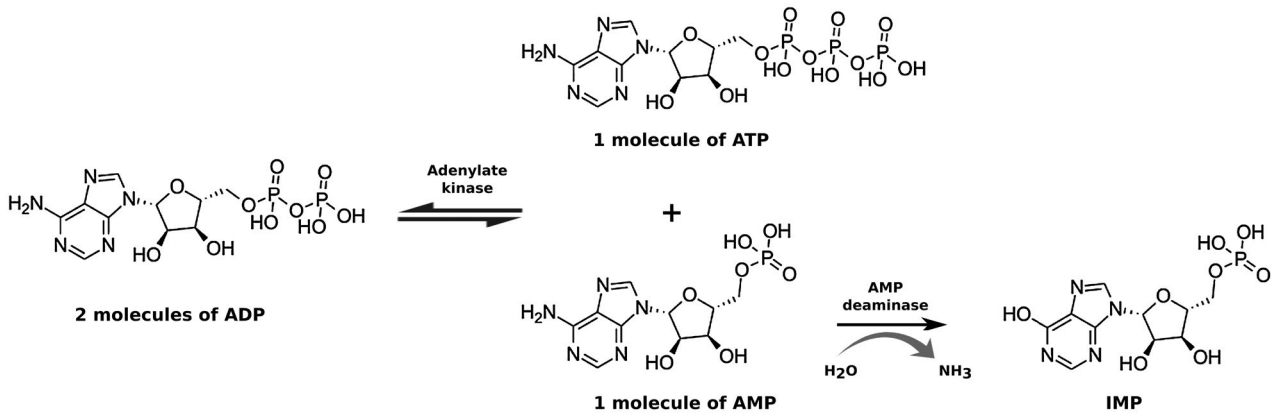
© 2019 John Wiley & Sons Ltd

parasite by examining one more enzyme involved in purine nucleotide metabolism, AMP deaminase (EC. 3.5.4.6), a previously uncharacterized protein.

AMPD belongs to amidohydrolase superfamily of enzymes characterized by a conserved $(\alpha/\beta)_8$-barrel core and a mononuclear metal centre (Seibert and Raushel, 2005). Salient features of AMPD in particular include, exclusive eukaryotic occurrence, presence of divalent zinc at the metal centre and a highly divergent N-terminus (Sabina and Mahnke-Zizelman, 2000; Marotta *et al*., 2009). AMPD is encoded by a single gene in lower eukaryotes whereas, in humans and other mammals three tissue-specific isoforms of AMPD are present, namely AMPD1 (skeletal muscle isoform), AMPD2 (soft tissue isoform) and AMPD3 (erythrocytic isoform). Extensive studies have been carried out on AMPD1 and more recently on AMPD2 and AMPD3 and mutations in these genes have been shown to have physiological consequences (Fishbein *et al*., 1978; Shumate *et al*., 1979; Morisaki *et al*., 1992; Hellsten *et al*., 1999; Akizu *et al*., 2013). Although detailed biochemical characterization of *S. cerevisiae* AMPD (ScAMPD) (Yoshino *et al*., 1979; Murakami, 1979; Murakami *et al*., 1980; Meyer *et al*., 1989; Merkler *et al*., 1989; Merkler Schramm, 1990, 1993), and other AMPDs (from rabbit skeletal muscle, goldfish, sea scorpion etc.) have been carried out earlier (Waarde and Kesbeke, 1981; Lushchak *et al*., 1998; Bazin *et al*., 2003; Mangani *et al*., 2003; Martini *et al*., 2007; Marotta *et al*., 2009), the only crystal structure available in the PDB database for this enzyme is from *Arabidopsis thaliana*, solved in 2006 by the group of Richard L Sabina (Han *et al*., 2006). Recently, Akizu *et al.,* identified mutations in AMPD2 in families where individuals were found to be suffering from a neurodegenerative brainstem disorder termed 'pontocerebellar hypoplasia' (Akizu *et al*., 2013). In addition to this, a new mechanism of action for the anti-diabetic drug metformin has been proposed by Ouyang *et al.,* where it was shown that AMPD inhibition in L6 rat skeletal muscle cells by metformin, led to an increase in AMP levels which in-turn activated AMP-activated protein kinase (AMPK) (Ouyang *et al*., 2011). Also, AMPD and AMPK have been reported to counter-regulate each other and are implicated in hepatic steatosis (Lanaspa *et al*., 2012).

AMPD can modulate AEC in a dual manner by being part of the purine nucleotide cycle as well as by independently regulating the equilibrium of the adenylate kinase reaction. Adenylate kinase catalyses a reversible reaction; where two ADP molecules are converted to one ATP and one AMP ($2ADP \leftrightarrows ATP + AMP$) (Atkinson, 1968; Chapman and Atkinson, 1973). This reaction maintains the three-way equilibrium between ATP, ADP and AMP levels in a cell. The ATP generated will be utilized by energy consuming processes, while AMP gets deaminated to IMP by AMPD (Scheme 1). In conditions where AMPD is not operating (either due to a mutation in case of the genetic disorder or a knock-out where the gene has been deleted) AMP accumulation takes place and this adversely affects the adenylate kinase reaction by shifting the reaction equilibrium towards ATP depletion. This leads to several consequences of which, most prominent in the literature is fatigue and muscle weakness reported in subjects suffering from myoadenylate deaminase deficiency, an autosomal recessive genetic disorder (Hellsten *et al*., 1999; Isackson *et al*., 2005). In the absence of AMPD activity, insufficient production of ATP and accumulation of AMP synergistically bring down the AEC of the cell. Further, in patients suffering from pontocerebellar hypoplasia, lack of AMPD activity results in accumulation of AMP which leads to inhibition of *de novo* purine biosynthesis pathway which eventually manifests in impaired protein production due to insufficient GTP pools. Also, AMPD2 and AMPD3 double knockout in mice has been found to be lethal at a post-natal stage, while mutation in AMPD gene (FAC1) was found to be embryonically lethal in *Arabidopsis*, making it a good herbicide target (Xu *et al*., 2005; Sabina *et al*., 2007; Akizu *et al*., 2013).

Studies have documented an increase in AMPD activity in the soil-living amoeba *Dictyostelium discoideum* in response to nutrient starvation or treatment with hadacidin (inhibitor of ADSS) (Jahngen and Rossomando, 1986). It was also found that loss of AMPD function resulted in increased AMP secretion, an impaired ratio of prestalk to prespore cells and reduced sporulation efficiency (Chae *et al*., 2002). In the context of malaria, a gain-of-function mutation in erythrocytic AMPD was found to increase erythrocyte turnover (increased reticulocyte formation and reduced erythrocyte half-life), conferring resistance in mice against *P. chabaudi* infection as they specifically infect mature erythrocytes. But *P. berghei* infection, which happens in reticulocytes was unaffected (Hortle *et al*., 2016). Also, an indirect evidence for the presence of AMPD activity in *Plasmodium* was provided by Cassera *et al.,* where it was shown that erythrocytic AMP can be taken up by the parasite and converted to IMP by the action of AMPD (Cassera *et al*., 2008). But, a detailed biochemical and physiological characterization of this enzyme from the parasite has remained hitherto unavailable. In the current report, we provide a comprehensive biochemical description of the *P. falciparum* enzyme. We have used a functional complementation assay to identify and validate essentiality of key conserved residues and our results throw light upon some of the key features of *P. falciparum* AMPD (PfAMPD) in comparison with human, *Arabidopsis* and yeast counterparts. Further, the *in vivo* genetic manipulation carried out in *P. berghei* (Pb), involving gene ablation and GFP tagging provides evidence for the dispensable nature of this cytosolic enzyme during all stages of parasite life cycle, while expression of wildtype GFP-tagged *P. berghei* AMPD (PbAMPD)



Scheme 1. Adenylate kinase and AMP deaminase reaction. Adenylate kinase catalyses the formation of ATP and AMP using two ADP molecules. ATP fuels energy utilizing cellular processes whereas AMP can be deaminated to IMP by AMP deaminase with concomitant release of ammonia.

protein through an episomal construct was found to be toxic in intra-erythrocytic stages.

Materials

Chemicals and reagents were procured from Sigma Aldrich, USA; Fischer Scientific; SRL, India. Media components were purchased from Himedia, Mumbai, India. Primers were custom synthesized from Sigma Aldrich, Bengaluru, India. Restriction enzymes, reverse transcriptase, Phusion DNA polymerase, Taq DNA polymerase and T4 DNA ligase were obtained from New England Biolabs, USA and used according to the instructions of the manufacturer. Trizol^{TM} was from Invitrogen, USA. Antibiotics ampicillin, tetracycline and chloramphenicol were bought from USB chemicals. G418 was bought from Sigma Aldrich, USA and Zeocin from Invitrogen, USA. Plasmid isolation, PCR clean-up and gel extraction kits were from Qiagen. *E. coli* strain XL-1 blue, and expression strain Rosetta (DE3) pLysS and plasmid pET-duet-1 were from Novagen. pJAZZ library clone (PbG02_B-44h05); plasmids, pSC101BAD, R6K Zeo/pheS and *E. coli* pir strains were procured from PlasmoGem, Sanger Institute, UK. *E. coli* TSA cells were obtained from Lucigen. Plasmid pBCEN5 was a gift from Dr. Shiroh Iwanaga, Japan. Wildtype *(BY4742; MATα; ura3Δ0; leu2Δ0; his3Δ1; lys2Δ0)*, *Δamd1 (BY4742; MATα; ura3Δ0; leu2Δ0; his3Δ1; lys2Δ0; YML035c::kanMX4)*, *Δade1 (BY4741; MATa; ura3Δ0; leu2Δ0; his3Δ1; met15Δ0; YAR015W::kanMX4)* and *Δade2 (BY4741; MATa; ura3Δ0; leu2Δ0; his3Δ1; met15Δ0; YOR128C::kanMX4) S. cerevisiae* strains were from EUROSCARF, Germany. Plasmid pYES2C/T was from Invitrogen, USA. Codon harmonised PfAMPD gene was synthesized and procured from Shinegene, China. *P. falciparum* 3D7 and *P. berghei* ANKA strain were procured from MR4. RPMI-1640 was from Sigma Aldrich, USA and Albumax-I, DMEM medium, antibiotic and antimycotic mix, and fetal bovine serum were from Gibco. Collagen was from Corning. Amaxa 4D nucleofector and P5 Nucleofection kit were from Lonza, Germany. Infusion assembly kit was from TaKaRa Bio, USA. Random primer kit was from BRIT, India. Gene sequencing by Sanger sequencing method was carried out in the in-house central instrumentation facility, JNCASR, Bangalore. Sequences of oligonucleotides used are provided in the section 'Supporting Information' (Table S1).

Experimental procedures

Details pertaining to bacterial and yeast transformation and recombinant protein expression, parasite genomic DNA isolation and genotyping of transgenic parasites and generation of parasite cell lysates for Western blotting is provided in 'Supporting Information'.

RNA isolation, cDNA synthesis and RT-PCR

Saponin released *P. falciparum* cell pellet from 40 ml of *in vitro* culture was treated with 1 ml Trizol^{TM} reagent at room temperature for 15 min and then centrifuged for 30 min at 18000 × g to remove the cell debris. The supernatant was transferred to a fresh tube and 200 µl of chloroform was added and kept at room temperature for 15 min. This was centrifuged at 18000 × g for 30 min at 4°C for phase separation. The top layer was aspirated to a fresh tube and 400 µl of isopropanol was added and kept at –20°C for 4 h. This was centrifuged at 18000 × g for 30 min at 4°C to obtain an RNA pellet. This pellet was washed once with 75% ethanol made in diethylpyrocarbonate (DEPC) treated water and allowed to air dry. The pellet was resuspended in 20 µl of DEPC treated water and stored at –80°C. For RNA isolation from *P. berghei*, blood was harvested from mice at 10–15% parasitemia and collected in heparin (200 units ml^{-1}). The cells were lysed by resuspending them in 10 volumes of erythrocyte lysis buffer (155 mM NH_4Cl, 12 mM $NaHCO_3$ and 0.1 mM EDTA) and kept at 4°C for 5

min. The cells were harvested by centrifugation at 500 × g for 10 min, the supernatant was discarded and the pellet was used for RNA isolation. The steps used for RNA isolation were identical to that described for *P. falciparum*. The cDNA was synthesized using gene-specific reverse primer (P1 for *P. falciparum* and P73 for *P. berghei*) and Moloney Murine Leukemia Virus (MMLV) reverse transcriptase according to manufacturer's protocol. This cDNA was used as a template for PCR amplification of AMPD gene.

Generation of plasmid constructs

All clones were generated in XL-1 blue strain of *E. coli* cells (Table S2 lists the plasmid constructs used in the study). Using cDNA as template PfAMPD gene was PCR amplified using primers P2 and P3. The PCR product was digested with EcoRI and HindIII and cloned into double digested pET-Duet-1 vector. Similarly, the truncated versions of PfAMPD gene were PCR amplified using the full-length clone as template and primer pairs P4, P5 for Δ59; P6, P7 for Δ94 and P8, P9 for Δ178. All PCR products were digested using EcoRI and HindIII enzymes and cloned into double digested pETDuet-1 vector. Using genomic DNA from yeast as a template, yeast AMPD gene was PCR amplified using primers P10 and P11. The PCR product was digested with SacI and XhoI enzymes and cloned into double digested pYES2/CT plasmid. Using full-length clone of PfAMPD (pETDuet-1_PfAMPD) as template and primers P12, P13 PfAMPD gene was PCR amplified, digested with KpnI and XbaI enzymes followed by cloning into double digested pYES2/CT plasmid. Harmonised PfAMPD gene segment was released from the pMD19_hPfAMPD vector using the enzymes KpnI and XhoI and subcloned into a pYES2/CT plasmid which was cut using the same restriction sites. eGFP was amplified using primers P14, P15 and pRS306 as template, double digested using enzymes BamHI and XhoI and ligated into the double digested pYES2/CT vector. Cloning of GFP tagged yeast and PfAMPD was done by ligating three DNA segments i.e., vector, gene fragment and GFP fragment. ScAMPD was amplified using primers P16, P17 followed by digestion with SacI and KasI enzymes. eGFP was amplified by using primers P18, P19 followed by digestion with KasI and XhoI enzymes. These two fragments were ligated with SacI, XhoI digested pYES2/CT plasmid. Similarly, PfAMPD was amplified using primers P20, P21 and pMD19_hAMPD as template, followed by digestion with KpnI and XbaI enzymes. eGFP was amplified by using primers P22, P23 followed by digestion with XbaI and XhoI enzymes. These two fragments were ligated with KpnI, XhoI digested pYES2/CT plasmid. PCR product for pYES2/CT_$(His)_6$_hPfAMPD_GFP construct was generated using primers P56, P55 and pYES2/CT_hPfAMPD_GFP (pYES2/CT clone containing harmonised PfAMPD gene with C-terminal GFP tag) as template. The PCR product was digested with enzymes KpnI and XhoI and cloned into a digested pYES2/CT plasmid. PCR product for pYES2/CT_hPfAMPD_GFP_$(His)_6$ construct was generated using primers P54, P57 and pYES2/CT_hPfAMPD_GFP as template. The PCR product was digested with enzymes KpnI and XhoI and cloned into a digested pYES2/CT plasmid.

Serial dilution and spotting of S. cerevisiae *cells*

Single colonies were inoculated into 5 ml SD-Ura medium containing glucose as carbon source and grown overnight at 30°C, 180 rpm. The cells were harvested by centrifugation at 5000 × g and washed once with sterile water. OD_{600} was determined and serial dilutions were made starting from 1 OD ml^{-1} to 10^{-3} OD ml^{-1}. 2 μl from each dilution was spotted on SD-Ura plate containing galactose as carbon source with or without 50 μg ml^{-1} S-adenosylmethionine (SAM). The plates were allowed to air dry and incubated at 30°C (37°C for temperature sensitivity studies) for 60–72 h. The plates were observed for cell growth and photographically documented.

Site-directed mutagenesis and PfAMPD truncations

Using pYES2/CT_hPfAMPD_GFP (pYES2/CT clone containing harmonised PfAMPD gene with C-terminal GFP tag) plasmid as template site-directed mutagenesis was performed by following overlap extension PCR and AQUA cloning protocol (Beyer et al., 2015). Partial amplicons for each mutant were obtained by PCR using Gal promoter-forward primer (P54)/ mutagenic-reverse primer and Cyc terminator-reverse primer (P55)/ mutagenic-forward primer pairs (Table S1). The fragments were gel purified and mixed with double digested (KpnI and XhoI) and gel purified pYES2/CT vector in a molar ratio 1:3:3:: vector:insert1:insert2. This mix was used to transform competent XL1-Blue *E. coli* cells and plated on LB plates containing 100 μg ml^{-1} ampicillin. The clones were confirmed by PCR, restriction digestion and sequencing. These constructs were used to perform functional complementation in Δ*amd1* yeast by serial dilution and spotting assay. PfAMPD lacking 60 and 180 residues from N-terminal end, hPfAMPD_Δ*N60* and hPfAMPD_Δ*N180* were PCR amplified using primer pairs P24, P55 and P25, P55 (Table S1); respectively. The PCR product was double digested (KpnI and XhoI) and cloned into a digested pYES2/CT plasmid.

Generation of P. berghei *transfection vectors*

The library clone for *P. berghei* AMPD (PbG02_B-44h05) was obtained from PlasmoGem. The procedures for knockout construct generation were described earlier (Godiska *et al.*, 2009; Pfander *et al.*, 2011). The intermediate vector and final knockout construct were confirmed by PCR and restriction digestion. The final knockout construct was subjected to NotI digestion, purified and used for transfection. For episomal expression of GFP-tagged PbAMPD, *P. berghei* AMPD gene was amplified by PCR using cDNA from *P. berghei* as template and primers P74, P75 (Table S1); followed by cloning into BamHI digested pBCEN5 plasmid using InFusion assembly kit from Takara. The clone was confirmed by PCR, restriction digestion and sequencing. H245A/H247A mutant of PbAMPD (pBCEN5_PbAMPD_H245A/H247A_GFP) was generated by AQUA cloning protocol as described earlier (Beyer *et al.*, 2015). Partial amplicons were generated using primer pairs P76, P79 and P77, P78 (Table S1) and pBCEN5_PbAMPD_GFP vector as template.

Culture of P. falciparum, P. berghei *and transfection in* P. berghei

Intra-erythrocytic stages of *3D7* strain of *P. falciparum* was cultured as described earlier (Trager and Jensen, 1976). Maintenance and transfection of *P. berghei* ANKA was according to published protocols (Janse *et al*., 2006).

Localization studies in Plasmodium

For *P. berghei*, parasites were harvested in heparin solution and centrifuged at 2100 × g for 5 min and the supernatant was discarded. The cells were resuspended in 1 × PBS containing Hoechst 33342 (10 μg ml^{-1}) and incubated at room temperature for 15 min. The cells were centrifuged at 2100 × g for 5 min and the supernatant was discarded. The cells were washed once with 1 × PBS and the pellet was resuspended in 70% glycerol. Cells were mounted on a glass slide using coverslips, then sealed and stored at 4°C. The cells were observed under oil immersion objective (100°C) of Zeiss LSM 510 Meta confocal microscope.

Determination of intra-erythrocytic growth rate of Δampd P. berghei

Glycerol stocks of wildtype and clone C1 of Δ*ampd P. berghei* were injected to two separate mice and parasitemia was monitored by Giemsa stained smears. Blood was harvested in heparin solution once parasitemia reached 0.5–1% and 10_5 parasites were injected into 5 fresh mice for both wildtype and Δ*ampd P. berghei*. Parasitemia was monitored by counting parasites in Giemsa stained smears regularly starting from day 1 post-injection and growth rate was determined by plotting percentage parasitemia on *y*-axis against time (number of days) on *x*-axis. The mortality rate among mice infected with either wildtype or Δ*ampd P. berghei* parasites was also determined by plotting percentage survival of mice on *y*-axis against time (number of days) on *x*-axis.

For enumeration of gametocytes 4×10^6 parasites were injected into 2 fresh mice for both wildtype and Δ*ampd P. berghei*. Parasitemia was monitored by counting parasites in Giemsa stained smears on day 2 post-injection. On day three all mice were fed with water containing sulfadiazine (30 mg in 100 ml) *ad libitum*. Giemsa stained smears were made on day 3 post sulfadiazine treatment and gametocytes were enumerated and female to male gametocyte ratio was also determined for wildtype and Δ*ampd P. berghei* parasites.

Maintenance of Anopheles stephansi *(*A. stephansi*) colony and phenotypic analysis of* Δampd P. berghei *in mosquito vector*

Adult *A. stephansi* mosquitoes were maintained at 28°C temperature, 80% humidity and fed on 10% sucrose solution. Female *A. stephensi* mosquitoes were used to study the developmental stages of Δ*ampd P. berghei* parasite line. The sexual cycle in the mosquitoes was initiated by allowing 5-day old mosquitoes to obtain a blood meal from Swiss Albino mice carrying gametocyte stages of either wildtype or Δ*ampd P. berghei* parasites. The infected mosquitoes were maintained at 20°C temperature and 80% humidity with 12/12 light and dark cycle. To analyze the zygote and ookinete stages of Δ*ampd P. berghei* parasites, mosquito midguts were dissected at 2–4 and 16–18 h post blood meal. The guts were disrupted by mechanical grinding using a plastic pestle. Approximately 0.2 to 0.5 μl of the sample was spotted on a glass slide. On day 14 and day 18–20 post blood meal, infected mosquitoes were dissected to observe the oocyst and salivary gland sporozoites. The samples were viewed at 100 × magnification through a DIC filter using a Nikon AR fluorescent microscope. For the morphological investigation of Δ*ampd P. berghei* midgut and salivary gland sporozoites, dissected midguts and salivary glands were pooled in a small volume of 20–25 μl of DMEM in a 1.5 ml Eppendorf tube. The tissues were disrupted using a plastic pestle to release sporozoites. The samples were centrifuged at 800 rpm for 3 min. Supernatants containing partially purified sporozoites were carefully separated and 0.2 to 0.5 μl sample was spotted on glass slides.

Immunofluorescence assay (IFA) for zygote, ookinete and sporozoites

The morphology of zygote, ookinetes and sporozoites was analysed by performing IFA. Briefly, the sample was fixed in 4% formalin solution for 30 min at 4 °C followed by nonspecific blocking in 3% bovine serum albumin (BSA) solution made in 1 × phosphate buffered saline (PBS), pH 7.2. The zygote and ookinete stages were stained with anti-p28 primary antibody (Winger *et al*., 1988) and sporozoites were stained with 3d11 monoclonal antibody specific to the repeat region of *P. berghei* CSP (Yoshida *et al*., 1980) for 1 h at 37 °C. The samples were washed three times sequentially in PBS, PBS-Tween (PBST) (0.05% Tween-20) and PBS. The immunoreactivity of p28 and CSP was revealed with Alexa fluor 594 anti-mouse secondary antibody. The parasite nuclei were stained with DAPI that was added in the secondary antibody solution. The samples were overlaid with mounting medium and covered with glass coverslip. The zygote, ookinete and sporozoites were visualized using a Nikon AR fluorescent microscope at 100× magnification.

Gliding motility assay

Day 19–20 post blood meal, the mosquito salivary glands harbouring WT and Δ*ampd P. berghei* sporozoites were dissected in medium containing DMEM and 10% FBS. The glands were disrupted using a plastic pestle. The released sporozoites were spotted on a clean glass slide and a coverslip was gently placed over it. The slides were observed at 100 × magnification using a Nikon AR fluorescent microscope and the video recording of the sporozoite gliding was performed under bright field using the NIS-Elements software Nikon© (movie S1 and S2).

In vitro *development of* Δampd P. berghei *exo-erythrocytic forms (EEFs)*

HepG2 (human liver carcinoma cell line) was used for studying the EEF development. The cells were maintained

in DMEM medium (Gibco) supplemented with 1 × antibiotic and antimycotic (Gibco) and 10% Fetal bovine serum (Gibco). Nearly 2×10^5 HepG2 cells were seeded on coverslips that were previously coated with 10 mg ml^{-1} concentration of collagen (Corning) for 4 h. After attaining 70–80% confluency, 5×10^3 wildtype or Δ*ampd P. berghei* sporozoites were added and centrifuged at 1500 rpm for 4 min. The cultures were maintained at 37°C in a CO_2 incubator to facilitate the growth of EEFs. At 12, 36 and 62 h time points, the coverslips were removed from 24 well plates and fixed in 4% formalin solution. Following non-specific blocking with 3% BSA in 1 × PBS, the cultures were immunostained for CSP (Yoshida *et al*., 1980) and UIS4 using 3d11 and anti-UIS4 antibodies (Mueller *et al*., 2005) that are markers respectively for the EEF membrane (Hopp *et al*., 2017) and parasitophorous vacuole (Mueller *et al*., 2005). DAPI was used for staining the host and parasite nuclei.

Infection of C57BL6 mice with Δampd P. berghei *sporozoites*

C57BL/6 mice were intravenously (i.v) injected with 3×10^3 and 1×10^4 sporozoites of wildtype or Δ*ampd P. berghei* parasite line in two independent experiments. The parasitemia was monitored daily from day 3 post-infection by examination of Giemsa-stained blood smears.

Results

Expression of AMPD in P. falciparum *and functional characterization by complementation*

PfAMPD gene (PlasmoDB gene ID: PF3D7_1329400) is 3173 bp in length encompassing 7 introns which upon splicing gives rise to a 2082 bp mRNA encoding a 693 amino acid protein. RT-PCR resulted in a 2.1 kb amplicon matching the description in the database (Fig. S1A).

Full-length recombinant PfAMPD with N-terminal $(His)_6$-tag, when expressed in *E. coli,* showed very high levels of degradation and both the full-length and degraded fragments were found to be present in the insoluble fraction of the lysate. Multiple clones of PfAMPD with $(His)_6$-tag at N- or C-terminal, GFP tag, truncated versions (ΔN59, ΔN94 and ΔN178) were made to produce intact soluble protein. None of these variants showed reduced degradation or increased solubility of the protein (Fig. S1B).

AMPD deficient yeast strain grows normally on either YPD medium or minimal medium but shows a distinct growth defect phenotype when grown in the presence of S-adenosyl methionine (SAM) (Fig. S2B). This is due to the accumulation of AMP in the cells which results in the inhibition of *de novo* purine biosynthetic pathway eventually resulting in depletion of GTP pools. This growth defect phenotype can be rescued by expression of a functional AMPD. This principle was utilized to determine the functionality of PfAMPD. The coding sequence of PfAMPD gene was cloned in yeast expression vector under GAL1 promoter and serial dilution and spotting assay was performed to check the functionality of PfAMPD. Rescue of the growth defect phenotype was not seen when compared to control strain expressing ScAMPD (Fig. 1A). Upon performing RT-PCR it was found that full-length transcript was not formed in yeast cells expressing PfAMPD. Instead, an aberrantly spliced product was observed (data not shown). Hence the experiment was performed using a codon harmonised (Angov *et al*., 2008) PfAMPD (hPfAMPD) gene. A clear rescue of growth phenotype was observed in this case showing that PfAMPD is a functional ortholog of ScAMPD (Fig. 1A).

Although codon harmonised PfAMPD with C-terminal $(His)_6$-tag showed functional complementation, the full-length protein was not detected by Western blot probed with anti-$(His)_6$ antibody. Hence, a C-terminal GFP tagged construct (pYES2/CT_hPfAMPD_GFP) was generated so that it would provide proof for the expression of the protein by microscopy and/or by Western blotting probed using anti-GFP antibody. The C-terminal GFP-tagged PfAMPD was also found to functionally complement yeast AMPD deficiency similar to the $(His)_6$-tagged protein and moreover, was also detected by Western blot when probed with anti-GFP antibody. Hence, to determine if the GFP tag was conferring stability to the protein, dual tagged PfAMPD constructs (i.e., pYES2/CT_$(His)_6$_hPfAMPD_GFP and pYES2/CT_hPfAMPD_GFP_$(His)_6$) were generated. Western blot was performed using cells expressing various constructs of AMPD i.e., pYES2/CT_hPfAMPD_$(His)_6$, pYES2/CT_$(His)_6$_hPfAMPD_GFP and pYES2/CT_hPfAMPD_GFP_$(His)_6$ which were probed with anti-$(His)_6$ antibody and pYES2/CT_hPfAMPD_GFP, pYES2/CT_$(His)_6$_hPfAMPD_GFP and pYES2/CT_hPfAMPD_GFP_$(His)_6$ which were probed with anti-GFP antibody. All GFP tagged hPfAMPD constructs were detected by anti-GFP antibody whereas among $(His)_6$-tagged constructs pYES2/CT_$(His)_6$_hPfAMPD_GFP alone was detected by anti-$(His)_6$ antibody whereas, the other two constructs (pYES2/CT_hPfAMPD_$(His)_6$ and pYES2/CT_hPfAMPD_GFP_$(His)_6$) were not detected going to show that the presence of GFP tag at C- terminal confers stability to the protein (Fig. S3A). It was also observed that both the constructs (i.e. pYES2/CT_$(His)_6$_hPfAMPD_GFP and pYES2/CT_hPfAMPD_GFP_$(His)_6$) were able to functionally complement yeast AMPD deficiency (Fig. S3B).

Characterization of PfAMPD mutants

Site-directed mutagenesis was performed on PfAMPD gene and mutants (Fig. S4) were characterized by serial dilution and spotting assay (Fig. 1A). It has to be noted that to date, no study using site-directed mutagenesis has been done to validate the role of different residues in PfAMPD. In AtAMPD, deletion of N-terminal 139 residues yielded active enzyme and crystals of diffraction

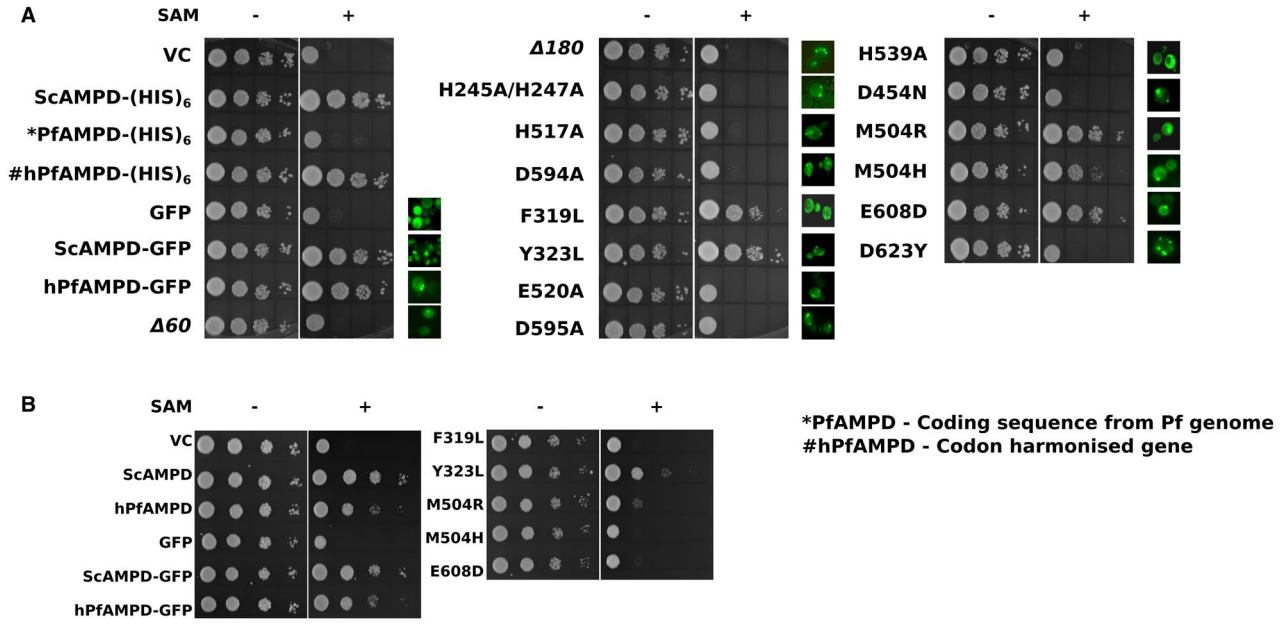


Fig. 1. Complementation of AMPD deficiency in *S. cerevisiae*.
A. Ability of truncated and mutant PfAMPDs to rescue the growth defect phenotype of Δ*amd1* yeast strain grown in the presence of SAM was used as a reporter to identify the role of specific residues in enzyme function. The phenotype of mutants was compared to that of vector control (VC, strain containing either pYES2/CT or GFP, pYES2/CT_GFP), ScAMPD, and wildtype PfAMPD expressing cells. The functional complementation assay was performed at 30°C. Panel A also shows microscopic images of GFP fluorescence as evidence for protein expression. B. Mutants that were able to rescue the growth defect phenotype at 30°C were further investigated for their ability to complement at 37°C and compared with that of wildtype ScAMPD and wildtype PfAMPD expressing cells. (Experiments have been performed in triplicates from two different batches of transformants and image from one experimental replicate is presented). [Colour figure can be viewed at wileyonlinelibrary.com]

quality (Han *et al*., 2006). Alignment of AMPD sequences shows that the catalytic core (180 to 680 residues, Pf numbering) is highly conserved (Fig. S5). Both ΔN60 PfAMPD that corresponds to the truncated version of AtAMPD with 139 residues at N-terminus deleted (found to be soluble and used for crystallization), and ΔN180 PfAMPD that corresponds to the catalytic core of the enzyme (Fig. S5) failed to functionally complement yeast AMPD deficiency going to show that in spite of the fact that AMPD sequences have a divergent N-terminus, the N-terminus of PfAMPD might be containing critical residues which are indispensable for activity or structural integrity of the protein. Residues H245, H247, H517 and D594 of PfAMPD that correspond to the residues H391, H393, H659 and D736 of AtAMPD, that coordinate with the divalent metal ion at the active site (Fig. S6); upon mutation to alanine rendered the protein inactive as cells expressing the mutant proteins failed to grow in the presence of SAM. In AtAMPD structure 2A3L, it was proposed that the residues F463 and Y467 might be involved in displacing the ribose sugar of the ligand coformycin monophosphate (Fig. S6) (Han *et al*., 2006). In our study, we have found that mutating the corresponding residues in PfAMPD, F319 and Y323 to leucine did not result in complete loss of enzyme activity. However, the F319L mutant did show slightly reduced growth when compared with Y323L or the wildtype. In the report by Han *et al*., 2006 it was proposed that H681 might be the catalytic base and in its absence, E662 might perform the same function although both these residues are conserved and are known to be required for catalysis by amino-hydrolases in general (Fig. S6). Hence, corresponding residues in PfAMPD i.e. H539 and E520 were mutated to alanine and it was found that the cells expressing these mutants failed to grow on SAM indicating that both these residues are indispensable for the activity of the protein and both might be involved in the catalysis. The residue D595 (highlighted in bold and italicized) is present in the conserved motif 'STD***D***P' which is seen in all AMP/adenosine deaminases (Han *et al*., 2006). Mutating this residue to alanine also resulted in the loss of activity. A chemical mutagen screen and sequencing study conducted by Xu *et al*., 2005 had identified a mutation (D598N) in AtAMPD that resulted in embryonic lethality (Han *et al*., 2006). Mutation of the corresponding residue in PfAMPD D454 to asparagine resulted in the loss of activity of the enzyme as observed by lack of rescue of yeast growth defect phenotype. Akizu *et al.,* had identified mutations in human AMPD2 (R674H, E778D and D793Y) which correlated with a neurological disorder called pontocerebellar hypoplasia (Akizu *et al*., 2013). R674 is conserved in human AMPD2, yeast and *Arabidopsis* AMPD

but is a methionine in PfAMPD (Fig. S5). This residue was mutated to arginine as well as histidine. Both M504R and M504H mutants were found to be active, but a slight growth defect was observed in M504H mutant compared to M504R and wildtype. E608D mutation in PfAMPD corresponding to E778 of human AMPD2 did not have any impact on the protein activity, whereas the D623Y mutant corresponding to D793 of human AMPD2 was inactive.

Expression of GFP-tagged PfAMPD and its mutants at the protein level was determined by Western blotting and also microscopy. Both full-length band corresponding to GFP fusion protein along with a band corresponding to free/degraded GFP was also observed (Fig. S7A and B). Interestingly, GFP tagged PfAMPD showed multiple localization patterns that included diffused cytosolic, cytoplasmic foci/punctate as well as a filamentous pattern (Fig. S7C-E). The mutants also showed foci/punctate like localization along with the diffused localization pattern (Fig. 1A).

Complementation assay was also performed at 37°C using wildtype ($(His)_6$-tag and GFP-tag) yeast AMPD and PfAMPD and mutants of PfAMPD which had shown rescue of growth defect phenotype at 30°C (Fig. 1B). Surprisingly, wildtype PfAMPD showed a minor yet observable reduction in the rescue of growth defect phenotype as compared to the yeast counterpart indicating sensitivity towards increased temperature. Among the mutants, only Y323L mutant of PfAMPD showed rescue of the growth defect phenotype similar to the wildtype, whereas the others completely failed to do so indicating that, they might also be playing a role in stabilizing the structure of the protein that is affected at higher temperatures.

PbAMPD is cytosolic in nature and over-expression causes toxicity

An episomal construct (pBCEN5_PbAMPD_GFP) where PbAMPD coding sequence was tagged with C-terminal GFP under PbEF1α promoter was used for localization of PbAMPD. When transfected with pBCEN5_PbAMPD_GFP, drug-resistant parasites were not obtained. As this result was reproducible with multiple transfection attempts a catalytically inactive mutant (H245A/H247A) of PbAMPD was cloned in pBCEN5 with C-terminal GFP tag and transfected into *P. berghei*. Drug-resistant parasites were obtained, genotyped (Fig. 2A) and a diffused cytosolic localization was observed (Fig. 2C). The GFP fusion protein was also detected by Western blotting (Fig. 2B).

pBCEN5_GFP (vector control), pBCEN5_PbAMPD_GFP and pBCEN5_PbAMPD_H245A/H247A_GFP were mixed in equal amounts (2.5 μg each) and co-transfected into wildtype *P. berghei* which resulted in a mixed population of drug-resistant parasites that were PCR positive for both vector control plasmid and plasmid containing either or both PbAMPD wildtype and mutant genes. Sequencing of the AMPD specific PCR product showed the presence of only the plasmid carrying the mutant gene and that the plasmid carrying the wildtype gene was not retained in the drug-resistant parasite population (Fig. 2D-H). These studies confirm that the expression of functional PbAMPD above the endogenous levels is toxic to the parasites.

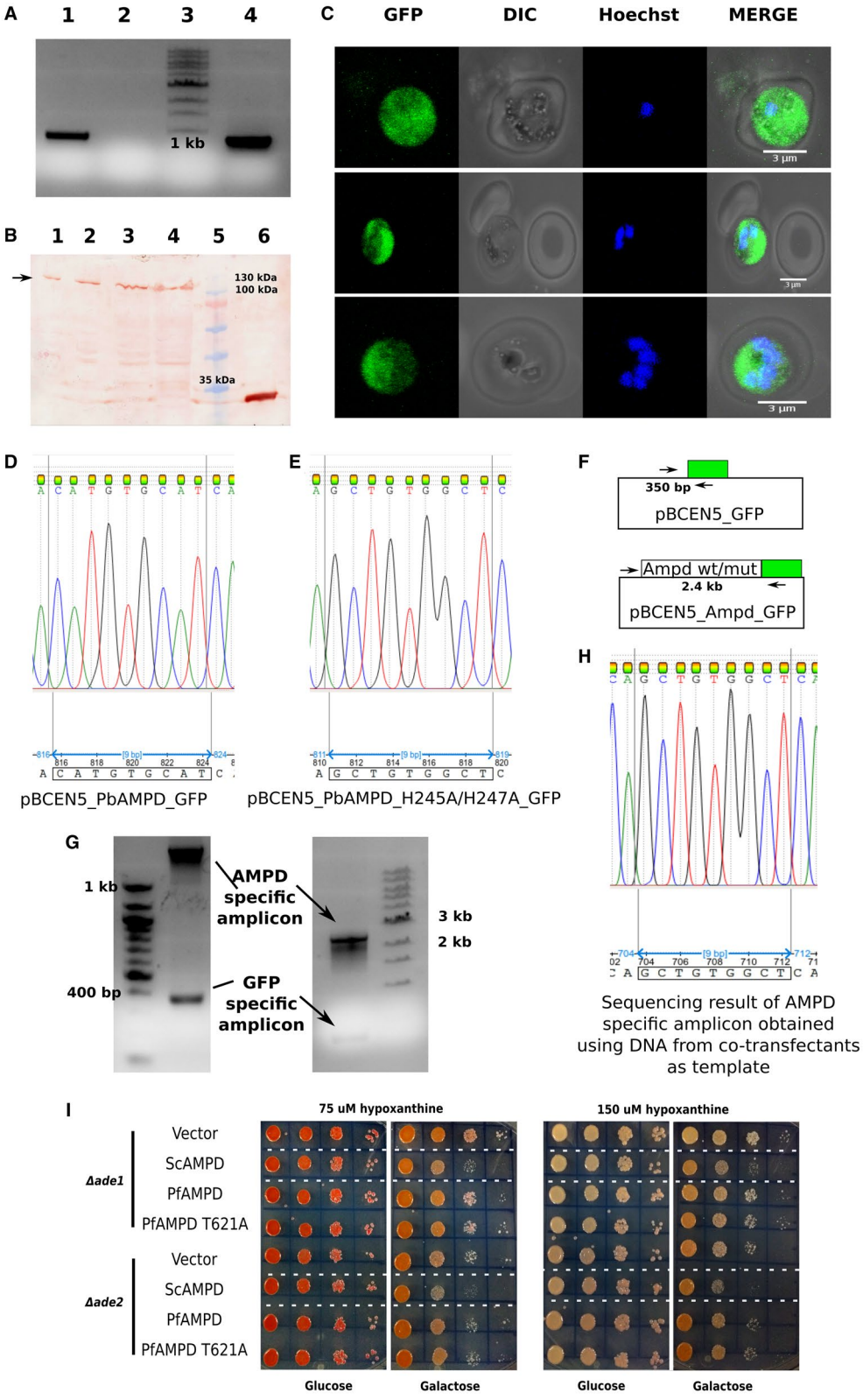
Supporting evidence for the above inference was also observed in yeast strains lacking a functional *de novo* purine biosynthetic pathway. Δ*ade1* and *Δade2 yeast* strains are deficient in enzymes of *de novo* purine biosynthetic pathway (N-succinyl-5-aminoimidazole-4-carboxamide ribotide synthetase and phosphoribosylaminoimidazole carboxylase) and hence have been used as mimics of the *Plasmodium* parasite in the context of nucleotide metabolism. Both Δ*ade1* and Δ*ade2* strains grown under conditions with a limited quantity of purine showed growth defect phenotype upon episomal expression of ScAMPD over and above the endogenous levels. Interestingly, episomal expression of PfAMPD in Δ*ade1* and Δ*ade2* strains grown under similar conditions did not result in growth defect phenotype (Fig. 2I). In addition to the expression of wildtype PfAMPD protein, T621A mutant (corresponds to a hyperactive mutation observed in human AMPD3 Hortle *et al*., 2016) was also expressed in Δ*ade1* and Δ*ade2*strains but a growth defect phenotype was not observed in this case also.

AMPD is non-essential during intra-erythrocytic stages in P. berghei

Δ*ampd P. berghei* parasites were generated using linear pJAZZok vector with homology arms flanking the marker gene, generated by recombineering strategy (Godiska *et al*., 2009; Pfander *et al*., 2011). The knockout parasites were genotyped by PCR and Southern blotting (Fig. S9), and by limiting dilution three clonal populations (C1, C2 and C3) were obtained that were genotyped by PCR (Fig. S10). One of the clonal populations (C1) was used for assessing the growth phenotype. Comparison of blood-stage growth rate measurements between wildtype and Δ*ampd P. berghei* parasites in mouse showed no significant difference (Fig. 3A and B), thus establishing that the gene is not essential for the parasite during the intra-erythrocytic stages. Also, enumeration of gametocytes did not show any significant difference in the number of gametocytes as well as the ratio of female to male gametocytes between wildtype and Δ*ampd* parasites (Fig. 3C and D).

Δampd P. berghei *parasites undergo normal development in* A. stephansi *and produce infectious sporozoites*

To assess if the Δ*ampd P. berghei* gametocytes are able to complete sexual reproduction in mosquito midguts, 2–4



Sequencing result of AMPD specific amplicon obtained using DNA from co-transfectants as template

Fig. 2. Episomal expression of PbAMPD in *P. berghei*. A. PCR confirmation of pBCEN5_PbAMPD_H245A/H247A_GFP transfectants. Lane 1, DNA isolated from transfectants as template; lane 2; no template control; lane 3, molecular weight marker; lane 4, +ve control (pBCEN5_PbAMPD_H245A/H247A_GFP). B. Western blot showing the presence of full-length GFP fused PbAMPD_H245A/H247A protein (arrowhead) expressed through pBCEN5 in *P. berghei*. Lane 1 to 4, different volumes (5, 10, 20, 40 μl) of lysate from transfectants expressing PbAMPD_H245A/H247A_GFP fusion protein and lane 6, lysate from *P. berghei* strain expressing GFP alone. C. Localization of episomally expressed PbAMPD_H245A/H247A_GFP in *P. berghei*. Images were acquired using Zeiss LSM 510 META confocal microscope under 100 × oil immersion objective and maximum intensity projections obtained using ImageJ are represented. D-H. Results pertaining to co-transfection experiments. *P. berghei* was co-transfected with pBCEN5_GFP (vector control), pBCEN5_PbAMPD_GFP, pBCEN5_PbAMPD_H245A/H247A_GFP. Chromatogram D and E show the difference in DNA sequence between the wildtype (**CAT** GTG **CAT**) and catalytically inactive mutant (**GCT** GTG **GCT**). F. Schematic of the primers selected for genotyping the parasites by PCR. A primer that binds to vector backbone and a GFP internal reverse primer were used that would amplify the DNA segment present in both vector control and PbAMPD (both wildtype and mutant). G. PCR was performed on DNA isolated from drug-resistant parasites which turned out to be positive for both vector control and the gene of interest i.e., PbAMPD (either wildtype or mutant or both). Bands corresponding to GFP alone and PbAMPD (wildtype or mutant or both) are indicated by arrow marks. The left image is of a 1% agarose gel that was used to visualize the presence lower molecular weight (vector control) PCR product and the right image is that of a 0.8% agarose gel that was used to visualize the presence of higher molecular weight (PbAMPD gene-specific) PCR product. The gene-specific PCR product was purified and sequenced to determine whether the sequence corresponds to wildtype PbAMPD or the mutant or a mixed population. As shown in chromatogram H the DNA sequence of transfectants bearing pBCEN5 plasmid containing PbAMPD gene turned out to be the mutant (**GCT** GTG **GCT**) and not the wildtype. I. Δ*ade1* and Δ*ade2* strains were transformed with vectors expressing ScAMPD or PfAMPD or PfAMPD-T621A mutant and grown on minimal medium containing 75 or 150 μM hypoxanthine as purine source. Glucose was used to repress protein expression and galactose for induction. Cells episomally expressing ScAMPD displayed a growth defect phenotype when compared to vector control or PfAMPD (wildtype or mutant) in both strains and at both concentrations of hypoxanthine (highlighted between white dashed lines). The appearance of a pink color in the colonies is due to the accumulation of P-ribosyl aminoimidazole under purine limiting conditions. [Colour figure can be viewed at wileyonlinelibrary.com]

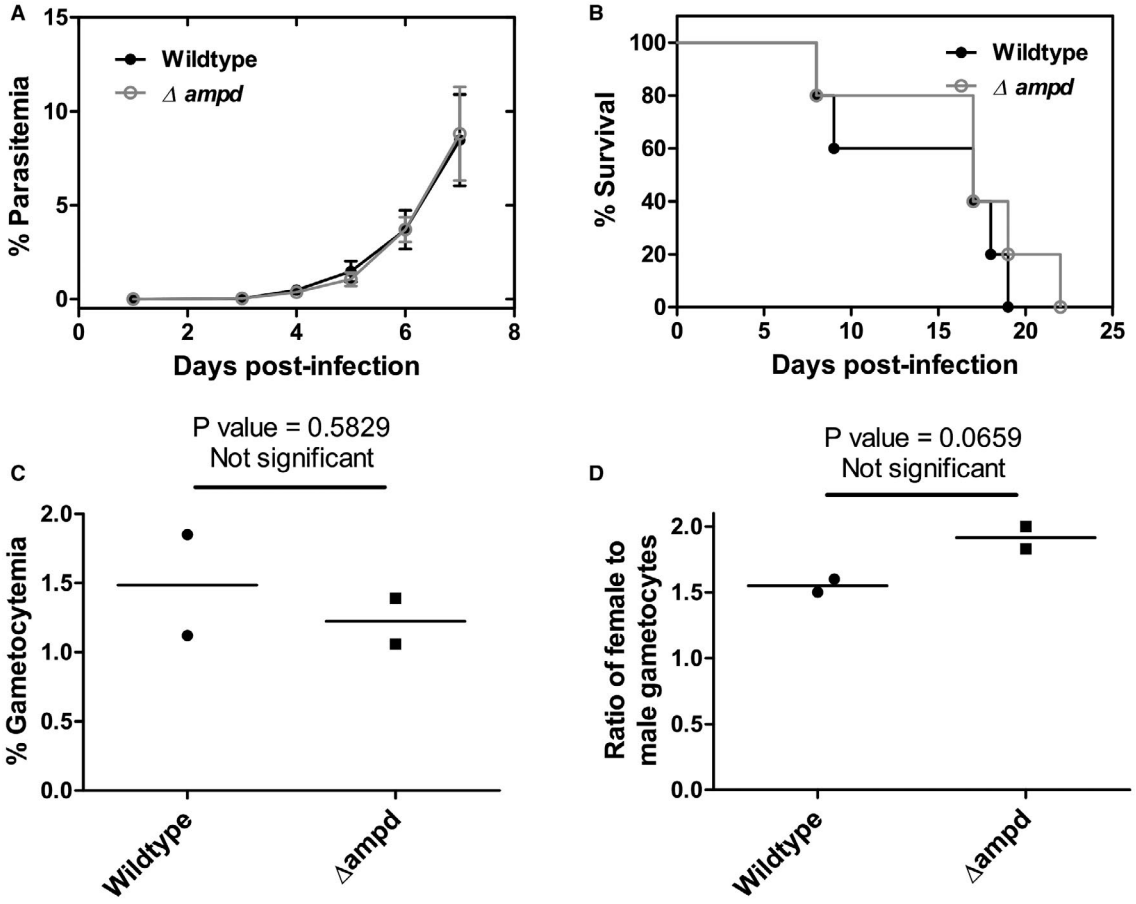


Fig. 3. Growth phenotype of wildtype and Δ*ampd P. berghei* parasites in intra-erythocytic stages. A. Comparison of growth rates of intra-erythrocytic wildtype and Δ*ampd P. berghei* parasites in mice. The data represents mean ± s.d. values obtained from five mice each infected with 10^5 wildtype or Δ*ampd P. berghei* parasites. Statistical analysis was done using Student's unpaired t-test using Graph Pad Prism V5. B. Percentage survival of mice ($n = 5$) infected with either wildtype or Δ*ampd P. berghei* parasites. The survival curves were found to be not significantly different according to the Log-rank (Mantel-cox) test (P value = 0.4157) and Gehen–Breslow–Wilcoxon test (P value = 0.5991).

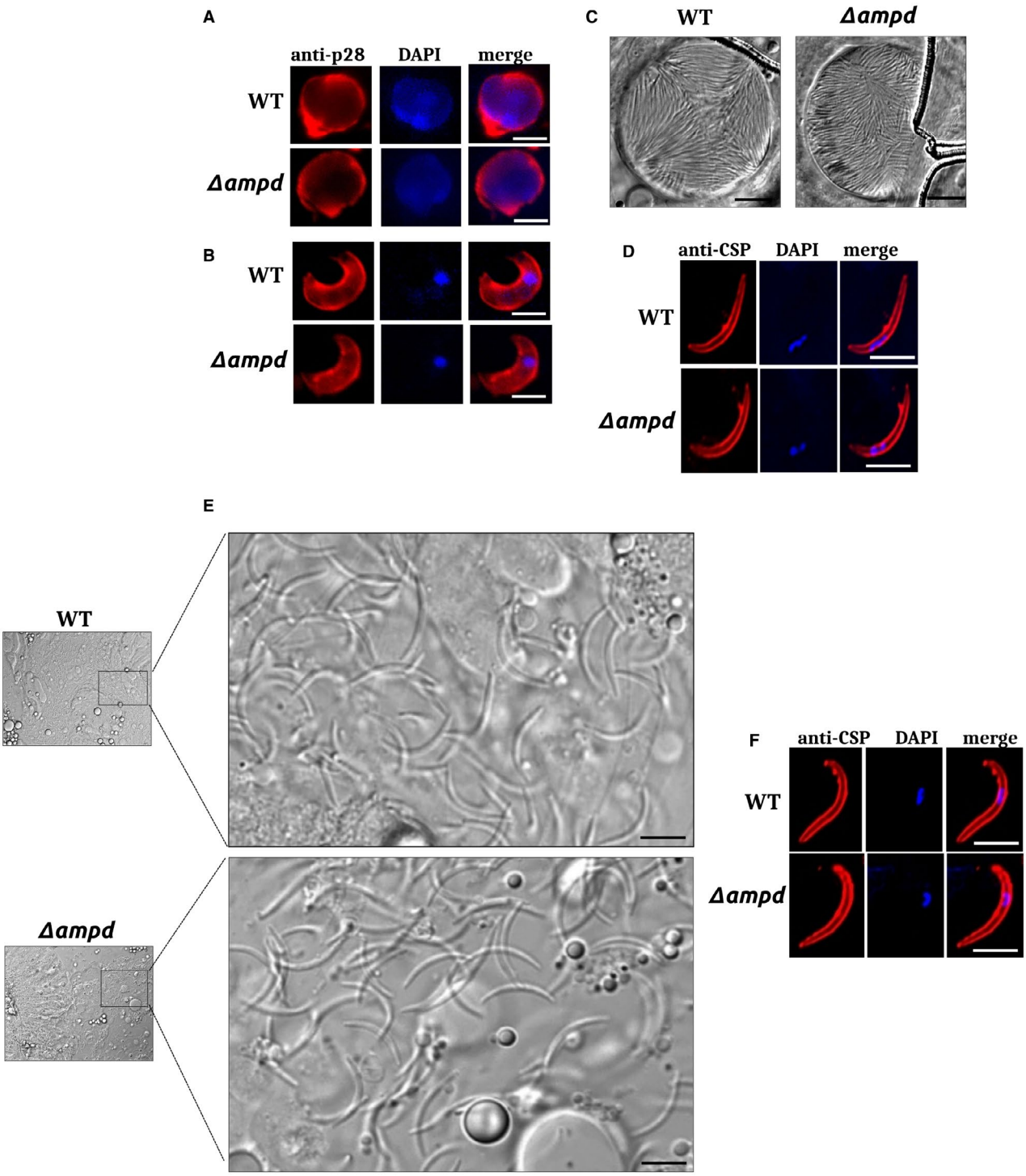


Fig. 4. Examination of wildtype and Δ*ampd P. berghei* parasites in mosquito stages. Sexual stages were stained with anti-p28 antibody. A. Zygote B. Ookinete. Scale 5 μm C. D14 Oocyst showing sporulation. Scale 20 μm. D. D14 midgut sporozoite stained with anti-CSP antibody and nuclei with DAPI. Scale 5 μm. E. Whole mount of D19–20 infected salivary glands. A small area is magnified to show sporozoites. F. Day 19–20 salivary gland sporozoites stained with anti-CSP antibody and nuclei with DAPI. Scale 5 μm. [Colour figure can be viewed at wileyonlinelibrary.com]

and 16–20 h post-blood-meal, samples were analyzed for the occurrence of zygotes and ookinete, respectively. Immunostaining of p28 revealed that Δ*ampd P. berghei* parasites produced zygotes and ookinetes whose morphology appeared indistinguishable from that of wildtype (Fig. 4A and B). These observations confirmed the ability of

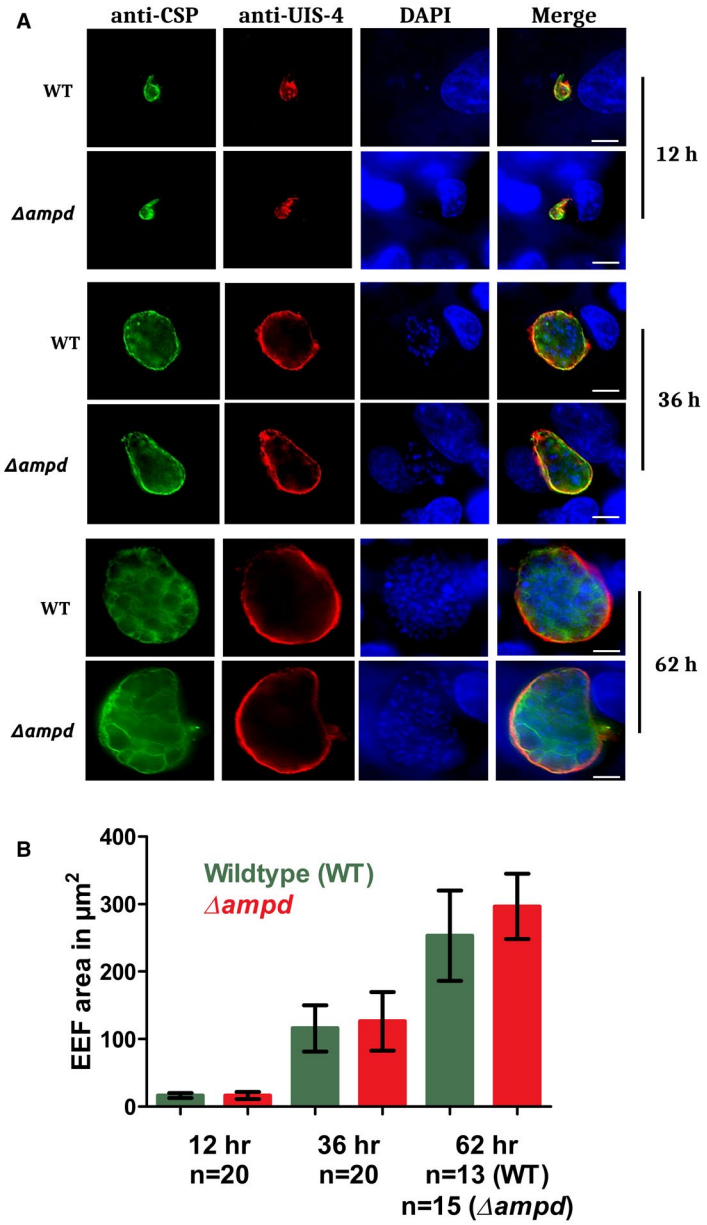


Fig. 5. *In vitro* liver stage development of wildtype and Δ*ampd P. berghei* parasites. A. *In vitro* liver stage development of wildtype and Δ*ampd P. berghei* parasites at 12, 36 and 62 h time points. The developing EEFs were stained with anti-CSP and anti-UIS-4 antibodies that are markers for parasite membrane and parasitophorous vacuole, respectively. The parasite and host nuclei were stained with DAPI. Scale 10 μm. B. Quantification of EEF size in wildtype and Δ*ampd P. berghei* parasites at 12, 36 and 62 h time points. [Colour figure can be viewed at wileyonlinelibrary.com]

Δ*ampd P. berghei* parasites to successfully complete sexual reproduction. Further, it was noted that Δ*ampd P. berghei* ookinetes were able to form oocyst also. Observation of several independent oocysts from multiple dissected midguts revealed sporulation pattern similar to wildtype (Fig. 4C). To analyse the qualitative aspects such as CSP distribution in D14 oocyst sporozoites, its levels were monitored by IFA. The pattern of CSP staining of Δ*ampd P. berghei* oocyst sporozoites was similar to that of the wildtype (Fig. 4D). The ability of oocyst sporozoites to navigate to salivary glands was also examined. Whole mount of dissected salivary glands on D19-20 post-infection showed successful colonization of Δ*ampd P. berghei* sporozoites in salivary glands (Fig. 4E). Further, the CSP staining pattern and size of Δ*ampd P. berghei* sporozoite were comparable to that of wildtype (Fig. 4F). Taken together we conclude that Δ*ampd P. berghei* parasites do not manifest any developmental defect within their vector host.

Δampd P. berghei *sporozoites exhibit normal gliding motility and transform into EEFs in HepG2 cells*

The salivary gland sporozoites manifest a characteristic substrate dependent locomotion referred to as gliding motility that involves an acto-myosin molecular motor (Kappe *et al*., 2004). In order to investigate whether depletion of AMPD affected gliding motility, freshly isolated sporozoites were observed for their ability to glide on glass slides. In multiple random fields observed under 100 × magnification, majority of Δ*ampd P. berghei* sporozoites exhibited gliding pattern that was similar to wildtype sporozoites. A representative video of sporozoite gliding motility was recorded for wildtype and Δ*ampd P. berghei* by using Ni-S elements software (movie S1 and S2).

We next analysed the ability of Δ*ampd P. berghei* sporozoites to transform into EEFs under *in vitro* condition. HepG2 supports complete development of *P. berghei* EEFs thus offering a convenient *in vitro* model system. Following the addition of Δ*ampd P. berghei* sporozoites, the HepG2 cultures were analysed at 12, 36 and 62 h time points (Fig. 5A). EEFs at indicated time points were stained with 3d11, a marker for EEF plasma membrane (Hopp *et al*., 2017) and anti-UIS-4, a marker for parasitophorous vacuolar membrane (Mueller *et al*., 2005). The pattern of staining for both markers was similar to wildtype suggesting that AMPD depletion did not abrogate EEF development. Also, at late liver stages, Δ*ampd P. berghei* parasites produced daughter hepatic merozoites as evident by DAPI staining (Fig. 5A 62 h). The measurement of EEF area was also performed at the aforementioned time points. At all 3 indicated time points, Δ*ampd P. berghei* did not differ with regard to wildtype in their growth characteristics (Fig. 5B)

Δampd P. berghei *sporozoites initiate a timely blood stage infection in C57BL6 mice*

In order to test if Δ*ampd P. berghei* liver stages were able to initiate a timely blood stage infection, Δ*ampd P. berghei* sporozoites were introduced intravenously into C57BL6 mice. In two independent experiments, (n = 3 mice per group and n = 2 mice per group), the mice received either 3×10^3 or 1×10^4 sporozoites of Δ*ampd* or wildtype *P. berghei*. Investigation of the pre-patent period revealed that Δ*ampd P. berghei* sporozoites gave rise to a breakthrough infection on D3.5 and D3 for 3×10^3 and 1×10^4 dose of sporozoites, respectively similar to wildtype (Table 1). The timely initiation of blood stage infection coincided with the ability of Δ*ampd P. berghei* liver stage to form hepatic merozoites (as seen *in vitro*, Fig. 5A, 62 h time point). These observations confirmed that egress of hepatic merozoites was not dependent on AMPD.

Discussion

AMPD belongs to amidohydrolase superfamily of enzymes and is a part of the purine nucleotide cycle involved in the cyclic interconversion of AMP and IMP. Studies on *Arabidopsis* and human AMPD have lead to the elucidation of the critical role of this enzyme in development, as impairment of its function affects AEC, as well as protein synthesis. To our knowledge, till date, there were no reports of comprehensive characterization of any parasitic protozoan AMP deaminase. Characterization of adenylosuccinate synthetase (ADSS) and adenylosuccinate lyase (ASL) from the malarial parasite *Plasmodium falciparum* has been reported earlier (Jayalakshmi *et al*., 2002; Eaazhisai *et al*., 2004; Bulusu *et al*., 2009; Mehrotra *et al*., 2010). These two enzymes that constitute one arm of PNC and involved in AMP generation have been found to be essential for the parasite's survival (Sanderson and Rayner, 2017). AMPD constitutes the second arm of PNC, regenerating IMP from AMP and had remained unexplored. This prompted us to conduct investigations towards elucidating the physiological role of AMPD in *Plasmodium*.

Our prime objective of performing biochemical characterization of recombinant PfAMPD was met with numerous hurdles owing to its insoluble and unstable nature. When expressed in *E. coli,* full length, as well as truncated versions of PfAMPD, showed a characteristic degradation pattern and all the fragments were present as inclusion bodies. Attempts to obtain soluble/stable protein by co-expressing with chaperones as well as refolding

Table 1. Analysis of pre-patency in Δ*ampd P. berghei* sporozoites

Experiment number	Parasite strain	Number of animals used for intravenous injection	Number of sporozoites injected per animal	Number of animals positive for blood stage infection	Pre-patent period (days)
Experiment 1	Wildtype	3	3×10^3	3/3	3.5
	Δ*ampd*	3	3×10^3	3/3	3.5
Experiment 2	Wildtype	2	1×10^4	2/2	3
	Δ*ampd*	2	1×10^4	2/2	3

Table 2. Residues selected for site-directed mutagenesis and their function in enzyme activity

Sl. No.	Residue	Protein	Corresponding residue in PfAMPD	Mutation	Description of the residue/mutation	Reference	Property of mutant PfAMPD*
1	H391	A *thaliana*	H245	H245A/H247 A	Zn^{2+} coordination	Han *et al.* (2006), Xu *et al.* (2005)	Inactive
2	H393	AMPD	H247				
3	H659		H517	H517A			Inactive
4	D736		D594	D594A			Inactive
5	F463		F319	F319L	Displacement of ribose ring		Active
6	Y467		Y323	Y323L			Active
7	E662		E520	E520A	Putative catalytic base		Inactive
8	H681		H539	H539A			Inactive
9	D737		D595	D595A	Present in STD'D'P motif		Inactive
10	D598		D454	D454N	Found in embryonic lethal mutant		Inactive
11	R674	*H. sapiens*	M504	M504R & M504H	Identified in pontocerebellar hypoplasia	Akizu *et al.* (2013)	Active
12	E778	AMPD2	E608	E608D			Active
13	D793		D623	D623Y			Inactive
14	T689	*H. sapiens* AMPD3	T621	T621A	Hyperactivity	Hortle *et al.* (2016)	Active

*Results from this study.

strategies were futile. Multiple expression systems and strategies were employed which included yeast (*S. cerevisiae* and *Pichia pastoris* using pYES2/CT and pGAPZ vectors, respectively), and *in vitro* cell-free protein synthesis system. None of these strategies was helpful in obtaining soluble and stable PfAMPD (data not shown). When expression was attempted in *S. cerevisiae* using a codon harmonised gene, the presence of a soluble and functional protein was established based on a growth phenotype readout in a functional complementation assay carried out using *Δamd1* yeast strain. Although we were able to express a functional PfAMPD in a heterologous system, the protein was not detected by Western blotting when yeast cell lysates were probed with anti-$(His)_6$ antibodies. Hence, we generated a PfAMPD-GFP fusion construct. Using this construct, expression of the protein was demonstrated both by microscopy and Western blotting. The observation that only the GFP-tagged protein can be detected by Western blotting and not the $(His)_6$-tagged counterpart indicated that the addition of GFP-tag had conferred stability to PfAMPD. In spite of successfully detecting full-length protein on Western blot, we were unable to purify the protein in sufficient quantities for *in vitro* assays.

The crystal structure of AtAMPD (PDB ID 2A3L) was used for addressing structure-function relationships in the *Plasmodium* enzyme (Fig. S6). Our study provides a comparative analysis of similarities and differences between yeast, *Arabidopsis*, human and *P. falciparum* AMPD. Establishing the essentiality of the divergent N-terminus and identification of structurally and catalytically important residues was performed using functional complementation assay on truncated protein and site-directed mutants. PfAMPD is different from any other AMPD as the N-terminal truncated version was found to be inactive, whereas N-terminal truncated versions of other AMPDs (yeast, *Arabidopsis*, human) have been reported to be active (Han *et al.*, 2006; Saint-Marc *et al.*, 2009). In comparison with the yeast enzyme, PfAMPD shows a mild temperature-sensitive phenotype (when grown in the presence of SAM at 37°C) which becomes distinct in the mutants F319L, M504R, M504H and E608D indicating the role of these residues in providing structural stability. Certain residues identified as vital for the functioning of human AMPD2 were found to be important for the *P. falciparum* counterpart as well (Table 2).

Attempts to express GFP-tagged PbAMPD from an episomal vector met with failure as multiple transfection attempts did not yield drug-resistant parasites. *Plasmodium* is completely dependent on the host for its purine source and operates predominantly via the HGPRT route for making IMP, which is then converted to AMP via the ADSS and ASL pathway and GMP via the IMPDH and GMPS reactions. AMP thus generated is utilized for various cellular processes including DNA

synthesis during cell division. In such a metabolic context, increased expression of an enzyme that catabolizes AMP might result in futile cycling of AMP/IMP interconversion probably leading to a deficit of AMP that would have a deleterious effect on actively dividing cells. This explains our inability to get drug-resistant parasites when transfected with a vector expressing active AMPD that would lead to higher levels of the enzyme in the cell. Whereas, drug-resistant parasites were obtained when transfection was done with pBCEN5 expressing a catalytically inactive mutant of PbAMPD. In addition to this, when *P. berghei* were co-transfected with three pBCEN5 plasmids expressing either GFP alone or GFP-tagged wildtype PbAMPD or GFP-tagged mutant PbAMPD, a mixed population of transfectants that were positive for only pBCEN5_GFP and pBCEN5_PbAMPD_H245A/H247A_GFP (inactive mutant) were obtained. This confirms our inference of cytotoxicity upon AMPD overexpression. Due to non-availability of inducible episomal expression systems in *Plasmodium,* we resorted to the yeast model to provide additional evidence for the detrimental nature of increased AMPD expression. We employed Δ*ade1* and Δ*ade2* strains which are very well characterized purine auxotrophs lacking functional *de novo* pathway (Ugolini and Bruschi, 1996) and solely depend on purine salvage by APRT or adenosine kinase or HGPRT (Fig. S8). These cells were grown on minimal medium containing only hypoxanthine as purine source, thereby, mimicking the *Plasmodium* parasite in the context of purine nucleotide salvage. Under these growth conditions when AMPD was episomally expressed, we observed growth defect when compared to the vector control or cells grown under repressive conditions (Fig. 2I). Although growth defect was seen only in cells episomally expressing ScAMPD, the lack of this phenotype in cells expressing PfAMPD might reflect on the catalytic efficiencies of the two enzymes and heterologous context of the host expression system. These observations in yeast and in *P. berghei*, in conjunction with a study on a hyperactive mutation in the erythrocyte isoform of AMPD resulting in decreased erythrocyte half-life (Hortle *et al.*, 2016), demonstrate that regulation of this enzyme activity is critical for survival in cells incapable of *de novo* purine biosynthesis. It should be noted that the T621A mutation in PfAMPD which corresponds to the hyperactive mutation reported in the erythrocytic isoform of AMPD, also failed to show growth defect phenotype when episomally expressed in Δ*ade1* and Δ*ade2* strains, although it was found to be active based on the complementation assay in AMPD knockout strain (Fig. S8D and 2I). The critical aspect that determines the cell viability in this scenario would be the relative fluxes between AMP generating arm including HGPRT, ADSS and ASL and the AMP depleting arm of AMP deaminase. From our observation in the yeast model, it is evident that the AMPD arm dominates the other arm (HGPRT, ADSS and ASL) upon increased expression of AMPD. Therefore, we conclude that increased expression of AMPD in an organism solely dependent on hypoxanthine salvage like *Plasmodium* might be toxic as it perturbs the AMP homeostasis by depleting AMP levels. Interestingly, episomal expression of ASL in *P. falciparum* and yeast adenosine kinase in *P. berghei*, both of which would increase the flux of AMP production was found to be non-lethal (unpublished data from our laboratory). As AMPD is known to be allosterically modulated by ATP, GTP and phosphate (Merkler *et al.*, 1989; Han *et al.*, 2006), allosteric activators of *Plasmodium* AMPD could exhibit anti-parasitic activity and development of an assay methodology for the identification of such molecules would be useful.

Plasmodium has two isoforms of adenylate kinase (AK1 and AK2) and two isoforms of adenylate kinase-like protein (ALP1 and ALP2). The loci of both AK and ALP were found to be refractory to knockout in *P. falciparum*, whereas in *P. berghei,* while AK1 was found to be essential, AK2 was dispensable during asexual stages (Sanderson and Rayner, 2017). Since AMPD activity can in-turn modulate AK activity, the essentiality of this gene was investigated in *P. berghei*. AMPD gene was successfully deleted in *P. berghei,* and the transgenic parasites did not show any difference in phenotype in comparison with wildtype counterpart during intra-erythrocytic stages, mosquito stages and liver stages as well. Hence, AMPD is not essential for the parasite's survival. It has to be noted that in a recent study by Zhang *et al.,* the gene loci was found to amenable for disruption in the intra-erythrocytic stages of *P. falciparum* using PiggyBac transposon-mediated saturation mutagenesis (Zhang *et al.*, 2018). The growth defect seen in *Δamd1* yeast strain manifests only in the presence of adenine or adenosine source (SAM) in the external medium, which results in the build-up of intracellular AMP levels by the action of APRT or adenosine kinase. This can be relieved only by expressing a functional AMPD or by supplementing hypoxanthine or guanine in the medium. In mammalian systems, it is the circulating adenosine levels that cause the defective phenotype in Δ*ampd* cells. But for the *Plasmodium* parasite that is harboured inside the erythrocyte, the enzymes APRT and adenosine kinase, which would add to AMP pools are absent. Even though the erythrocyte compartment has both APRT and adenosine kinase, and AMP generated via this route can enter the parasite (Cassera *et al.*, 2008); hypoxanthine is the key precursor for purines in *Plasmodium*. Interestingly, in *Dictyostelium* that has adenosine kinase and APRT and *Toxoplasma gondii* that has adenosine kinase, loss of AMPD results in a developmental/growth defect phenotype (Chae *et al.*, 2002; Sidik *et al.*, 2016). Also, both adenosine kinase and APRT

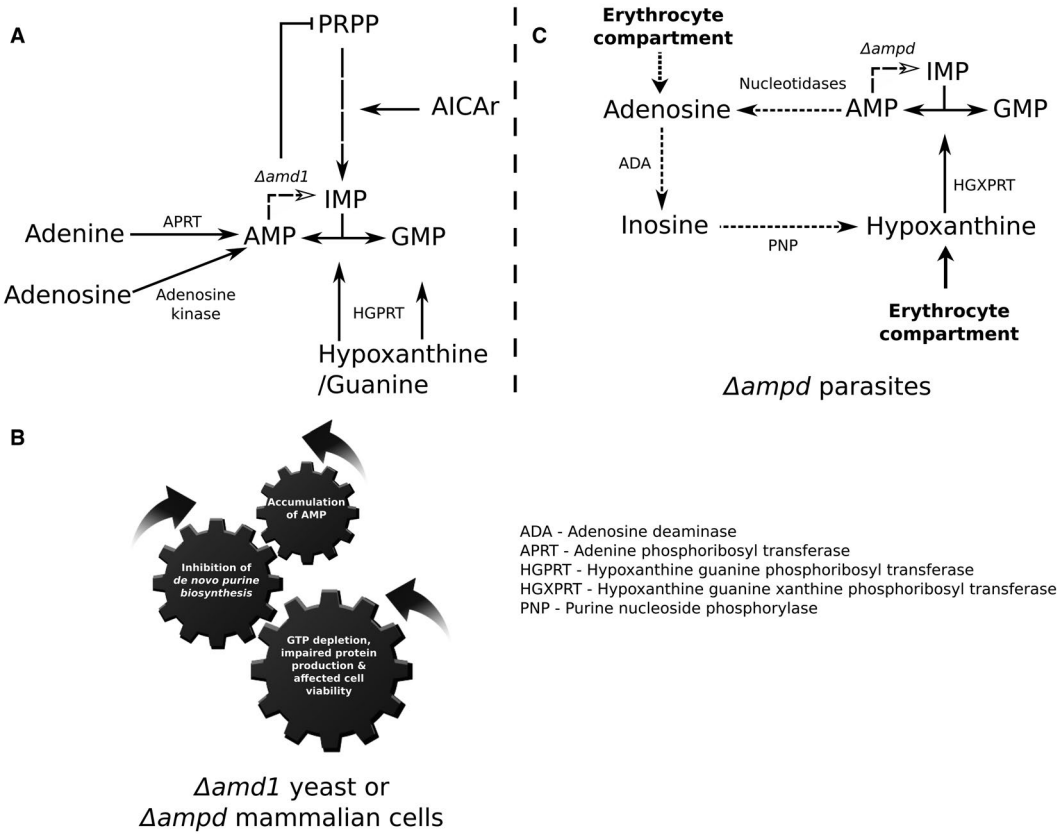


Fig. 6. Schematic of AMP metabolism in yeast, mammalian cells and *Plasmodium*. A. Modes of AMP generation (adenosine phosphoribosyltransferase-APRT and adenosine kinase pathways), consequences of increased AMP concentration in AMPD knockout yeast or mammalian cells and mode of metabolite mediated rescue (HGPRT pathway). B. The interlinked gears depict how the accumulation of AMP eventually manifests as a growth defect. C. Mode of AMP metabolism in Δ*ampd* parasites (note: Enzymes APRT and adenosine kinase which would have lead to AMP accumulation are absent in the parasite). In addition to the salvage of hypoxanthine by HGXPRT other possible routes for IMP generation from adenosine/AMP is also shown (dashed arrow).

genes are present in *Chromera velia* which is a free-living ancestor of *Plasmodium* (Aurrecoechea *et al*., 2016). An inherently advantageous metabolic wiring that is deficient of adenosine kinase and APRT seems to have enabled the parasite to survive even in the absence of AMPD in all stages (Fig. 6).

In summary, this study is the first report of comprehensive biochemical and physiological characterization of AMPD from an apicomplexan parasite. Apart from providing evidence for the expression of the protein in *Plasmodium* by RT-PCR, we have also demonstrated that the protein is enzymatically functional by making use of a complementation assay in an AMPD knockout yeast strain. In addition, critical residues have been identified that are required for the functionality of this protein and the dispensable nature of this enzyme-function in asexual stages of the parasite's life cycle has been established. Having demonstrated that overexpression of AMPD is toxic, one can ascertain that regulation of its activity is vital and it would be interesting to investigate the mode of regulation of this enzyme, employed by the parasite.

Acknowledgements

HB acknowledges financial support from Department of Biotechnology, Ministry of Science and Technology, Government of India (BT/PR11294/BRB/10/1291/2014, BT/PR13760/COE/34/42/2015, and BT/INF/22/SP27679/2018); Science and Engineering Research Board, Department of Science and Technology, Government of India (EMR/2014/001276); and institutional funding from the Jawaharlal Nehru Centre of Advanced Scientific Research, Department of Science and Technology, India. KAK acknowledges the financial support from DBT (BT/PR2495/BRB/10/950/2011) and DST (EMR/2016/006331). LKN acknowledges CSIR for junior and senior research fellowships. DS and SD acknowledge CSIR for direct SRF. We thank Dr. Photini Sinnis (Johns Hopkins University) for UIS4 antibody and Dr. Oliver Billiker (Wellcome Sanger Institute) for the p28 antibody.

Conflict of interest

The authors declare that they have no conflicts of interest with the contents of this article.

Author contributions

HB and LKN conceived the project. LKN generated all the plasmid constructs and conducted the experiments using bacteria and yeast model systems. LKN generated the knockout parasite cell line and examined intra-erythrocytic stages including the gametocyte stages. LKN conducted the over-expression study in *P. berghei* and in yeast. Mosquito colony maintenance, initiation of infection in the mosquito, sexual stages analysis, oocyst analysis, gliding motility video recording, salivary gland sporozoite count, IFA of EEFs and salivary gland sporozoites were performed by DS and SD. IFA of oocyst sporozoites, *in-vitro* exoerythrocytic stage development, and determination of *in vivo* infectivity of sporozoites by intravenous injection to mice was conducted by DS. Day 14 infected mosquito dissections and day 18 salivary gland sporozoites dissections were done by KAK. LKN, HB and KAK wrote the manuscript with inputs from DS and SD.

Ethics statement

Male/female BALB/c mice aged 6–8 weeks were used for cultivation and transfection of *P. berghei*. 6-8 weeks old female Swiss albino (SA) mice were procured from National Institute of Nutrition NIN, Hyderabad, India. The mice were used for gametocyte production required for initiation of the sexual cycle in mosquito and generation of sporozoite stages. Female C57BL/6 mice (5-6 week old) were procured from Hylasco Biotechnology (India) and were used to determine the pre-patent period of Δ*ampd P. berghei* parasites. Whole blood for *P. falciparum* culturing was collected from healthy volunteers with written informed consent. Animal experiments involving the handling of mice were performed by adhering to the standard protocols prescribed by the Committee for the Purpose of Control and Supervision of Experiments on Animals (CPCSEA), a statutory body under the Prevention of Cruelty to Animals Act of 1960 and Breeding and Experimentation Rules of 1998, Constitution of India. The current study (project no. HB002/201/CPCSEA and UH/IAEC/KAK/2018-1/24) was approved by Institutional animal ethics committee (IAEC) of JNCASR and the University of Hyderabad that come under the purview of CPCSEA.

References

Akizu, N., Cantagrel, V., Schroth, J., Cai, N., Vaux, K., McCloskey, D., et al. (2013) AMPD2 regulates GTP synthesis and is mutated in a potentially treatable neurodegenerative brainstem disorder. *Cell*, **154**(3), 505–517.

Angov, E., Hillier, C.J., Kincaid, R.L. and Lyon, J.A. (2008) Heterologous protein expression is enhanced by harmonizing the codon usage frequencies of the target gene with those of the expression host. *PloS One*, **3**(5), e2189.

Atkinson, D.E. (1968) Energy charge of the adenylate pool as a regulatory parameter. *Interaction with feedback modifiers. Biochemistry*, **7**(11), 4030–4034.

Aurrecoechea, C., Barreto, A., Basenko, E.Y., Brestelli, J., Brunk, B.P., Cade, S., et al. (2016) Eupathdb: the eukaryotic pathogen genomics database resource. *Nucleic Acids Research*, **45**(D1), D581–D591.

Aurrecoechea, C., Brestelli, J., Brunk, B.P., Dommer, J., Fischer, S., Gajria, B., et al. (2008) Plasmodb: a functional genomic database for malaria parasites. *Nucleic Acids Research*, **37**(suppl_1), D539–D543.

Bahl, A., Brunk, B., Coppel, R.L., Crabtree, J., Diskin, S.J., Fraunholz, M.J., et al. (2002) Plasmodb: the *Plasmodium* genome resource. An integrated database providing tools for accessing, analyzing and mapping expression and sequence data (both finished and unfinished). *Nucleic Acids Research*, **30**(1), 87–90.

Bahl, A., Brunk, B., Crabtree, J., Fraunholz, M.J., Gajria, B., Grant, G.R., et al. (2003) Plasmodb: the *Plasmodium* genome resource. A database integrating experimental and computational data. *Nucleic Acids Research*, **31**(1), 212–215.

Bazin, R.J., McDonald, G.A. and Phillips, C. (2003) UK Patent GB2373504.

Beyer, H.M., Gonschorek, P., Samodelov, S.L., Meier, M., Weber, W. and Zurbriggen, M.D. (2015) Aqua cloning: a versatile and simple enzyme-free cloning approach. *PloS One*, **10**(9), e0137652.

Bulusu, V., Srinivasan, B., Bopanna, M.P. and Balaram, H. (2009) Elucidation of the substrate specificity, kinetic and catalytic mechanism of adenylosuccinate lyase from *Plasmodium falciparum*. *Biochimica et Biophysica Acta (BBA)-Proteins and Proteomics*, **1794**(4), 642–654.

Cassera, M.B., Hazleton, K.Z., Riegelhaupt, P.M., Merino, E.F., Luo, M., Akabas, M.H., et al. (2008) Erythrocytic adenosine monophosphate as an alternative purine source in *Plasmodium falciparum*. *Journal of Biological Chemistry*, **283**(47), 32889–32899.

Chae, S.-C., Fuller, D. and Loomis, W.F. (2002) Altered cell-type proportioning in *Dictyostelium* lacking adenosine monophosphate deaminase. *Developmental Biology*, **241**(1), 183–194.

Chapman, A.G. and Atkinson, D.E. (1973) Stabilization of adenylate energy charge by the adenylate deaminase reaction. *Journal of Biological Chemistry*, **248**(23), 8309–8312.

de Koning-Ward, T.F., Fidock, D.A., Thathy, V., Menard, R., van Spaendonk, R.M., Waters, A.P., et al. (2000) The selectable marker human dihydrofolate reductase enables sequential genetic manipulation of the *Plasmodium berghei* genome. *Molecular and Biochemical Parasitology*, **106**(2), 199–212.

Downie, M.J., Kirk, K. and Mamoun, C.B. (2008) Purine salvage pathways in the intraerythrocytic malaria parasite *Plasmodium falciparum*. *Eukaryotic Cell*, **7**(8), 1231–1237.

Eaazhisai, K., Jayalakshmi, R., Gayathri, P., Anand, R., Sumathy, K., Balaram, H., et al. (2004) Crystal

Received: 19 July 2016 | Revised: 4 January 2017 | Accepted: 7 January 2017

DOI: 10.1111/cmi.12723

WILEY

RESEARCH ARTICLE

Modulation of host cell SUMOylation facilitates efficient development of *Plasmodium berghei* and *Toxoplasma gondii*

Mulaka Maruthi[1] | **Dipti Singh**[1] | **Segireddy Rameswara Reddy**[1] | **Babu S. Mastan**[1] | **Satish Mishra**[2] | **Kota Arun Kumar**[1]

[1] Department of Animal Biology, School of Life Sciences, University of Hyderabad, Hyderabad, India

[2] Division of Parasitology, CSIR-Central Drug Research Institute, Lucknow, India

Correspondence
Kota Arun Kumar, Department of Animal Biology, School of Life Sciences, University of Hyderabad, Hyderabad 500046, India.
Email: kaksl@uohyd.ernet.in

Funding information
Department of Biotechnology (DBT, India), Grant/Award Number: BT/PR2495/BRB/10/950/2011 to KAK; Council for Scientific and Industrial Research (CSIR); Department of Biotechnology (DBT); DBT Ramalingaswami Fellowship, Grant/Award Number: GAP0142

Summary

SUMOylation is a reversible post translational modification of proteins that regulates protein stabilization, nucleocytoplasmic transport, and protein–protein interactions. Several viruses and bacteria modulate host SUMOylation machinery for efficient infection. *Plasmodium* sporozoites are infective forms of malaria parasite that invade mammalian hepatocytes and transforms into exoerythrocytic forms (EEFs). Here, we show that during EEF development, the distribution of SUMOylated proteins in host cell nuclei was significantly reduced and expression of the SUMOylation enzymes was downregulated. *Plasmodium* EEFs destabilized the host cytoplasmic protein SMAD4 by inhibiting its SUMOylation. SUMO1 overexpression was detrimental to EEF growth, and insufficiency of the only conjugating enzyme Ubc9/E2 promoted EEF growth. The expression of genes involved in suppression of host cell defense pathways during infection was reversed during SUMO1 overexpression, as revealed by transcriptomic analysis. The inhibition of host cell SUMOylation was also observed during *Toxoplasma* infection. We provide a hitherto unknown mechanism of regulating host gene expression by Apicomplexan parasites through altering host SUMOylation.

KEYWORDS

conjugation enzyme E2, host SUMOylation, *Plasmodium* EEFs, SMAD4, SUMO1, *Toxoplasma*

1 | INTRODUCTION

Malaria infection is initiated when sporozoites are introduced in the mammalian host by the bite of a female *Anopheles* mosquito. The sporozoites selectively invade hepatocytes and develop into exoerythrocytic forms (EEFs) inside a parasitophorous vacuole (Prudencio, Rodriguez, & Mota, 2006). The intrahepatic development of *Plasmodium* is an obligatory step before the onset of disease. Very little is known about the parasite liver stage and their interactions with host cell. Apicomplexan parasites subvert their host cell functions to access essential nutrients and escape from host defense mechanisms. The host processes that are targeted include modulation of gene expression, protein synthesis, membrane trafficking, antigen presentation, and apoptosis (Plattner & Soldati-Favre, 2008). In addition to the orchestration of the above host cellular mechanisms, parasites have evolved to manipulate specialized host cellular processes—the posttranslational modifications (PTMs). The first study providing evidence for a pathogen-derived toxin in catalyzing PTM of host protein was reported 5 decades ago (Collier & Cole, 1969). Since then, significant numbers of host PTMs induced, mediated, or counteracted by different pathogens have been reported (Randow & Lehner, 2009; Ribet & Cossart, 2010).

In addition to ubiquitin, a family of substrates called ubiquitin-like proteins (UBLs) is covalently linked to the target protein and influences diverse biological processes. One such member of UBLs is small ubiquitin-like modifier (SUMO), a 12-kDa polypeptide found ubiquitously in the eukaryotic kingdom. SUMOylation, the covalent linkage of SUMO moiety on Lys residue of the target protein, is mediated by the sequential action of three enzymes: E1-SAE1/SAE2 heterodimer (activating enzyme), E2/Ubc9 (conjugating enzyme), and E3 enzymes (ligating enzymes). SUMOylation is essential for many cellular functions such as transcription regulation, intracellular transport, maintenance of genome integrity, protein stability, stress responses, and many other biological functions (Zhao, 2007).

 © 2017 John Wiley & Sons Ltd

Consistent with the indispensable role of SUMOylation in the host cell, the exploitation of host SUMOylation by bacterial pathogens such as *Listeria* (Ribet et al., 2010), *Salmonella* (Verma et al., 2015), *Anaplasma* (Beyer et al., 2015), and many viral pathogens (Boggio & Chiocca, 2006) is well documented. However, there are no reports till date showing the modulation of host SUMOylation by Apicomplexan parasites. In this study, we provide evidence for manipulation of host cell SUMOylation by two well-studied Apicomplexan parasites—*Plasmodium* and *Toxoplasma*. We demonstrate for the first time that both parasites downregulate host SUMOylation machinery for efficient infection and growth.

2 | RESULTS

2.1 | Altered cellular distribution of SUMO1 during development of *Plasmodium berghei (P. berghei)* EEFs

While addressing the role of sporozoite-induced SUMOylation changes in the HepG2 cells, we used *P. berghei* ANKA mCherry transgenics (Surendra K. K. and Kumar K. A., personal communications) for all experiments. We investigated SUMO1 immunoreactivity in the nuclei of cells that were harboring EEFs at 36 hr. We found significantly less SUMO1 immunoreactivity in nuclei of infected cells (Figure 1a-A) as compared to mock-infected cells (Figure 1a-B), suggesting that developing EEFs precluded the translocation of SUMOylated proteins into host nucleus. Such observations were consistent, in some instances, with the preferential accumulation of SUMOylated proteins towards the nuclear periphery of infected host nuclei (Figure 1a-A). Figure 1a-C,D shows respectively the SUMO1 pixel intensity along the line in the nuclei of infected and mock-infected cell. From three independent experiments, we quantified SUMO1 intensity in 50 infected and mock-infected host nuclei, and cytosol and values were normalized with size of host nuclei and cell, respectively. While we observed more than three-fold decrease in the SUMO1 intensity in infected cell nuclei (Figure 1a-E), we noticed a trend towards significant increase in the SUMO1 intensity in the cytosol of infected cell (Figure S1a,b).

2.2 | Transient overexpression of SUMO1 in HepG2 cells does not compromise *P. berghei* sporozoite entry into the host cells, but attenuates intracellular growth of the parasite

In order to investigate how the cellular levels of SUMOylation may impact the intrahepatic transformation of sporozoites, we transiently overexpressed SUMO1-FLAG in HepG2 cells and analyzed the fate of developing *P. berghei* EEFs. At 48-hr postinfection with sporozoites, the parasite burden in transfected cultures was analyzed by quantifying the *Pb18SrRNA* copy number by quantitative reverse transcription polymerase chain reaction (qRT-PCR). We observed six- to seven-fold decrease in the parasite burden in SUMO1-FLAG-overexpressing HepG2 cells (Figure 1b). In order to investigate whether the observed decrease in parasite burden was due to compromised invasion of sporozoites or block in EEF development, we performed sporozoite invasion assay and quantified the infectivity of sporozoites. We observed that invasion efficiency of sporozoites was almost the same in SUMO1-FLAG overexpressing and control HepG2 cells (Figure 1c). We next analyzed the development of EEFs in HepG2 cells overexpressing SUMO1-FLAG. At 48-hr time point, the EEFs were drastically attenuated in their growth in SUMO1-overexpressing cells (Figure 1d-A) as compared to those growing in control cells (Figure 1d-B). We conclude that transient overexpression of SUMO1 has detrimental effect only on EEF development and does not affect sporozoite infectivity.

2.3 | A minimal induction of SUMO1-GFPt (Green Fluorescent Protein) in HepG2 cells using Tet-regulated expression system attenuates the growth of the *P. berghei* EEFs

To reiterate our findings on the detrimental effect of SUMO1 overexpression on EEF development in vitro, we generated a Tet-regulated SUMO1-GFP expression system in HepG2 cells. Towards this end, we first generated HepG2 cells expressing TetR transactivator. Western blotting revealed that clone 6 expressed high levels of TetR (Figure 1e). The TetR expressing HepG2 cells was further transfected with pTRE3G-SUMO + GFP plasmid that is responsive to doxycycline. The cultures were exposed to different concentrations of doxycycline, and the expression of Tet-SUMO1 + GFP expression was observed at a minimum concentration of 10 ng/ml (Figure 1f). Under these conditions, the cells were infected with sporozoites and monitored for EEF growth. At 48-hr postinfection, we observed EEF growth attenuation in Tet-SUMO1 + GFP-expressing cells (Figure 1g-A). As an appropriate control, we transfected the TetR HepG2 cells with pTRE3G-GFP plasmid and observed no defect in EEF development in cells expressing Tet-GFP (Figure 1g-B). In fact, the EEF development was indistinguishable in Tet-GFP-transfected cell and nontransfected cell (Figure S2). We quantified the EEF size from HepG2 cells expressing Tet-GFP and Tet-SUMO1 + GFP and noted a seven-fold decrease in EEF size in Tet-SUMO1 + GFP-expressing cells (Figure 1g-C). We conclude that a minimal expression of SUMO1 likely activates effector mechanisms in host cells that limit growth of EEFs.

2.4 | Short hairpin RNA-mediated silencing of host *E2/Ubc9* facilitates better development of *P. berghei* EEFs

Because overexpression of SUMO1 was unfavorable for EEF development, we next analyzed if downregulation of any one of the host SUMOylation enzymes would favor growth of EEFs. We transfected HepG2 cells with short hairpin RNA (shRNA) GFP reporter constructs specific for host *Ubc9* (four variants and one scrambled) and added sporozoites to these cultures. We monitored the growth of EEFs at 32 hr by measuring its size. We found significant increase in the size of EEFs transfected with shRNA 83 and 84 (Figure 2a-A). We also confirmed these findings independently by measuring the parasite *18srRNA* burden (Figure 2a-B). However, we observed some discrepancy in EEF size (Figure 2a-A) versus parasite *18srRNA* burden (Figure 2a-B) and a likely explanation for this may be the

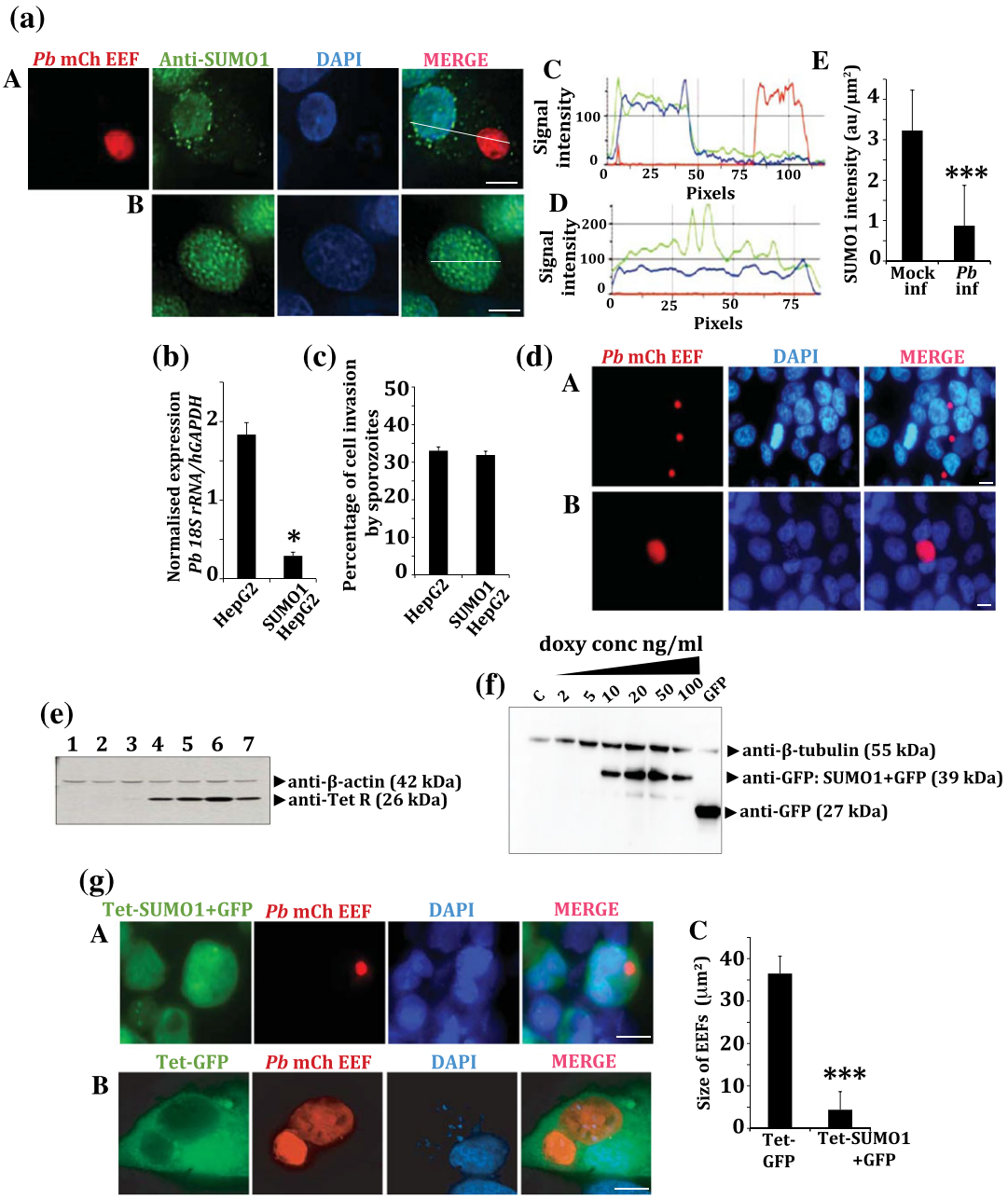


FIGURE 1 Alterations in SUMOylation levels of HepG2 cells during *Plasmodium berghei* ANKA (Pb) exoerythrocytic form (EEF) development. (a) Immunofluorescence assay of HepG2 cultures at 36-hr postinfection with *Pb* mCherry (mCh) sporozoites. SUMO1 was stained with rabbit anti-SUMO1 monoclonal antibody, and immunoreactivity was revealed using goat antirabbit Alexa 488 secondary antibody. Nuclei were stained with DAPI. (A) HepG2 cell harboring *Pb* mCh EEF precludes the nuclear translocation of SUMO1. (B) Nuclear translocation of SUMO1 in mock-infected cell (scale bar: 10 µm, magnification 60×). The staining intensity of nuclear SUMO1 is shown along the line for (C) infected and (D) noninfected cell. Pixel intensity was measured using NiS-elements AR software. (E) Nuclear intensity of SUMO1 in mock-infected HepG2 cells (mock inf) and *Pb* sporozoite-infected HepG2 cells (*Pb* inf). Error bars: SEM, $n = 50$, ***p value < .0001. (b) *Pb 18SrRNA* levels in pCDNA3.1-SUMO1-FLAG-transfected HepG2 cells as quantified by quantitative reverse transcription polymerase chain reaction. The gene expression values were normalized to host *GAPDH* (h*GAPDH*), error bars: SEM, $n = 4$, *p value < .05 compared with control. (c) Average number of intracellular parasites per field calculated from sporozoite inside and outside assay. Error bars: SEM, $n = 25$, not significant. In both (b) and (c), HepG2 refers to nontransfected cells and SUMO1-HepG2 refers to cells transfected with pCDNA3.1-SUMO1-FLAG. (d) Growth of *Pb* mCh EEF in (A) HepG2 cultures stably transfected with pCDNA-SUMO1 + FLAG plasmid and (B) in nontransfected cultures at 48 hr. (scale bar: 10 µm, magnification 40×). (e) Western blot showing expression of TetR transactivator protein in clones 4, 5, 6, and 7. Anti-β-actin was used as loading control. (f) Western blot showing the expression of SUMO1 + GFP induced in the presence of varying doxycycline (doxy) concentrations (2, 5, 10, 20, 50 and 100 ng/ml); C = control HepG2 cells; GFP = positive control. The blot was probed with anti-GFP antibody, and anti-β-tubulin antibody was used as loading control. (g) The minimal induction of Tet-SUMO1 + GFP in TetR HepG2 cells inhibits the development of *Pb* mCh EEF. *Pb* mCh sporozoites were added to cultures and 2-hr postinfection, SUMO1 + GFP expression was induced with 10 ng/ml of doxycycline. Growth of *Pb* mCh EEF in TetR transactivator HepG2 cell line transfected with (A) pTRE3G-SUMO1 + GFP (Tet-SUMO1 + GFP) plasmid and (B) pTRE3G-GFP (Tet-GFP) plasmid. The EEF development was monitored at 48 hr (scale bar: 10 µm, magnification 60×). (C) Measurement of EEF size in HepG2 cells transfected with pTRE3G-GFP (Tet-GFP) and pTRE3G-SUMO1 + GFP (Tet-SUMO1 + GFP). Error bars: SEM, $n = 100$, ***p value < .0001

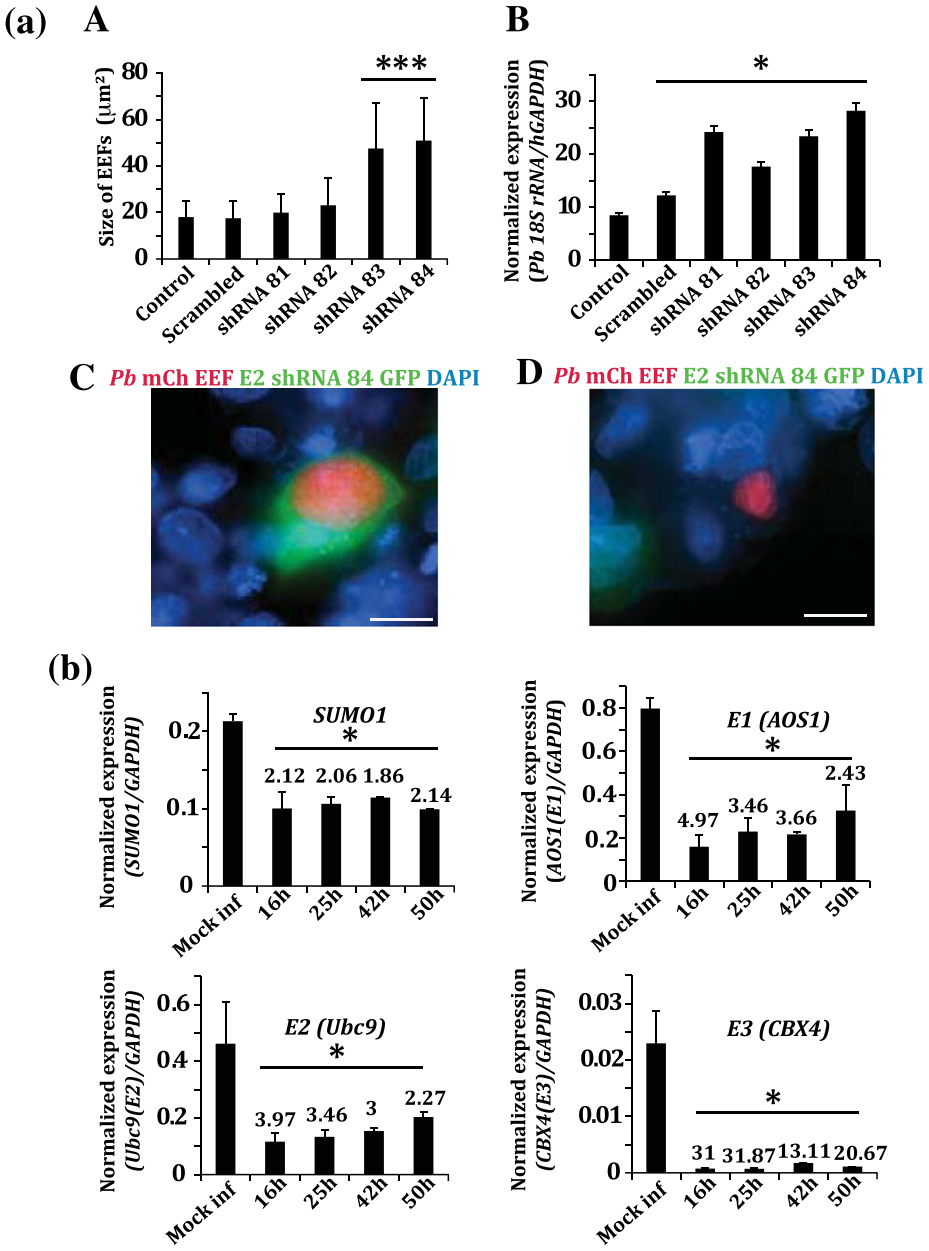


FIGURE 2 Silencing of *Ubc9/E2* in HepG2 cells promotes development of *Pb* exoerythrocytic forms (EEFs). (a; A) Measurement of EEF size in HepG2 cells transfected with different short hairpin RNAs (shRNAs) against *Ubc9/E2*. Error bars: SEM, $n = 25$, ***p value < .0001 compared with control. (B) *Pb 18SrRNA* levels in *Ubc9/E2* silenced HepG2 cells as quantified by quantitative reverse transcription polymerase chain reaction (qRT-PCR). The expression values were normalised to host *GAPDH* (h*GAPDH*), $n = 4$, *p value < .05 compared with control. Fluorescent microscopy showing *Pb* mCh EEF at 32 h post infection in (C) *Ubc9* shRNA-transfected cells (GFP expressing) and (D) nontransfected cells (scale bar: 10 µm, magnification 60×). (b) *Pb* sporozoite infection of HepG2 cells downregulates the expression of SUMO machinery enzymes. Complementary DNA samples were generated from infected HepG2 cultures at indicated time points. Mock-infected (mock inf) HepG2 cultures were kept as controls. Expression of SUMO1 and enzymes of the SUMOylation machinery were quantified by qRT-PCR. Gene expression values were normalized to host *GAPDH* (h*GAPDH*). Error bars: SEM, $n = 4$, *p value < .05 compared with control

detection of parasite *18srRNA* copy number from EEFs maturing within shRNA-transfected and nontransfected cells. However, at the cellular level, fluorescent microscopy analysis of HepG2 cells showed maximal EEF growth in cells transfected with shRNA 84 (Figure 2a-C) as compared to nontransfected cells (Figure 2a-D) within the same culture. The efficacy of shRNA-mediated silencing of *Ubc9/E2* was confirmed by immunoblotting using anti-Ubc9/E2 antibody (Figure S3A) that revealed varying but significant reduction in the levels of Ubc9/E2 in cells transfected with shRNA variants 81, 82, 83, and 84. Further, the shRNA-transfected cell lysates were also analyzed for overall SUMO conjugation to cellular proteins. Western blot analysis using anti-SUMO1 antibody revealed an overall decrease in SUMO1 conjugation to cellular proteins (Figure S3B). We conclude that depleting Ubc9/E2 enzyme of the host SUMO machinery favors the maturation of *P. berghei* EEFs by promoting its growth.

2.5 | Developing *P. berghei* EEFs downregulate the expression of SUMO1 and enzymes of the SUMOylation machinery

Having shown that host cell SUMOylation is modulated during EEF development, we next analyzed if expression of *SUMO1* and enzymes of the SUMOylation machinery was also affected. Quantitative reverse transcription polymerase chain reaction revealed downregulation in expression of *SUMO1* and the enzymes of SUMOylation machinery in the range of two to 31 folds during 12- to 50-hr postinfection (Figure 2b). These observations suggest a possible interference of developing EEFs with components of host SUMOylation machinery at transcription level.

2.6 | Transcriptomic analysis revealed induction of defense-related genes associated with SUMO1 overexpression that likely inhibits the growth of *P. berghei* EEFs

As the role of SUMO1-tagged transcription factors in activation and repression of global gene expression is well known, we wanted to investigate how SUMO1 overexpression differentially regulates the host gene expression in the presence of sporozoites. By using human whole genome microarray, we investigated the differential gene expression in HepG2 cells under four different conditions: (a) mock infection (Mock inf), (b) sporozoite infection (Spz+), (c) SUMO1 overexpression (SUMO1+), and (d) SUMO1 overexpression and sporozoite infection (SUMO1 + Spz+). From the raw data and heat maps (Figure 3a-A-C), we pooled certain genes whose transcription factors are likely to be SUMOylated and generated heat maps for genes involved in pathways regulating signal transduction, stress response, defense response, and apoptosis (Figure 3b-d). Overall, the effects of sporozoite infection (Spz+) gave an indication that *P. berghei* usurps host SUMOylation process to create an antiapoptotic, proliferative environment that favors the parasite development. This was evident by altered expression of *PTGS2*, *IL1B*, *PLA2G4*, *HERC5* (Figure 3d-A), *KIT* (Figure 3d-B), *NOS2* (Figure 3d-C), and *SOCS3* (Figure 3d-E) following infection with sporozoites that likely promote the EEF growth. However, SUMO1 overexpression, when concommitant with Spz + infection (SUMO1 + Spz+) resulted in upregulation of several defense responsive genes such as *CCL5*, *IFIT2* (Figure 3d-A), *IFNG*, *IL10*, *NOS2* (Figure 3d-C), and *IL4* (Figure 3d-E), whose products may successfully revert the parasite-induced effects resulting in its growth arrest. Validation of microarray data was done by qRT-PCR analysis of six genes randomly selected from the expression data. For all six genes, we observed correlation between expression values from microarray and qRT-PCR (Figure S4).

2.7 | Several aspects of modulation in host cell SUMOylation by *Plasmodium* are conserved during *Toxoplasma gondii (T. gondii)* infection

We also noted a similar phenomenon in *T. gondii* where cells harboring the parasites revealed a reduced SUMO1 immunoreactivity in the host nucleus (Figure 4a-A) as compared to noninfected cells (Figure 4a-B) at 24 hr. Figure 4a-C,D shows respectively the SUMO1 pixel intensity along the line in the nuclei of infected and noninfected cell. Next, we analyzed the *T. gondii* burden in HepG2 cells transfected with pTRE3G-SUMO + GFP plasmid. We observed four-fold less parasite burden in Tet-SUMO1 + GFP-expressing cells as compared to nontransfected (control) cultures (Figure 4b). The ability of *T. gondii* to form tachyzoites was compromised in the Tet-SUMO1 + GFP-overexpressing HepG2 cells (Figure 4c-A) as compared to nontransfected (control) cells (Figure 4c-B). Downregulation of *SUMO1* and enzymes of SUMOylation machinery was also noted in *T. gondii* at 24-hr postinfection (Figure 4d); however, the fold change in expression of genes investigated varied from 1.8 to 5.3 fold, which was far less dramatic as compared to *P. berghei*.

2.8 | Translocation of SUMOylated SMAD4 complex to nucleus is precluded in HepG2 cells harboring *Plasmodium* EEFs and *T. gondii*

In order to understand how intracellular parasites block nuclear translocation of SUMOylated proteins, we investigated a signaling pathway mediated by transforming growth factor (TGF)-β, which enhances the nuclear accumulation of SMAD4 complex by SUMOylation (Lin et al., 2003). We therefore analyzed the transcriptional activity of SMAD4 using a TGF-β-SMAD4 reporter assay (Figure S5). We observed nearly 50% decrease in transcriptional activity of SMAD4 in the presence of *Plasmodium* EEFs (as compared to mock infection) and *T. gondii* (Figure 4e). We infer that both parasites reduce the nuclear translocation of SUMOylated SMAD4 complex. In line with such prediction, we indeed noted downregulation of SMAD4 target such as *IRF2BP2*, *CDKN1A* (*p21*), and *SKIL* (*SnoN*) in 24-hr cultures infected with *P. berghei* sporozoites and *T. gondii* (Figure 4f). We conclude that both *Plasmodium* and *Toxoplasma* inhibit SUMOylation of SMAD4 likely to minimize the expression of SMAD4 responsive genes.

3 | DISCUSSION

Several lines of evidence suggest that viruses and intracellular pathogens modify the host SUMOylation machinery for successful establishment of infection. The spectrum of activities altered by modulating SUMO conjugation includes signal transduction, gene expression, chromatin structure, and maintenance of genome (Gill, 2004). In this study, we investigated the mechanism used by *P. berghei* EEFs and *T. gondii* to alter the host cell SUMOylation during their intracellular growth. Because overexpression of SUMO1 inhibited the intracellular growth of both parasites, we studied the mechanism that lead to the parasite growth arrest. Previous studies (Lin et al., 2003) have shown that SMAD4 mediates the transcriptional response for TGF-β. In cells overexpressing SUMO1, the SUMOylation of SMAD4 is enhanced resulting in rescuing from ubiquitin-dependent degradation and promoting its transcriptional activity. We integrated this known information of SMAD4 regulation by SUMOylation and demonstrated that developing *Plasmodium* EEFs and *T. gondii* precluded the nuclear translocation of SMAD4 by preventing its SUMOylation to downregulate

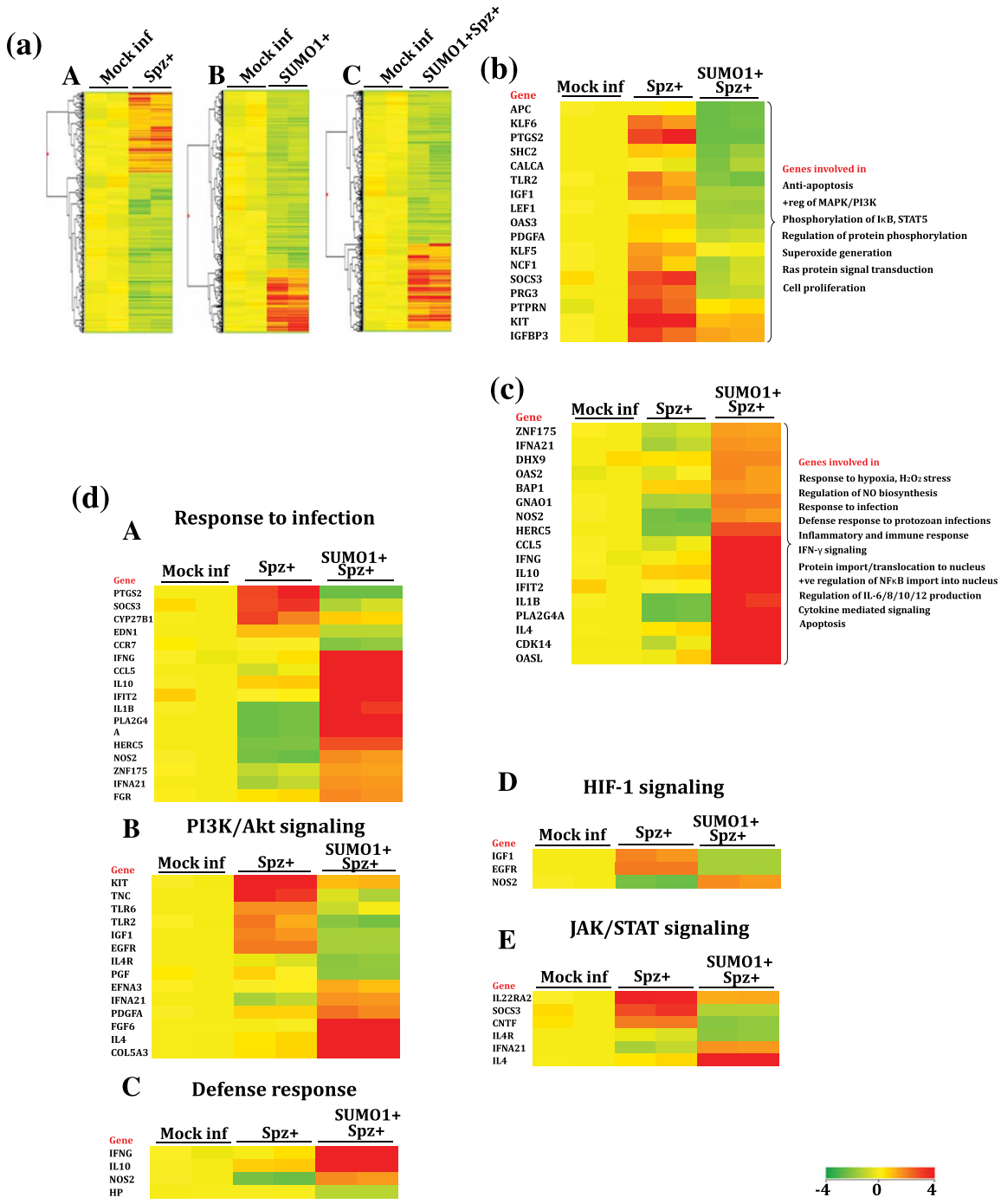


FIGURE 3 Transcriptomic analysis of SUMO1-overexpressing HepG2 cells infected with *P. berghei* sporozoites. (a) Heat maps of differentially expressed genes under conditions of (A) mock infection (mock inf) versus *Pb* sporozoite infection (Spz+), (B) mock infection versus SUMO1 overexpression (SUMO1+), and (C) mock infection (mock inf) versus SUMO1 overexpression and *Pb* sporozoite infection (SUMO1 + Spz+). (b) and (c) Heat maps showing differentially expressed genes for indicated pathways in mock-infected cultures (mock inf), *Pb* sporozoite-infected cultures (Spz+), and SUMO1-overexpressing cells infected with *Pb* sporozoite (SUMO1 + Spz+). (d) Heat maps showing differentially expressed genes for pathways involved in (A) response to infection, (B) PI3K/Akt signaling, (C) defense response, (D) HIF1 signaling pathway, and (E) JAK/STAT signaling pathway in mock-infected cultures (mock inf), sporozoite-infected cultures (Spz+), and SUMO1-overexpressing cells infected with sporozoite (SUMO1 + Spz+)

the expression of its target genes such as *CDKN1A* (*p21*), *SKIL* (*SnoN*), and *IRF2BP2* that likely mediate antiparasitic effects. These target genes are involved in regulation of cell cycle, inhibition of tumorigenesis, and *p53*-mediated apoptosis (Chen et al., 2015; Koeppel et al., 2009; Pan, Zhu, Conboy, Conboy, & Luo, 2012). In fact, the critical processes of resistance to host cell apoptosis and suppression of host *p53* during EEF development have already been documented (van de Sand et al., 2005). Thus, infection-induced conditions that alter SMAD4 translocation to host nucleus may likely be envisaged in suppression of *p21*-induced apoptosis and also prevent *SKIL*-mediated activation of *p53*. Nuclear translocation of SMAD4 is dependent on phosphorylation of the regulatory SMAD2 and SMAD3 that form complex with SMAD4. It needs to be investigated if *Plasmodium* and *Toxoplasma* interfere with phosphorylation of regulatory SMADs. Taken together,

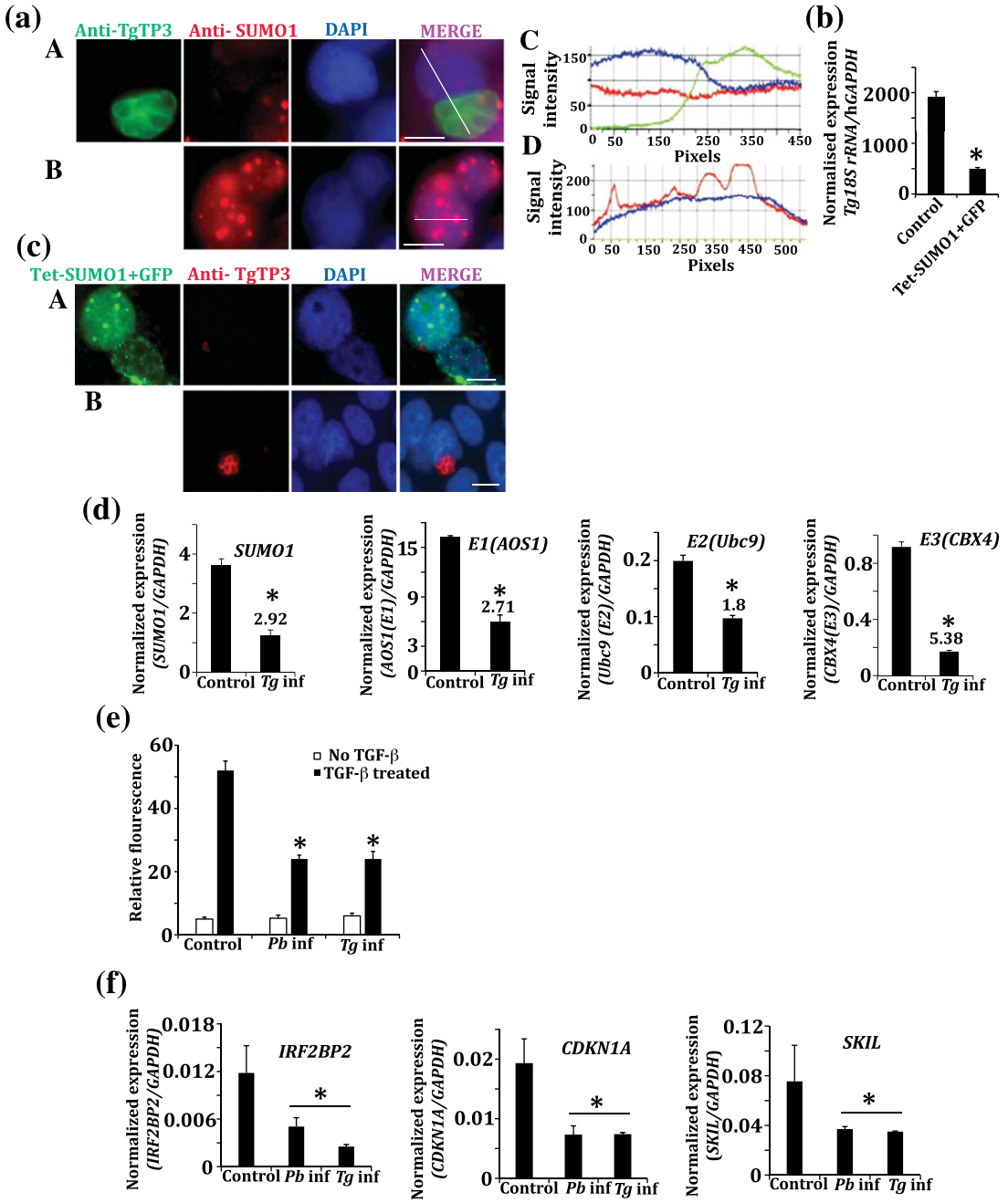


FIGURE 4 *Toxoplasma gondii* (*Tg*) infection alters the host SUMOylation machinery. (a) Immunofluorescence assay (IFA) of *Tg*-infected HepG2 cells at 24 hr. *Tg* was stained with mouse anti-TgTp3 antibody, and immunoreactivity was revealed using rabbit antimouse Alexa 594 secondary antibody. SUMO1 was stained with rabbit anti-SUMO1 monoclonal antibody, and immunoreactivity was revealed using goat antirabbit Alexa 488 secondary antibody. Nuclei were stained with DAPI. (A) *Tg*-infected cell and (B) noninfected cell (scale bar: 10 μm, magnification 100×). The staining intensity of nuclear SUMO1 is shown along the line for (C) infected and (D) noninfected cell. Pixel intensity was measured using NiS-elements AR software. (b) *Tg18SrRNA* levels in HepG2 transfected with pTRE3G-SUMO1 + GFP plasmid as quantified by quantitative reverse transcription polymerase chain reaction (qRT-PCR). The values were normalized to host *GAPDH* (h*GAPDH*), error bars: SEM, $n = 4$, $^*p$ value < .05 compared with control. (c) The minimal induction of SUMO1 + GFP in HepG2 cells reduces the multiplication of *Tg*. The TetR transactivator HepG2 cells were transfected with pTRE3G-SUMO1 + GFP plasmid and infected with *Tg* tachyzoites. Following 2-hr postinfection, the SUMO1 + GFP expression was induced with 10 ng/ml of doxycycline. The intracellular multiplication of *Tg* was monitored at 24 hr. The cells were fixed and permeabilized prior to IFA. (A) *Tg* tachyzoites in pTRE3G-SUMO1 + GFP-transfected cell (Tet-SUMO1 + GFP) and (B) *Tg* tachyzoites in nontransfected cell (scale bar: 10 μm, magnification 60×). (d) *Tg* infection of HepG2 cells downregulates the expression of SUMO machinery enzymes. Expression of *SUMO1* and SUMOylating enzymes were quantified by qRT-PCR at 24-hr postinfection. Expression values were normalized with host *GAPDH* (h*GAPDH*). Error bars: SEM, $n = 4$, $^*p$ value < .05 compared with control. (e) *Plasmodium* exoerythrocytic forms (EEFs) and *Toxoplasma* inhibit the SUMOylation of host SMAD4 and its transcriptional activity. The GFP fluorescence was quantified in HepG2 cells transfected with SMAD4-GFP reporter plasmid followed by treatment with or without transforming growth factor beta in the presence of *Plasmodium berghei* (*Pb*) and *Toxoplasma* (*Tg*), error bars: SEM, $n = 4$, $^*p$ value < 0.05 compared with control. (f) The qRT-PCR quantification of SMAD4 targets *IRF2B2*, *CDKN1A*, and *SKIL* in noninfected HepG2 cells (control) and cells infected with *P. berghei* sporozoites (*Pb* inf) and *Toxoplasma* tacyzoites (*Tg* inf), error bars: SEM, $n = 4$, $^*p$ value < 0.05 compared with control

these observations strongly support the ability of infected cells to resist apoptosis for the successful propagation of both parasites. Other than SMAD4, STAT1 is a target for modification by SUMO1 (Ungureanu, Vanhatupa, Gronholm, Palvimo, & Silvennoinen, 2005). Studies in *Plasmodium* (Liehl et al., 2014) and *Toxoplasma* (Kim, Fouts, & Boothroyd, 2007) have shown that IFN-γ activates several immune-responsive genes that likely confer resistance for completion of intracellular growth of both parasites by altering host gene expression, an effect mediated by STAT1. Induction of IFN-γ, an activator of STAT1, was revealed in our transcriptomic analysis in HepG2 cells overexpressing SUMO1. Nonetheless, a definitive proof for SUMOylation of STAT1 awaits further investigation.

The better growth of EEFs following shRNA-mediated silencing of *E2/Ubc9* suggested that an overall decrease in SUMOylation status of host cell benefits growth of *Plasmodium*. Interestingly, a similar mechanism was reported in *Listeria monocytogenes (L. monocytogenes)*, where degradation of Ubc9 led to higher infection levels. Although these studies highlighted the role of Listeriolysin as an effector in modulating the host cell SUMOylation, it is currently unknown how *Plasmodium* achieves the same. The scenario may not be as simple as *L. monocytogenes* that reside in the cytoplasm and have access to directly alter the host SUMO machinery. *Plasmodium* and *Toxoplasma* that reside in membrane-bound parasitophorous vacuolar compartment may have more elaborate mechanisms of protein export that may directly interact with the components of SUMO machinery or indirectly regulate expression of its enzymes by some unknown mechanism. Because overexpression of SUMO1 or silencing of *Ubc9/E2* impacted the EEF growth, it is likely that sporozoites destined for the transformation may only interfere with host SUMOylation process rather than during their transient association with hepatocyte cytoplasm, prior to productive invasion. However, further investigation is needed to clarify the latter statement. We did not observe any changes in the expression of the de-SUMOylase (SENP4) suggesting that this pathway was not affected by both *Plasmodium* and *Toxoplasma* (Figure S4).

Comparison of differentially expressed genes during sporozoite infection in the absence (Spz+) or presence of SUMO overexpression (SUMO1 + Spz+) revealed that during EEF development, *P. berghei* takes over the host SUMOylation to create an antiapoptotic, proliferative environment that is beneficial for its growth. We observed the levels of PTGS2, KIT, and SOCS3 were upregulated in sporozoite-infected cultures (Spz+). PTGS2/COX-2 is responsible for production of the inflammatory prostaglandins, which plays important roles in resistance to apoptosis and proliferation (Greenhough et al., 2009). In *Trypanosoma cruzi*, celecoxib-mediated downregulation of COX-2 impairs parasite entry into cardiac cells (Malvezi et al., 2014), and in *Leishmania infantum*, production of the Prostagalandin E2 mediated by COX2 benefits the parasite survival (Saha et al., 2014). Thus, in *Plasmodium* hepatic stages, it may be envisaged that a similar strategy for modulation of host COX2 pathway occurs to establish successful infection. SOCS3 plays a role in regulation of STAT3 signaling in the outcome of infection with *Mycobacterium tuberculosis* (Rottenberg & Carow, 2014). C-KIT (KIT) plays an important role in regulation of cell proliferation and survival, stem cell maintenance, and migration. KIT can activate several signaling pathways including activation of Akt/PI3K, STAT1/3/5, and PLCG1. PI3K pathway is required for successful infection of intracellular bacteria (Jiwani et al., 2012; Kuijl et al., 2007; Micheva-Viteva, Shou, Nowak-Lovato, Rector, & Hong-Geller, 2013). In *Plasmodium* HGF/MET signaling protects infected host cells via activation of PI3K pathway (Leiriao et al., 2005).

However, contrary to this scenario during SUMO1 + Spz + condition, several defense-responsive genes such as *NOS-2*, *IFN-G*, *IL1-B*, *IL10*, *IL4*, *CCL5*, *IFIT2*, and *HERC5* were upregulated whose products may be recruited to revert the parasite-induced effects and promote parasite growth arrest. The function of these gene products in other infection models indeed reveals their role as effectors in limiting infection. For example, *NOS2* (iNOS) activity produces NO, which is a messenger molecule having tumoricidal and bactericidal actions. Nitric oxide has been proposed to have a relevant role in malaria pathogenesis, but its mechanisms of action in different stages of infection remain unknown. Further, *NOS2* acts downstream to HIF1 signaling. HIF1 signaling reduces the susceptibility to mycobacterial infection via a nitric oxide-dependent mechanism (Elks et al., 2013). IGF1, a component of HIF1 signaling, is upregulated during Spz + condition. IGF1 is likely associated with promoting cell growth activity, which is reversed during SUMO1 + Spz + condition.

IFNG activates JAK/STAT pathway, leading to synthesis of IRF1 and stimulation of NOS2 expression. NOS2 expression in phagocytes results in efficient killing of *Leishmania* parasites in vitro and is critical for controlling the infection in vivo (Olekhnovitch, Ryffel, Muller, & Bousso, 2014). Interleukin 1 beta is an important mediator of inflammatory response and is involved in apoptosis, cell proliferation, and differentiation. Interleukin 1 beta is critical for host resistance during *M. tuberculosis* infection (Mayer-Barber et al., 2010). HERC5 broadly targets the newly synthesized proteins for ISG15 conjugation, a PTM modification that enable its targets to mediate diverse cellular pathways including RNA splicing, chromatin remodeling or polymerase II transcription, cytoskeleton organization and regulation, translation, glycolysis, stress responses, interferon signaling, and antiviral responses. HERC5 upregulation during SUMO1 + Spz + condition may have protective role against *Plasmodium* infection to hepatocytes similar to its role in HIV infections where it inhibits HIV-1 replication (Woods et al., 2011).

The upregulation of IFIT2 in SUMO1 + Spz + condition may direct the cells to undergo apoptosis. The RNA-binding ability of IFIT2 protein is required for antiviral activity and to promote apoptosis (Reich, 2013). Further, IFIT2 is also known to modulate the microtubule network implicated in cell reorganization during *Anncaliia algerae* infection as a host response to clear infection (Panek et al., 2014). The cytokines CCL5 and IL4 are part of the cascade of events leading to efficient parasite control in *Leishmania major* (Santiago et al., 2004) and *Listeria* (Kaufmann, Emoto, Szalay, Barsig, & Flesch, 1997) infections, respectively. Thus, SUMO1-mediated upregulation of CCL5 and IL4 may play an important role in host cell defense. In *Leishmania*, the promastigotes engage PI3K/Akt signaling, which confers to the infected cell, the capacity to resist cell death from activators of apoptosis. Our studies showing upregulation of Akt pathway during SUMO1 + Spz + condition may likely hint to a similar host cell resistance mechanisms being activated that counteract the effects of *Plasmodium* EEFs.

Our transcriptome data from *P. berghei*-infected HepG2 cells (Spz+), when compared to previous study of transcriptional landscape

of murine hepatoma (Hepa1-6) cells infected with *P. berghei* sporozoites (Albuquerque et al., 2009), revealed similarity in the differential expression of several host genes such as *AARS*, *CHAC1*, *DPP7*, *GPR137*, *KIF5C*, *KLF4*, *MAF*, *NR4A2*, *NRP*, *PROC*, *PTPN14*, and *SLC16A4*. The differential regulation of similar genes in two independent transcriptomic profiling studies suggests that the observed changes in the transcriptional patterns are indeed true. Other common pathways differentially expressed in both studies are involved in apoptosis, stress response, and regulation of gene expression. The interacting partners of JAK/STAT1 signaling pathway are significantly changed in HepG2 cells but not in infection to Hepa1-6 cells. Our study shows that *Plasmodium* modulates the JAK/STAT1 pathway as it occurs during *Toxoplasma* infection (Kim et al., 2007); however, the changes are reversed under conditions of SUMO1 overexpression and sporozoite infection (SUMO1 + Spz+). The pro- and antiapoptotic gene expression were modified in both Hepa1-6 and HepG2 cells infected with *P. berghei* suggesting a tendency of infected cells to undergo apoptosis and the modulation of host cell by the parasite for host cell survival. In contrast, in SUMO1 + Spz + condition, the host cell responses are clearly biased towards the suppression of cell proliferation and promoting apoptosis favoring the parasites' growth arrest and clearance. We further observed upregulation of toll-like receptor (*TLR2*) and *TLR6* in Spz + condition. During *Brucella abortus* infection, the mitogen-activated protein kinase (MAPK) signaling is impaired in *TLR2* and *TLR6* KO dendritic cells (de Almeida et al., 2013) likely hinting that TLR2 and TLR6 act as positive regulators of MAPK pathway. Although our studies do not demonstrate a direct role of MAPK pathway in Spz + condition, we nonetheless hypothesize that the TLR2 and TLR6 upregulation observed in our study may involve MAPK loop.

In conclusion, we provide evidence for the first time that Apicomplexan parasites such as *Plasmodium* and *Toxoplasma* hijack SUMOylation process to globally alter the gene expression of the host. Downregulation of SMAD4 SUMOylation is one of the mechanism opted by both parasites to prevent expression of host genes that likely elicit antiparasite effects. Destabilization of SUMO machinery by depletion of *Ubc9/E2* favored *Plasmodium* EEF growth, suggesting that the normal Ubc9 activity of host cell may limit parasite-induced effects. The parasites may interfere in the process of host SUMOylation by multiple yet to be deciphered mechanisms, and takeover of host cellular machinery may negatively regulate the expression of SUMO enzymes. The involvement of players such as *NOS2*, *IFNG*, *IL1B*, *IL10*, *IL4*, *CCL5*, *IFIT2*, *HERC5*, *PI3K*, and *MAPK* during SUMO1 overexpression may hint to the activation cellular effector mechanisms to defend the host against the parasite. Thus, activation of host SUMOylation machinery may have important implications for therapeutic interventions to treat protozoan infections.

4 | EXPERIMENTAL PROCEDURES

4.1 | Maintenance of rabbits, BALB/c, C57BL/6, and Swiss albino mice

Rabbits, BALB/c, C57BL/6, and Swiss albino mice were maintained at the animal house facility of University of Hyderabad. All animal experiments were performed in compliance with the Committee for the Purpose of Control and Supervision of Experiments on Animals (CPCSEA) national guidelines. The animal protocols were approved by Institutional Animal Ethics Committee (IAEC).

4.2 | Plasmids

Respectively, pCDNA3.1-SUMO1-FLAG and pTRE3G-SUMO1-GFP encode mature forms of SUMO1 with C-terminal FLAG and GFP tags. pCMV-Tet3G (Clonetech) plasmid was used to generate stable clones of HepG2-expressing transactivator protein. Cignal SMAD4 reporter plasmid encodes GFP gene under minimal CMV promoter and tandem repeats of SMAD4 transcriptional response elements (SABiosciences).

4.3 | Doxycycline-regulated expression of SUMO1 in HepG2 cells

HepG2 cells were initially transfected by the pCMV-Tet3G plasmid to express the transactivator protein required for binding to the Tet promoter in the pTRE3G response plasmid. The transfected cells were kept on drug selection with Geneticin (Invitrogen) at a concentration of 700 μg/ml. The drug resistant colonies were subcultured separately and analyzed for transactivator protein expression by Western blotting. The clonal population with maximal expression of transactivator protein was passaged and used for further experiments. A second round of transfection was done on transactivator cell line with a pTRE3G-SUMO1-GFP response plasmid, carrying tetracycline-responsive elements. The responsiveness of pTRE3G-transfected cells to doxycyline was tested at different concentration (10 ng–100 ng/ml) by analyzing the expression of recombinant SUMO1 + GFP by Western blotting using rabbit anti-GFP antibody. After 24 hr of transfection with response plasmid, cells were infected with *P. berghei* mCherry sporozoites or *T. gondii* tachyzoites as mentioned below. After 2 hr of infection, cells were replenished with fresh culture medium with 10 ng/ml of doxycycline and incubated for the indicated time period.

4.4 | Infection of HepG2 cells with *Plasmodium* sporozoites

HepG2 cells were cultured in Dulbecco's Modified Eagle Medium supplemented with 10% fetal bovine serum and maintained at 37 °C and 5% CO_2. Approximately 2×10^5 cells per well were seeded in a 24-well plate. *P. berghei* mCherry sporozoites were isolated from salivary glands of infected *Anopheles stephensi* mosquitoes and added to HepG2 cells. As an appropriate control, we also generated lysates from uninfected salivary glands and added to HepG2 cell that served as mock-infected culture. After 3 hr, cells were washed and replenished with fresh culture medium. For qRT-PCR analysis, the samples were harvested at 16, 25, 42, and 50 hr. For other experiments, the infected HepG2 cells were maintained for indicated time points. Samples for microarray were harvested at 48-hr postinfection.

4.5 | Culturing of *T. gondii* tachyzoites and infection to HepG2 cells

Human foreskin fibroblast cells were maintained similarly as described above. The cells were grown to 90% confluency, and cryopreserved *T. gondii* RH tachyzoites were added to cultures and maintained for 4 days to allow the parasites to multiply. Infected cells were harvested by scraping, and the tachyzoites were purified by passing the cells through 24G syringe and subsequently filtering through 5-μm filter. The parasites were counted and added to HepG2 cells at a multiplicity of infection of 0.5. Infected samples were collected at 24-hr postinfection for microscopy and real-time PCR.

4.6 | Immunofluorescence assay

HepG2 cells were infected with *P. berghei* and *T. gondii* as described above. Cells were washed with phosphate-buffered saline (PBS) and fixed with 4% paraformaldehyde (PFA) for 15 min at room temperature. The cells were permeabilized with precooled acetone and methanol in a ratio of 1:3 for 15 min. The nonspecific blocking was done with 3% bovine serum albumin (BSA) in PBS for 1 hr. The cells were incubated for 1 hr with anti-SUMO1 rabbit primary antibody (Abcam) at 1:250 dilution or anti-Tg TP3 mouse primary antibody (Abcam) at 1:300 dilution or anti-CSP mouse primary antibody (3d11) in 1:1,000 dilution made in 3% BSA. Cells were washed sequentially with Tris buffered saline (TBS), TBST, and TBS for 15 min each. Immunoreactivity was visualized under fluorescent microscope using secondary antibodies—goat antirabbit IgG-Alexa Flour 488 (Invitrogen) at 1:200 dilution or goat antimouse IgG-Alexa Flour 594 (Invitrogen) at 1:250 dilution and DAPI (1 μg/ml) (sigma). All secondary antibody dilutions were made in 3% BSA and incubated for 1 hr. Cells were washed sequentially with TBS, TBST, and TBS for 15 min each. Following completion of staining procedure, coverslips were mounted on a glass slide using Prolong Gold (Invitrogen) antifade reagent and stored at 4 °C before and after microscopy. Stained cells were analyzed using Nikon AR fluorescence microscope.

4.7 | Western blot analysis

Protein samples were prepared by lysing the cultured cells in RIPA buffer (20 mM Tris-HCl (pH 7.5), 150 mM NaCl, 1 mM Na_2EDTA, 1 mM EGTA, 1% NP-40, 1% sodium deoxycholate, 2.5 mM sodium pyrophosphate, 1 mM β-glycerophosphate, 1 mM Na_3VO4, and 1 μg/ml leupeptin). Samples were resolved by sodium dodecyl sulfate polyacrylamide gel electrophoresis, transferred to nitrocellulose membrane, blocked in 3% skimmed milk in TBS, and probed with antibodies. Primary antibodies used in this study were mouse anti-TetR (Clonetech) used at 1:2,000 dilution, rabbit anti-Ubc9 (Abcam) used at 1:3,000 dilution, rabbit anti-SUMO1 (Abcam) used at 1:3,000 dilution, mouse anti-actin (Abcam) used at 1:5,000 dilution, rabbit anti-GFP antibody used at 1:200 dilution, and mouse anti-β tubulin (Millipore) used at 1:5,000 dilution. Secondary antibodies were horse radish peroxidase-linked goat antirabbit IgG and goat antimouse IgG (both from Biorad) used at a dilution of 1:5000. Blots were developed using ECL prime Western blotting detection kit (Amersham), and images were scanned using Versadoc (Bio-Rad).

4.8 | Inside and outside assay to quantify *P. berghei* sporozoite invasion

HepG2 cells were grown in Lab-Tek Chamber Slides and transfected with pCDNA3.1-SUMO1-FLAG plasmid. Approximately 2×10^4 *P. berghei* mCherry sporozoites were added to HepG2 cells that were either nontransfected or transfected with pCDNA3.1-SUMO1-FLAG and incubated at 37 °C for 2 hr. Medium was gently removed, and the sporozoites were fixed with 4% PFA for 15 min. Immunofluorescence assay was performed with anti-CSP antibody (3d11) without permeabilization to stain the extracellular sporozoites. The immunoreactivity was revealed using rabbit antimouse IgG Alexa Flour 488 (Invitrogen) secondary antibody used at 1:250 dilution. The slide was observed under fluorescent microscope to score for red (total) and green (extracellular) sporozoites in 25–30 random fields. The number of sporozoites that invaded per field was calculated using the formula: total number of sporozoites (outside and inside) minus extracellular sporozoites (only outside).

4.9 | Microarray analysis of HepG2 cells

For microarray analysis, an Agilent custom human gene expression microarray slide having 8 × 60 k format was used. The microarray slide contains 900 × 10 replicates of biological probes and 96 × 10 positive control probes. The hybridization, scanning, data extraction, and data analysis were performed under project number SO_3724 at Genotypic Technology Private Limited, Bangalore, India.

4.10 | Isolation of RNA from infected samples

Total RNA was isolated from the cultured cells using PureLink micro-to-midi total RNA purification system (Ambion). Briefly, cells were washed with 1× sterile PBS, lysed in lysis buffer, and passed through 35G insulin syringe for efficient cell lysis. The RNA was precipitated with 70% ultrapure ethanol and applied to the silicon membrane column. Following two washes with wash buffer and one additional dry spin to remove residual ethanol, RNA was eluted in RNase free water and assessed for concentration and purity using Nanodrop® ND-1000 spectrophotometer. RNA was stored at −80 °C until further use.

4.11 | Generation of complementary DNA

Complementary DNA (cDNA) was generated using the total RNA as template. The reaction mixture for cDNA synthesis consisted of Moloney murine leukemia virus reverse transcriptase, dNTPs, $MgCl_2$, RNase inhibitor, random hexamer primer (for short length cDNA fragments), or Oligo dT (for full length cDNA). Nearly 1–2 μg of RNA was used to perform reverse transcription in a volume of 30 μl reaction mixture. Using following thermal cycling conditions, cDNA was generated: 25 °C for 10 min, 42 °C for 20 min, 98 °C for 5 min, and 5 °C for 5 min.

4.12 | Labeling and microarray hybridization

The samples for gene expression analysis were labeled using Agilent Quick Amp Labeling Kit (p/n5190-0442). Five hundred nanograms each of total RNA were reverse transcribed at 40 °C using Oligo dT primer tagged to a T7 polymerase promoter, and RNA was converted to double stranded cDNA. Synthesized double stranded cDNA were used as template for cRNA samples generation. By in vitro transcription, cRNA was generated, and the dye Cy3-CTP (Agilent) was incorporated during this critical step. The cDNA synthesis and in vitro transcription steps were carried out at 40 °C. Labeled cRNA was purified using Qiagen RNeasy columns (Qiagen, Cat No: 74106) and quality assessed for yields and specific activity using the Nanodrop ND-1000.

4.13 | Hybridization and scanning

Six hundred nanograms of labeled cRNA sample were fragmented at 60 °C and hybridized on to an Agilent Human Gene Expression Microarray 8 × 60 K (AMADID No: 39494) arrays. Fragmentation of labeled cRNA and hybridization were performed using the gene expression hybridization kit from Agilent Technologies (in situ hybridization kit, part number 5190-0404). Hybridization was carried out in Agilent's SureHyb Chambers at 65 °C for 16 hr. The hybridized slides were washed using the Agilent gene expression wash buffers (Agilent Technologies, part number 5188-5327), and slides were scanned using the Agilent microarray scanner (Agilent Technologies, part number G2600D).

4.14 | Feature extraction: image analysis

Data extraction from images was done using Agilent Feature Extraction software.

4.15 | Microarray data analysis

Feature-extracted raw data was analyzed using Agilent GeneSpring GX software. Normalization of the data was done with GeneSpring GX using the 75th percentile shift method. Percentile shift normalization is considered as a global normalization, where the locations of all spot intensities in the array are adjusted. This normalization takes each column in an experiment independently and calculates the nth percentile of the expression values for this array, across all the spots (where n has a range from 0 to 100 and $n = 75$ is the median). It subtracts this value from the expression value of each entity, and fold change values were obtained by comparing test samples with respect to specific control samples. Significant genes upregulated fold > 0.6 (log base2) and downregulated <−0.6 (log base2) in the test samples with respect to the control sample were identified. Statistical Student's *t* test *p* value among the replicates was calculated on the basis of volcano plot algorithm. Differentially regulated genes were clustered using hierarchical clustering based on the Pearson coefficient correlation algorithm to identify significant gene expression patterns. Genes were classified on the basis of functional category and pathways using Biological Analysis tool DAVID (http://david.abcc.ncifcrf.gov/).

4.16 | The shRNA-mediated silencing of Ubc-9 expression

HepG2 cells were transfected with p-GFP-VRS-UBE2I plasmid variants encoding shRNA targeting human Ubc9 mRNA (Origene TG300697). Cells were infected with *P. berghei* mCherry sporozoites (3×10^4 per well) and incubated for 48 hr prior to processing.

4.17 | TGF-β reporter assay

HepG2 cells were transfected with SMAD4 reporter plasmid (SABiosciences) and 24-hr posttransfection; the cells were infected with *P. berghei* sporozoites (3×10^3 per well) or *T. gondii* tachyzoites (multiplicity of infection 0.5). After 2 hr of infection, cells were incubated with recombinant human TGF-β1 (20 ng/ml) for 20 hr. Intensity of GFP fluorescence was measured using Tecan Infinite 200 microplate reader with 480-nm excitation and 515-nm emission filters. Intensities were normalized to nontransfected HepG2 cells.

4.18 | TA cloning to generate standards for qRT-PCR quantification

For quantification of target gene expression, real-time PCR analysis was done by absolute quantification method. Briefly, primers were designed for genes as indicated in Table S1. Primers spanning the exon-exon junctions were selected that amplified a product in the range of 100–150 bp. The PCR products were ligated into TA vector (pTZ57 R/T, Thermo). The recombinant TA clones were used to prepare the gene standards based on the size.

4.19 | Real-time PCR quantification

Real-time PCR was performed with Mastercycler ep realplex (Eppendorf) using IQ SYBR green super mix (Biorad). Gene expression was determined by absolute quantification method. Data normalization was done by obtaining ratio of target gene copy number and host *GAPDH* (h*GAPDH)* copy number. Microsoft excel was used to plot the graphs and for statistical analysis.

4.20 | Microarray data accession number

The complete microarray data set can be accessed from the NCBI GEO database (accession code GSE72049).

ACKNOWLEDGEMENTS

This work was supported by Department of Biotechnology (DBT, India) Grant BT/PR2495/BRB/10/950/2011 to KAK. MM and SRR were supported by Council for Scientific and Industrial Research (CSIR); BSM was supported by Department of Biotechnology (DBT). SM is supported by DBT Ramalingaswami Fellowship grant (GAP0142). We thank Dhanasekharan Shanmugam from NCL Pune for providing *Toxoplasma gondii* RH strain. We thank Surendra Kumar Kolli for assistance with preparing figures.

Anti-Plagiarism report

Functional insights into a Plasmodium sporozoite membrane protein (SIMP) and a Cysteine protease (SERA-3) reveals a role in maintaining pre-erythrocytic infectivity

by Dipti Singh

Submission date: 14-Jun-2022 02:54PM (UTC+0530)
Submission ID: 1856614206
File name: Dipti_Singh.pdf (4.43M)
Word count: 31158
Character count: 176671

Functional insights into a Plasmodium sporozoite membrane protein (SIMP) and a Cysteine protease (SERA-3) reveals a role in maintaining pre-erythrocytic infectivity

ORIGINALITY REPORT

30%	7%	29%	2%
SIMILARITY INDEX	INTERNET SOURCES	PUBLICATIONS	STUDENT PAPERS

PRIMARY SOURCES

1	Dipti Singh, Smita Patri, Veeda Narahari, Rameswara R. Segireddy et al. " A Conserved Structural Integrity Maintenance Protein ( ) is associated with sporozoite membrane and is essential for maintaining shape and infectivity ", Molecular Microbiology, 2022 Publication	16%
2	Dipti Singh, Smita Patri, Veeda Narahari, Rameswara R. Segireddy et al. " A conserved structural integrity maintenance protein ( ) is associated with sporozoite membrane and is essential for maintaining shape and infectivity ", Molecular Microbiology, 2022 Publication	5%
3	www.ncbi.nlm.nih.gov Internet Source	1%
4	Bianca B. Kojin, Zach N. Adelman. "The Sporozoite's Journey Through the Mosquito: A Critical Examination of Host and Parasite	1%

from our publication